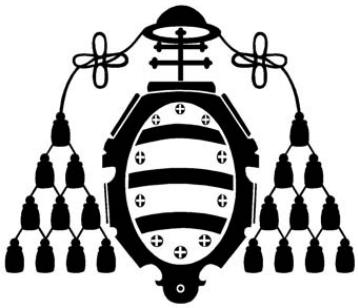

UNIVERSIDAD DE OVIEDO

Departamento de Ingeniería Eléctrica, Electrónica, de Computadores y de Sistemas

Doctor of Philosophy

Technical and Economical Analysis of Isolated Microgrids

Ahmed Mohamed Abd el Motaleb

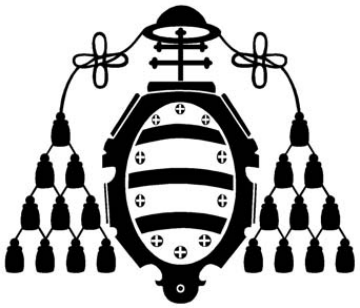

Departamento de Ingeniería Eléctrica, Electrónica, de Computadores y de Sistemas

Doctor of Philosophy

Technical and Economical Analysis of Isolated Microgrids

Author: Ahmed Mohamed Abd el Motaleb

Director: Guzmán Díaz González

Co-Director: Cristina González Morán

March 2013

ACKNOWLEDGEMENTS

First of all, the author would like to express his sincere appreciation and gratitude to his supervisor, Dr. Guzmán Díaz González, for his invaluable guidance, patience, encouragement and support throughout the course of this research work and in the preparation of this thesis.

The author would like to express his sincere gratitude to Dr. Cristina González Morán for her guidance, insightful comments and suggestions during the research work.

The author would like to thank all colleagues at Escuela Politécnica de Ingeniería de Gijón for their support and help.

The author would like to thank Ministerio de Ciencia e Innovación for the financial support by the scholarship FPI-ene2010-14899.

Finally, the author would like to take this opportunity to acknowledge the constant encouragement and support from his family and ex-director. Hazem Makram. The author presents this thesis as a gift to them.

Contents

List of Figures

List of Tables

Nomenclature

Abbreviations

AGC	Automatic generation control
AIC	Akaike information criterion
ARMA	autoregressive moving average time series model
AVR	Automatic voltage regulator
BIC	Bayesian information criterion
CCS	Carbon capture and storage
CDF	Cumulative distribution function
CF	Capacity factor
CHP	Combined heat and power
CIGRE	International Council on Large Electric Systems
COE	Cost of Energy
CPF	Continuation power flow
DGs	Distributed generators
DERs	Distributed energy resources
DFIG	doubly-fed induction generator

DNOs	Distribution network operators
EMS	Energy management system
ESS	Energy storage systems
GSC	grid side converter od doubly-fed induction generator
GRR	Generator to rotor ratio
LHS	Latin Hypercube Sampling
MCS	Monte Carlo Sampling
MG	Microgrid
MSUs	Microgrid supporting units
NCP	Nonlinear complementarity problem
NLP	Nonlinear programming problem
NPV	Net Present Value
NR	Newton-Raphson
ODEs	Ordinary differential equations
PCC	Point of common coupling
PDF	Probability density function
Pll	Phased locked loop
PI	Proportional integral controller
$p(w)$	Distribution probability of wind speed
RES	Renewable energy sources
RSC	rotor side converter od doubly-fed induction generator
SNB	Saddle node bifurcation
SRU	System reserve unit

SPB	Simple payback
SS	Static switch
WECS	Wind energy conversion systems
WTGs	Wind turbine generators

Variables

AAR	wind turbine average annual revenue
ACE	area control error
AEP_{bat}	annual energy production of the battery
AEP_{wt}	annual energy production of the wind turbine
$C_{st_{bat}}$	energy stored in the battery bank
C_p	wind turbine power coefficient
E_{bat}	Energy production of the battery
e_i	current error in current controller of droop inverter
e_v	voltage error in voltage controller of droop inverter
E_{wt}	Energy production of the wind turbine
$F(x)$	distribution function vertical axis
f_{COE}	cost of energy function
F_{P_g}	wind power cumulative distribution function
F_w	wind speed cumulative distribution function
g	algebraic variables vector
$g(x)$	inequality constraints vector
$h(x)$	equality constraints vector
i_b	input current to DC-link circuit

i_c	filter capacitor current
i_{Cdc}	DC-link capacitor current
i_g	output current from doubly-fed induction generator to the microgrid
i_i	inductance filter current
i_{line}	distribution line current
i_{load}	static load current
i_m	doubly-fed induction generator magnetization current
i_o	output filter current of droop inverter
i_r	doubly-fed induction generator rotor current
i_s	doubly-fed induction generator stator current
K	uncertain variables or parameters
n	Sampling moment
N	number of samples
P	active operating inverter power
P_{demand}	demand power
P_g	wind turbine power
P_g^0	Nominal power of MSUs, where the frequency is nominal
P_g^{max}	Nominal power of MSUs, where the frequency is nominal
$P_t^{E_c}$	battery power charge
$P_t^{E_d}$	battery power discharge
P_{tie}	tie line power among different areas
P_{wt}	instantaneous wind turbine power

$\tilde{p}$	instantaneous active power
Q	reactive operating power
$\tilde{q}$	instantaneous reactive power
r_r	wind turbine rating ratio
$r_{x,y}$	cross-correlation between two variables
T_e	doubly-fed induction generator electromagnetic torque
T_m	doubly-fed induction generator mechanical torque
u	control variables vector
v_c	tension of capacitor filter
v_{dc}, v_b	similar terms of DC-link tension
v_g	microgrid node tension
v_i	input filter tension of droop inverter
v_{L_c}	coupling inductance voltage drop
v_{L_f}	filter inductance voltage drop
v_m	doubly-fed induction generator magnetization circuit tension
v_o	filter capacitor tension
v_r	doubly-fed induction generator rotor tension
v_s	doubly-fed induction generator stator tension
w	instantaneous wind speed sample
w_{avg}	mean wind speed
x	state variables vector
x^i_{max}	maximum interval limit of distribution function

x^i_{min}	minimum interval limit of distribution function
y	output variables vector
δ	angle between droop inverter synchronous frame and the microgrid common synchronous frame
ζ_{dc}, ζ_{i_b}	integral terms of dc-link circuit
ζ_i	integral term of current controller state variable
ζ_{i_b}	integral term of DC-link circuit
ζ_{i_r}	integral term of doubly-fed induction generator rotor side converter
ζ_{pll}	integral term of phased-locked loop circuit
ζ_Q	integral term of doubly-fed induction generator rotor side converter state variable
θ_{pll}	angle between doubly-fed induction generator synchronous frame and the microgrid common synchronous frame
λ_i	wind turbine blade tip speed ratio
μ	average value
σ	standard deviation
Φ_v	integral term of voltage controller
Ψ_s	doubly-fed induction generator stator flux linkage
ω	operating frequency
ω^0	Nominal value of frequency
ω_{pll}	doubly-fed induction generator pulsation frequency
ω_r	wind turbine mechanical speed

Parameters

C_{bat}	battery capital cost
$C_{bat_{st_{max}}}$	maximum energy stored
$C_{bat_{st_{min}}}$	minimum energy stored
C_f	filter capacitor of droop inverter
C_{wp}	initial capital cost of wind turbine
D	wind turbine rotor diameter
F	wind turbinefriction constant
FCR	fixed rate of charge
H	wind turbine height
i	discount rate
J	wind turbine inertia constant
k_{ii}	current controller integral gain
k_{iv}	voltage controller integral gain
k_{pi}	current controller proportional gain
k_{pv}	voltage controller proportional gain
L	life time of wind turbines in years
LRC	levelized replacement cost
L_c	coupling inductance of droop inverter
L_f	output filter inductance of droop inverter
L_{line}	distribution line inductance
L_{load}	static load inductance
L_m	doubly-fed induction generator mutual inductance

L_r	doubly-fed induction generator rotor inductance
L_s	doubly-fed induction generator stator inductance
m_p	active droop constant
nq	reactive droop constant
$O\ \&\ M$	operation and maintenance cost
p	doubly-fed induction generator poles number
$P_E^{c_{max}}$	maximum charge rate
$P_E^{d_{max}}$	maximum discharge rate
P_{max}	maximum real power of inverter droop
P_{rated}	rated power of wind turbine
Q_{max}	maximum reactive power of inverter droop
R_c	internal resistance of coupling inductance of droop inverter
R_f	internal resistance of output filter inductance of droop inverter
R_{line}	resistance of distribution line
R_{load}	static load resistance
R_r	doubly-fed induction generator rotor resistance
R_s	doubly-fed induction generator stator resistance
UC_e:	Unit cost of input electricity for charging batteries
V_{max}	maximum voltage
w_f	wind turbine furling speed
w_i	wind turbine cut-in speed
w_n	wind turbine blending speed

w_r	wind turbine rated speed
X_m	doubly-fed induction generator mutual reactance
η_c	charge efficiency
η_d	discharge efficiency
ϑ	model parameter
ω_{max}	maximum frequency

Matrices

A	open loop state variables matrix
A_c	closed loop state variables matrix
B	control matrix
C	output matrix
D	feed-forward matrix
j_{1A}	state variables coefficients matrix of state variables equations
j_{2A}	algebraic variables coefficients matrix of state variables equations
j_{1C}	state variables coefficients matrix of output variables equations
j_{2C}	algebraic variables coefficients matrix of output variables equations
j_3	state variables coefficients matrix of algebraic variables equations
j_4	algebraic variables coefficients matrix of algebraic variables equations

k	system gains matrix
ϕ	right eigenvector
ψ	left eigenvector

Operators and reference systems

dq	synchronous reference related to each droop inverter
DQ	common synchronous reference of the microgrid
s	laplace operator
Δ	linearized variables operator
Δp	synchronous reference differential operator
∇	gradient vector

Superscripts and subscripts

$*$	superscript indicates to reference variable
dq	subscript means that the variable is referred to droop inverter synchronous reference
DQ	subscript means that the variable is referred to microgrid common synchronous reference
i, j	subscripts indicates to microgrid elements of the same type, such as DFIGs but related to nodes i and j

Introduction

As affordable and adequate energy is considered the main path towards economic prosperity, by 21th century the EU countries are confronted with moving from centralized conventional generation methods, which depend mainly on fossil fuels, to another trend of generation based on distributed generation. Fossil fuels release damaging gases, the combustion of such sources creates some acids as sulfuric and carbonic, which rise into the atmosphere and return as acid rain, and subsequently damages soil and water. In addition, these released gases cause rapid heating and adverse effects on climate change.

According to the latest available information from EUROSTAT in 2005, thermal power plants, fuelled mostly by fossil fuels, accounted for 54% of the total installed capacity in EU, followed by hydro, nuclear generation and other sustainable sources. As a result of the latest EUROSTAT statistics, some important issues need to be addressed, such as global warming; average temperature rose by 0.6C, because conventional generation fuelled by fossil fuels are the main emitters of carbon dioxide (CO_2) that is the basic contributor to global warming. Another issue regarding security of energy supply, as EU imports 50% of its energy requirements and the dependency on imports is to be increased to 70% by 2030. More drawbacks of the centralized conventional generation can be briefed in the following points: (1) The transmission and distribution costs amount up to 30% of the delivered electricity cost, due to high line transmission and conversion losses. (2) It is required to upgrade the transmission and distribution networks by huge investment. (3) The centralized generation can offer adequacy mostly, but cannot ensure the required power quality for certain network areas.

Several studies have been conducted to ensure the main shortfalls of the centralized generation and to detail the motivation of the customers towards a new architecture of generation which is distributed generation as a primary source of electricity or as a backup generation source.

In order to overcome such drawbacks, the European Commission proposed a new energy policy in January 2007 based on distributed generation, for reduction greenhouse gas emission, improving power quality and increase the contribution of sustainable energy sources to 20%. Figure 1 shows the growing

dependency of EU electricity generation on fossil fuel resources, followed by nuclear energy, wind energy and other renewable energy sources (RES), according to EUROSTAT.

In order to reduce the dependency on centralized fossil fuel generation sources, improve power quality and increase the contribution of sustainable energy sources, the study and analyses of the new developed generation trend which depends on distributed energy sources are necessary.

This thesis concentrates on a new architecture of generation known as Microgrid (MG), which is supplied by distributed generators (DGs). In late 1990s, the major issues related to the distributed generation have been extensively investigated by the working groups of the International Council on Large Electric Systems (CIGRE). The new era of generation is under continuous investigation to overcome the negative sides of the centralized power utilities, in order to enhance the electric and thermal energy, optimize power quality, minimize pollutant deposition and contributes to ancillary services.

The main objective of the thesis is to conduct several technical and economic analyses in such new architectures of generation, such as providing an insight about site matching suitability for droop-regulated microgrids supplied by wind generators, optimizing both energy production and economic performance for isolated microgrids supplied by wind energy and different energy storage systems and finally predicting some stability constraints for generation sources by small signal stability analysis.

This thesis is divided into five chapters; Chapter 1 shows the state of the art, to clear the main difference of operation and control between the conventional power utility grid and microgrids; moreover, the problems of supplying microgrids by non-dispatchable generation as wind energy are highlighted, to illustrate the main challenges of supplying microgrids by such intermittent energy sources. Finally, thesis contributions are listed, and comparisons between thesis contributions and other recent researches regarding microgrids are shown. In Chapter 2, capacity factor analyses of droop-regulated microgrids are performed based on a reliable wind speed sampling strategy, by reducing the variance of wind speed samples, and also including the correlations among wind speeds. In Chapter 3, the idea of site matching suitability of droop-regulated microgrids supplied by wind generators is more detailed, by considering both energy production and economic performance of isolated mi-

crogrids supplied by wind energy and different energy storage systems. The optimization function in this Chapter is conducted to minimize the cost of energy, which is a function of both capital costs and energy production of the generation sources. In Chapter 4, microgrid stability analyses are conducted by the small signal stability criteria. The analyses are carried out to illustrate the stability margin and to determine the critical eigenvalues of isolated microgrids supplied by doubly-fed induction generators and inverter-interfaced distributed generators, when applying common actions to share the power among generation sources, and also through different wind speed levels. Finally, the conclusions of the thesis are listed in Chapter 5.

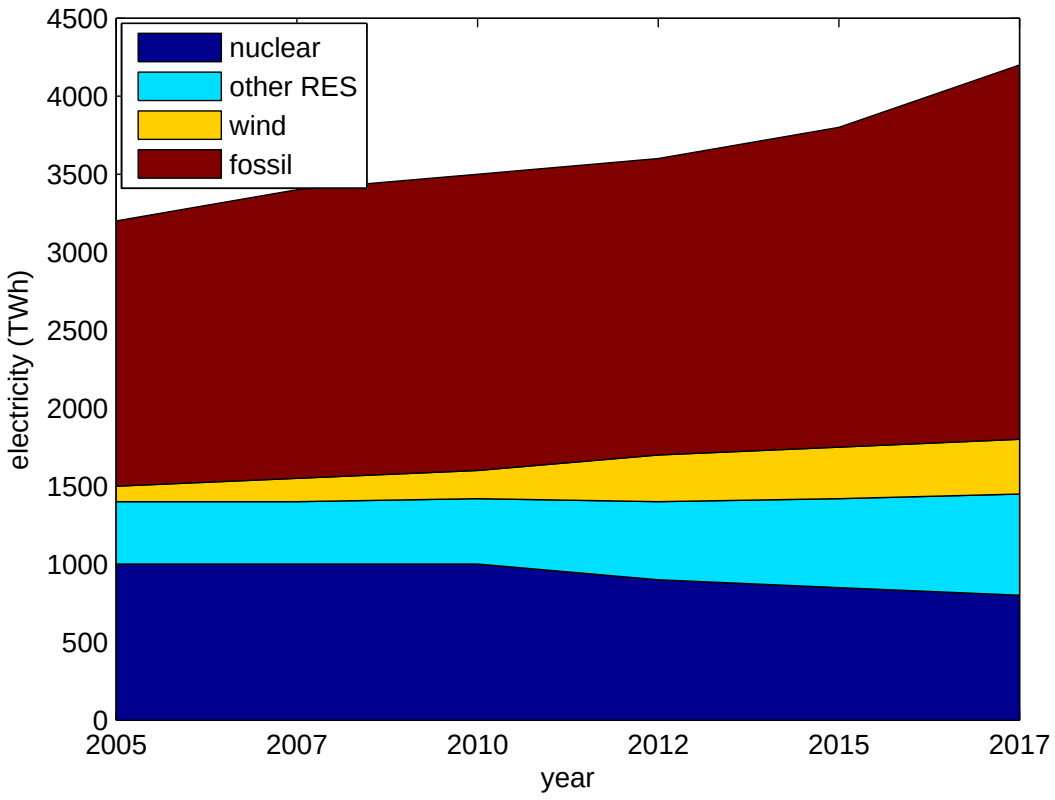

Figure 1: EU electricity generation by different energy resources

Chapter 1

State of the Art

1.1 Introduction

The world's first power station was built in the Bavarian town of Ettal and went into operation in 1878. The first public power station was the Edison Electric Light Station, built in London, which started operation in January 1882. In September 1882, the Pearl Street Station was established by Edison to provide electric lighting. Through the first few decades of the 20th century, central stations became larger, using higher steam pressures to provide higher efficiency. Interconnection by hydroelectric power was allowed to be in service by 1906; however, a great generation capacity expansion has been achieved through steam turbines in central stations, as they have played the primary role in the generation level. Generators were no longer limited by slow speed of reciprocating engines and could grow to greater sizes, represented mainly by *Synchronous Generators*, which are considered the main sources of generation level in centralized power utilities.

As the synchronous generators play the main role in the generation level of the centralized power utility grids, they can be classified as either high-speed generators, driven by steam or gas turbines called *turbogenerators*, or low-speed generators driven by water turbines *hydro generators*. Both mentioned generators have two main magnetic parts termed as the stator and rotor; both of them are manufactured from magnetic steels. The armature winding carries the load current and supplies power to the system. The rotor excitation winding is supplied by a direct current to produce a rotating magnetic flux. This rotating magnetic flux induces an electromotive force in each phase of the

three-phase stator armature winding which forces alternating current to flow out to the power system. Typically, the operation of synchronous generators depends mainly on the electromechanical interaction between the stator and rotor circuits. Thus, the rotor plays an important rule for power control and stability. The details regarding control and stability of synchronous generators are beyond the scope of this thesis. For more details, it is recommended to refer to [2] and [3].

Through the last decades, the conventional power systems have faced some problems related to gradual depletion of fossil fuel resources, poor energy efficiency, environmental pollution, low power quality and power market monopoly policies. Firstly, the transmission and distribution costs amount up to 30% of the delivered electricity cost on average. Secondly, it is required to upgrade the transmission and distribution networks by huge investments [4]. Thirdly, the centralized generation can supply the energy requirements of the consumers at all times, but cannot ensure the required power quality for certain network areas [4]. Fourthly, the catastrophic environmental impact of the centralized generation is clear due to the dependence on fossil fuels [5].

These problems have led to a new trend of locally power generation at distribution voltage level by using non-conventional/renewable energy sources like natural gas, biogas, wind power, solar photovoltaic cells, fuel cells, combined heat and power (CHP) systems, microturbines and stirling engines. This type of power generation is termed as distributed generation (DG) and the energy sources are termed as distributed energy resources (DERs). The term distributed generation has been devised to distinguish this concept of generation from centralized conventional generation. Distribution networks become active with the integration of DGs, subsequently the are termed as active distribution networks.

In contrast to conventional power systems, the distributed generation sources have proved more positive impacts over the centralized generation. Firstly, the distributed generation can alleviate the loading of the transmission and distribution. Consequently, the network transmission and distribution losses can be minimized, which leads to lower energy tariffs. Secondly, the distributed generation can be employed to locally control the power quality according to customer requirements even on an hourly basis. Thirdly, the distributed generation can reduce system expansion costs of the main power utility by limiting

the utility transmission capacity expansion and offering the best utilization of the current transmission capacity. Fourthly, the distributed generation can effectively reduce the emissions and environmental warming, due to high dependency on renewable energy sources. Fifthly, the distributed generation is capable to restart its generation after a total system collapse without importing any external power to restore, at least, a portion of the power system to service after the collapse (black start capability).

The operational differences between conventional generation and distributed generation can be clarified by some main features, such as DGs have small generation capacities, DGs are located near to customers and DGs are interfaced to networks via electronic inverters to synthesize their productions.

In order to reduce the dependency on centralized fossil fuel generation sources, improve power quality and increase the contribution of sustainable energy sources, this thesis concentrates on a new architecture for generation known as Microgrid (MG), which is supplied by distributed generators. Microgrids are considered as clusters of distributed energy sources, loads and controls organized to deliver the optimum energy service [6].

The proposed microgrid models in this thesis are supplied mainly by DGs interfaced to the microgrids via electronic inverters. Moreover, intermitted energy sources which are wind energy connected to the grids directly without interfaces. Thus, the generation supply depends on inverter-interfaced distributed generators and intermittent energy sources, unlike the centralized generation. The droop control strategy is adopted in the thesis, to enhance real-reactive power exchange among the DGs interfaced by inverters. The droop control uses only local power to detect changes in the system and adjust the operating points of the generators accordingly.

The main objective of this thesis is to conduct several technical and economic analyses in microgrids; therefore, some pivotal aspects are illustrated, such as providing an insight about site matching suitability of droop-regulated microgrids supplied by wind generators, optimizing both the energy production and economic performance of isolated microgrids supplied by wind energy and different energy storage systems and finally predicting the stability constraints of the generation sources by small signal stability analysis. The following text outlines the main objectives of the thesis.

A conventional generation unit is capable of generating rated power during

normal operation. Typically, the capacity factor of a conventional generator is its actual average generation as a function of its rated power; the capacity factor can be defined as the ratio of the actual energy produced from a generation unit, in a given period, to its potential output at full capacity. Thus, the capacity factor of a conventional generator is dependent only on power demand. On the other hand, for intermittent wind energy sources, the capacity factor depends on the wind speed probability distribution and on the characteristics of wind turbines, and so the determination of the wind generation capacity, which can share supply microgrids with other distributed generators, is relatively complex. Moreover, the capacity factor for a droop-regulated microgrid cannot be conducted by considering the microgrid as a large generator that is built up from several minor wind generating units, because droop control imposes restrictions on the maximum loadability. Thus, the thesis conducts a capacity factor analysis of droop-regulated microgrids that serves to evaluate the site-matching suitability of a combination of wind generators and wind speeds, by an advanced technique, known as *Latin Hypercube* (LHS), based on [7], for accurate wind speed sampling.

In conventional power grids, the uncertainties of system reserves are efficiently reduced and well-settled. Although, the conventional generation suffers from the volatility of conventional energy prices, their variability is still much lower than uncertainty of the wind power. In contrast, in the case of microgrids supplied by wind energy, some doubts emerge regarding the impact of wind variability on the generation capacity and economic considerations. The characteristics of such grids require scheduling more reserve for ensuring adequate security and reliability levels, but the higher reserve requirements may substantially deteriorate the economy of these supply systems. Usually, electric energy storage systems, including different types as batteries, capacitors and flywheels are required to supplement the wind generators, during the moments of demand shortfall. Hence, the energy storage systems as batteries can handle such problems by managing the power control during the transient moments. For this purpose, the thesis introduces a study based on optimizing both energy production and economic performance of isolated microgrids, supplied by wind energy and batteries. Hence, the maximum possible energy production at the lowest energy cost can be clarified.

In conventional generation systems, the possibility of system restoration

and reducing power swings among different generation units is high, in case of disturbances, as an adequate reserve can be supplied from neighboring generation units to restore the operation. Moreover, in the conventional generation systems, some standards and recovery strategies from power imbalances have been set and handled from decades. In addition, the stability analysis of conventional generation has been conducted in many studies, and the most dominant variables which can violate the stability of networks are well-known. In contrast, the situation is different in the case of isolated microgrids, as the system reserve and capabilities of the whole system to recover from disturbances are limited, especially when the microgrid is supplied by intermittent sources as wind energy. Moreover, microgrids suffer from lack of standards to overcome disturbance and power swing problems, as it is considered as a new architecture of generation. Therefore, the thesis introduces the small signal stability analysis of isolated microgrids, supplied by wind energy and also generation sources interfaced via inverters, under different scenarios. Thus, the dominant variables which violate the microgrid stability can be recognized, and so in future work, an appropriate control strategy can be developed to keep the microgrid stable.

This chapter shows the state of the art to clear the main differences of operation and control, between the conventional power utility grid and microgrids supplied by distributed generators. In addition, the problems of supplying microgrids by non-dispatchable generators as wind energy are studied, to unfold the challenges to microgrids development.

This Chapter is divided into nine sections. In Sections 1.2-1.5.2, the concepts of microgrids operation and control are introduced, to reveal the operational differences between microgrids and centralized power utilities. In Section 1.5.3, the integration of non-dispatchable generators to microgrids is explained, to illustrate the challenges faced by microgrids, supplied by non-dispatchable energy sources. In Section 1.6, the topic of capacity factor analysis of droop-regulated microgrids is addressed; this topic is studied through Chapter 2. Section 1.7 shows the necessity of optimizing both energy production and economic performance in isolated microgrids; this topic is detailed in Chapter 3. Section 1.8 illustrates the stability analysis of isolated microgrids, supplied by non-dispatchable energy sources, as microgrid stability analysis is performed in Chapter 4. Finally, Section 1.9 illustrates the thesis contributions.

Through this thesis, the DGs are employed in microgrids either in the isolated microgrid mode or grid-connected mode. Clearly, the modelling and dynamics of DGs are far from synchronous generation units; hence, the mentality and concept of microgrids operation must be detailed to explain how microgrids can benefit from the diversity of generation sources, in order to optimize their operations and overcome problems arisen by conventional generation units.

1.2 Operational Concepts of Microgrids

Electricity networks are in the era of major transition from stable passive distribution networks with unidirectional electricity transportation, to active distribution networks with bidirectional electricity transportation. Distribution networks without any DG units are passive since the electrical power is supplied by the main utilities to the customers embedded in the distribution networks. The grid becomes active when DG units are added to the distribution system leading to bidirectional power flow in the networks [8].

The present *fit-and-forget* operational strategy of DG units must be changed for management of active networks. Active networks incorporate DGs in distribution networks and demand side management, by motivating the distribution network operators (DNOs) towards better asset utilization and management by deferral of replacement of age-old assets. The application of active network management can greatly support more connections of DGs as compared to passive networks.

A microgrid is essentially an active distribution network, because it is an aggregation of DG systems and different loads at distribution voltage level. The microgrid generators (microsources) are usually integrated renewable/non-conventional DERs to generate power at distribution voltage [9]. Such generators must be equipped with power electronic interfaces to synchronize all DERs together and provide the required power quality [10]. This control flexibility allows the microgrid to present itself to the main utility power system as a single controlled unit that meets local energy needs for reliability and security.

Figure 1.1 shows the energy flow for both a centralized conventional grid and a microgrid supplied by distributed resources, also the figure shows the single point of connection to the utility called point of common coupling (PCC);

moreover, the static switch (SS) is responsible for isolating or connecting the microgrid from/to the utility power grid. Basically, the key differences between the microgrid and the conventional power grid can be accounted in the following points: (1) The small capacity of microsources in respect to power generators in conventional networks. (2) Microsources can feed power directly to distribution networks. (3) Microsources are installed close to customers, and so the optimum local power quality can be ensured. (4) The operation of generators employed in conventional power utilities depend mainly on electromechanical interaction, between the stator and rotor circuits of those generators, whereas most DERs depend mainly on power electronic interfaces, to synthesize their productions and ensure stable level of power exchange.

The operation of a microgrid in different modes is controlled through a local controller of each microsource and a central controller for the whole microgrid. The main function of the local microsource controller is to independently control the power flow and load voltage profile of the microsource in response to any disturbance and load change, without any communication with the central controller, whereas the main function of the central controller is to perform protection coordination and provides the power dispatch and voltage set points for all the controllers of the microsources [11].

1.3 Impacts of Microgrids

Microgrids have remarkable impacts on existing electricity and gas markets. In order to harness their impacts, their market participation must be encouraged. Suitable market reforms must be made to allow such participation and financial incentives must be provided for owners to invest in microgrids. Major changes in conventional electricity markets have already been initiated in some countries. Once market participation is assured, there is a vast opportunity for microgrids to supply quality service to the main utility distribution system. Microgrids can naturally provide significant ancillary services to the utility. The impacts of microgrid can be summarized in the following items:

- Heat Utilisation: By installing CHP microsources near to customer premises, then CHP can operate at very high energy efficiencies and the generated heat can be effectively used to supply local heat loads [5];

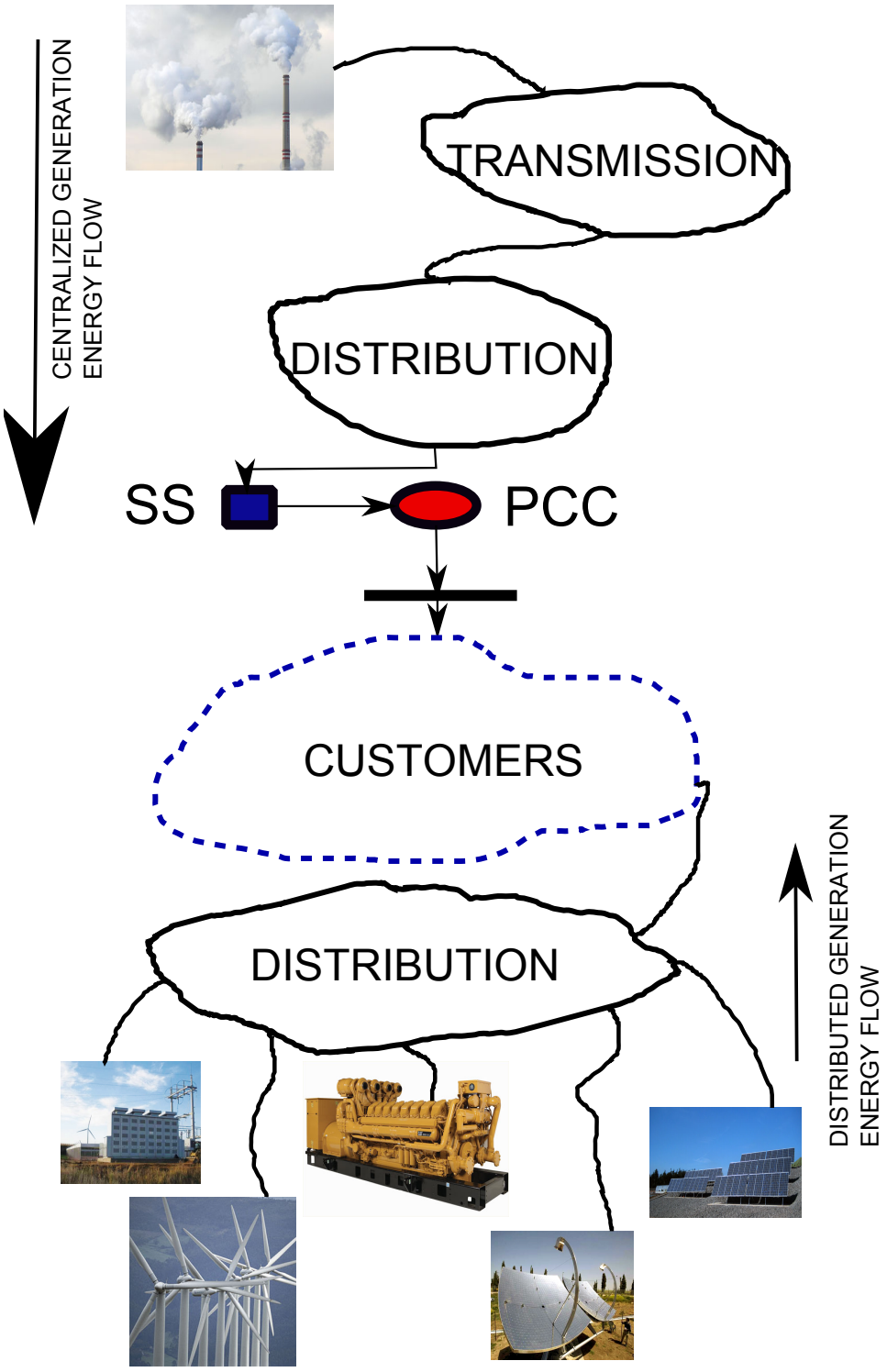

Figure 1.1: Centralized vs distributed generation

- Power Quality: Microgrids can be employed to control the power quality locally according to customers requirements even on an hourly basis. It is quite difficult for a utility grid to be attentive to special power

quality needs of a particular customer. The conventional utility grid normally provides a uniform level of quality and service to all customers, within a given area and does not easily differentiate among their needs. Microgrid power quality services can be accounted in some items, such as reactive power and voltage control, supply of reserves, regulation and load following [12];

- Optimizing Utility Expansion: Microgrids normally reduce system expansion costs of the main power utility, by limiting the utility transmission capacity expansion and offering the best utilization of current transmission capacity, and consequently the customers benefit well from this impact, as this cost is realized from the tariff imposed on them. Without this benefit, the customers have to pay heavily for power supply due to interregional transmission congestion;

- Environmental Impact: Low-carbon microsources can effectively reduce emissions and environmental warming. This is one of the major criteria to support the microgrid operation, as the central controller of a microgrid is capable to be programmed for operational decisions based on the lowest net emission production [4];

- Black Start Capability: The black start is defined as the capability of a power system to restart its generation after a total system collapse, without importing any external power to restore at least portion of the power system to service again after the collapse. The microgrid black start involves a sequence of control actions, defined through a set of rules and conditions to be checked during the restoration stage. These rules are identified in advance and embedded in the software of any microgrid central controller.

For the best utilization of microgrid benefits, a microgrid may be employed by one of two modes. Firstly, the isolated mode, where the microgrid is fully isolated from the power utility grid. Secondly, the grid-connected mode, where the microgrid is connected to the power utility grid.
The operational modes of a microgrid are more detailed hereunder:

1. Stand-Alone: The microgrid may be isolated due to faults, maintenance purposes or as predetermined control sequence. In the stand-alone mode,

there is no connection to the host grid. Thus, the DERs control is responsible for frequency regulation. In addition, a voltage regulation strategy is required to maintain the network voltage. Moreover, the DERs control is also responsible for managing the real and reactive power contribution of DERs, such that load power is shared among different DERs in the microgrid;

2. Grid-Connected: In the grid-connected mode, the magnitude and frequency of the system terminal voltages are imposed by the utility grid. Thus, the control task can be summarized as the regulation of the real and reactive power is undertaken through the exchange among the DERs and the host network.

From the previous mentioned microgrid modes, it is clear that the power electronic interface of each microsource plays the main role to synchronize the microgrid sources in the both operational modes. In addition, the presence of DGs introduce an additional supplying nodes and change the power flow in microgrids. The presence of DGs directly affect voltage profiles along feeders by changing the direction and the magnitude of real and reactive power flows. The directional characteristics of voltage regulation circuitry must also be considered. Up to now, it is evident that the main difference between the conventional centralized grid and the microgrid emerges from two points:

- Power flow analysis;
- Power exhange control concept, in order to exchange real-reactive power and to synchronize different microsources.

Therefore, it is required to illustrate the classical distribution power flow models; on the other hand, some solving techniques related to microgrid power flow models. Furthermore, the control concepts of microsources which depend mainly on power electronic interfaces.

1.4 Power Flow in Microgrids

The first requirement for planning, operation, control, protection and management of microgrids is the availability of accurate power-flow analysis results. The conventional power-flow analysis based on the system positive-sequence

representation, which is widely used for large power transmission systems is not directly applicable to microgrids, for some reasons can be termed in the following points: (1) The presence of unbalanced three-phase loads, single and two-phase loads. (2) The presence of microsources with electronically coupled interfaces, which are managed by various control strategies. (3) The presence of different types of three-phase rotating machines related to microsources, with various control strategies. (4) The presence of non-dispatchable microsources, as wind turbines and photovoltaic generators.

The power flow software tools, which have been developed for large-system are not tailored for the microgrid analyses, because they lack the flexibility to accommodate DER models and operating characteristics, particularly those of electronically-coupled DER units. In addition, another limitation is imposed on the steady-state modelling of electronically-coupled microsources, as the available models assume only positive-sequence microsources representation for power-flow analysis.

Some authors have developed new updates to power flow theories, in order to accommodate new features of the microgrid concept which can consider the full sequence modelling of power electronic interfaces.

In [13] Arturo proposed an object-oriented power flow analysis, to include different DGs models; numerical applications were presented to evidence the features of the algorithm and the flexibility of the software tool, to overcome the drawbacks of the classical Newton-Raphson algorithm for power flow analysis.

In [14] Hassan proposed a two-step power flow analysis approach that can represent electronically coupled DG units accurately, which is capable to solve for the internal variables of each DG unit in a non-iterative fashion based on the presented closed-form DER models.

In [15] Zakaria provided a three-phase power-flow algorithm in the sequence-component frame for a microgrid, which can accommodate single-phase laterals, unbalanced loads and three/four-wire distribution lines. The author considered the steady state sequence component frame models of DGs for the developed power flow approach, under balanced/unbalanced conditions.

In [16] Zhang showed a capable algorithm, to cope with the disadvantages of classical power flow models, which do not account for the unbalances. The author introduced a decomposition model based on the sequence components

frame. The three-phase unbalanced power flow was decomposed into three separate subproblems with weak mutuality. The subproblem corresponding to the positive sequence component was solved by using a Newton-Raphson iterative scheme, while the other two subproblems were formulated into two sets of linear simultaneous equations.

The proposed model of the microgrid power flow in this thesis accounts for dissimilarities between single and three phase loads, also considers the full dynamic modelling of loads, non-dispatchable generators. The proposed power flow is based on decomposing the electrical phasor quantities into direct-quadrature components. All loads and generators are referred to one master source of generation. This master is the infinite bus, in case of the grid connected mode, while the master is considered to be a certain microsource, in the microgrid isolated mode. The full details of the microgrid dynamic model are shown in Chapter 4.

After setting the microgrid power flow model, which is proved as totally different from the power flow models of centralized utility grids, it is necessary to move to another important point that is the control concept of real-reactive power exchange among microsources or between microsources and utility grids. For this sake, a special attention must be paid to the microsource electronic interface algorithm to handle the power exchange in the microgrid.

1.5 The Interface Control of Microgrids

When a microgrid is connected to a utility grid, then the utility grid is the only responsible for determining the dynamics of the system through the direct interface of synchronous generators. In contrast, during the isolated microgrid mode, the power electronic interfaces and their sequences of control are the only responsible for determining the dynamics of the microgrid, by controlling the power production and synchronizing DGs with the microgrid.

1.5.1 Power Electronic Interface

The power electronic interface has some characteristics can be termed in the following points: (1) The electronic interface contains the necessary circuitry to convert power from one form to another one. This may include both a rec-

tifier and an inverter or just an inverter. (2) The power electronic interface is compatible in voltage and frequency with the electric power system to which it will be connected to and contain the necessary output filters.

Typically, the electronic interfaces are comprised of four basic components, such as semiconductor switches, control system for switch gating, inductive components and capacitive components. The inductive and capacitive components are used to dynamically store energy for circuit power flow dampening, filtering and transformation. By using electronic interfaces, the power quality of DGs improves through the ability to control harmonic contents of the output voltage and current; moreover, to provide fast operation to switch modes between utility connected and stand-alone modes.

The electronic interfaces are self-commutated and can produce an AC-voltage of arbitrary amplitude and phase; therefore, this allows the DGs to produce any power amount at any power factor. The electronic interfaces have a wider operating power factor range than synchronous generators. This can be an extremely useful, if the DGs are allowed to regulate voltage and/or supply reactive power to the system, whereas the voltage regulation in conventional power systems is normally maintained using active-reactive power capability of synchronous generators, load-tap-changing transformers at substations and line-voltage regulators.

Usually, microgrids combine capabilities of several DGs technologies and can be extremely beneficial when integrating different types of DGs together; as an example, energy storage is often integrated with photovoltaic generators or wind systems, to provide power when there is no solar or wind resource available. Typically, there is a DC bus within the electronic interface that can be used to integrate a variety of DGs technologies at a common point. The use of a common DC bus can also allow the integration of several DGs technologies inverters. The employed control strategies of microgrid power inverters can be divided into two different strategies:

1. *PQ-mode*: The inverter only injects the power available at its input into the grid. Usually, this mode is applicable to non-dispatchable generators employed to track the maximum power point of sustainable sources.

2. *Vf-mode*: The inverter is controlled to feed the grid with reference values of voltage and frequency, according to a specific control strategy that is

similar to the behaviour of a synchronous machine.

Usually, distributed generators are interfaced to a microgrid by electronic inverters, unlike synchronous generators, where their inertias contribute directly to conventional power utility, and so their responses contribute to the system stability. In the microgrid case, the employed PQ-mode distributed generators are usually interfaced to the microgrid by inverters and their inertias are far from contributing to power system dynamics, in order to track the maximum available power from the sustainable sources. However, there is a trend to treat this problem of non-dispatchable generators, which operate through the PQ-mode as wind turbines, by *deloading* their capacities. Thus, some kinetic energy can be stored in the rotating parts, as the drive train part of the wind turbine, in order to be used during voltage and frequency dips. Consequently, this stored energy can contribute to improving the grid stability, by restoring reference values of the voltage and frequency of the grid.

Some authors have discussed this important point. In [17] Morren proposed a control strategy for wind turbines, to turn them more sensitive to power system frequency dip, by means of an additional controller that adapts the torque set point as a function of the grid frequency deviation. The emulated inertia is proportional to the controller constant, and this loop is activated when the grid frequency exceeds certain frequency deviation limits. In [18] Rogério adopted another control strategy of a wind generator to supply the primary frequency regulation by a mechanical strategy, which utilized the pitch control, by adjusting the rotor speed and active power according to the deloaded optimum power extraction curve. In [19] Anaya showed a controller which can dynamically manipulate the position of a wind turbine rotor, to slow down the wind generator, allowing for a temporary power surge in case of a frequency dip.

However, The option of deloading the operating point of a wind turbine is *temporary* option, as it can be employed for the moment of frequency dip only. Otherwise, the wind turbine will suffer from stalling as it loses all its kinetic energy. The main strategy which must be adopted to control the dispatchable generators and even non-dispatchable generators interfaced by electronic inverters is called *droop control*. The droop control strategy can enforce all distributed generators to participate in a system restoration in case of disturbances, and also to enhance real-reactive power exchange in a microgrid.

1.5.2 Droop Control in Microgrids

Microgrid distributed generators can be assigned to regulate the voltage and frequency at the point of common coupling. Usually, there are multiple DGs operating in parallel and feeding the microgrid, and so DGs must participate in the grid stabilization and voltage regulation. The frequency-droop and voltage-droop control strategies are used to manage the real-reactive power share in a microgrid among various generation sources.
In case of a frequency or voltage deviation from nominal values, then frequency-droop $P-\omega$ and voltage-droop $v-Q$ must be activated. This is achieved by dynamically changing the power sharing levels to set the frequency and voltage at new values.

Some authors discussed this important point. In [20] Lopes showed the feasibility of the droop control strategy for an isolated microgrid, by assigning the microgrid operation to single/multi master operations.

In [21] Milan proposed wave form quality control, in terms of harmonics of an isolated microgrid loaded by unbalanced and non-linear loads. This duty is shared equally among different DGs. The proposed control separates the tasks in the frequency domain, as power sharing and voltage regulation are controlled by the droop strategy.

In [22] Moreira showed the capability of electronic interfaces to perform a black start, by sequence of actions as the interfaces are controlled by the droop strategy.

In [23] Barklund introduced an energy management strategy for a droop-controlled isolated microgrid, which successfully implements optimal generation dispatch levels by selecting the droop constants from a region where a stable operation of the microgrid can be guaranteed.

In [24] Seon proposed power exchange among different DGs by droop regulation based on feeder flow control.

The proposed control among DGs in this thesis is based on the droop strategy without any need of communication among DGs. Therefore, connecting/disconnecting any DG from/to the microgrid without changing the control algorithm is possible; moreover, the droop control is handled by *Fischer-Burmeister* algorithm, which reduces the complexity of problem solving, by formulating the problem as a complementarity problem, through substituting the

piecewise-defined droop function by an only scalar function that makes computations of operating points of microgrids to be solved by means of Newton-Raphson-like methods. The algorithm is detailed in Chapter 3.

At this point, the main operational concepts of microgrids were illustrated and the differences between microgrids and conventional grids were detailed. However, the full scope of integrating non-dispatchable generators as wind turbines in microgrids is not clear so far. One of the benefits in a microgrid strategy is to fully benefit from sustainable sources, as a trial to reduce carbon and toxic emissions. Some vital terms as generation capacity, economic performance and stability of such non-dispatachable generators must be taken into consideration. Next Section will explain the challenges faced by microgrids, when being supplied by non-dispatchable generators.

1.5.3 Microgrids Supplied by Non-Dispatchable Generators

Introduction of generation based on renewable sources becomes an important topic at present; however, these renewable resources are usually given by very fluctuating and uncontrollable stochastic parameters. These fluctuations can lead to severe problems, such as system frequency oscillations and/or violations of power lines capability. The generation patterns resulting from these renewable sources may have some similarities with the electricity demand patterns, but they usually record deviations from the demand patterns. Consequently, a supplemental production is required to keep the demand and supply in balance.

In [22] Moreira showed that during the black start, the connection of uncontrollable generators, as photovoltaic and wind generators must be during the last step of the black start in order to smooth voltage and frequency variations, due to power fluctuations of the uncontrollable generators.

In [25] Emanuel showed a critical case may occur, as a load demand may be lower than the available power from photovoltaic solar arrays, and subsequently the battery bank can be overcharged with unrecoverable damage consequences. Therefore, he proposed a control algorithm for efficient battery charging based on the microgrid line frequency.

Albert in [26] proposed a methodology to improve the reliability of non-

dispatchable generators based on predicting consumers demands for a day ahead, then processing an objective function to enhance the power quality for all consumers.

In [27] Marcelo highlighted the possibility of overcoming wind fluctuation by a superconducting magnetic energy storage system, which can share the demand supply of a microgrid with wind generators; the results show a capability to meet the demand peaks without any shortfall.

In [28] Changhee proved that synchronization in an isolated microgrid is disturbed by wind turbines fluctuations.

Alba in [29] proposed a method for tracking the deviations between wind fluctuations and load demands. Thus, a set of batteries were installed to backup such deviations of real-reactive power through electronic interfaces with a microgrid.

Obviously, the major difference of generation between the wind power and conventional power is related to the intermittent nature of the wind. The effectiveness of the wind power control is highly dependent upon the available generation margin, which is decided from the available wind speed. In order to have an accurate margin assessment in hand, an accurate capacity factor analysis of wind energy based on efficient wind speed sampling can play a key role.

As mentioned from the last Section, the first objective of this thesis is to provide an insight about site matching suitability of droop-regulated microgrids supplied by wind generators. For this reason, capacity factor analyses of droop-regulated microgrids are carried out in Chapter 2, based on a reliable wind speed sampling strategy, by reducing the variance of wind speed samples, and also including the correlations among wind speeds. Thus, each wind energy source status can be determined accurately.

Most researches related to wind power have used *Monte Carlo* for wind speed sampling, taking into consideration that Monte Carlo technique accumulates the samples in certain areas of the wind speed probability domain. Moreover, this technique is time consuming; thus, a more advanced technique is employed in Chapter 2, which is Latin Hypercube, for accurate wind speed sampling. This technique is capable to spread wind speed samples equally overall the wind speed probability domain. Consequently, a better determination of wind power can be ensured.

Usually, the increase of wind energy penetration requires also attention to reserve requirements. For isolated microgrids, sources of reserve are always required, to share microgrids supply with intermittent energy sources, as generation must always be as close as possible to system loads. The problem of keeping the power balance is still more difficult for stand-alone microgrids, supplied by intermittent generators. The characteristics of such grids require scheduling more reserve for ensuring adequate security and reliability levels, but high reserve requirements may substantially deteriorate the economy of these supply systems.

Figure 1.2 shows a sample of two interconnected areas. The tie line power flow between both areas P_{tie} is managed by the automatic generation control (AGC) of each area. In conventional power grids, the function of AGCs is to control power flow among interconnected areas. In conventional power grids, the control parameters of AGCs are updated according to annual load demand changes. Thus, uncertainties of providing reserve are efficiently reduced. Although, conventional generation suffers from the volatility of conventional energy prices, their variability is still much lower than uncertainty of the wind power.

In contrast, in the case of microgrids supplied by intermittent generators, some urgent questions emerge, regarding the optimum economical sizing of microgrids. Moreover, the debate about the capacity needed from intermittent generators to contribute to supplying microgrids with constraints of power quality is pivotal. For this sake, the purpose of Chapter 3 is to provide a study based on optimizing both energy production and economic performance for isolated microgrids, supplied by wind energy and batteries. Hence, the maximum possible energy production at the lowest energy cost can be clarified.

However, the objective of optimizing the energy production and economic feasibility for microgrids must be extended to include additional constraints related to the operation of microgrids, as the objective is to enhance the minimum generation cost with stable power flow limits in the islolated mode or interconnected mode of microgrids.

For the microgrid interconnected mode and during a stable operation in each area, it is assumed that summation of the total power generation, load demand and net tie-line interchange power is nearly zero. During an unstable operation, the tie-line interchange power is assumed to flow from high capac-

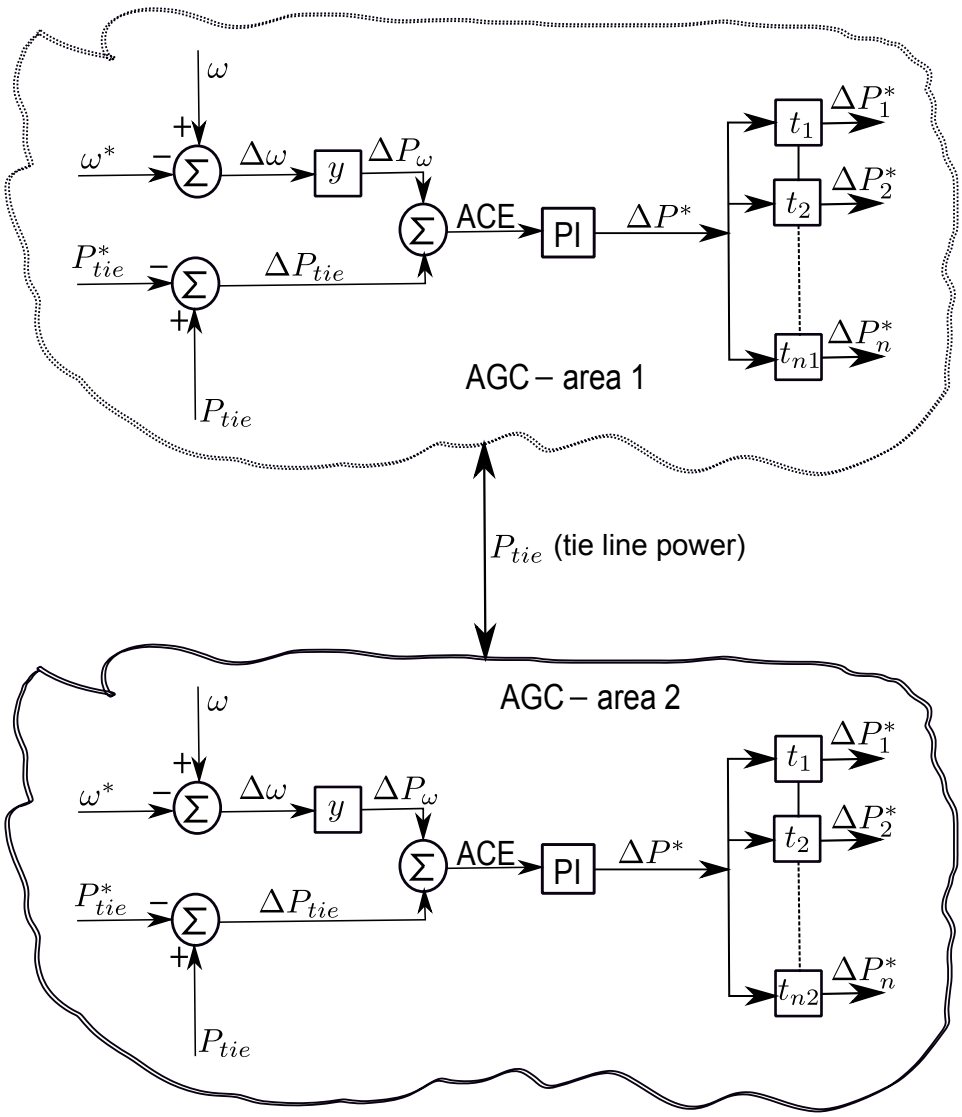

Figure 1.2: Interconnected systems power exchange

ity areas to low capacity areas. When the tie-line capacity is small and power imbalance among different areas is large, then large oscillations in the tie-line power will occur and the possibility of resynchronization among different generation units will be small. Thus, some generation units will be disconnected from the operation. On the other hand, in the isolated microgrid mode, the large penetration of DG units in distribution networks may not only lead to problems under faulty conditions, but also to instability under small disturbances, such as small changes in loads and power transfers that occur during the normal power system operation.

Figure 1.3 shows the mechanical analogue of a disturbed multi-machine

system, based on Elgerd (1982). The disturbance near to one of the power stations distorts the power balance at the neighbouring stations. The resulting electromechanical swings in the power system can be compared with the way that masses swing in a mechanical system.

For conventional generation systems, some standards and recovery methods from power imbalances have been set and handled from decades. These standards can be briefed in the following terms: (1) Power system stabilizers in rotor circuits. (2) Fast valving for steam turbines. (3) Braking resistors for hydro turbines. (4) Defence plan strategy to handle the operation of turbines and feeding pumps. (5) Recovery plan by series-shunt compensators.

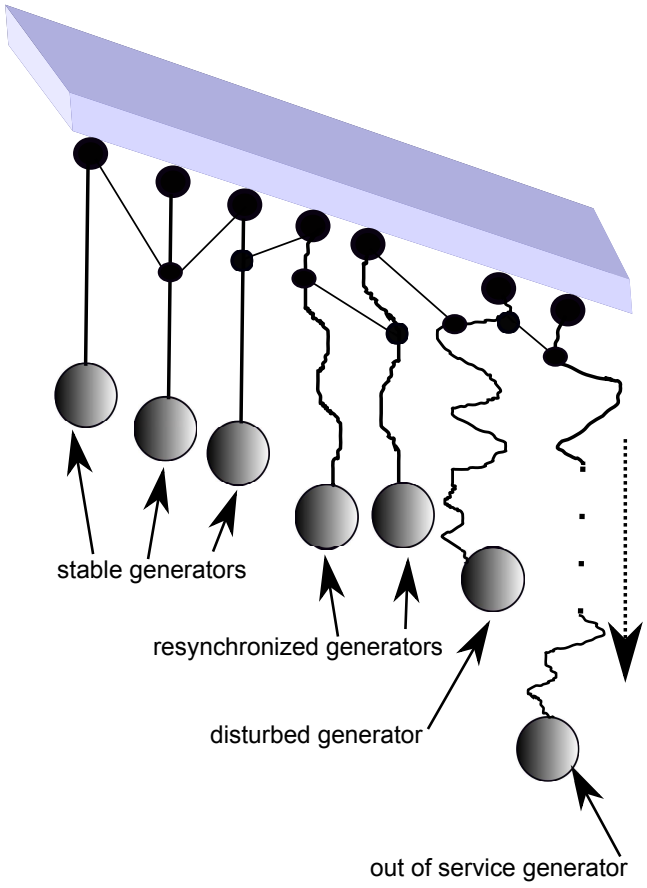

Figure 1.3: Mechanical analogue of swings in a multi-machine system

In order to clear the necessity of stability analysis of microgrids, Zhixin [30] conducted a small signal stability analysis of an isolated microgrid, supplied by a synchronous generator and distributed generators interfaced by electronic inverters. The analysis proved that the dominant variables which could violate

the system stability of the both synchronous generators and distributed generators interfaced by inverters are different. These result showed a necessity for stability analysis of microgrids, because the generation sources in the case of microgrids are non-conventional and their modellings are totally far from synchronous generators. Stability analysis is required to identify the impacts of microgrid controllers, system characteristics and the intermittent behaviour of wind generation units on the stability of the whole network.

For this important matter, some recent articles have discussed the small signal stability of power systems supplied by wind energy. In [31] Ostadi proved that stability in a grid supplied by wind turbines and a grid utility varies under different levels of wind penetration.

In [32] Yateendra showed that the stability of a network supplied by wind turbines and a utility grid varies under different wind speeds, and proposed a damping controller for the dominant variables.

In [33] and [34], both Lihui and Yang respectively proved that the stability of a power system varies under different wind speeds, and determined the dominant variables.

For the previous considerations, the small signal stability analysis are conducted in Chapter 4, for isolated microgrids, supplied by doubly-fed induction generators and also generation sources interfaced via inverters, under different scenarios, such as different levels of wind penetration, power demand increment and different levels of real-reactive power exchange by droop manipulation.

The three topics of this thesis, which were discussed briefly in this Section will be more detailed through the following Sections. The first topic belongs to capacity factor analysis of droop-regulated microgrids based on a reliable wind speed sampling strategy will be introduced in Section 1.6. The second topic belongs to optimizing both energy production and economic performance of isolated microgrids supplied by wind energy and different energy storage systems will be shown in Section 1.7. The third topic belongs to small signal stability analysis will be shown in Section 1.8. Finally, the thesis contributions will be detailed in Sections 1.9.

1.6 Capacity Factor Analysis of Droop-Regulated Microgrids

Conventional generation units are capable of generating rated power during normal operation. Reliability evaluation techniques for these units are well established and are routinely used in the capacity planning of electric power utilities. Contradictory to Conventional generation units, the wind energy sources are always dependent on climate stochastic parameters, and so wind energy sources are hourly and seasonal fluctuating. Thus, capacity determination of power systems including wind energy conversion systems (WECs), which can share supply microgrids with other distributed generators is relatively complex.

Through last decades, power networks in Europe and North America involved in several blackouts; however, in each case the blackout was caused by a specific technical problem. The unprecedented concentration of blackouts has driven many observers to argue that there are underlying reasons for such large number of disturbances. The increased liberalization of electricity supply industry by the beginning of 1990 has resulted in a significant increase of inter-area problems. Those problems have been compounded by the penetration of wind energy. Large changes of wind power due to changing weather patterns mean that the actual network flow may be quite different from the predicted one.

With the increase of wind energy penetration in power networks, it becomes important matter to conduct accurate capacity factor analysis of wind energy. The reason for the interest in capacity factor analysis of a wind generator is that the analysis provides a smart, summarized indication about the combined interaction between the generator and the site that is between wind power curve and stochastic wind speed. Subsequently, the accurate wind energy capacity determination reduce the need for balancing energy and reserve power, which are needed to integrate wind power into the balancing of supply and demand in electricity supply systems. Thus, power plant scheduling optimization can be ensured. In addition, the grid operator needs to know the current and future wind power feed-in at each grid connection point. This leads to lower integration costs for wind power, lower emissions from conventional power plants used for balancing, and subsequently to a higher value of

wind power.

The capacity factor is widely studied in Chapter 2, for autonomous droop-regulated microgrids, supplied by distributed wind generators. The main concern about capacity factor analysis in such grids is that the proposal of considering the droop-regulated microgrid as a large generator that is built up from several wind generation units, cannot be solved as a simple sum of individual rated and average power of wind generation units. This fact can be explained as the micogrid load is shared among the intervening generators by means of the droop control, and so particular restrictions on the maximum loadability of the microgrid may occur that make it possible for the maximum delivered power to be less than the sum of power injections. However, before conducting the capacity factor analysis of the proposed droop-regulated microgrids, an accurate wind speed sampling strategy is needed to appropriately determine the status of wind generators.

Figure 1.4a shows the wind time series during a day by different averaging times in Germany, Ernst (five minute and an hour) sampled wind time series. It is observed that wind is more fluctuating when the wind speed samples are taken every five minutes. The average value of the one hour sampled wind series was 3.6 m/s, whereas the average value of the five minutes sampled wind series was 4.4 m/s. Thus, this figure explains well that the five minutes sampled wind series are spread over a wider area of wind speed values.

Figure 1.4b shows the relation of correlation coefficients between different wind farm turbines and the distance separating these turbines. Normally, the wind is driven by weather fronts and a daily pattern caused by the sun; depending on these dominants, there is a significant diurnal pattern in the wind production.

According to [35], the wind speed correlations among wind turbines based on distances separating them can be modelled by an exponential fitting with a decay parameter ranges from 500 to 700. Regardless the issue of correlations, it is clear that the variations smooth out faster when the time scale is small. The conclusion of this figure coincides with the conclusion of Figure 1.4a that the wind speed series of the same wind distribution parameters, but at different sampling periods are spread over different values. Both figures indicate the impossibility that the wind speed sampling can concentrate on a specific range of the wind speed probability domain.

Most researchers have used the conventional sampling technique *Monte Carlo Sampling* (MCS) to estimate wind speed samples. Typically, MCS has some engrained weak points, such as disappearance of stratifications through the whole range of the event probability domain, and so the sampling process can not cover all wind speed probabilities. Moreover, MCS is characterized by an intensive computationally nature. These weak points of MCS applied for wind power sampling typically lead to a degree of risk analysis and give the superiority always to conventional generation units, and subsequently a less dependency on wind generators.

For this reason, the wind speed sampling process based on LHS is adopted in Chapter 2, in order to provide more accurate and reliable wind speed sampling. Thereafter, the status of wind generators can be determined accurately. The proposed LHS sampling technique can stratify equally all wind speed samples overall the wind speed probability domain. In Chapter 2, some comparitive simulations are conducted to clear the superiority of the LHS over the conventional MCS.

The reliability of wind generators does not depend only on efficient determination of wind speed samples, but also on a wind speed correlation which must be considered among different wind farm turbines. Clearly, wind speed does not maintain a specified stable level, and so multi-state model must be used to estimate a reliable wind energy system.

In [36] Dimitrios used a neural network training to produce correlated wind speed samples for a wind farm.

In [37] Wijarn employed an autoregressive moving average (ARMA) time series model, which considers the time lagging effect among different wind turbines.

In [38] Gao used a genetic algorithm method to adjust the ARMA models and simulate hourly wind speed samples based on the degree of wind speed correlations among wind sites.

A simple method is adopted in Chapter 2 to introduce correlations among different wind turbines based on Cholesky decomposition technique. The method has the following desired properties: (1) It can be applied to all types of input distribution functions. (2) The simplicity, as there is no need for complex mathematical computations. (3) The marginal distribution of wind speed samples remain intact.

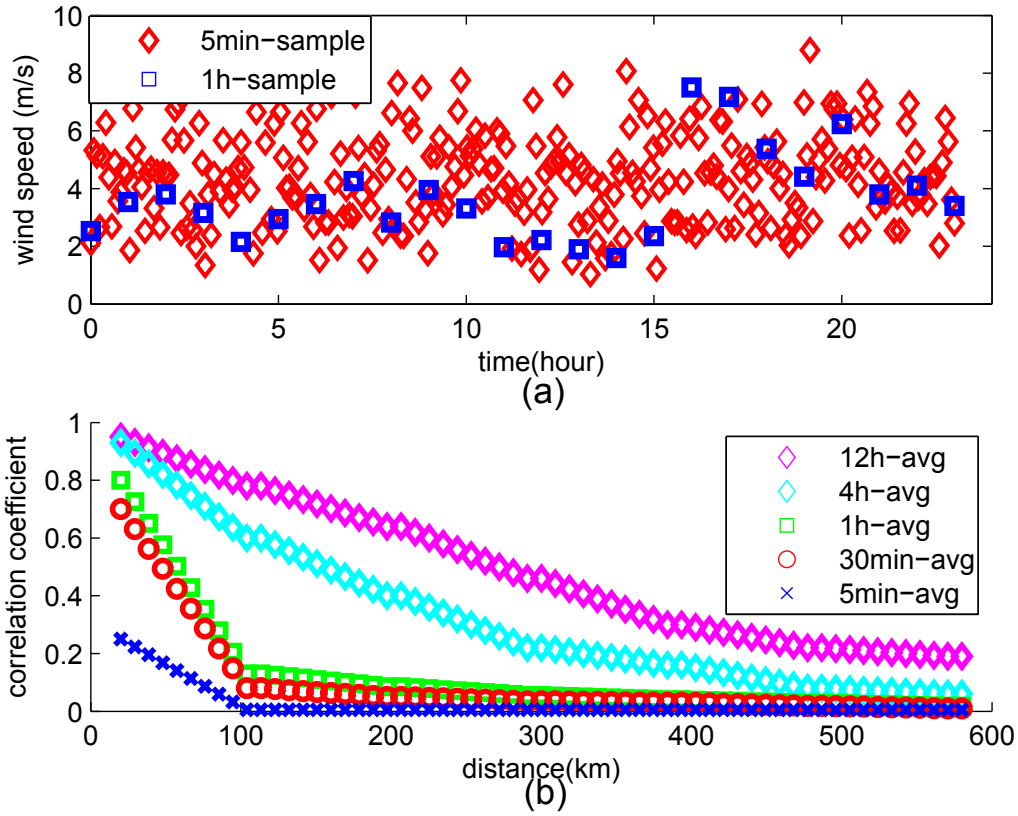

Figure 1.4: An example of wind measurements at different sampling rates in Germany, Ernst: (a) Wind speed. (b) Correlation coefficients vs distance.

After introducing a reliable wind speed sampling technique and introducing a correlation among different wind turbines, several simulations are processed in Chapter 2 by an optimized load flow, under different mean wind speeds and different wind turbines, in order to determine the maximum loadability of microgrids supplied by wind turbines. The maximum loadability provides an insight about the capacity factor of droop-regulated microgrids. Consequently, the capacity factor analysis can be used to evaluate the site-matching suitability of a combination of wind generators and wind speeds.

Unlike conventional generation units, where the capacity and reserve of each conventional generator is known in advance, the capacity and reserve of a microgrid supplied by wind turbines are vital issues, as it affects both the stability and economic performance of the whole microgird. In Chapter 3,

the idea of site matching suitability for droop-regulated microgrids supplied by wind generators and different energy storage systems is more detailed, by considering analysis of energy production and economic performance.

1.7 Benefit Evaluation of Microgrids Using Capacity Factor and Economic Analysis

Power system operators are always responsible for maintaining the system reliability, as generation must always be as close as possible to the system load, to ensure the system frequency is maintained at the nominal values. When generation levels can be easily determined, then achieving this responsibility is easy. However, in the case of intermittent generators integration as wind energy, additional capacity is needed to meet actual load demands. The characteristics of such grids require scheduling more reserve for ensuring adequate security and reliability levels, but high reserve requirements may substantially deteriorate the economy of these supply systems.

With the market liberalization and occurrence of competitive markets, vital questions are always conducted regarding the optimum economical sizing of microgrids. Moreover, the debate about the capacity needed from intermittent generators to contribute to supplying microgrids, considering power quality constraints is pivotal. For this sake, technical and economic analyses are necessary, in order to meet the requirements in competitive markets.

In general, the most efficient wind turbine might not be the most effective for transforming wind power in electric power on a specific site, and so the main goal is to maximize the wind annual energy production [39]. The energy production from a wind turbine depends on several factors, such as wind speed conditions from the area and the characteristics of the wind turbine itself, including the cut-in, rated and cut-off wind speed parameters.

The selection of the optimal wind turbine has been discussed in some papers based on maximization of the capacity factor [40]. In addition, other studies have been conducted regarding site matching of wind turbines. The site matching is based on identifying optimum turbine parameters, to yield higher energy production at higher capacity factor.

The matching of a wind turbine to a site using normalized power and

capacity factor curves was discussed in [40], but in general the economic considerations of the turbine are not provided through wind site matching studies.

Other studies have focused on the matching of wind turbines to wind farms from the viewpoint of both performance and economic considerations, as in [41] and [42]. In [43], [44] and [45] Sureshkumar, Razak and Srivastava respectively presented economic analyses of microgrids by HOMER Energy software.

Usually, HOMER Energy software analyses the economic feasibility of hybrid energy systems, but it does not take into consideration the droop regulation of microgrid interfaces, and also does not account for the reserve issue, because it is based on historical data only. Therefore, the HOMER Energy software cannot be reliable to determine the definite optimum model from the viewpoint of both performance and economic considerations.

However, for isolated microgrids, storage systems are always required, to share microgrids supply with the intermittent wind energy, as generation must always be as close as possible to system loads. The problem of keeping the power balance is still more difficult for stand-alone microgrids supplied by intermittent generators. The total requirements for these storage systems are unclear at present, because most of the recent studies which have optimized the capacity factor and economics of wind energy production, have not taken into consideration the operation of storage systems, which share supply with wind energy. Thus, the optimum point of operation is totally different, when considering the dynamics of storage systems. The performance and economic aspects of such storage systems are significant and must be brought into the economic evaluations.

Therefore, the proposed study in Chapter 3 is based on optimizing both energy production and economic performance for isolated microgrids, supplied by wind energy and various batteries via a multi-objective function. The optimization function is conducted to minimize the cost of energy, which is a function of both capital costs and energy production. Hence, the maximum possible energy production at the lowest cost of energy can be ensured, taking into consideration the droop regulation of microgrid interfaces and dynamic operation of batteries (charging-discharging). In addition, the economic analyses are conducted also by simple payback and net present value.

However, the objective of optimizing the energy production and economic feasibility for microgrids must be extended to satisfy the power balance and

generation limit among different microgrid generators; a stable operation must be ensured without power swings and resynchronization problems. Small signal stability analysis is conducted in Chapter 4, and the purpose of the analysis will be more detailed in the following Section.

1.8 Microgrids Stability Analysis

As mentioned in the last Section, the objective of optimizing the energy production and economic feasibility must be extended to include additional constraints related to the operation of microgrids, such as flow limit between two successive areas and stability constraints of each DG supplying microgrids, because all these constraints may cause perturbations, and subsequently instability. Such perturbations in microgrids affect important operating variables, such as frequency and voltage. Therefore, different microgrid perturbations must be well studied, to avoid power network collapses.

The proposed microgrid in Chapter 4 is supplied by DGs interfaced through electronic inverters and intermittent sources which are doubly-fed induction generators (DFIGs). A large penetration of DG units interfaced by electronic inverters in distribution networks may not only lead to problems under faulty conditions, but also to instability under small disturbances, such as small changes in loads and power transfers, which occur during normal power system operation. Moreover, the modelling of DFIGs are totally far from synchronous generators. Consequently, analyses and design frameworks of microgrid supplied by intermittent sources are required to ensure stable performance and robustness. Analyses are required to identify the impacts of microgrid controllers, system characteristics and the behaviour of intermittent wind generation units on the stability of the whole system.

The most common perturbations in power networks can be analysed by the small signal stability study. Small signal stability is the ability of a power system to maintain stability, when it is subjected to small disturbances. A disturbance is considered to be small, if the linearized system around the equilibrium point still adequately represents dynamics of the original nonlinear system under this disturbance [2].

The small signal stability analyses of conventional power systems have been studied in many works. In [46] and [47], Wang and Evandro studied the small

signal stability of conventional power systems, with respect to system parameters changes.

The production of electricity in a conventional utility is secured primarily using synchronous generators, and for this reason, it is important to secure their synchronism and parallel operation. Thus, the question of stability in a conventional power system is mainly based on the stability of synchronous machinery and on the relationship between the active power and rotor angle of the generator. In contrast to conventional power systems, the proposed microgrids in this thesis are supplied by electronic interfaces operating by high frequencies and intermittent energy sources which are DFIGs. Therefore, the stability analysis in such microgrids must include all these elements.

Microgrid small signal stability analyses have been conducted in some recent papers. In [33] and [34], both Lihui and Yang respectively presented stability analyses of microgrids supplied by wind energy, in grid-connected modes.

In [48] Pogaku conducted a stability analysis in an isolated microgrid supplied by distributed generators, and interfaced to the microgrid through electronic inverters.

All the previous microgrid stability studies belong to either microgrid supplied by wind generators and connected to utility grids, or to isolated microgrids supplied by distributed generators interfaced by electronic inverters and without penetration of any intermittent energy sources.

When a microgrid is connected to the main utility, the possibility of system restoration and reduction of power swings among different generation units is high. In the case of grid-connected mode, the utility grid can provide an adequate reserve, in the case of demand shortfall. Unfortunately, the situation is different in the case of isolated microgrid, as the available reserve and capabilities of the whole system to recover from disturbances are limited, especially when the microgrid is supplied by intermittent sources. Hence, in Chapter 4, the small signal stability analysis of isolated microgrids, supplied by DFIGs and also DGs interfaced through inverters are conducted, under different scenarios, such as different levels of wind penetration, power demand increment and different levels of real-reactive power exchange by droop manipulations.

Thus, in future work, the controllers of DFIGs and inverter-interfaced distributed generators can be set appropriately, and an adequate control strategy

can be developed to keep the microgrids stable.

1.9 Thesis Contributions

The Chapter mentioned several doubts and weak points of isolated microgrids, supplied by intermittent energy sources. These weak points are accounted by the following terms: (1) The uncertainties of the generation capacity for microgrids, supplied by intermittent energy sources. (2) The full insight regarding the economic and technical feasibility evaluation for microgrids are unclear at present. (3) Usually, microgrids are supplied by DGs via electronic interfaces, or through renewable energy sources; thus, the modelling and the behaviour of such DGs are totally far from conventional generation units. Therefore, stability analysis of microgrids supplied by such DGs is required to ensure stable performance and robustness.

For the all mentioned doubts, the thesis analyses and proposes solutions for these problems regarding capacity factor analysis of droop-regulated microgrids, optimizing both energy production and economic performance for isolated microgrids and finally small signal stability analysis.

Thesis contributions are summarized in the following points, also some comparisons between thesis contributions and other recent researches are shown hereunder:

- Concerning a reliable wind speed sampling method to determine the penetration and capacity of intermittent wind energy, in [49] Andréa proposed a model for a probabilistic representation of a wind farm to provide an annual estimation of energy production. This model included all operational information of wind turbines, as failure and repair rates regarding wind farm. The model was sampled by Monte Carlo Markov chain.

  In [50] Roy explained reliability effects of wind energy penetration on a composite generation and a transmission system, using the state sampling Monte Carlo simulation technique.
  Vallée in [51] showed some clustering algorithms for wind turbines, in order to group wind parks with close statistical behaviour, allowing highly

correlated wind parks into the same cluster to be integrated in a realistic way, and the evaluation was processed by the non sequential Monte Carlo sampling.

In this thesis, a modified algorithm for wind speed sampling *Latin Hypercube Sampling* (LHS), based on [7] is adopted. The algorithm avoids disappearance of stratifications through the whole range of the event probability resulting from Monte Carlo Sampling. Furthermore, the algorithm avoids intensive computations, which result from Acceptance Rejection and Markov chain Monte Carlo Sampling;

- The reliability of wind generators does not depend only on determination of wind speed samples, but also on wind speed correlations among wind turbines based on the distance separating them. The wind speed does not maintain a specified stable level, and so a multi-state model must be used to estimate a reliable wind energy system.

  In [36] Dimitrios used a neural network training, to produce correlated wind speed samples for a wind farm. In [37] Wijarn employed the ARMA time series model, which considers the time lagging effect among different wind turbines. In [38] Gao used a genetic algorithm method to adjust ARMA models, and to simulate hourly wind speed samples based on the degree of wind speed correlation among wind farm turbines.

  A simple method is adopted in this thesis, to introduce correlations among different wind turbines based on the Cholesky decomposition technique. The proposed correlation method has some desired properties, as it can be applied on all types of input distribution functions, simplicity as there is no need for complex mathematical computations and the marginal distribution of wind speed remain intact;

- In order to determine the feasibility of wind farm installations from the viewpoint of performance and economic considerations, some authors have discussed this matter.
  In [41] Tai determined the feasibility of a wind farm, via the capacity factor of each wind turbine, under different values of tower height and

rated wind speed, and determined the feasibility of the wind farm as a function of the energy cost and mean wind speed.
In [42] Wang processed simulations for wind turbines under different hub heights, diameters and mean wind speeds, to determine the most feasible case. As wind turbine is considered an intermittent source of energy and wind power always fluctuates depending on stochastic parameters, it is not logic to optimize the capacity factor and economic performance of wind turbines without considering other storage systems or dispatchable generators, which share the operation with wind farms.

In this thesis, the issue of optimizing both energy production and economic performance is shown for microgrids supplied by different wind turbines and different types of batteries. Several authors have optimized the capacity factor and economics of wind turbines production, but have not taken into consideration the dynamic operation of storage systems, which share the supply with wind generators. Therefore, the optimum point of operation is totally different when considering the dynamics of storage systems, if both wind turbines and storage systems are employed together in a multi-objective function.

This thesis provides benefit evaluations for microgrids from the perspective of energy production and economic performance. Several analyses are processed for microgrids supplied by composite generation of wind energy units and batteries, all economic evaluations in the thesis are conducted by several economic evaluation models, such as cost of energy, simple payback and net present value.

In addition, some comparative simulations among various batteries based on their capital costs-efficiencies are shown, in order to clear the possibility of enhancing the microgrid economic performance and energy production by high capital cost-high efficient batteries. The cost of a battery is typically related to its performance, including the discharge rate, energy density, operational losses and life time. Through the thesis, some simulations show the possibility of improving the economic performance of high capital cost-high efficient batteries by employing them with wind

turbines in a multi-objective function;

- Regarding an adequate real-reactive power exchange strategy in a microgrid, the droop regulation of each distributed generator supplying a microgrid must be performed in a quick efficient manner, and also the economical aspects must be taken into consideration. Some authors proposed a centralized energy management in microgrids. Regardless the high cost that entails communication establishment between all distributed generators and central controller of a microgrid, the concept of *plug & play* cannot be confirmed. Through the thesis, the real-reactive power exchange among different distributed generators in microgrids is based on the droop control. Therefore, if power flow level changes in a microgrid, the change can be met directly by droop regulation without any need of central controller management;

- As the droop control strategy can enforce all distributed generators to participate in a system restoration in case of disturbances, and also manage the real-reactive power exchange in the system, several authors have discussed this strategy.

  In [52] Katiraei addressed a real-reactive power management of electronically interfaced distributed generators, which is based on locally measured signals and droop characteristic, in order to provide complimentary frequency restoration.
  Barklund in [23] proposed an energy management strategy for a standalone droop-controlled microgrid based on frequency-droop gains of different distributed generators, which adjusts generators output power, to minimize the fuel consumption and also ensures a stable operation.
  In [53] Majumder explained a method for power flow control between an utility and a microgrid through back-to-back converters, which facilitates the desired real and reactive power flow between the utility and microgrid, based on droop characteristics of different generators.

  All the previous authors proposed strategies to optimize the power flow in microgrids through the droop control based on considering two operational constraints for each distributed generator. The first constraint

is for droop regulation, while the second constraint is for maximum power limit of each distributed generator. Thus, realizing an equilibrium point requires employing heavy computations by the conventional Newton-Raphson algorithm. In this thesis, another strategy based on *Fischer-Burmeister* is proposed, to handle the droop control. The proposed strategy is based on a nonlinear complementarity problem that substitutes the piecewise droop function by an only scalar function, and makes the problem to be solved easier by less iteration process;

- The objective of optimizing the energy production in microgrids must be extended to satisfy the power balance and generation limit among different microgrid generators, such a stable operation must be ensured without power swings and resynchronization problems. Some authors have discussed the stability analysis of microgrids.

  In [31] Ostadi proved that the stability of a microgrid supplied by wind turbines and a grid utility varies, under different levels of wind penetration.
  In [32] Yateendra showed variations in the stability of a microgrid supplied by wind turbines and a utility grid, under different wind speeds, and proposed a damping controller for the dominant variables.
  In [33] and [34], both Lihui and Yang respectively proved that the stability of a power system supplied partially by wind energy varies under different wind speeds, and determined the dominant variables.
  In [48] Pogaku conducted a stability analysis of an isolated microgrid supplied by distributed generators, and interfaced to the microgrid through electronic inverters, and without penetration of any intermittent energy sources as wind turbines.

  All the previous stability studies belong to either microgrids supplied by wind energy and connected to utility grids, or to isolated microgrids supplied by distributed generators and without penetration of any intermittent energy source. Through this thesis, the stability analyses are performed for isolated microgrids supplied by intermittent energy sources which are DFIGs and also other DGs interfaced by inverters. The reason

of conducting such analyses is to determine the critical state variables which can violate the stability of microgrids. The analyses are processed under different scenarios, such as different levels of wind penetration, power demand increment and different levels of real-reactive power exchange by droop manipulations.

Chapter 2

Capacity Factor Analysis of Droop-Regulated Microgrids

2.1 Introduction

The main function of an electric power system is to meet its customers demand with electrical energy by minimum possible cost; at the same time, continuity and power quality must be ensured [54]. Advanced electric power systems around the world have undergone de-regulation with major changes in structure, operation and regulation.

Each part of the power chain, as power plant owners, transmission system owners, operators, regulators and finally the customers are all involved in this chain. The development process in any modern society is mainly dependent on power availability and quality. Any modern society, can appreciate perfectly how main necessities of daily life would be without energy. From statistics, it is expected that necessity for available and high quality of power supply will continue to increase.

The reliability associated with a power system is a measure of the overall system ability to satisfy the customer demand for electrical energy. Power system reliability can be further subdivided into two different categories, system adequacy and system security [54], as shown in Figure 2.1.

The reliability of the energy infrastructure is indication of the whole infrastructures capacity to meet the customers demand of the electrical energy. Power system reliability can be clearly categorized to different branches of system adequacy and security [54] as shown in Figure 2.1.

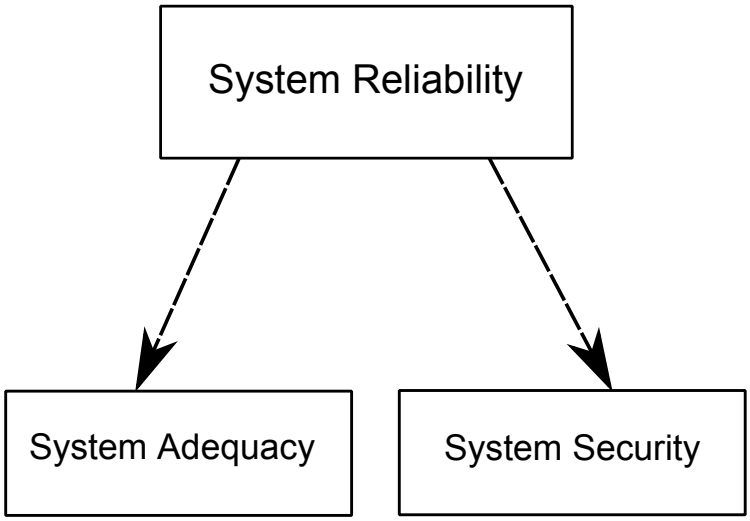

Figure 2.1: Categories of system reliability

System adequacy is considered as indication of sufficient facilities within the system to meet the customer demand. These facilities include those parties of the power chain to generate energy starting from power plants to transmission and finally distribution networks required to transport the energy to the actual consumer load points. On the other hand, system security is related to the ability of the system to respond to originating disturbances within that system [54]. Therefore, to ensure a reliable power system, both reliability terms must be well evaluated.

The proposed isolated microgrid in this Chapter is supplied by wind turbines, interfaced to the microgrid by inverters, and so the main reliability challenge results from intermittent nature of wind energy sources.

Wind energy is one of the fastest growing renewable energy sources; Figure 2.2 shows the total wind capacity installed around the world from 1980, to 2008. Total of 120,791 MW of wind capacity was installed throughout the world [55] by the year 2008. The cost of energy from wind has dropped to the point that in some sites it is nearly competitive with conventional sources. The current total installed wind capacity in Canada is 2,577 MW, which is about 1% of Canada's total electricity demand [56]. Saskatchewan city, currently has 171.2 MW of installed wind capacity with the completion of the 150 MW centennial wind project in 2006 [56].

The World Energy Council has estimated that the wind energy capacity worldwide may reach as high as 474,000 MW by the year 2020 [55]. In Canada,

Ontario, Nova Scotia and Prince Edward Island have committed to generate 10%, 5% and 15% respectively of the total electricity production from renewable energy sources by the year 2010 [56]. Many countries around the world implement different policies to promote the growth of renewable energy.

Renewable energy policies, such as the Fixed Feed-in-Tariffs in Germany, Denmark, Spain [57] and Renewable Obligation in the UK [58] have driven the development of wind power in these countries.

Figure 2.2 explains the gradual increase in the wind energy production around the world, as mentioned in [59].

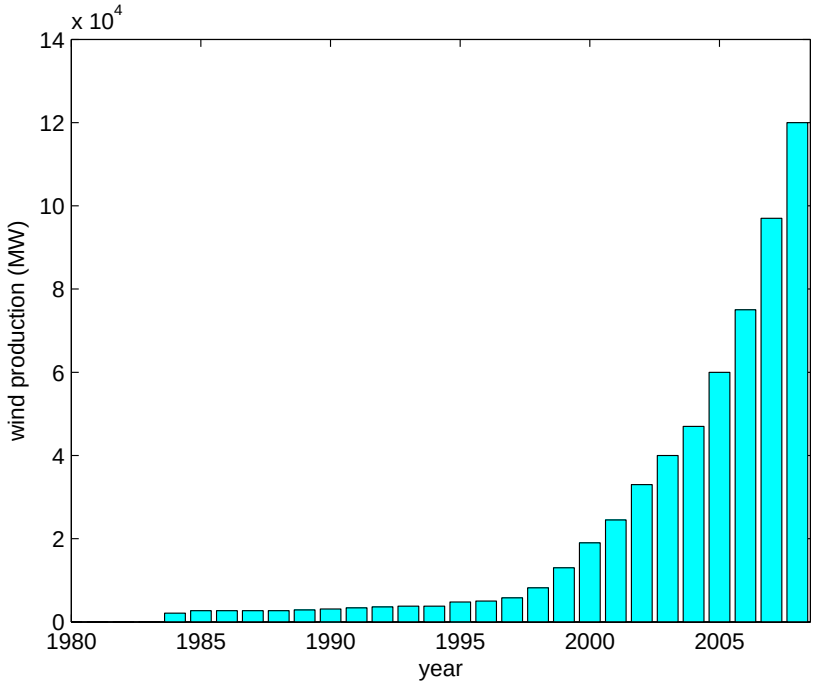

Figure 2.2: World wind energy generation

As a result of continuing growth and penetration of the wind energy in the traditional power systems, it has been urgent necessity to consider the reliability evaluation for wind power production. Typically, the conventional generating units are capable of generating rated power during normal operation; reliability evaluation for these units are well established and are routinely used in the capacity planning of the electric power utilities. Wind energy sources are always dependent on the climate stochastic parameters, and so it is usually hourly and seasonal fluctuating, unlike conventional generating units. Through last decade, the power networks in Europe and North America involved in sev-

eral blackouts, due to the increased penetration of wind energy.

The increased liberalization of electricity supply industry by the beginning of 1990 has resulted in a significant increase in the inter-area problems. Those problems have been compounded by increased penetration of the wind generation.

Large changes of wind power due to changing weather patterns mean that an actual network flow may be quite different from a predicted flow. Thus, the reliability evaluation of power systems icluding the wind energy conversion systems (WECS) is relatively complex.

Determination of non-dispatchable generator reliability, as in case of the wind turbine generator (WTG) unit can be performed by different techniques. Analytical methods evaluate the reliability indices by using numerical solutions from mathematical models, which represent the power system.

A considerable research activity has been dedicated to the area of power system reliability including wind energy in the past several years. The wind generator unit has been modelled as a multi-state unit to evaluate the effect of the wind power on the reliability indices of power systems by analytical techniques, as shown in [60], [61] and [62].

In [61], a methodology was proposed to classify the impact of wind generation, which is dependent on time variation and climatic change on the reliability of the power system.

In [63], the author proposed a method to clarify the multi-state of wind turbines, due to dependency on wind speed variation.

The reliability study has been extended in [62] to investigate the effect of the wind power generation by a probability theory on the power system.

On the other hand, the capacity factor is a measure of operating efficiency, which indicates the ability of a generating plant to deliver its full capacity; thus, it is considered as an indicator of the reliability of supply.

The reason of the interest in capacity factor analysis of a wind generator is that the analysis provides a smart, summarized indication about the combined interaction between the generator and the site that is between the wind power curve and stochastic wind speed. Subsequently, the accurate wind energy capacity determination reduce the need for balancing energy and reserve power, which are needed to integrate wind power into the balancing of supply and demand in electricity supply systems.

Moreover, the main concern about capacity factor analysis in droop-regulated microgrids that the proposal of considering the droop-regulated microgrid as a large generator that is built up from several wind generation units cannot be solved as a simple sum of individual rated and average power of wind generation units. This fact can be explained as the micogrid load is shared among the intervening generators by means of the droop control, and so particular restrictions on the maximum loadability of the microgrid may occur, which make it possible for the maximum delivered power to be less than the sum of power injections.

For this reason, the capacity factor analysis of droop-regulated microgrids is performed in this Chapter based on a reliable wind speed sampling strategy, by reducing the variance of wind speed samples, and also including the correlations among wind speeds; thus, each wind energy source status can be determined accurately. Finally, capacity factor analysis can provide an insight about site matching suitability for droop-regulated microgrids supplied by wind generators.

However, before conducting the capacity factor analysis of the proposed droop-regulated microgrids, an accurate wind speed sampling strategy is needed, to determine appropriately the status of wind generators.

Most wind energy reliability studies have been conducted by one of the most well-known sampling methods which is Monte Carlo sampling (MCS). Typically, MCS has some engrained weak points, such as disappearance of stratifications through the whole range of the event probability domain, and so the sampling process can not cover all wind speed probabilities, as shown in Figure 2.3 where the simulation is processed by ten samples, at wind scale parameter equals to three. Wind speed samples by MCS are accumulated over certain areas of the wind speed distribution probability. Moreover, MCS is characterized by an intensive computationally nature.

The MCS weak points typically lead to a degree of risk analysis and give the superiority always to conventional generator units, and a less dependency on wind generators. For this reason, a modified strategy for wind speed sampling is adopted in this Chapter; the proposed sampling technique is *Latin Hypercube* (LHS), which can stratify equally all wind speed samples overall the probability domain, by simple calculations and non-time consuming manner.

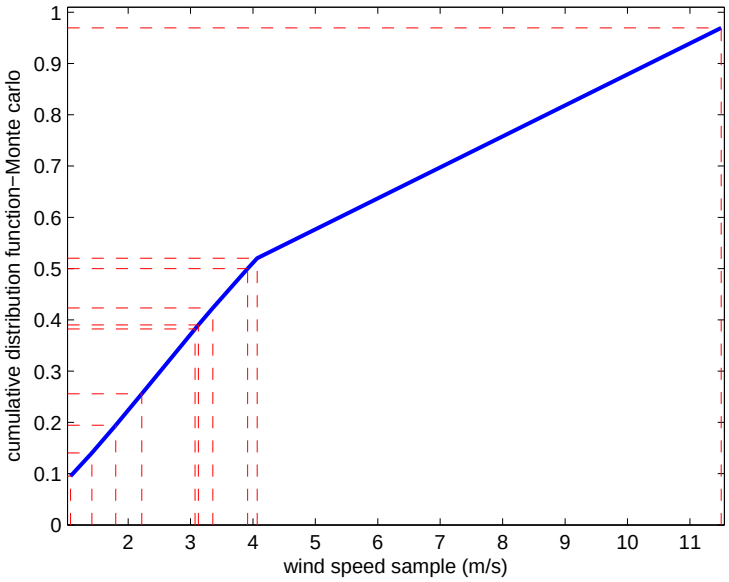

Figure 2.3: Monte Carlo transformation method

Furthermore, the reliability of a wind generator does not depend only on an efficient sampling technique for the wind speed, but also on a wind speed correlation which must be considered. In this Chapter, a simple method is adopted to introduce correlations among different wind turbines based on Cholesky decomposition technique. The method has some desired properties, as it can be applied on all types of input distribution functions, simplicity as there is no need for complex mathematical computations and the marginal distribution of wind speed samples remain intact.

The following Section, explains the organization of this Chapter. Starting by sampling the wind speed by LHS strategy, then introducing the correlation among wind turbines. Therefore, a microgird supplied by wind energy can be processed by an optimized power flow, and consequently the maximum loadability of the microgid can be accurately determined.

2.1.1 Chapter Outlines

As mentioned in Chapter 1, the first concern of this thesis is to conduct capacity factor analysis of droop-regulated microgrids based on a reliable wind speed sampling strategy, by reducing the variance of wind speed samples, and also including the correlations among wind speeds. Thus, the states of

wind turbines can be obtained in an accurate manner and wind turbines adequacy term can be determined later more precisely by capacity factor measures, through an optimized power flow.

This Chapter concentrates mainly on the following items:

- Developing a reliable sampling strategy for wind speed samples. Through this Chapter, a strategy based on Latin Hypercube Sampling is adopted;
- The reliability of wind generators does not depend only on a sampling technique of the wind speed, but also on correlation among wind turbines, which must be considered. Therefore, a simple method is adopted in this Chapter, to introduce the correlation among different wind turbines;
- Furthermore, in this Chapter an efficient curve fitting for a wind turbine is proposed, taking into consideration the null wind speeds;
- A piecewise-definition of the wind power cumulative distribution function (CDF) is proposed, and so wind power samples can be obtained directly by the probability distribution of the wind speed;
- Another important issue is shown through this Chapter that is the maximum loadability of an isolated microgrid, as it provides an insight about the capacity factor of microgrids. A global optimization technique *Global Search* is used to calculate the maximum loadability of the microgrid;
- Measures of the relative goodness of fit were employed by *Akaike* and *Bayesian* to set the distribution fitting of the injected power to the microgrid from the wind turbines, explaining the effect of seasonal or locational wind speed variations on the shape of the output power, and so an accurate estimation of generators capacities can be clarified;
- Capacity factor estimations for both wind turbines and microgrids are conducted. Thus, the adequacy term can be evaluated according to capacity factor measures;
- In addition, the bifurcation analysis is performed by the Continuation Power Flow (CPF), to determine the feasibility of microgrids, under different scenarios;

- Finally, several case studies are conducted to measure the capacity factor of a microgrid, by suppling the microgrid by various wind turbines and under different values of droop constants of the microgrid supporting units (MSUs). Thereafter, some important conclusions can be obtained.

The main outlines of the Chapter are shown hereunder:

1. Providing LHS technique (Section 2.2);
2. Applying a correlation technique among wind turbines (Section2.3);
3. Conducting a curve fitting for wind turbines (Section 2.4)
4. Performing a cumulative distribution function of wind power samples (Section 2.5);
5. Microgrid layout (Section 2.6);
6. Maximize the microgrid loadability by the global search technique (Section 2.7);
7. Processing simulations and conclusions (Section 2.8);
8. Applying Akaike and Bayesian techniques to the microgrid injected power (Section 2.9);
9. Capacity factor estimation for both wind turbines and microgrid (Section 2.10);
10. Bifurcation analysis (Section 2.11);
11. Case studies (Section 2.12).

2.2 Latin Hypercube Sampling

History and Definition

By 1975, W. J. Conover of Texas Tech University was asked to develop a method for improving the efficiency of simple Monte Carlo, to characterize the uncertainty of inputs to computer models. The research resulted in a stratified model of Monte Carlo called *Latin hypercube sampling* (LHS), and so LHS has been applied to some computer modelling applications at Sandia National Laboratories [64].

The Latin Hypercube Sampling uses a stratified sampling to cover the whole domain of a distribution function of a random variable X_j. The stratification is processed by dividing the distribution function vertical axis $F(x)$ into (N) non-overlapping intervals of equal length, where N is the number of samples to be processed. Therefore, by deriving $F^{-1}(x)$, the distribution function horizontal axis is stratified into N equiprobable and non-overlapping intervals.

The main four steps of LHS are listed as follows:

1. Definition of the probability density function (PDFs), or the Cumulative Distribution Function (CDFs) of parameters and state variables, which will be sampled;
2. Calculating the number of simulations (N);
3. Dividing each parameter into equiprobable intervals;
4. Creating the LHS table.

2.2.1 Distribution Functions of Parameters and State Variables

Probability density functions (PDF) or cumulative distribution functions (CDF) are assigned to uncertain parameters or state variables, depending on the nature of the parameters or state variables.

As mentioned in [65], [66] and [67] regarding the wind speed distribution probability, it has been assumed that wind speed distribution probability is formed as weibull distribution function by two parameters, scale and shape parameters.

Other authors, as in [68] and [69] considered that the probability distribution of the wind speed of specific wind farms cant not be formed as weibull distribution, due to geographical nature of such wind farms.

The only considered parameters in this Chapter is the wind speed distribution probabilities; also wind speed probability is assumed to be distributed as weibull, by two parameters, scale and shape parameters, and sampled through the CDF.

2.2.2 Calculating the number of samples

The LHS design involves sampling without replacement; therefore, if a mathematical model of a problem contains uncertain variables (K), then the minimum limit of samples must be $K+1$; In [70], the author showed a necessary condition that $(N > 4/3K)$. Moreover, the desired partial rank correlation coefficient is important factor to determine (N). In this Chapter, N is assumed to be 100.

2.2.3 Dividing the range of each of the parameters into equi-probable intervals

By assuming the parameter being sampled is x and its CDF is $f(x)$, and must be divided into (N) non-overlapping equiprobable intervals, as shown in Figure 2.4, where the simulation is processed for ten samples.

Each interval is indexed by i, and so the limits of each interval (x^i_{min} and x^i_{max}).

The integral of $f(x)$ is assumed to be $F(x)$, and so the transformation of the probability values into the sample x is conducted by using the inverse of the cumulative distribution function $F(x)$, as shown by equation (2.1).

$$x^i = F(x)^{-1} \tag{2.1}$$

The lower interval limit of the interval i is (x^i_{min}) and the upper interval limit (x^i_{max}) is determined from equation (2.2).

$$x^i_{max} = F^{-1}[F(x^i_{min}) + 1/N] \tag{2.2}$$

The minimum value for the next interval x^{i+1}_{min}, is set to be equal to the maximum value of the previous interval x^i_{max}, and this process is repeated for

the remaining intervals.

Regarding the wind speed sampling, the CDF of the wind speed is divided into N intervals, according to the proposed number of simulations, then above equations are applied to generate the samples from CDF function as shown in Figure 2.4, as the simulation is processed by ten samples, at wind speed scale parameter equals to three.

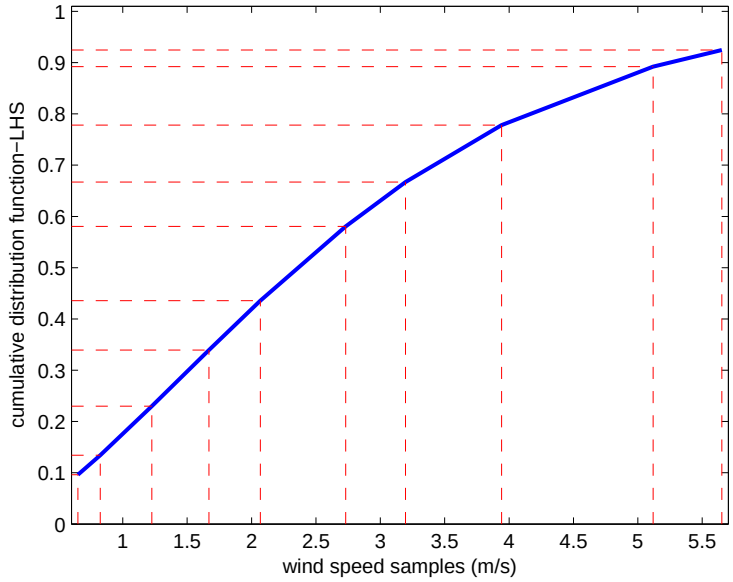

Figure 2.4: Stratified wind speed samples by LHS

2.2.4 Creating the LHS table

The LHS design involves random sampling without replacement; the equiprobable interval of each input variable is sampled once. LHS table is generated as $(N \times K)$ matrix, where N is the number of simulations and K is the number of the sampled input variables.

The LHS design was first proposed in [70]; a computer program based upon this methodology is available for generating LHS tables [71].

The N sampling indices of the first variable are combined randomly, with the N sampling indices of the second variable. These N pairs are then paired randomly with the N values of the third variable. The random pairing continues until all the K parameters are included and the $N \times K$ matrix is generated [71].

Figures 2.5a and 2.6a represent the LHS sampling at wind speed scale parameters: 3 and 5; while, Figures 2.5b and 2.6b represent MCS sampling at wind speed scale parameters: 3 and 5.

Clearly, Figures 2.5 and 2.6 show the superiority of the LHS over MCS at wind speed scale parameters: 3 and 5.

The LHS ensures a better spread of the sample points over the sampling space, while MCS lacks stratification and that is clear from MCS figures, where some samples are accumulated over each other without equiprobable distribution.

After conducting such a reliable sampling technique, inducing correlations among wind turbines is a must. Next Section will propose a correlation method to be introduced among wind turbines.

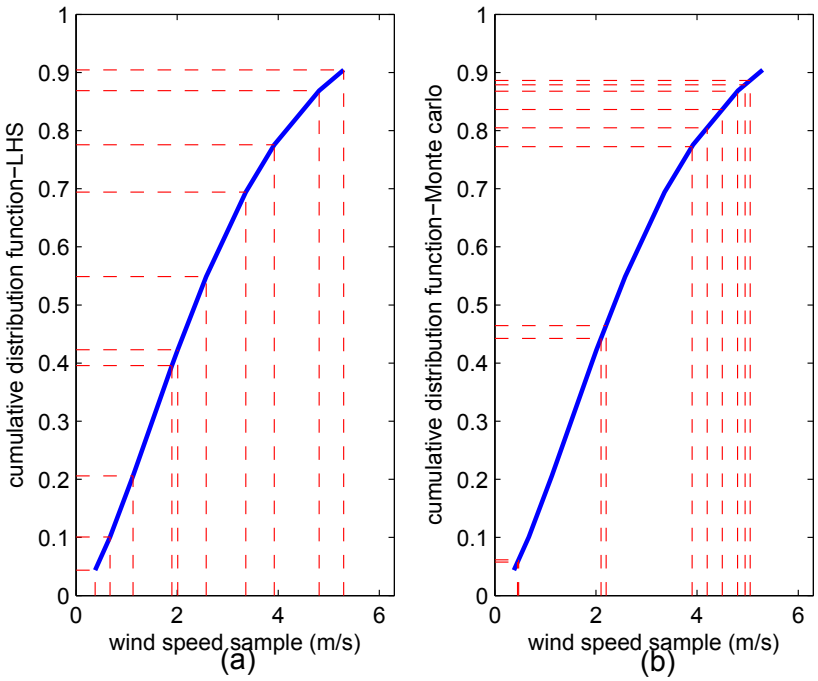

Figure 2.5: Wind speed sampling at scale parameter (3) processed by: (a) LHS. (b) MCS.

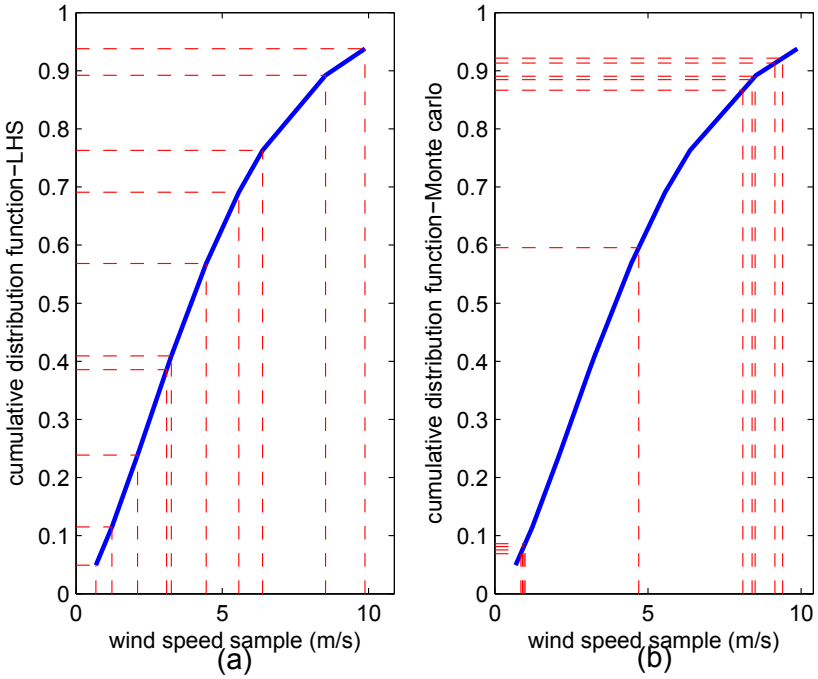

Figure 2.6: Wind speed sampling at scale parameter (5) processed by: (a) LHS. (b) MCS.

2.3 Correlation among Different Wind Turbines

The wind is driven by weather fronts and a daily pattern caused by the sun; depending on these dominants, there is a significant diurnal pattern in the production. When combining the generation of variable sources, an averaging effect occurs, if the time series of generators are uncorrelated or only partly correlated.

For an analysis of this behaviour, a correlation coefficient of (1) means that time series are perfectly correlated, and hence go up and down in exactly the same manner. A coefficient of (0) means that time series are randomly distributed. On the other hand, when the correlation coefficient is (-1) meaning, if there is a tendency of decreasing a production at one site, a production increases at the another site.

There is a significant variation in the cross-correlation coefficients for similar distance, the correlation becomes weak when it reaches below 0.5, with distance 200-500 km. Cross-correlation ($r_{x,y}$) is a measure of how two time

series follow each other, as indicated by equation (2.3).

$$r_{x,y} = \frac{\frac{1}{n}\sum_{i=1}^{n}(x_i - \mu_x)(y_i - \mu_y)}{\sigma_x \sigma_y} \tag{2.3}$$

Where μ is related to the average value, σ is the standard deviation, n is the number of points in the times series and $r_{x,y}$ is the coefficient of correlation between two variables.

When distributing the wind power production to larger area, the total production will be smoother and less variable, if the correlations among the site turbines are high.

There is no significant change in correlation coefficients calculated from different years. The cross correlation can be modelled by an exponential fitting as shown in Figure 2.7, with decay parameter ranges from 500 to 700, based on [35].

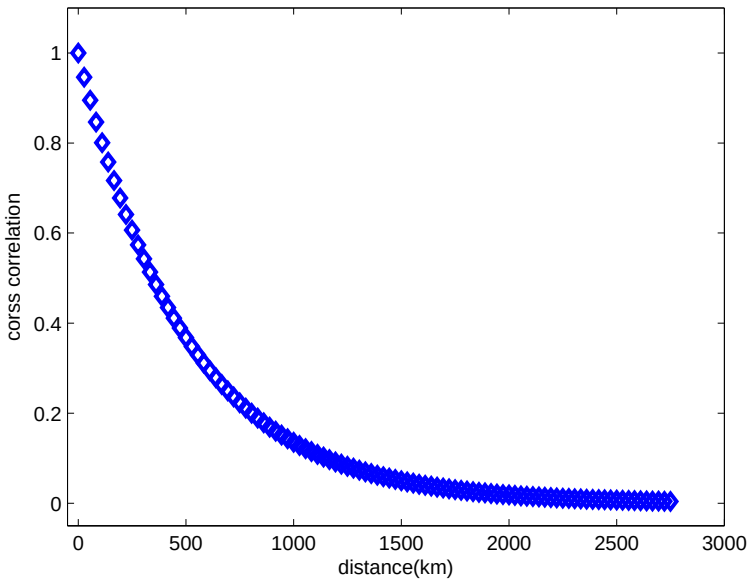

Figure 2.7: Cross-correlation vs distance.

As a result of the important effect of the wind speed correlation among wind farms on power system reliability, this issue have been discussed through many papers, as [72] and [73]. In [74], the correlation among wind farms based on wind speed and wind directions was proposed.

Other papers have discussed the correlation issue for single time series, but with time lags (auto-correlation). For the wind power, the auto-correlation

decreases soon with increasing the time lag. Some authors discussed this important matter as in [37], by employing the ARMA time series model, which considers the time lagging effect, noise and residual effects; thus, by choosing a certain instant the correlation coefficients among wind farms can be produced.

The sampling time was found to influence significantly the forecasting error [75], as wind variation in one site affects the another site when a delay time is considered. The Neural Network in [36] was used as a training technique to produce the wind speed samples, after considering an auto-correlation.

All the previous correlation methods are based on intensive computational techniques; a simple method is adopted in this Chapter to introduce correlations among wind turbines based on Cholesky decomposition technique. The method has some desired properties as it can be applied on all types of input distribution functions, simplicity as there is no need for complex mathematical computations and the marginal distribution of wind speed samples remain intact.

The LHS design is proposed for models, where all of input variables are statistically independent. One approach to incorporate dependences is to consider linear combinations of the independent random variables to achieve the desired correlation structure. In case of normal random variables and random sampling, this approach is well-known to produce multivariate normal input vectors.

However, if the samples are stratified as in the LHS case, then this approach destroys the integrity of the stratified samples, and so the values obtained from linear combinations will no longer map back into each of the original structure.

Moreover, the linear combinations of non-normal variables will adversely affect both the random samples and stratified samples, as the marginal distribution may no longer resemble the original marginal distribution desired on the input variables.

The adopted strategy in this Chapter for introducing the correlations among wind turbines is based on [7], the methodology replaces the random pairing of the (N) values of each input parameter with a restricted pairing. This new technique may be appropriate for both dependent and independent variables, because the restricted pairing can reduce spurious correlations and induce the desired rank correlation among the input variables.

2.3.1 Correlation Steps

The method is based on the Cholesky decomposition of the correlation matrix. Suppose matrix X is composed of independent random variables, with correlation matrix I and C is the desired correlation matrix. The matrix C can be written as $C = PP'$, where P is the lower triangular matrix. Similar to the simple random sampling, multiplying vector into P' yield random variables, with correlation matrix C. Therefore, the objective is to rearrange the input variables close to the target correlation matrix. The main steps of correlation:

1. Generating matrix R using Latin hypercube sampling of (K) variables at sample size (N);

2. Calculating T, the correlation matrix of R;

3. Calculating P, the lower triangular matrix of the target correlation matrix C using Cholesky factorization $C = PP'$, and also Q, the lower triangular matrix of T; $T = QQ'$;

4. Solving to obtain matrix S such that $STS' = C$, which is calculated from $S = PQ^{-1}$;

5. Calculating target correlation matrix $R^* = RS'$, which has a correlation matrix equal to C;

6. Rearranging the values of each variable in R, so they have the same rank order as the target matrix R^*.

The statistical dependencies can be performed by the rank sorting approaches as shown by Iman and Conover in [7] or by Stein in [76]. Stein's method applies the rank sorting approach when the input variables are related in a non-monotonic way, and requires producing samples with definite joint distribution, by then it is not the purpose of the current study. Thus, Iman's and Conover's method is applied in this Section to induce correlations among wind speed samples. In order to clear the effectiveness of the proposed method, the proposed correlation strategy is applied to correlate among wind speed samples of separated wind turbines, as shown in Figure 2.8, according to correlation values from Figure 2.7. By measuring the distance among the dispersed wind turbines at nodes 8, 12 and 14 in Figure 2.7, the correlation

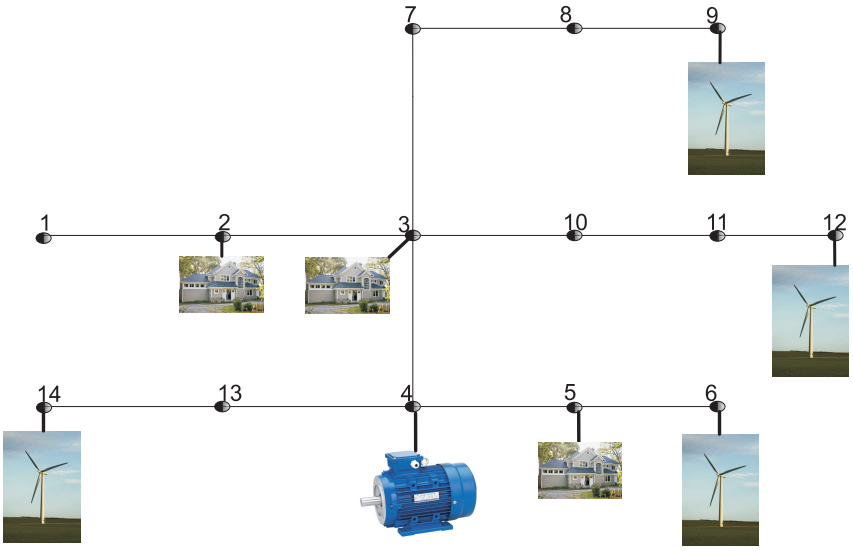

Figure 2.8: Microgrid layout

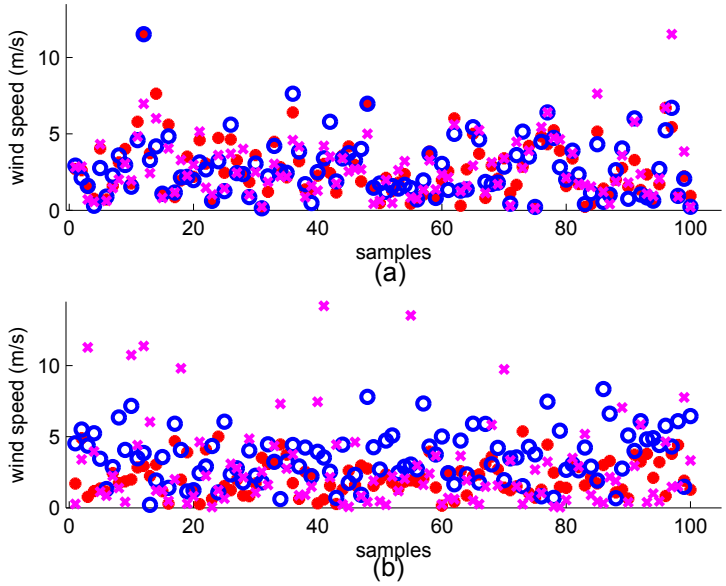

Figure 2.9: Wind speed time series processed by scale parameter (3): (a) Correlation included. (b) Correlation excluded.

factor ranges from 0.75 to 0.9.

Figure 2.9 clears the deviation between each turbine sample and its correspondent in the other turbines at the same time. Figure 2.9a represents the deviations in time series among wind turbines samples, in case of applying correlation. Figure 2.9b represents the deviations in time series among wind

turbines samples without correlation. Uncorrelated samples show large deviations.

In order to obtain accurate outputs from wind turbines, after conducting efficient sampling and correlation techniques among separated wind turbines, a curve fitting for the wind turbines must be conducted, which can take into consideration null wind speed samples. Therefore, steps for conducting curve fitting of the proposed wind turbine in this Chapter will be shown in the next Section.

2.4 Curve Fitting of the Wind Turbine Enercon-E40

A simple model of wind turbine curve fitting derivation has been proposed in [77], but this model did not account well for different regions of operation; moreover, null wind speed region was not well considered.

In order to correctly fit the power curve of a wind turbine, this Section proposes a curve fitting which can describe well the nonlinearity of the turbine operation through all possible wind speed ranges, including the null wind speed region.

The selected turbine for fitting is Enercon-E40 600 kW rated power, cut-in (w_i), cut-out (w_f) and rated speeds (w_r): 2.5, 28 and 12.5 m/sec respectively. The collected wind turbine energy is null below w_i; also wind turbine energy is null above w_f, because of dramatic increase in wind energy, and so the pitch control is activated to protect the mechanical parts of the turbine. The blending speed (w_m=10 m/s) is selected to separate two regions (II) and (III), as shown in Figure 2.10, in order to reduce the fitting errors which may occur between the two regions.

The selection of the blending speed w_m is based on finding a reduced least square residuals of the turbine curve. Contrary to [78], where the author applied two third polynomials to fit the turbine curve and resulted in difficulties for curve inversion.

The different operating regions of the wind turbine are shown in Figure 2.10 and can be justified as follows:

- Regions I and V, where $w < w_i$ and $w > w_f$;

- Regions II and III, where the wind power varies according to wind speed, as $w_i \leq w \leq w_r$;

- Region IV, where the turbine power is always constant and equals to the rated power, as $w_r \leq w \leq w_f$.

The fitting of the whole wind turbine is shown in Figure 2.10, manufacturer data are shown by diamonds; also different operating ranges of the wind turbine are cleared by equation (2.4).

$$P_g = \begin{cases} 0 & \text{if } w < w_i \ \ or \ \ w > w_f, \\ a_3 w^3 + a_0 & \text{if } \ w_i \leq w \leq w_r, \\ \frac{b_1}{1+e^{(}-(w-b_2)^{b_3})} & \text{if } \ w_m \leq w \leq w_r. \end{cases} \tag{2.4}$$

Considering, $a_3 = 6.847 \times 10^{-4}$, $a_0 = -9.332 \times 10^{-3}$, $b_1 = 1.001$, $b_2 = 9.278$ and $b_3 = 1.074$.

After conducting the curve fitting, a piecewise-definition of the wind power cumulative distribution function (CDF) is presented in the next Section, in order to obtain the wind power samples directly from wind speed samples by an inversion process.

2.5 Cumulative Distribution of Wind Power

The piecewise-definition of the wind power cumulative distribution function (CDF) is conducted in this Section, in order to inverse the operating regions of the wind turbine. It can serve to determine directly the turbine power from the probability function of the wind speed. Thereafter, the CDF can be employed to calculate the capacity factor of each wind turbine that serves the microgrid.

In the previous Section, a direct relation to obtain the turbine power samples from wind speed samples was shown as $P_g = g(w)$, such a relation makes it difficult to infer a closed form of the (power CDF) $F_{P_g(y)}$ from the (wind CDF) $F_w(g^{-1}(y))$. As a result of the turbine power curve has separate and different representations, the definition of the wind power cumulative distribution function must be inferred by another way. As shown in Figure 2.10, there are five operating regions of the wind turbine, and so the power CDF must be divided also into five separate regions ($F_{P_g^I(y)}, F_{P_g^{II}(y)}, F_{P_g^{III}(y)}, F_{P_g^{IV}(y)}$

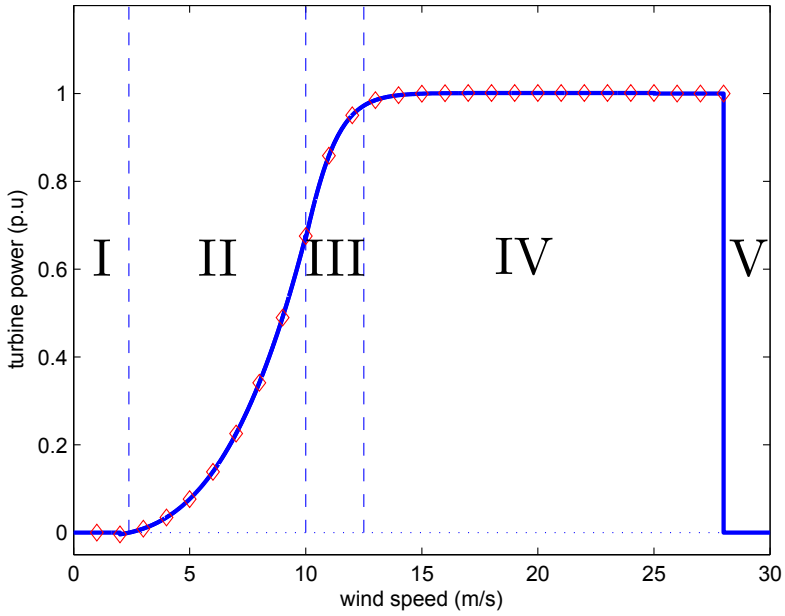

Figure 2.10: Curve fitting of Enercon-E40 600 kW, manufacturer data indicated by (asterisks).

and $F_{P_g^V(y)}$) as indicated by equation (2.5).

$$F_{P_g(y)} = \begin{cases} 1 + F_w(w_i) - F_w(w_f) & \text{if } w < w_i \text{ or } w > w_f, \\ 1 + F_w(g^{-1}(y) - F_w(w_f)) & \text{if } w_i \leq w \leq w_m, \\ 1 + F_w(g^{-1}(y) - F_w(w_f)) & \text{if } w_m \leq w \leq w_r, \\ 1 & \text{if } w \geq w_f \end{cases} \tag{2.5}$$

Figure 2.11a shows the cumulative distribution of the wind power at wind speed scale parameter equals to three, while Figure 2.11b shows the cumulative distribution of the wind power at wind speed scale parameter equals to eight. Clearly, if the wind scale parameter is low, then a higher probability of calm wind speed samples, and subsequently null wind power production results.

After conducting the formula of the probabilistic wind power CDF, now the turn is for a wind power sample derivation (P_g) from a given wind speed

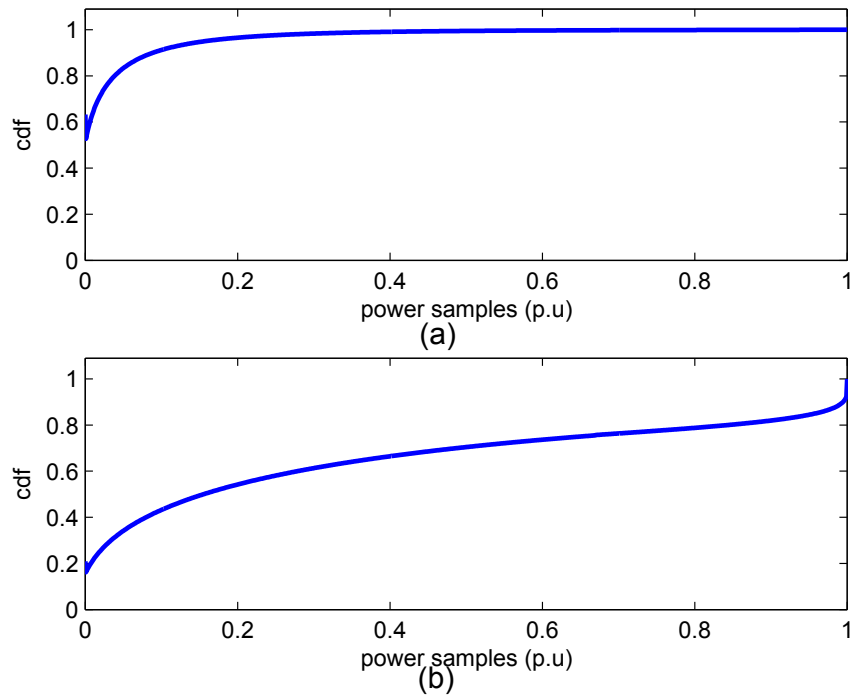

Figure 2.11: Cumulative distribution of Enercon-600kW: (a) Processed at wind speed scale parameter (3). (b) Processed at wind speed scale parameter (8).

probability sample ξ, as indicated by equation (2.6).

$$F_{P_g^{-1}(\xi)} = \begin{cases} 0 & \text{if } 0 \leq \xi \leq F_{P_g}(0), \\ F^{-1}_{P_g^{II}(\xi)} & \text{if } F_{P_g}(0) \leq \xi < F_{P_g}(g(w_m)), \\ F^{-1}_{P_g^{III}(\xi)} & \text{if } F_{P_g}(g(w_m)) \leq \xi < F_{P_g}(g(w_r)), \\ 1 & \text{if } otherwise. \end{cases} \tag{2.6}$$

The proposed microgrid layout is detailed in the following Section, in order to show the locations of the wind turbines where the wind speed samples are applied, the static loads and the microgrid supporting units (MSUs).

2.6 Microgrid Layout

The proposed isolated microgrid is configured as shown in Figure 2.12, and the main elements of this microgrid are briefed hereunder:

- Fourteen nodes distribution system;
- Five microgrid supporting units (MSU), which are fed from Enercon-E40 wind turbines at nodes (1, 6, 8, 12 and 14);
- Distributed static loads at all microgrid nodes;
- Three dynamic loads, mainly induction motors at nodes (2, 4 and 9).

The power and frequency are regulated by the droop control constants (5×10^{-6} rad/W/s) of the MSUs, the nominal power of each MSU is 0.12 MW and the base power of the microgrid is 1.27 MW. Thus, each wind turbine has 0.472 p.u, as a rated power. The balance between the demand and supply

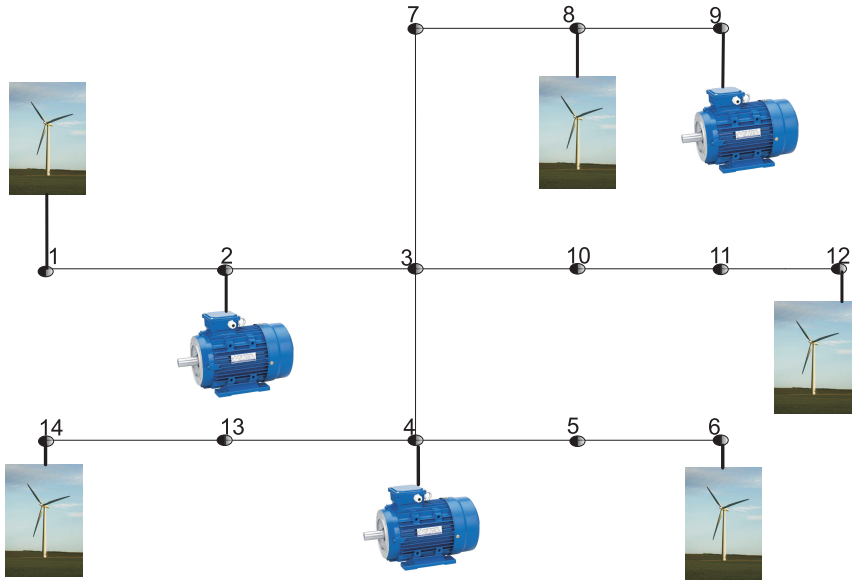

Figure 2.12: Microgrid layout

is handled by the droop control strategy. Figures 2.13 and 2.14 show $P-\omega$ and $v-Q$ droop control by MSU interfaces. Equations (2.7) and (2.8) explain the operational characteristic of the droop regulation by each MSU in the microgrid, where ω is the operating frequency, ω_{max} is the maximum frequency, P is the active operating MSU power, Q is the reactive operating MSU power, m_p is the active droop constant, n_q is the reactive droop constant, ω_{max} is the maximum frequency and v_{max} is the maximum voltage.

$$\omega_0 - \omega_1 = -m_p(P_1 - P_0) \tag{2.7}$$

$$v_0 - v_1 = -n_q(Q_1 - Q_0) \tag{2.8}$$

The next step is to obtain the maximum loadability of the microgird, in

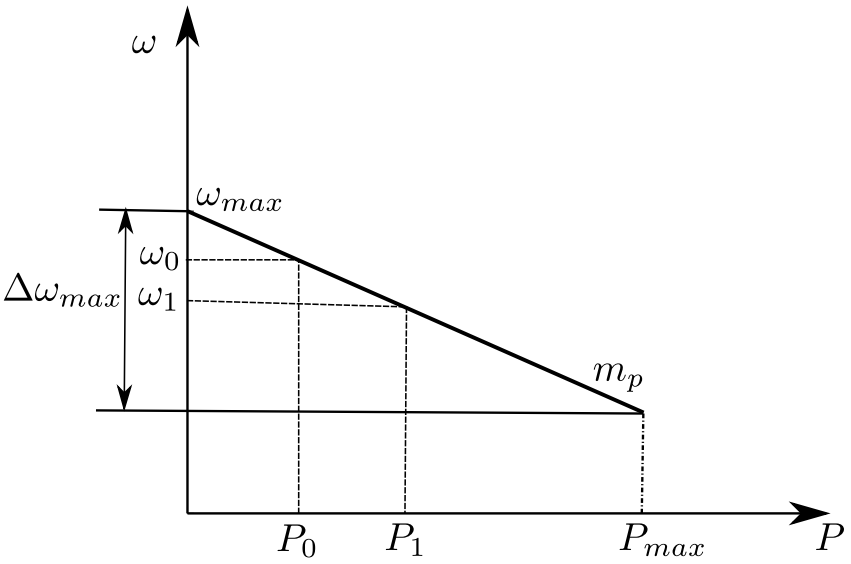

Figure 2.13: Active power vs frequency droop characteristics

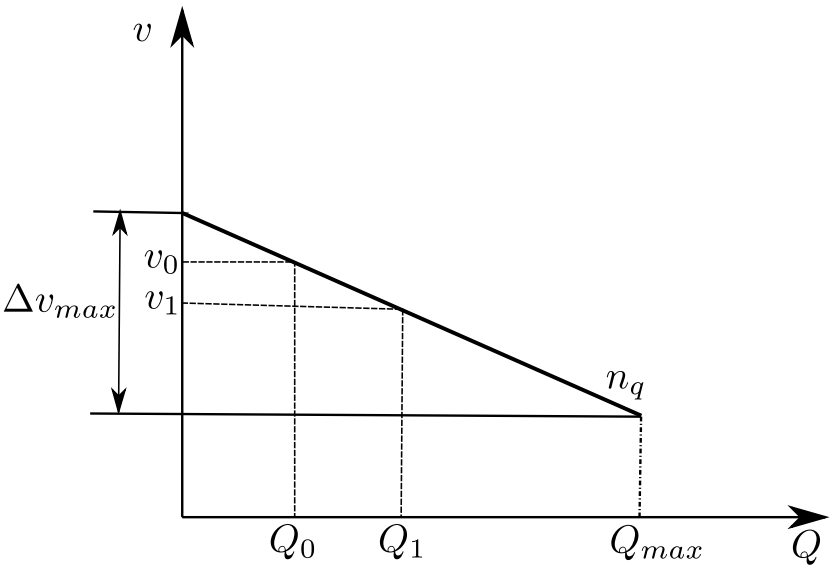

Figure 2.14: Reactive power vs voltage droop characteristics

order to evaluate the capacity factor of the wind turbines. A global optimization technique *Global Search* will be used in the following Section to obtain

the maximum loadability of the microgrid, overcoming the shortcomings from other optimization techniques, which usually attain only local maximum loadabilties.

2.7 Nonlinear Optimization

The maximum loadabiltiy problem is aimed at determining the maximum power demand that the microgird can meet. The maximum loadability can provide an insight about the capacity factor of droop-regulated microgrids. The maximum loadability can be conducted through non-linear optimization problem.

The applied optimization function to attain the maximum loadability of the microgrid is shown by equation (2.9). Where θ is the objective function that represents load increment; the set x represents the microgrid variables; h and g respectively represent the microgrid equality and inequality constraints.

$$\begin{aligned} & max_{\theta} \qquad \theta \\ s.t \qquad & h(x,\theta) = 0 \qquad g(x,\theta) \leq 0 \end{aligned} \tag{2.9}$$

The mathematical optimization is usually considered as selection of a best element from some set of available alternatives. This process must be employed within nonlinear programming problem (NLP) [79].

The NLP is the process of solving a system of equalities and inequalities, collectively termed constraints over a set of unknown real variables along with an objective function, to be maximized or minimized, where some of the constraints or the objective function are nonlinear.

The general nonlinear programming problems are represented by the following form:

$$\begin{aligned} min \qquad & f(x) \\ s.t \qquad & h(x) = 0 \qquad g(x) \leq 0 \end{aligned} \tag{2.10}$$

The constraints $h(x) = 0$, $g(x) \leq 0$ are considered as the functional constraints. The inequality constraints $g(x) \leq 0$ are said to be active at a feasible point x, if $g(x) = 0$ and inactive at x, if $g(x) < 0$.

The necessary conditions to obtain the point of global optimization are defined by two conditions. Therefore, the two main conditions must be met

by an optimization solver.

The first condition is dedicated to obtain the local point of optimization and the second condition is to ensure the global point of optimization.

The First-Order Necessary Condition

By assuming (x^*) to be a point satisfying the constraints of equation 2.11, and **J** is a set of indices j for which $g_j(x^*) = 0$, x^* is regular point of the constraints (2.11), if the gradient vectors $\nabla h_i(x^*), \nabla g_j(x^*)$ are linearly independent, then x^* is considered as regular minimum point for the problem (Karush-Kuhn-Tucker condition). The optimization function is considered by the form shown in equation (2.12); also complementary slackness condition must be met, as shown from equations (2.13) and (2.14). Stating $g_j(x^*) < 0$ implies that $\mu_j = 0$ and $\mu_j > 0$ implies $g_j(x^*) = 0$.

$$h(x^*) = 0, \quad g(x^*) \leq 0 \tag{2.11}$$

$$\begin{aligned} min \quad & f(x) \\ s.t \quad & h(x) = 0 \qquad g(x) \leq 0 \end{aligned} \tag{2.12}$$

$$\nabla f(x^*) + \lambda^T \nabla h(x^*) + \mu^T \nabla g(x^*) = 0 \tag{2.13}$$

$$\mu^T g(x^*) = 0 \tag{2.14}$$

The Second Order Condition

The sufficient conditions for a point x^* satisfying (2.11) to be a strict relative minimum is to realize equations (2.15)-(2.17). Moreover, the second derivative of (2.17) must be positive definite.

$$\mu \geq 0 \tag{2.15}$$

$$\mu^T g(x^*) = 0 \tag{2.16}$$

$$\nabla f(x^*) + \lambda^T \nabla h(x^*) + \mu^T \nabla g(x^*) = 0 \tag{2.17}$$

2.7.1 Global Optimization Search

General nonlinear optimization problems are difficult to solve due to a large number of local minima in the search space. A good local minima are difficult

to be found by local search methods, because solver stops at each local minimum. Therefore, to obtain global optimal solutions, a global search method is provided in this Section, to realize only global peaks.

2.7.2 Applied Global Search Optimization Methodology

The applied Global Search solver in this Section presents an attempt to locate the optimum solution as shown in Figure 2.15. This methodology can efficiently realize the global solution; moreover, it converges with high dimensional systems.

Figure 2.15 explains the steps of this technique. The main steps of Global Search can be briefed as follows:

1. The global solver generates trial points, by employing a Scatter Search method. These trial points are then filtered by checking an initial condition, as if the distance between the trial points and expected local solver points are greater than the preset standard distance, then these trial point are accepted and the optimization process starts from each of the filtered points;

2. A continuous direction update from the trial points to local solvers is processed, taking into consideration the following condition:

    - If the penalty Factor, which is used to determine the update amount of a set of rejected trial point threshold is greater than this threshold value, then the threshold value must be updated.

3. Check if all trial points are rejected, if so the global solver generates other starting trial points and repeats the optimization process again;

4. After analyzing a set of accepted trial points by the scatter search algorithm, the best quality point is chosen.

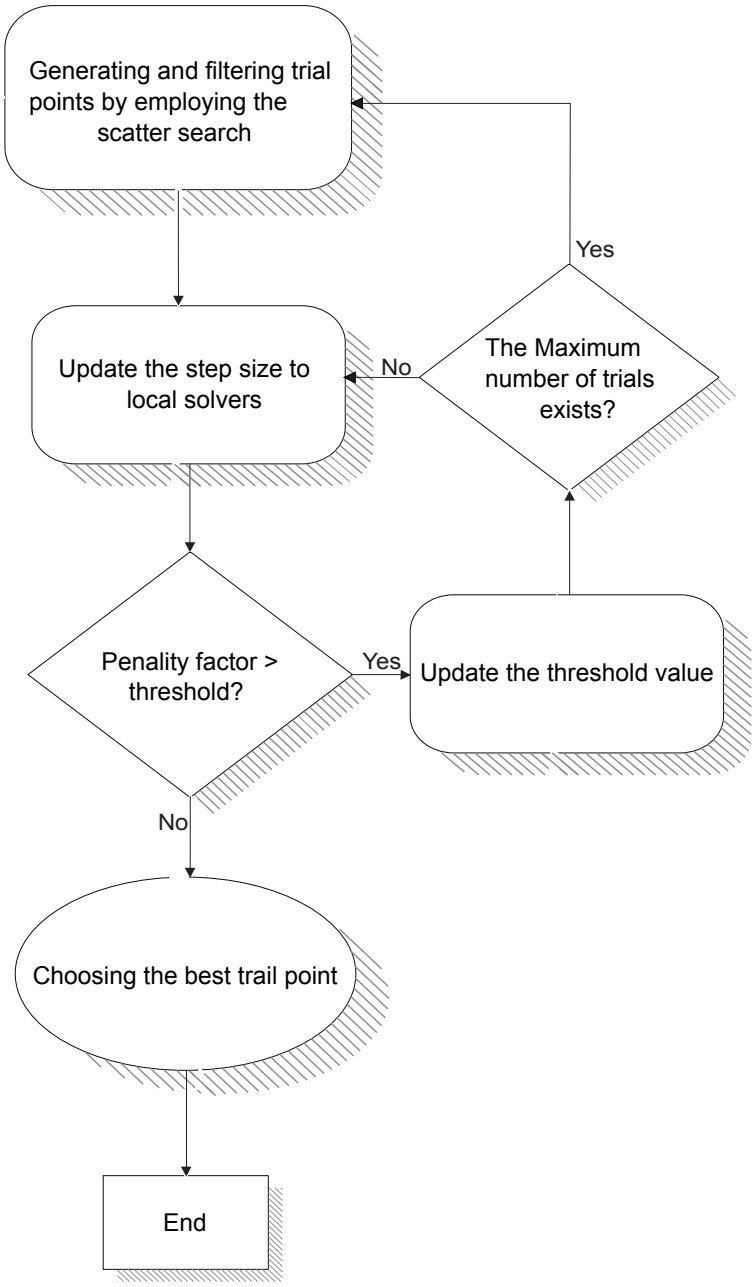

Figure 2.15: Flow chart of the Global Search

2.8 Processing Simualtions and Conclusions

Figure 2.16 shows histograms of 100 samples of injected power from each wind turbine, interfaced by a droop-regulated MSU, at droop constants $m_p =$ 0.5 p.u. The wind distribution is assumed as Weibull of scale 8.0 and shape 1.4. As mentioned from Section 2.6, the base power of the whole microgrid is 1.27 MW, while the rated power of each wind turbine is 600 kW, which represents 0.47 p.u.

Figure 2.16 contains two arrows, arrow 1 indicates a bulk of five histograms, each histogram represents the frequency of occurrence of each wind turbine power samples. Arrow 2 indicates the total injected power to the microgrid.

The group of power histograms represented by arrow 1 ranges from 0to 0.47p.u, while the total injected power represented by arrow 2 ranges from 0 to 2.74p.u.

It is observed that each histogram of the five histograms related to arrow 1 in Figure 2.16 have two peaks at the beginning and the end of each histogram; left peak represents the null power production, when the wind speed samples are lower than the cut-in speed of the wind turbine, whereas the right peak represents the rated power production, if the wind speed samples are higher than the rated speed of the wind turbine.

Worthy to mention, the two peaks left and right ones of each histogram depend on the stochastic parameters of the wind speed. If the wind scale parameter is high, then the histogram will shift to the right side much more and the frequency of the injected power will be distributed all over the horizontal axis of the injected power domain. On the other hand, if the wind scale parameter is low, then the left histogram peak will be more salient and the right histogram peak will be nearly invisible.

An important conclusion must be mentioned regarding Figure 2.16 that the distribution frequency of the total injected power to the grid differs from the total injected power by all wind generators in microgrid. Therefore, the injected power estimation into the microgrid cannot be measured by multiplying directly the injected power of one generator by number of generators connected to the grid. Regardless the losses in each branch among the microgrid nodes, the correlations among generators plays an important role in such discrepancies.

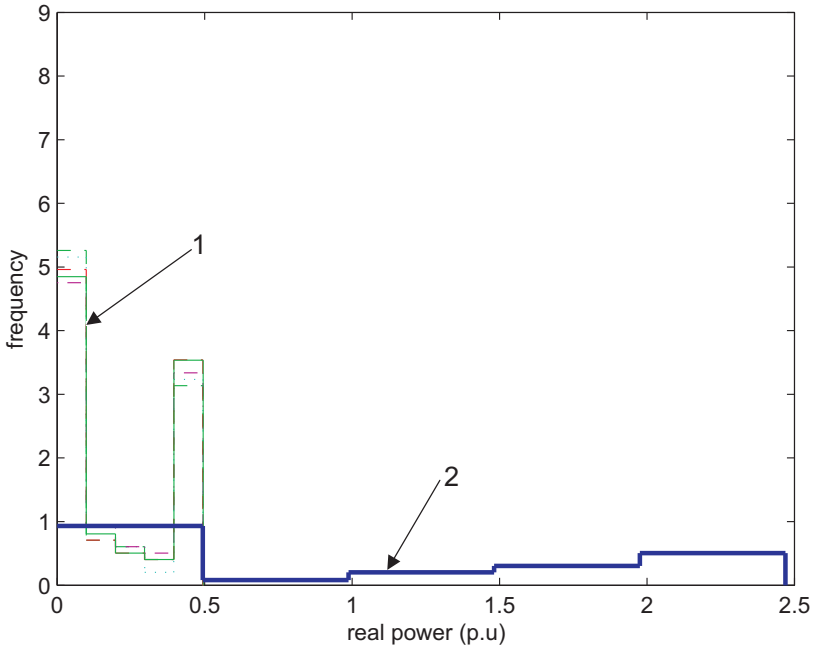

Figure 2.16: Histograms of wind turbines and microgrid power samples. Individual powers indicated by (thin lines) and aggregated injected power indicated by (blue, thick line).

Unlike many researchers who have concentrated on finding the distribution functions for wind speed samples only, the model selection criteria will be applied in the next Section to obtain the distribution fitting of the injected power to the microgrid and to indicate that distribution fittings may change depending on the mean wind speed and the wind turbine characteristic.

2.9 Model Selection

Usually, most papers have discussed the derivation of wind speed distribution functions by model selection criteria, in order to obtain the wind power samples from wind turbines curve fittings.

In this Section, the model selection criteria are conducted to infer the distribution of the output power from the wind turbines and microgrid directly. Therefore, the analysis can be used as an index for the total microgrid energy production and capacity factor, according to mean wind speeds, wind turbine

characteristics and droop constants of MSU interfaces. Consequently, an efficient model selection criterion must be adopted.

Many recent researches are concerned with the question of the model choice; researchers usually collect data in form of measurements and observations; consequently they are in need to study how such data affect the outcome. Both frequentist and Bayesian schools have discussed this issue by different methodologies, such as Spawning methods, Akaike Information Criterion (AIC), Bayesian Information Criterion (BIC) and others [80].

If there are K models, indexed by k, model k has parameters $\vartheta_k \in \Omega_k$, then the whole parameter space is $(M, \vartheta_1, \vartheta_2, \ldots\ldots, \vartheta_k)$, where M denotes the model. In each statistical model, the estimation may be thought as the choice of a single value of the parameter chosen according to some criterion to represent the distribution. There may be occasions just as with estimation in general, when one model clearly dominates the others that the choice is unobjectionable, and other occasions, when the choice is misleading.

Model selection is best seen as a way of approximating, rather than identifying full reality. The idea can be briefed by adding parameters to a model, an improvement in a distribution fitting is obtained to some degree, but at the same time the parameter estimates are worse, because less data per parameter exist.

Many techniques have been developed to cope with the difficulty of distinguishing among true statistical differences. Typically, any fitted model is never going to be a true model, and so the efficiency of a statistical modelling is based on its ability to compare large numbers of competing statistical models simultaneously.

The Information criteria balance the model complexity with a goodness-of-fit, to select a simple model with the highest predictive power in a parsimonious fashion [81]. Comparability and parsimony are basic traits in informational modelling not found in classical statistical methods.

The model selection is a classical topic in statistics, the idea of selecting a model via penalizing a log-likelihood type criterion goes back to the early seventies with the pioneering works of Mallows and Akaike.

Akaike and Bayesian methods can compare multiple nested or non-nested models, examine model uncertainty and estimate model parameters efficiently. Therefore, the two methods, Akaike Information Criterion [82] and the Bayesian

Information Criterion [83] are applied through this Chapter; the aim of these methods is to penalize the error of the model on the training data, to estimate the error on unseen cases.

The objective is to estimate distribution fittings of the injected power to the microgrid. Before proceeding in the both criteria, the error measure (likelihood) must be introduced, because both criteria AIC and BIC depend on the likelihood measure.

2.9.1 The likelihood measure

The likelihood concept is used to measure the strength of statistical evidence; it equates the amount of evidence against a null hypothesis. This measure is a probability, and so it is bounded between [0, 1], one represents the certainty that the model can generate the data set and zero represents the impossibility that this model is able to generate the data.

The likelihood measure can be represented as shown in equation (2.18).

$$l[P(X|\Theta)] = \prod_{i=1}^{N} P(x_i|\vartheta) \tag{2.18}$$

Where $l[\bullet]$ is the likelihood measure, X is the data set, x_i is a particular datum, N is the number of observations and ϑ is the list of the model parameters. The likelihood is always a very small number which results in underflow in modern computers. A good solution to the underflow problem is to use the logarithmic transformation, as shown by equation (2.19).

$$\begin{aligned} log(l[P(X|\Theta)]) &= log[\prod_{i=1}^{N} P(x_i|\vartheta)] \\ &= \sum_{i=1}^{N} log([P(x_i|\vartheta)]) \\ &= ll[P(X|\Theta)] \end{aligned} \tag{2.19}$$

Where $ll[\bullet]$ is the log-likelihood. This new function is bounded between [-∞, 0], minus infinity represents the incapacity of the model to generate the data set and zero represents the certitude that this model can efficiently generate the data. This criteria is to evaluate the error in measurements and is called *negative log-likelihood*.

2.9.2 Akaike Information Criterion

One of the most commonly used information criteria is AIC. The idea of AIC [82] is to select the model that minimizes the negative likelihood penalized by the number of parameters as shown from equation (2.20).

$$AIC = 2[-ll(data)] + 2d \tag{2.20}$$

Considering N is the number of observations and d is the number of free parameters. Only the error measure ($-ll[\bullet]$) and the number of the free parameters in the model are needed. The model which has the minimum AIC value will be chosen. AIC is aimed at finding the best approximating model to the unknown true data, while penalizing the model for its complexity.

2.9.3 Bayesian Information Criterion

The BIC [83] is similar to the AIC [82], except that it is motivated by the Bayesian model selection principle [84]. In addition to the information required to compute the AIC, the number of observations must be provided. The Bayesian has the following form:

$$BIC = 2[-ll(data)] + log[N]d \tag{2.21}$$

BIC differs from AIC only in the second term, which depends on the sample size N. The model with the smallest BIC is equivalent to the model with the highest probability. BIC can be used not only to choose the best model, but also to assess the merit of each of the tested models.

In [85], the simulation results indicated the ability of AIC to select a true model rapidly increases with the sample size, but at larger sample sizes it continued to exhibit a slight tendency to select complex models.

Contrary to AIC, BIC tends to outperform AIC in large sample size and appears to perform relatively poorly in small samples size.

By employing both AIC and BIC for obtaining the best probabilistic representation of the injected power to the microgrid, the models with the lowest AIC and BIC are considered as the best distribution probability of the micorgid power. By taking into consideration there is no unique distribution fitting for all scenarios, the distribution fitting always depends on the mean wind speeds and characteristics of wind turbines; thus, it may change from one scenario to

another.

Figure 2.17 explains the goodness of fit of the total injected power by 100 samples to the micorgrid, at scale and shape parameters of wind speed 8 and 1.4 respectively. The distribution fitting is plotted by cumulative distribution functions. Figure 2.18, explains the error between the empirical distribution and each fitted distribution.

The concept of the choice is based on choosing the minimum value of AIC and BIC as shown from Table 2.1. The minimum values record always first; such fitted distributions depend also on the stochastic parameters of the wind speed.

However, the main purpose is beyond estimation of distribution fittings of the injected power. Usually, the main reason of the wind energy analysis is always to determine the capacity factor, which wind turbines can provide, in order to evaluate their feasibilities for service. The capacity factor calculations for both wind turbines and the whole microgid will be shown in the next Section.

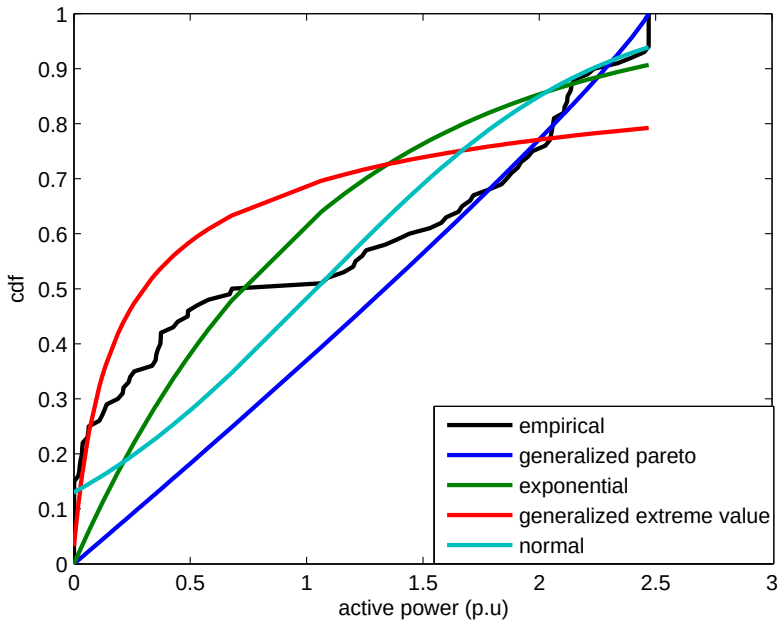

Figure 2.17: Cumulative distribution functions of the microgrid injected power processed at wind speed scale and shape parameters (8) and (1.4) respectively.

Table 2.1: Model Selection

Input weibull	
scale	8
shape	1.4
Generalized pareto	(1)
BIC	171.66
AIC	163.84
shape	-1.12
scale	2.77
threshold	0
Exponential	(2)
BIC	212.70
AIC	210.09
scale	1.04
Generalized extreme value	(3)
BIC	265.62
AIC	257.80
shape	1.89
scale	0.29
location	0.14
Normal	(4)
BIC	276.40
AIC	271.19
location	1.04
scale	0.92

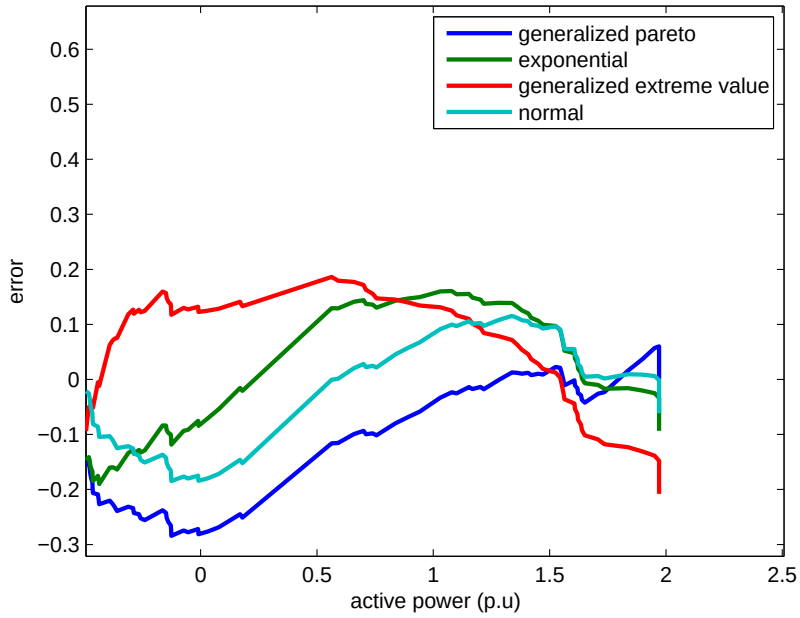

Figure 2.18: Errors between the empirical distribution and a set of fitted distirbution functions of the microgrid injected power processed at wind speed scale and shape parameters (8) and (1.4) respectively.

2.10 Microgrid Capacity Factor

As a result of continuous growth in the wind energy penetration in the power systems around the world, it has been a must to consider the capacity credits of the wind energy systems. In [86] and [87], the authors focused on the capacity credit calculations of the wind energy system, which is associated with the average wind power.

The increase in the penetration of the wind generation in the recent years has led to a number of challenges for the planning and operation of the power systems.

The power system reliability is divided into two basic aspects, system security and system adequacy as shown in Figure 2.1. The system is secure, if it can be up to a loss of power supply as generators or transmission lines. Adequacy can be attained by a set of generators probably have different characteristics; the capacity of each individual generator is the contribution that

this individual generator can ensure to overall system [88]-[89].

Adequacy can be defined as the amount of additional loads which can be served due to the addition in generation capacity, and at the same time maintaining the existing levels of reliability. The variability of the stochastic nature of wind rises the challenges must be met by wind generators.

The capacity factor (CF) of a wind generator is the ratio of the actual output turbine power over a period of time, to its full nameplate capacity output for the same period of time. For wind generation, the capacity factor depends on the probability distribution of the wind speed, also on the characteristics of the wind turbine, such as cut-in, cut-out and rated wind speeds. It is a percentage of the electrical power that a wind turbine is able to supply from an available wind at a specific wind farm.

The CF provides a summarized indication about the combined interaction between a wind generator and a site that is between the wind power curve and the stochastic wind speed. CF was introduced in other researches as a simple quotient between delivered and rated energy over a given period of time as in [90], whereas in [40] and [91], it was conducted from the mean cubic wind speed.

Through this Section, the capacity factor of the wind energy is studied to serve an important issue which is the site-matching with the isolated microgrid. The comparison between the capacity factor of each wind turbine and the capacity factor of the whole microgrid is a must, because the capacity factor of the droop-regulated microgrid cannot be considered as a large generator that is built up from several minor wind generation units, because the droop control imposes restrictions on the maximum loadability.

Table 2.2 shows a summary of the mean injected power to the microgrid, the capacity factor of the individual wind turbines and the capacity factor of the whole microgrid. The capacity factor of the wind turbines ranges from 42.3% to 45.6%, while the capacity factor of the whole microgrid records only 42.16%. Therefore, it can be concluded that the droop regulation of the MSU interfaces causes a drop in the capacity factor of the microgrid. The droop constants of MSUs play an important role in restricting the maximum power of the micorgrid. This conclusion explains the behaviour of MSU when it reaches its P_{max}, which indicates the start of frequency degradation limit. Consequently, whenever the bifurcation occurs, the microgrid can never support any more

power.

Moreover, the capacity factor of each wind turbine is different from the other turbines, and also different from the capacity factor of the whole microgrid, as shown in table 2.2. This conclusion indicates a possibility of different bifurcation limits of the microgrid, under different mean wind speeds and MSUs droop constants. The detailed bifurcation analysis will be conducted in the following Section.

Table 2.2: Microgrid Capacity Factor

Input weibull	
scale	8
shape	1.4
Enercon E40	
Mean power (p.u)	$0.19 \leq P \leq 0.215$
Capacity factor	$42.3\% \leq \text{CF} \leq 45.6\%$
Microgrid	
Mean power (p.u)	1.04
Capacity factor	42.16%

2.11 Microgrid Bifurcation Analysis

The load demand increase leads to negative consequences on voltage stability; typically, a system enters a state of voltage instability when an increase in load demand causes a progressive and an uncontrollable drop in voltage. During such instability moments, the reactive power demand may be higher than the supply reactive power and the voltage starts to decrease. Consequently, the difference between the reactive power supply and reactive power demand increases and the voltage falls to a very small value (Voltage Collapse).

Nowadays, power networks are characterised by heavy loading and operations at their maximum stable margins [92] and [93].

The continuation power flow (CPF) is a technique used to compute the stability margin, as the distance to saddle node bifurcation (SNB) from the current loading point, by increasing the loading level until a voltage, a current or a voltage stability limit is detected in the power flow model. The CPF is based on a predictor-corrector scheme to find the complete equilibrium profile or bifurcation (PV curve) of a set of power flow equations, with respect to a given scalar variable. This scalar parameter is typically known as the bifurcation parameter or loading factor.

The previous results of capacity factor in Section 2.10 can be interpreted by another way via applying CPF to the maximum microgrid loadability samples as shown in Figure 2.19. The figure explains the behaviour of MSU interfaces when restricting their P_{max}; solid line curve shows MSUs without power limits; dashed line curve shows one MSU with power limitation; and dotted line curve shows two MSUs with power limitation.

The CPF explains well the behaviour of the microgrid when tightening the power limitation of MSU interfaces, as each MSU can deliver power from zero to P_{max}, while when it reaches its P_{max}, the voltage degradation limit starts to occur. Consequently, the bifurcation occurs and the microgrid can never support any more power.

It is clear that the more restriction on power limitation, the earlier bifurcation will occur, because the voltage is continuously degraded down to a point in which a saddle-node bifurcation occurs; the same results were shown in [94].

As bifurcation limit appears under different microgrid power limits, mainly related to wind power availability, as shown in Figure 2.19. Thereby, several

simulations under different scenarios, such as different wind turbines, different wind speeds and different MSUs droop constants will be shown in the following Section, in order to clear this phenomena and observe which is the most reliable scenario, and so the microgrid can meet the increased demand.

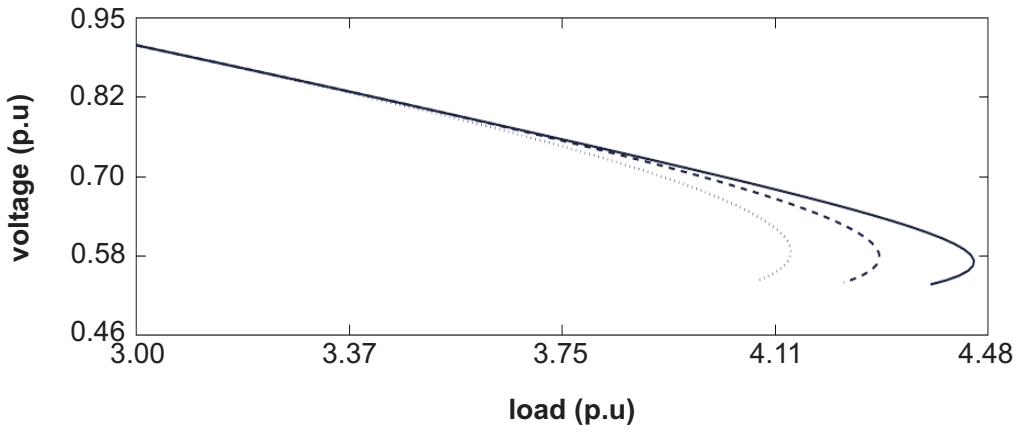

Figure 2.19: Microgrid loadability by CPF. Solid line: MSUs without power limits; dashed line: one MSU with power limitation; dotted line: two MSUs with power limitation. Source: [1]

2.12 Case Studies

Several cases are summarized in Figure 2.20, to highlight the effect of droop regulation and wind speed stochastic parameters on the microgrid capacity factor. All cases of simulations in Figure 2.20 are processed for 100 sample, based on [1]; each box represents the lower and upper quartiles (Q1 and Q3); the horizontal line within the box shows the median (Q1), while maximum and minimum values are represented by whiskers; the average value of each case is plotted by ($\diamond$), while capacity factor of each case is plotted by ($*$). The details of each case are shown hereunder:

1. Case1$\longrightarrow$ wind speed scale and shape parameters: 8, 1.4 respectively, while the droop regulation constant is 0.5 of the base droop, and the employed wind turbines are Enercon E40-600 kW;

2. Case2$\longrightarrow$ wind speed scale and shape parameters: 8, 1.4 respectively, while the droop regulation constant is 0.25 of the base droop, and the

employed wind turbines are Enercon E40-600 kW;

3. Case3⟶ wind speed scale and shape parameters: 8, 1.4 respectively, while the droop regulation constant is 0.1 of the base droop, and the employed wind turbines are Enercon E40-600 kW;

4. Case4⟶ wind speed scale and shape parameters: 8, 1.4 respectively, while the droop regulation constant is 0.5 of the base droop, Enercon E40-600 kW turbines located at nodes 12 and 14 had been replaced by Vestas V52-850 kW;

5. Case5⟶ wind speedscale and shape parameters: 8, 1.4 respectively, while the droop regulation constant is 0.25 of the base droop, Enercon E40-600 kW turbines located at nodes 12 and 14 is replaced by Vestas V52-850 kW;

6. Case6⟶ wind speed scale and shape parameters: 8, 1.4 respectively, while the droop regulation constant is 0.1 of the base droop, Enercon E40-600 kW turbines located at nodes 12 and 14 is replaced by Vestas V52-850 kW;

7. Case7⟶ wind speed scale and shape parameters: 4, 1.4 respectively, while the droop regulation constant is 0.1 of the base droop, and the employed wind turbines are Enercon E40-600 kW;

8. Case8⟶ wind speed scale and shape parameters: 4, 1.4 respectively, while the droop regulation constant is 0.1 of the base droop, Enercon E40-600 kW turbines located at nodes 12 and 14 is replaced by Vestas V52-850 kW;

9. Case9⟶ wind speed scale and shape parameters: 6, 1.4 respectively, while the droop regulation constant is 0.1 of the base droop, and the employed wind turbines are Enercon E40-600 kW;

10. Case10⟶ wind speed scale and shape parameters: 6, 1.4 respectively, while the droop regulation constant is 0.1 of the base droop, Enercon E40-600 kW turbines located at nodes 12 and 14 is replaced by Vestas-V52 850 kW.

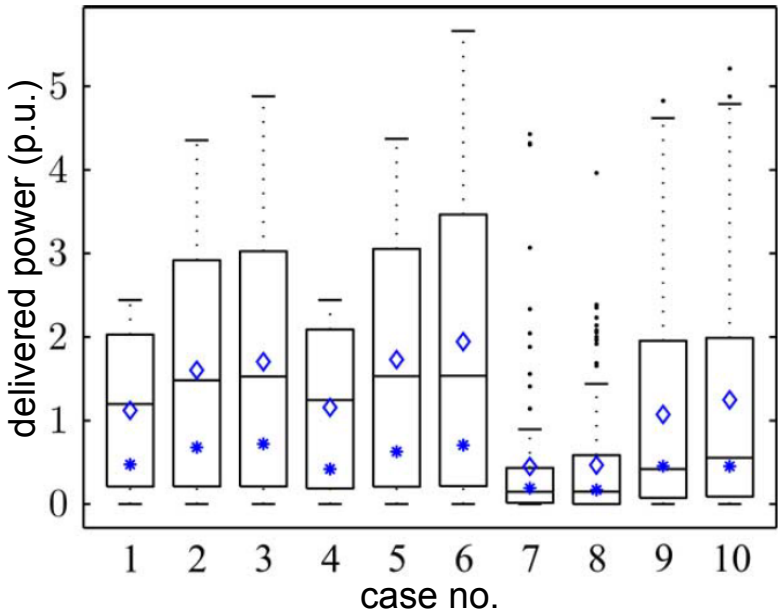

Figure 2.20: Box plot of several scenarios.

The cases from one to three explain the gradual increase in the maximum power limitation of each MSU; as shown, the highest limitation occurs when the droop is high, as in the first case. Thus, both the average power and capacity factor are lower than the third case, because the droop of MSUs is the highest among the three cases.

The cases from four to six ensure again the same results obtained from cases one to three, as some of wind turbines are replaced by higher capacity wind turbines. Therefore, the results as shown from Figure 2.20 indicate the mean power and the capacity factor of the cases four to six are slightly higher than their correspondents of the cases from one to three. By decreasing the MSUs droops, the capacity factor and the average power rise again.

One of the interesting results that the cases nine and ten, where the wind scale parameter equals six have average power and capacity factor higher than cases one and two, where wind scale parameter equals eight. The clue of this conclusion can be verified, as both the first and second cases show a higher restriction on MSUs by high droops, and this conclusion clears the dramatic effect of the high MSU droop constant.

The previous cases show the effect of changing the droops of MSU interfaces, as the highest droop leads to the highest restriction on the delivered power. The conditions are different in cases seven to ten, as the parameters

which are tested through these cases are the stochastic parameters of the wind speed. The scale parameter is reduced to four in cases seven and eight, while in cases nine and ten the scale parameter is six. Figure 2.20 shows the lowest scale parameter causes a dramatic fall in the average power and the capacity factor of the grid.

Regarding Figure 2.20, it is clear that the delivered power varies according to the wind turbines characteristics, the mean wind speed and the MSUs droop constants.

The results of this Chapter show that the capacity factor of droop-regulated microgrids supplied by wind generators depends on some terms, such as wind speed stochastic parameters, droop regulation values of MSUs and the characteristic of wind turbines. Unlike conventional generation units, where the capacity and reserve of each conventional generator is known in advance, the capacity and reserve of a microgrid supplied by wind turbines are vital issues, as it affects both the stability and economic performance of the whole microgird.

In Chapter3, the idea of site matching suitability for droop-regulated microgrids supplied by wind generators and different energy storage systems is more detailed, by considering analysis for both energy production and economic evaluations.

Chapter 3

Benefit Evaluation of Microgrids Using Capacity Factor and Economic Analysis

3.1 Introduction

In rural areas, it is very difficult as well as uneconomical to transmit power over long distances through transmission lines to supply such areas. The lack of an electrical network to supply remote areas, high connection cost of grid extension and rough topography often leads to other options to supply energy.

Stand-alone hybrid systems which are dependent on renewable sources are found promising ways to satisfy the energy supply requirements for these areas [95].

The need for efficient electric power sources in remote locations is a driving force for research in hybrid energy systems [96].

In [97], the research focused on economical drawbacks of supplying energy to rural areas, as in the case of Alaskan communities. Alaskan communities pay economic penalties for electricity, because they import diesel as a primary fuel for electric power production, paying heavy transportation costs. In addition, the local negative environmental impact caused by excessive consumption of fossil fuels. In these remote locations, renewable resources and advanced technologies, coupled with energy storage systems, can compete efficiently with conventional generation sources.

The wind power is considered as one of the main possible energy sources

in operation of rural areas, similarly to microgrids. The huge growth in the wind power utilization through last years, environmental concerns and the rising cost of fossil fuel generation in many developing parts of the world have led the energy cost of the wind power to fall one seventh of the cost in the early 1980s [98]. In the United States, the wind energy production has shown average annual growth 24% during the past 5 years [99]. Also in Europe, the growth of wind energy production has shown extraordinary records before 2010 [100].

Typically, the cost of conventional electricity production is determined by three main components: (1) Fuel cost. (2) Operation and maintenance costs. (3) Capital cost.

When conventional generation units are substituted by wind energy, the avoided energy cost by wind power depends on the degree to which wind power substitutes each of the three components.

In general, wind energy avoids the full fuel cost and a considerable portion of Operation and maintenance costs of the displaced conventional units. However, the level of avoided capital costs depends on the extent to which wind power capacity can displace the conventional units, and so this level is directly related to the capacity factor of wind plants [55].

However, the drawbacks of the wind power production is based mainly on the uncertainty nature that it is unpredicted source of energy, and so the wind power production cannot be estimated accurately.

Wind speed is characterized by its high variability *spatially and temporally.* Therefore, the planners and the operators of the wind plants are concerned about the effect of the wind speed variation on the operating costs of the systems. The system must maintain the balance between the demand and total generated power from the wind energy. The costs associated with maintaining this balance are referred as to ancillary-services costs [101].

With the market liberalization and occurrence of competitive markets, vital questions are always conducted regarding the optimum economical sizing of intermittent wind generators, to contribute to supplying microgrids with constraints of power quality. For this sake, technical and economic analyses of wind energy sources are necessary, in order to meet the requirements in competitive markets.

In the new model of power markets, the plant dispatch is performed by

independent system operators, and the contracts between generators and customers are either negotiated bilaterally or accomplished through power pools, this subsequently means a drastic increase in risk for generators [102]. Hence, the investors tend to favour generation technologies characterised by low capital costs, such as gas turbines, despite their high operating costs. Consequently, the wind energy, which is characterised by high capital cost, is hurt by the shift to low capital cost technologies.

Moreover, in a competitive market, the generators must submit bids a week, day or hour in advance, offering to provide a given quantity of generation at a given price during a particular hour. The failure to meet the committed generation capacity as declared on the previous day is penalised.

As the wind is a fluctuating energy source, the viability of wind power in day-ahead markets is highly dependent on several factors, such as accurate wind speed forecasting, degree of penalties charged by the market operator to generators which are unable to meet their commitments and finally the wind generators efficiencies to provide power reserves as much as possible [103].

As a result, there is a growing difficulty for financing wind power projects in the absence of a guaranteed long-term revenue stream, leading to a serious challenge for continued wind power development.

This chapter performs several economic evaluations and capacity factor analysis for microgrids, supplied by wind energy and energy storage systems, in order to show a clearer perspective of the most efficient generation profiles from both economic evaluation models and generation capacities views. These profiles can be adopted to enhance and promote the wind energy contributions in competitive markets.

In this Chapter, the results of economic evaluations and energy productions are illustrated; moreover, pie charts are shown, to explain the daily power generation percentage, distributed between the load demand and system reserve unit, to clarify the ability of microgrids supplied these generation sources to meet load demands and provide power reserves as well.

In general, the most efficient wind turbine might not be the most effective for transforming wind power into electric power on a specific site, and so the main goal is to maximize the wind annual energy production [39]. The energy production of a wind turbine depends on several factors, such as wind speed conditions from the area and the characteristics of the wind turbine itself, in-

cluding the cut-in, rated and cut-off wind speed parameters.

The suitability of a wind turbine to a specific location is given by the capacity factor. The selection of optimal wind turbines has been discussed in some papers based on maximization of the capacity factor [40]. The choice of turbines involves choosing parameters that lead to maximizing this factor.

In conclusion, the optimization of the wind turbine components leads to magnifying the wind turbine output and contributes to a reduction of the cost of energy [104], which is the main parameter used to compare economic performances of systems.

In addition, other studies have been conducted regarding site matching of wind turbines. The site matching is based on identifying optimum turbine parameters to yield higher energy production at higher capacity factor.

The matching of a wind turbine to a site using normalized power and capacity factor curves were discussed in [40], but in general the economic considerations of the turbine are not provided through wind site matching studies.

Other studies have focused on the matching of wind turbines to wind farms from the viewpoint of both performance and economic considerations, as in [41] and [42].

However, for isolated microgrids, storage systems are always required to share microgrids supply with wind energy sources, as the generation must always be as close as possible to system loads. The problem of keeping the power balance is still more difficult for stand-alone microgrids supplied by intermittent generators. The characteristics of such grids require scheduling more reserve for ensuring adequate security and reliability levels, but the higher reserve requirements may substantially deteriorate the economy of these supply systems. The total requirements for these storage systems are unclear at present, because most of the recent studies which have optimized the capacity factor and economics of wind energy production, have not taken into consideration the operation of storage systems that share supply with wind energy. Thus, the optimum point of operation is totally different when considering the dynamics of storage systems.

The performance and economic aspects of such storage systems are significant and must be brought into the economic evaluation, so the microgrid can work at optimum conditions in terms of investment and power system reliability requirement.

Therefore, the proposed study of this Chapter is based on optimizing both energy production and economic performance for isolated microgrids supplied by wind energy and various batteries, by a multi-objective function. The optimization function in this Chapter is conducted to minimize the Cost of Energy (COE), which is a function of both capital costs and energy production of the generation sources. Hence, the maximum possible energy production and the lowest cost of energy can be ensured, taking into consideration the droop regulation of microgrid interfaces and the dynamic operation of the batteries (charging-discharging). Moreover, the economic analyses are performed also by Simple Payback (SPB) and Net Present Value (NPV).
Before conducting the proposed simulations, the sources of data which are used through this Chapter will be shown in the following Section.

3.2 Sources of Data

The sources of data include the layout of the proposed microgrid, the droop regulation of MSUs by *Fischer-Burmeister* algorithm, the daily operation of the batteries, the characteristics of several wind turbines and finally the employed economic evaluation models in the Chapter.

3.2.1 Microgrid Layout

The layout of the microgrid is shown in Figure 3.1. The power and frequency of MSUs are regulated by droop constants: (9.4×10^{-6} rad/W/s); the base power of the microgrid is 900 kW; the rated power of each MSU is 5 p.u. The main configuration of the microgrid is briefed by the following points:

- Fourteen nodes distribution system;
- Three wind turbine at nodes (6, 12 and 14), the rating of these turbines will be set according to purpose of each simulation and will be specified in the following Sections;
- Three microgrid supporting unints supplied by Lead Acid batteries at nodes (1, 4 and 8);
- Distributed static loads at all microgrid nodes;

- Group of aggregated motors at node (4);
- System Reserve Unit (SRU); the function of SRU is to store the excess of generated power by wind turbines or MSUs, if the generated power is higher than the load demand. The stored power in SRU can be used in case of power shortfall or to charge the batteries.

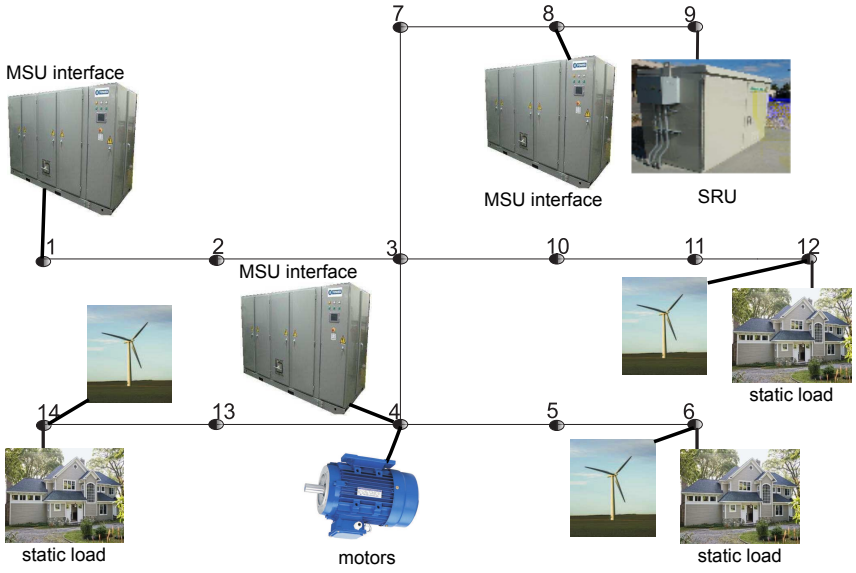

Figure 3.1: Microgrid layout

3.2.2 Droop Regulation by Fischer-Burmeister

Microgrids with a large number of MSUs may suffer from reactive power oscillations without proper voltage control. Voltage control function of MSUs alleviates the large circulating reactive currents amongst MSUs. The circulating currents can be controlled by using voltage-reactive power $v - Q$ droop controllers. In addition, the MSUs employ a local $P - \omega$ control to change the operating point, in order to achieve a local power balance among MSUs.

Equations (3.1) and (3.2) explain the operational characteristic of the MSUs droop regulation, where ω is the operating frequency, ω_{max} is the maximum frequency, P is the active operating inverter power, Q is the reactive operating inverter power, m_p is the active droop constant and n_q is the reactive droop constant.

$$\omega_0 - \omega_1 = -m_p(P_1 - P_0) \tag{3.1}$$

$$v_0 - v_1 = -n_q(Q_1 - Q_0) \tag{3.2}$$

The droop formulation depends on two possible states (with and without power limit reached). In the first state, the generated power P_g is less than the maximum limit of power generation P_g^{max}, whereas the second state considers the generated power as constant, because the power limit is reached. The frequency can freely vary in both states, searching for an equilibrium in the load share among all the generation units. The problem can be reformulated by equation (3.3).

$$f = \begin{cases} P_g^{max} - P_g & \text{if } P_g^{max} \geq P_g. \\ \omega^0 - \omega + m_p(P_g^0 - P_g) & \text{if } P_g < P_g^{max}. \end{cases} \tag{3.3}$$

By assuming the following variables:

f: Represents an equation of the microgrid model;

P_g^0: Nominal power of MSUs, where the frequency is nominal;

ω^0: Nominal value of frequency;

ω: Equilibrium point of frequency.

The problem of droop formulation in a microgrid lies in that the equilibrium power of a droop-regulated generation source that decides which is the state that will be active upon the operating point computation is not known in advance, because it is dependent on the equilibrium power of other droop-regulated generation sources owning different settings and nominal values, which means that the solution by Newton-Raphson-like methods might be hindered.

The applied methodology through this Chapter employs *Fischer-Burmeister* algorithm based on nonlinear complementarity problem (NCP), as in [105], by substituting the piecewise droop function by only a scalar function. Thus, the provided algorithm solves the problem easier by less iteration process to find the equilibrium point. The NCP reformed equation (3.3) to equation (3.4).

$$0 \leq (P_g^{max} - P_g) \perp [\omega^0 - \omega + m_p(P_g^0 - P_g) \geq 0] \tag{3.4}$$

Equation 3.4 can be formulated by means of Fischer-Burmeister function, as $\Psi : R^2 \rightarrow R$ satisfying:

$$\Psi(a,b) = 0 \Leftrightarrow a \geq 0, b \geq 0, ab = 0 \tag{3.5}$$

Where $b = P_g^{max} - P_g$ and $a = \omega^0 - \omega + m_p(P_g^0 - P_g)$. Equation (3.5) which is general formula of NCP can be reformulated by Fischer-Burmeister as shown in (3.6).

$$\Psi(a,b) = \sqrt{a^2 + b^2} - (a + b) \tag{3.6}$$

3.2.3 Daily Operation of Batteries

The daily operation of the batteries must be verified to ensure that every day the batteries start supplying loads with the same capacity as the previous day.
Typically, each battery is rated to a certain capacity (kW) and feeds MSUs, which are tuned by droop rules of $(P - \omega)$ and $v - Q$. Each MSU has a maximum power constraint P_{max}, which the inverter can never surpass.

During the first daily simulation sample, the maximum power constraint P_{max} must be equal to the rated capacity of each battery, but after each sample, if the battery discharges, the maximum power constraint of the inverter P_{max} must be subtracted from the consumed energy of the battery, till the battery depth of discharge is higher than 0.99 and the maximum power constraint nearly equals zero. Thus, the battery must be out of service for the charging process.

During the charging process of the battery, the wind turbines or other discharging batteries can supply the charged battery till the maximum power constraint equals to the rated capacity of the charged battery again.

Usually, the energy is stored in the form of electrochemical energy in the batteries, in order to obtain the desired voltage and capacity. A Battery consists of a set of cells connected together in series, parallel or both. Each cell consists of two conductor electrodes and an electrolyte, placed together in a special sealed container and externally connected to a source or load. The electrolyte enables the exchange of ions between the two electrodes, while the electrons flow through the external circuit.

The charging-discharging battery process is based on [106] and must com-

ply with the following equations:

$$\begin{aligned} Discharging: \;\; C_{st_{bat}}(t+1) &= C_{st_{bat}}(t) - \Delta t P_t^{E_d/\eta_d} \\ Charging: \;\; C_{st_{bat}}(t+1) &= C_{st_{bat}}(t) + \Delta t P_t^{E_c/\eta_c} \end{aligned} \tag{3.7}$$

Subject to the following power Limits:

$$\begin{aligned} 0 \leq P_t^{E_d} \leq P_E^{d_{max}} \\ 0 \leq P_t^{E_c} \leq P_E^{c_{max}} \end{aligned} \tag{3.8}$$

Stored energy limits:

$$C_{bat_{st_{min}}} \leq C_{bat}(t) \leq C_{bat_{st_{max}}} \tag{3.9}$$

By assuming the following variables:

$P_t^{E_d}$: Power discharged by the battery bank during the time period (t);

$P_t^{E_c}$: Power charged by the grid to the battery bank during the time period (t);

$C_{st_{bat}}$: Energy stored in the battery bank;

Δt: Duration time of each interval;

η_d: Discharge efficiency;

η_c: Charge efficiency;

$P_E^{d_{max}}$: Maximum discharge rate;

$P_E^{c_{max}}$: Maximum charge rate;

$C_{bat_{st_{min}}}$: Minimum stored energy;

$C_{bat_{st_{max}}}$: Maximum stored energy.

Worthy to mention that during the first and last sample every day, the consumed energy of each battery must be zero, and the remaining capacity must equal to rated capacity of the corresponding battery.

The daily operation of the battery is shown by Figure 3.2, the figure explains the charging-discharging process of a simulated battery, taking into consideration that the simulation is processed at base power equals to 150 kW.

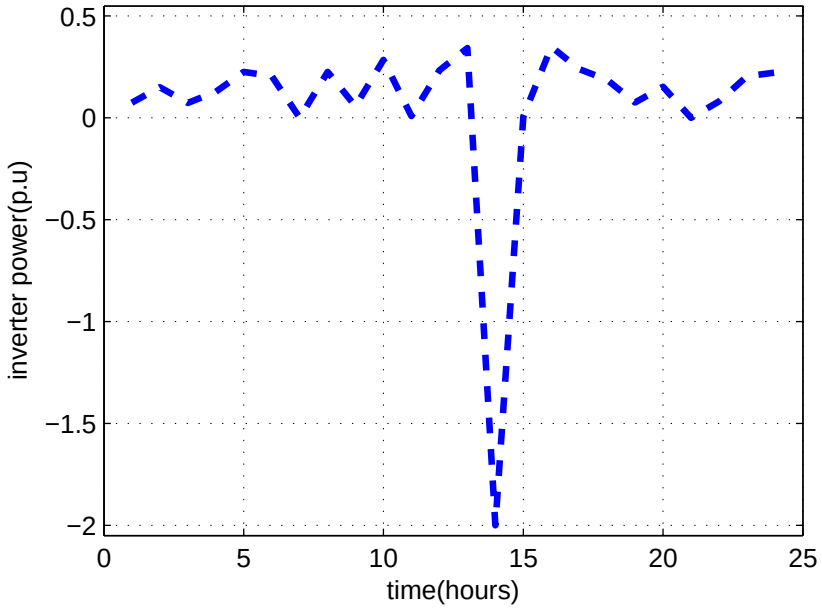

Figure 3.2: Daily battery charging-discharging process

3.2.4 Wind Turbines Characteristics

Typically, the wind turbine is classified by the cut-in speed, rated speed and fluring speed that complies with equation (3.10). Through this Chapter, several turbines are simulated as shown in Table 3.1.

The daily operation of each turbine is shown in Figure 3.3. When the wind turbine power is higher than demand load, the rest wind power will be transferred to the SRU, to be used later in case of higher load demand, or to charge batteries.

$$P_{wt} = \begin{cases} P_{rated}\frac{(w^2 - w_i^2)}{w_r^2 - w_i^2} & \text{if} \quad w_i \leq w \leq w_r. \\ P_{rated} & \text{if} \quad w_r \leq w \leq w_f. \\ 0 & \text{if} \quad otherwise. \end{cases} \tag{3.10}$$

By assuming the following variables:

P_{wt}: Instantaneous wind turbine power;

P_{rated}: Rated power of wind turbine;

w: Instantaneous wind speed sample;

w_i: Cut-in speed of the turbine;

w_r: Rated speed of the turbine;

w_f: Fluring speed of the turbine.

Table 3.1: Wind Turbines Characteristics

Turbine	Rated power kW	Cut-in speed	Rated speed	fluring speed
Enercon-E33	330	3	13	28
Enercon-E40	600	2.5	12.5	28
Enercon-E44	900	3	16	28
Enercon-E82	2000	2	13	28
Vestas-V80	1800	4	15	25

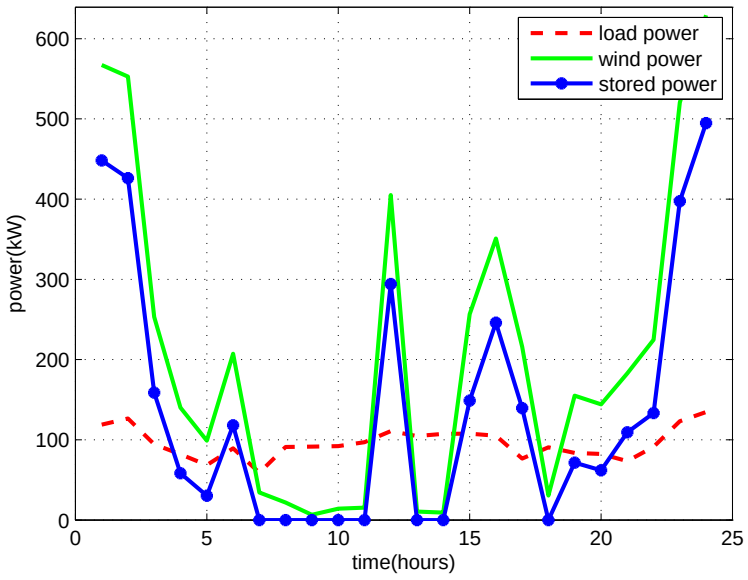

Figure 3.3: Daily operation of wind turbines

3.2.5 Economic Evaluation Models

Usually, the economic evaluation provides a framework for a specific decision and considers both the effectiveness and cost data for two or more comparative technologies being compared within the analysis. The choice to evaluate an investment is determined by several factors, these factors include the investor's perspective, regulation, risk, financing, cash flow, comparison of mutually exclusive alternatives, similarity of alternative benefits and whether the investment is fully defined in terms of its size and use.

Most economic measures are valid for most investments, and it is usually a good idea to compute several of the measures to better evaluate the investment. Economic evaluation has usually been implemented by different models.

The selection criteria guide is based on suggesting which economic measures are the most appropriate for a specific analysis. Different economic measures apply to different situations, and it is generally a good idea to use several measures when evaluating an investment.

In this Chapter, comprehensive economic evaluations for several case studies of microgrids supplied by wind turbines and batteries are explained, to show the most feasible case for the microgrid. The main concern regarding the economic evaluation belongs to cost of energy analysis (COE), but other economic evaluation models, such as simple payback (SPB) and net present value (NPV) are also conducted, in order to determine the profitable gains of each generating unit. Moreover, it is an asset, because most researches have considered cost of energy issue only.

Levelized Cost of Energy

The levelized cost of energy is the cost of producing one kilowatt-hour (kWh) of electricity including some items, such as the total cost of the generating plant, operating the plant over its life time, the financing costs, the return on equity and the depreciation factor. COE is a keen method to compare technologies and designs of different generation infrastructures. The applied COE model for wind turbines is based on [107] and is represented by equation (3.11).

$$COE = \frac{FCR \times C_{wp} + LRC + C_{O\&M}}{AEP_{wt}} \tag{3.11}$$

While, The applied COE model for batteries is represented by equation (3.12).

$$COE = \frac{FCR \times C_{bat} + C_{O\&M} + UC_e}{AEP_{bat}} \tag{3.12}$$

By assuming the following variables:

FCR: Fixed rate of charge, assumed as 0.1;

C_{wp}: Capital cost of wind turbine;

AEP_{wt}: Wind turbine annual energy production in kWh;

AEP_{bat}: Battery annual energy production in kWh;

C_{bat}: battery capital cost;

UC_e: Unit cost of input electricity for charging batteries;

$C_{O\&M}$: Annual operation and maintenance cost;

LRC: Levelized replacement cost.

Through current study, LRC of wind turbines is assumed zero, as it is originally a little value and approximated to 0.7% of the C_{wp} [107]. Therefore, by ignoring this term, the COE would result in the same design as minimizing SPB. The fixed charge rate FCR is the annual amount per dollar of the initial capital cost needed to cover the capital cost items, such as debt payments and return on equity. In this thesis, FCR is assumed as 0.1; moreover, the thesis assumes a constant operation and maintenance cost of 0.007\$/kWh for wind turbines, based on [107]. In addition the annual operation and maintenance cost for batteries ranges from 2\$/kW-year to 15\$/kW-year, according to the battery type, based on [108] and [109], whereas the variable operation and maintenance cost for batteries are neglected. The unit cost of input electricity for charging batteries is assumed as 0.1\$/kWh, according to [110].

For simplicity, the numerator terms of equations (3.11) and (3.12) will be referred in the following Sections as $F_{wt}(E_{wt})$ and $F_{bat}(E_{bat})$ respectively.

The AEP corresponds to the integral of the power which is injected into the grid over a year, taking into consideration that this thesis adopts an average availability of 0.9 for wind turbines. Thus, the annual energy production of a wind turbine depends on the turbine power output and the probability of

wind speed.

The levelized cost of energy mentioned in this Section has some limitations, such as it does not allow for variable equity return and assumes that the debt-term lifetime equals to the lifetime of equipments.

Simple Payback

Another economic measure of generation plants is to consider the time-dependent valuation of the electricity in determining the optimal design; typically, COE is not indication to this issue. Thereby, another measure must be considered. Simple payback (SPB) is the number of years which the plant takes to recover the initial capital cost of an investment, without discounting future profits [42]; SPB is calculated as shown in equation (3.13).

$$SPB = \frac{C_{wp}}{AAR} \tag{3.13}$$

By assuming the following variables:

C_{wp}: Initial capital cost;

AAR: Average annual revenue based on hourly production,

and calculated from equation (3.14).

$$AAR = CF \times T \times P_{rated} \times COE \tag{3.14}$$

Considering the following variables:

CF: Capacity factor of wind turbine;

T: Time in hours;

P_{rated}: Rated power of turbine;

COE: Levelized cost of energy.

The model assumes the wind turbine will produce the same amount of electricity each year. As the simple payback does not consider the discount rate or life of the project, the optimal design obtained using simple payback analysis will not be dependent on these values.

Net Present Value

The Net present value (NPV) is another model for economic evaluation which takes into consideration the time value of money, as money value of today will worth more some years later. Any amount of money to be invested backs a return higher than the rate of inflation. Therefore, the future profits must be discounted. NPV is considered as the present value of benefits minus the present value of costs [111].

The present value of the costs is the initial capital cost C_{wp}, assuming that the wind power production is the same from year to year, considering the produced electric energy and annual revenue are always constant from year to year, and so the uniform cash flow must be discounted as it occurs in the future. NPV is calculated as shown by equation (3.15).

$$NPV = AAR \times \left(\frac{(1+i)^L - 1}{i(1+i)^L} \right) - C_{wp} \tag{3.15}$$

By considering the following variables:

i: Discount rate;

L: Life time of wind turbine in years;

C_{wp}: Initial capital cost;

AAR: Average annual revenue.

Usually, the profitable project is based on maximizing the value of NPV to be greater than zero. If there is a comparison between two mutually exclusive projects, the one with highest NPV will be chosen, taking into consideration both discount rate and investment life of the project are effective items in any profitable project, as they directly affect the optimal design of a wind turbine.

All the mentioned economic evaluations models in this Section will be directly applied to the all simulated microgrids in this Chapter, for the purpose of determining the economic performance of microgrids supplied by wind energy and energy storage systems.

The mentioned sources of data in this Section will be used later for the economic evaluations and capacity factor analysis of several microgirds. As mentioned before, the purpose of this Chapter is to optimize both the energy

production and economic performance for isolated microgrids supplied by wind turbines and batteries.

However, the optimization process must start by optimizing the characteristics of wind turbines to be installed at microgrids firstly. Next Section will show an interesting manner for optimizing the wind turbine specific rating.

3.3 Economic Evaluation for a Scaled Down Wind Turbine

The energy production from a wind turbine depends on some factors, such as wind speed conditions from the area and the characteristics of the wind turbine itself, including the cut-in, rated and cut-off wind speed parameters.

The turbine of high power rating might not be the most effective for transforming wind power into electric power on a specific site, and so the main goal becomes the maximization of the annual energy production [39], or the minimization of the cost of energy [107].

In [112], the author proved that cost of energy optimization is possible since an annual energy production can be obtained with different turbine designs and the one should be chosen where the cost of energy is the minimum.

The turbine rotor diameter is the main element which determines the turbine size, energy production, and subsequently its capital cost [107].

The cost model of the wind turbine is suitable for extrapolation in terms of the rotor diameter (D) and rated power, and is shown by Table 3.2, based on [107]. The cost model is used to calculate the cost of turbines with rotor diameters from $D = 20$ m to $D = 200$ m and rated power up to 10 MW [112].

Thus, if the components of the turbine can be scaled down, mainly the rotor diameter, then minimizing the wind turbine capital cost will be possible. The optimal wind turbine rating for a given application is determined by the wind turbine rating ratio (r_r): the ratio of the turbine rated wind speed w_r to the mean speed of the wind regime w_{avg} [113].

Figure 3.4 shows the power curve of turbines with reduced rating ratios have more spacious area between the rated turbine speed and cut-out speed; each zone shown in this figure explains a different value of the rating ratio r_r. Therefore, the scaled down turbine, which has lower r_r spends more time

to produce power at rated capacity and it is more capable to produce higher capacity factor than other turbines of higher r_r. Moreover, Figure 3.5 explains that wind turbine capital cost decline with reduction of the rating ratio, based on [113].

The objective of this Section is to scale down a wind turbine and to check this effect on its cost of energy and annual energy production.

The simulation scenario consists of two steps:

1. Scaling down a wind turbine by minimizing its capital cost;
2. Minimization of the energy cost of both wind turbines and batteries, which share supply the proposed microgrid, as shown Figure 3.1.

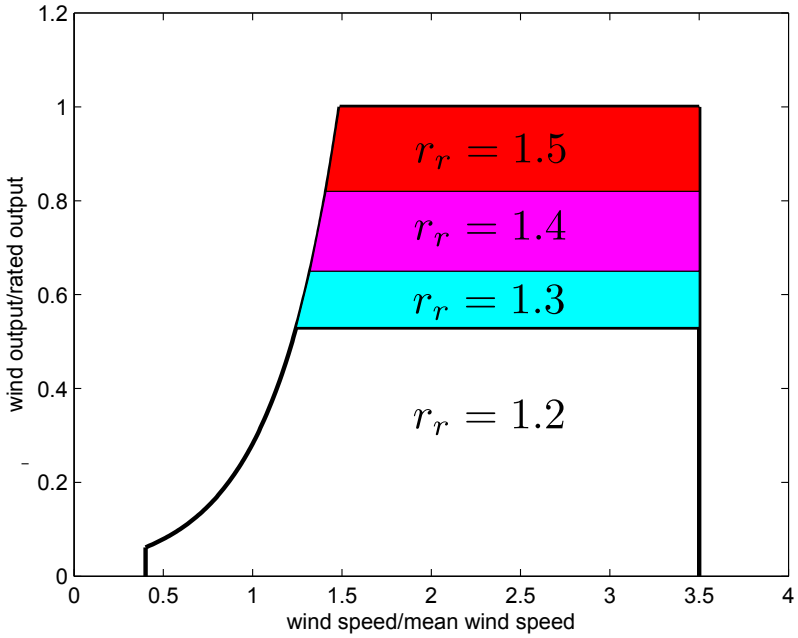

Figure 3.4: Wind turbine output power according to several rating ratio values

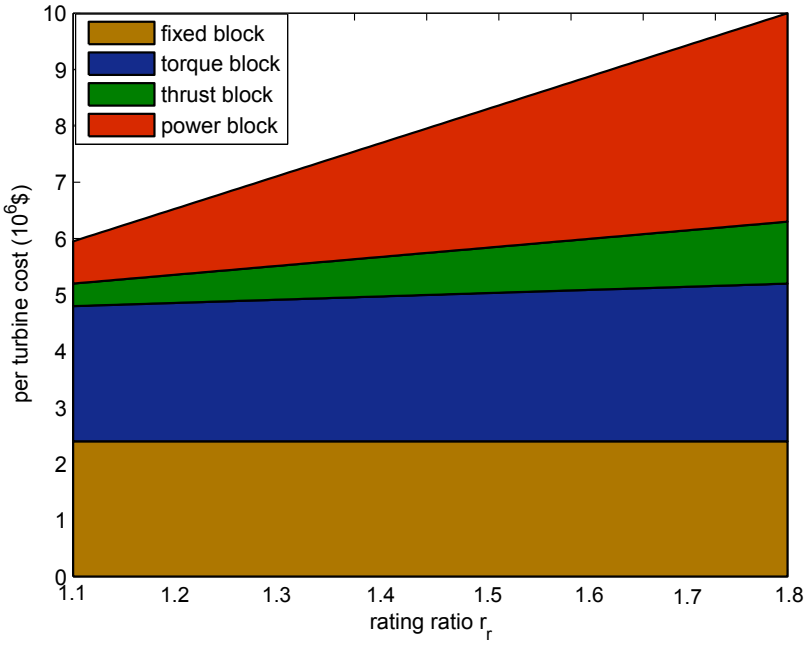

Figure 3.5: Wind turbine capital cost vs rating ratio

Table 3.2: Items of Wind Turbine Capital Cost

Item	Equations
Blade	$0.0703\times D^3 + 0.6781\times D^{2.5025}$ - 29471
Hub	$0.0817\times D^{2.53} + 5680.3$
Pitch system	$0.4802\times D^{2.6578}$
Bearing	$1.2267\times10^{-4}\times D^{3.5}$ - $3.0360\times10^{-4}\times D^{2.5}$
Brake	$1.9894\times P_{rated}$ - 0.1141
Generator	$219.33\times P_{rated}$
Yaw system	$0.0678\times D^{2.964}$
Main frame	$627.28\times D^{0.85}$
Railing Platform	$1.3354\times D^{1.953}$
Electric connections	$40\times P_{rated}$
Cooling	$12\times P_{rated}$
Nacelle	$11.537\times P_{rated} + 3849.7$
Tower	$0.2116\times H\times D^2 + 2669$
Foundation	$275.06\times(H\times D^2)^{0.4037}$

Table 3.2: Continued-Items of Wind Turbine Capital Cost

Item	Equations
Roads	$2.17\times10^{-6}\times P_{rated}^{2}$ - $0.0145\times P_{rated}$ + 69.54
Assembly	$1.965\times(\mathrm{H}\times\mathrm{D})^{1.1736}$
Converter	$79\times P_{rated}$

Where:

D: Rotor diameter;

P_{rated}: Rated power of the turbine;

H: Height of the turbine.

3.3.1 The First Step of Optimization

The first optimization step in this Section is to scale down a wind turbine, by minimizing its capital cost at a specific base load power. The objective function for this purpose can be conducted as follows:

$$min \sum C_{wp}(D, P_{rated}) \tag{3.16}$$

By assuming the following variables:

C_{wp}: Capital cost of wind turbine, as function of turbine diameter D and the rated power;

P_{rated}: Rated power of each wind turbine;

D: Diameter of each wind turbine.

The optimization solver is run at average wind speed 4 m/s, and reaches to a turbine of 40 m diameter and rated power 600 kW, which coincides with Enrecon-E40 600 kW.

3.3.2 The Second Step of Optimization

It is important to evaluate the effect of scaling down a wind turbine on the energy production and economic performance. Several elements must be taken into consideration, as initial capital cost (ICC), operations and maintenance cost $C_{O\&M}$ and annual energy production (AEP).

The impacts of scaling down a wind turbine are not clear; for example, decreasing ICC of the wind turbine may reduce its AEP. If one step does not balance out the another one, the proposed scaled down wind turbine may actually has a negative effect. It is necessary to study the impact of scaling down a wind turbine on energy production and economic performance. Therefore, a comparative simulation study between the scaled down turbine (Enercon-600 kW) and another turbine with higher rating which is chosen to be (Enercon-900 kW) is conducted, to minimize the cost of energy.

A wind speed time series of average value 4 m/s and a duration curve of load demand are applied for the proposed comparative simulation. Thus, the cost of energy is minimized during every time series sample. The purpose of this step is to force the wind turbine and batteries to produce the maximum available power at the lowest cost of energy. The objective function of this step is shown by equation (3.17).

Figure 3.6a shows the curve fitting of Enercon-600 kW; Figure 3.6b shows the curve fitting of Enercon-900 kW. The diamonds in Figure 3.6 indicate the manufacturer data.

$$min \sum_{i=1}^{n} \left(\frac{F_{wt}(E_{wt})}{E_{wt}} + \frac{F_{bat}(E_{bat})}{E_{bat}} \right) \tag{3.17}$$

By assuming the following variables and parameters:

E_{bat}: Energy production of the battery;

E_{wt}: Energy production of the wind turbine;

$F_{wt}(E_{wt})$: Wind turbine cost function;

$F_{bat}(E_{bat})$: Battery cost function.

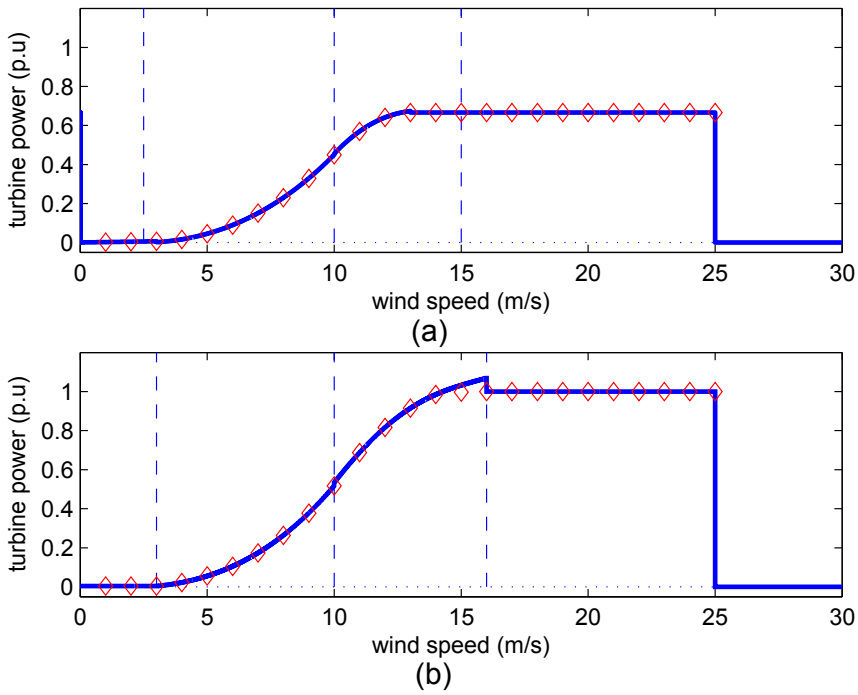

Figure 3.6: Wind turbines curve fitting: (a) Enercon-600 kW. (b) Enercon-900 kW

3.3.3 Optimization Results

From Table 3.3, it can be concluded that the decision of choosing (Enrecon-E40 600 kW) is more optimal than choosing (Enrecon-E44 900 kW), from the energy production and economic evaluation view.

The capital cost, cost of energy and simple pay back of the 600 kW turbine are lower than the correspondent results of the 900 kW turbine. Moreover, the net present value, capacity factor and annual energy production of the 600 kW turbine are higher than the correspondent results of the 900 kW turbine.

These results coincide with the results of [113] and [40], as the authors proved if a turbine has higher (w_i/w_r) and (w_f/w_r) ratios taken together than other turbines, then it proves higher capacity factor, because the turbine works closer to its rated speed. From Table 3.1, the (Enrecon-E40 600 kW) has higher (w_i/w_r) and (w_f/w_r) than (Enrecon-E44 900 kW).

The same comparative simulation procedure is repeated at wind speed time series of average value 5 m/s. In the case of average wind speed 5 m/s, the behaviour of (Enrecon-E44 900 kW) starts to improve and its annual energy

production is higher than (Enrecon-E40 600 kW), although its cost of energy is still higher than (Enrecon-E40 600 kW). This result indicates that (Enrecon-E44 900 kW) can provide higher energy production than (Enrecon-E44 600 kW), in case of installation at sites of high mean wind speeds.

Table 3.3: Enercon-600 kW Versus Enercon-900 kW at Mean Wind Speed: 4 m/s

Item	900 kW turbine	600 kW turbine
Capital Cost	4.5710×10^5	3.2381×10^5
Capacity factor	0.0698	0.1168
Diameter	44	40
Cost of energy	0.1010	0.0642
Simple pay back	8.4202	8.3283
Net present value (15 years)	-3.9891×10^4	-2.8259×10^4
Annual wind turbine production	1.6286×10^6	1.8169×10^6

Table 3.4: Enercon-600 kW Versus Enercon-900 kW at Mean Wind Speed: 5 m/s

Item	900 kW turbine	600 kW turbine
Item	900 kW turbine	600 kW turbine
Capital Cost	4.5710×10^5	3.2381×10^5
Capacity factor	0.0952	0.1247
Diameter	44	40
Cost of energy	0.0741	0.0601
Simple pay back	8.3308	8.3371
Net present value (15 years)	-3.9891×10^4	-2.8259×10^4
Annual wind turbine production	2.2214×10^6	1.9388×10^6

Figure 3.7a shows the power generation percentage of both wind turbines and batteries, distributed between the loads and the SRU in the case of Enercon-600 kW turbine, at mean wind speed 4 m/s. Figure 3.7b shows the power generation percentage of both wind turbines and batteries, distributed between the loads and the SRU in the case of Enercon-900 kW, at mean wind speed 4 m/s. It is clear that the energy production in the case of the 600 kW turbine is higher than the case of 900 kW. Therefore, this power shortage in the case of 900 kW turbine is compensated by the batteries, as the batteries power production is higher in the case of 900 kW than 600 kW scenario.

The economic evaluation was conducted in this Section, assuming that the microgrid is supplied by wind turbines of the same power rating. However, in microgrids it is common to supply power by different ratings of wind turbines, and so the economic evaluations must be performed in such cases. Next Section will show the economic evaluation of a microgrid supplied by wind turbines of different power ratings.

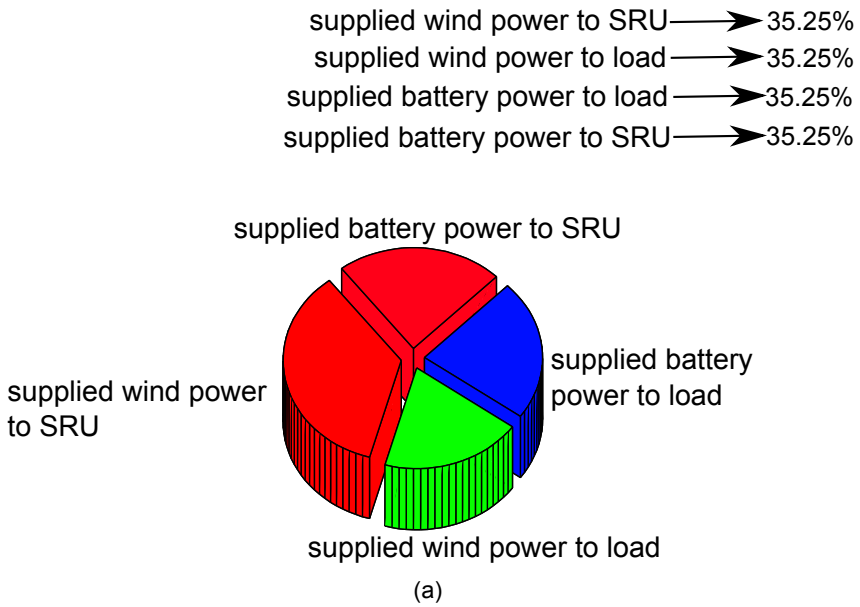

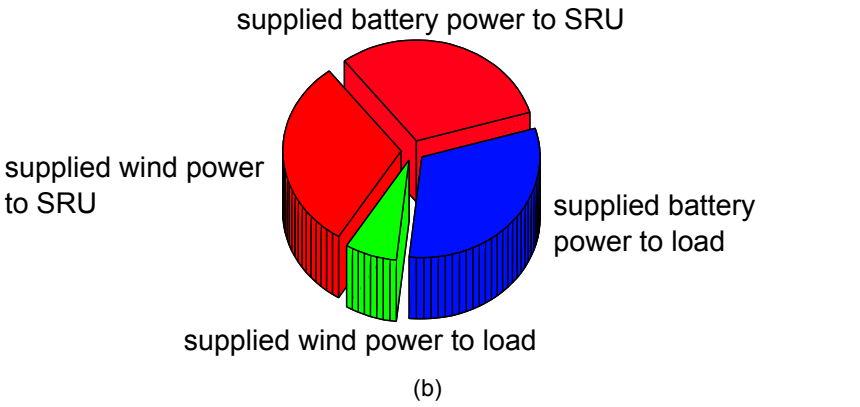

Figure 3.7: Daily power generation percentage: (a) Enercon-600 kW. (b) Enercon-900 kW.

3.4 Economic Evaluation for a Microgrid Supplied by Wind Turbines of Different Power Ratings

Through this Section, the microgrid is supplied by wind turbines of different power ratings and also by Vanadium Redox batteries interfaced through MSUs, as shown in Figure 3.8. The microgrid is simulated to minimize the cost of energy and maximize the energy production, according to equation (3.17). Simulations are processed at wind speed time series of average values 2, 4 and 5 m/s. The analyses of each turbine are performed, according to the cost of energy, the simple pay back and the net present value.

Figure 3.9a shows the curve fitting of Enercon-330 kW; Figure 3.9b shows the curve fitting of Enercon-900 kW; Figure 3.9c shows the curve fitting of Enercon-2000 kW; diamonds indicate the manufacturer data. Power ratings of the contributing wind turbines are shown hereunder:

1. Enercon-E33-330 kW
2. Enercon-E44-900 kW
3. Enercon-E82-2000 kW

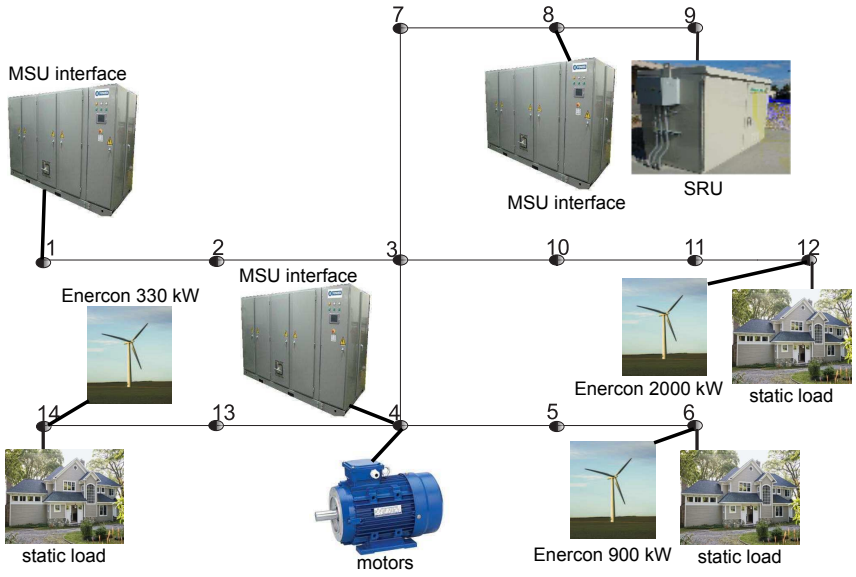

Figure 3.8: Layout of a microgrid supplied by wind turbines of different power ratings

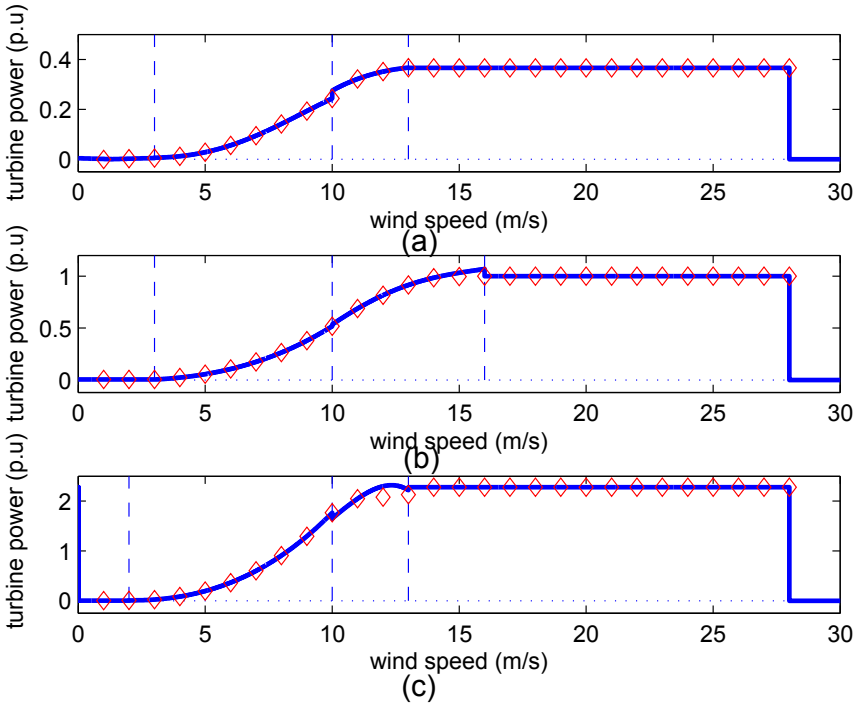

Figure 3.9: Curve fitting of contributing wind turbines: (a) Enercon-330 kW. (b) Enercon-900 kW. (c) Enercon-2000 kW.

3.4.1 Optimization Results

The economic analysis is carried out to evaluate the economic performance of each turbine. The results are shown in Figures 3.10, 3.11 and 3.12. The main conclusions of these simulations are shown as follows:

1. The capacity factor of both 330 kW and 2000 kW turbines are higher than the capacity factor of the 900 kW turbine. As concluded previously the turbines which have higher (w_i/w_r) ratios, have higher generation capacities. From Table 3.1, the 900 kW turbine has the lowest (w_i/w_r) ratio;

2. The cost of energy decreases with increasing the wind speed and still the 900 kW shows the highest cost of energy, even though at high wind speeds;

3. The simple payback improves slightly at higher wind speeds;

4. From Figures 3.13, 3.14 and 3.15, the net present value of the 330 kW turbine is the lowest after 10 years, but the 2000 kW turbine has the best record from economic view after 20 years, indicating more profitable gains;

5. The optimum cases from the economic evaluation view are related to the 330 kW and 2000 kW turbines, as they have the highest capacity factor and the lowest cost of energy. Moreover, if the profitable gains are taken into consideration, the 2000 kW turbine is the best choice, because it has the highest NPV after 20 years.

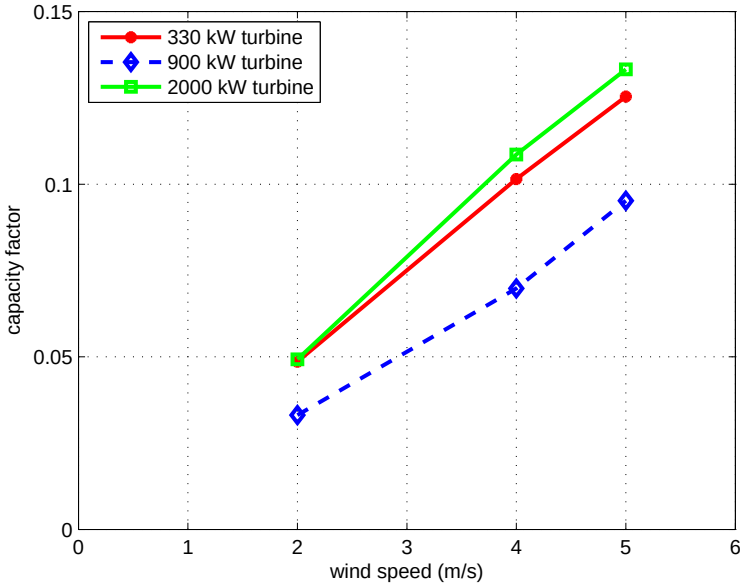

Figure 3.10: Capacity factor vs wind speed

The previous results through this Section were aimed at analysing the economic evaluation of the wind turbines only. However, an interesting result of the batteries daily production which entails the simulations at wind speed time series of average values 2 and 5 m/s respectively, must be considered, to show the role of the multi-objective optimization function, which is used to minimize the cost of energy for both wind turbines and batteries. The optimization function was shown by equation equation (3.17) and will be mentioned hereunder again for convenience.

$$min \sum_{i=1}^{n} \left(\frac{F_{wt}(E_{wt})}{E_{wt}} + \frac{F_{bat}(E_{bat})}{E_{bat}} \right) \tag{3.18}$$

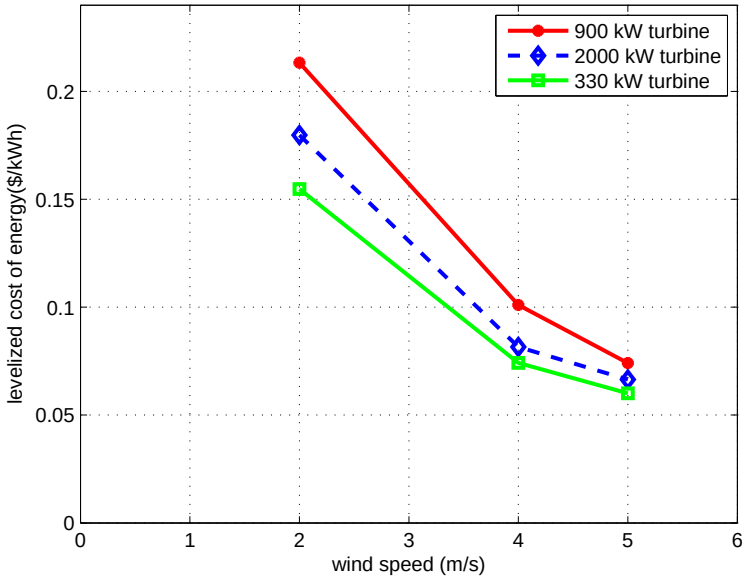

Figure 3.11: Wind turbines levelized cost of energy vs wind speed

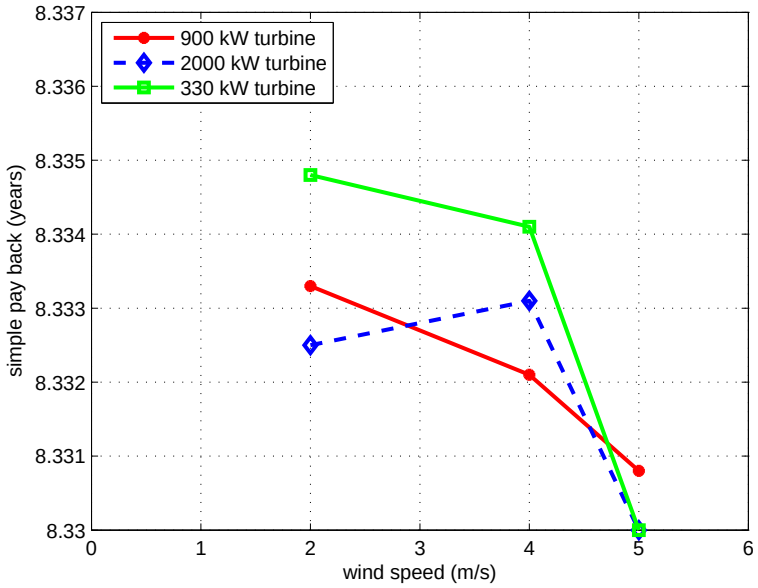

Figure 3.12: Simple payback vs wind speed

The first half of the equation (3.17) is dedicated to the wind turbine term, while the second half is dedicated to the batteries. In the case of wind speed time series of high average value as 5 m/s, the energy production of the wind turbines increase, and so the term $\left(\frac{F_{wt}(E_{wt})}{E_{wt}}\right)$ of the wind turbines is much

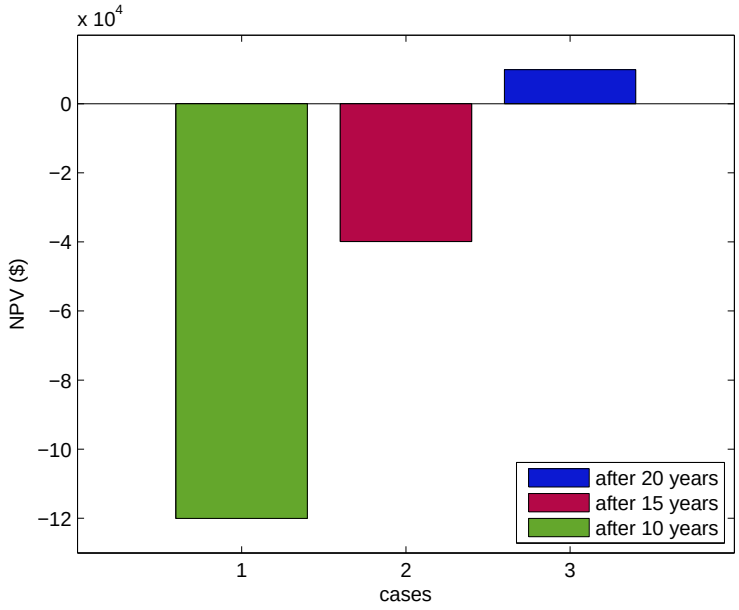

Figure 3.13: Net present value of Enercon-900 kW turbine measured at different periods of time

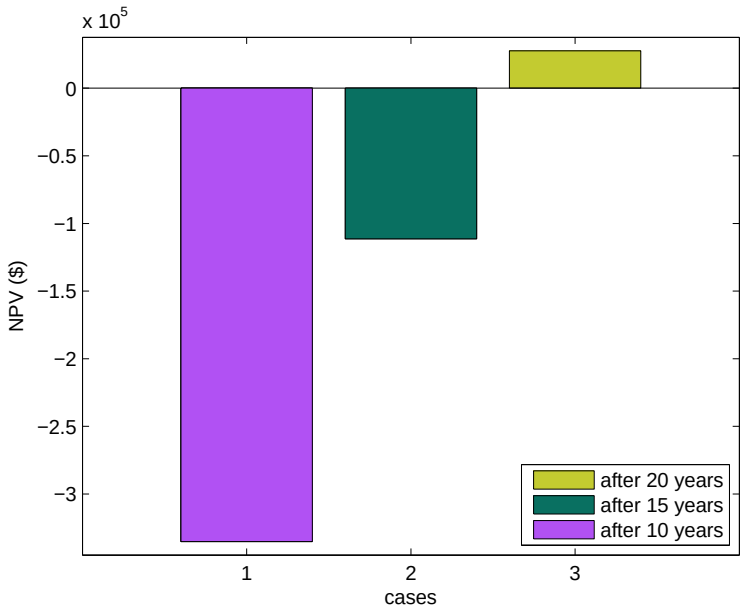

Figure 3.14: Net present value of Enercon-2000 kW turbine measured at different periods of time

lower than the term $\left(\frac{F_{bat}(E_{bat})}{E_{bat}}\right)$ of the batteries, but both terms of the wind turbines and batteries must have the same weight to get minimized, because the both terms are employed in the multi-objective function. Subsequently,

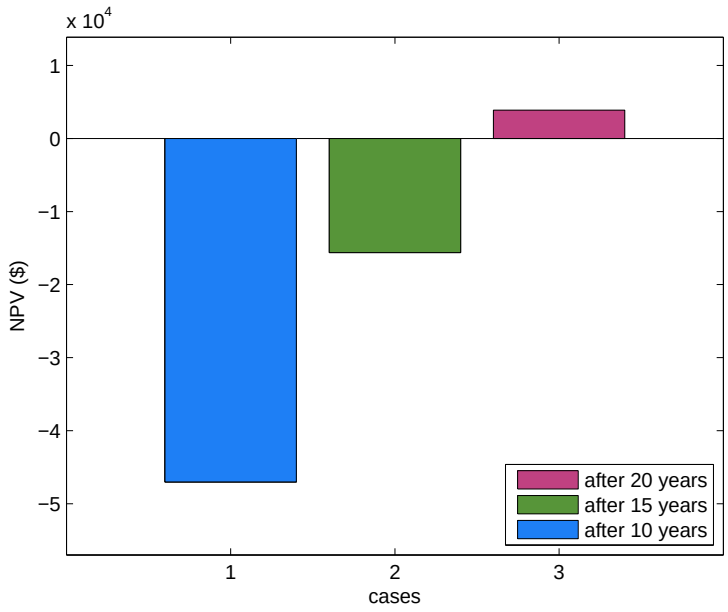

Figure 3.15: Net present value of Enercon-330 kW turbine measured at different periods of time

the optimization solver search for more optimal equilibrium points, in order to balance the both terms.

Figures 3.16 and 3.17 explain the daily production of the wind turbines and batteries in the case of wind speed time series of average values 2 m/s and 5 m/s respectively. In Figure 3.17, the slope of the wind production part is higher than the slope of wind production in Figure 3.16, due to wind speed increase. Moreover, the axis of the battery production in Figure 3.17 reaches higher values than the axis of the battery production in Figure 3.16.

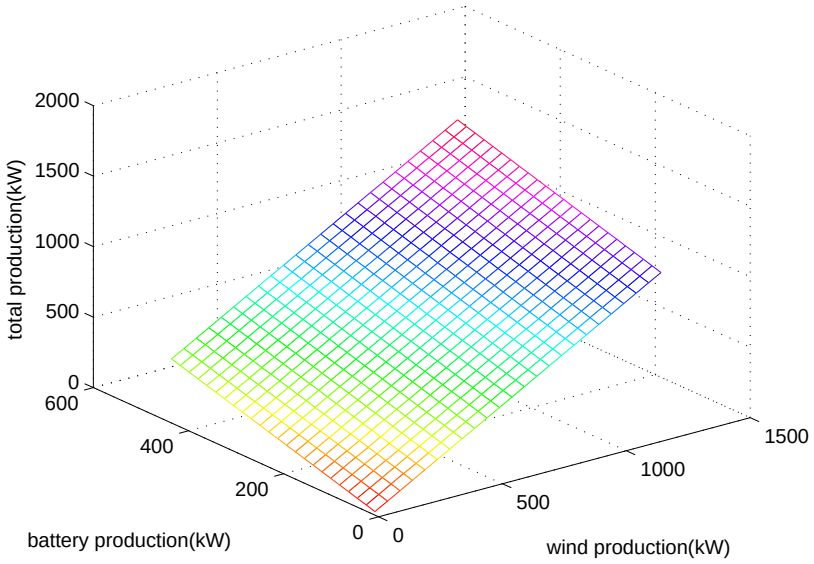

Figure 3.16: Daily power production at average wind speed 2 m/sec

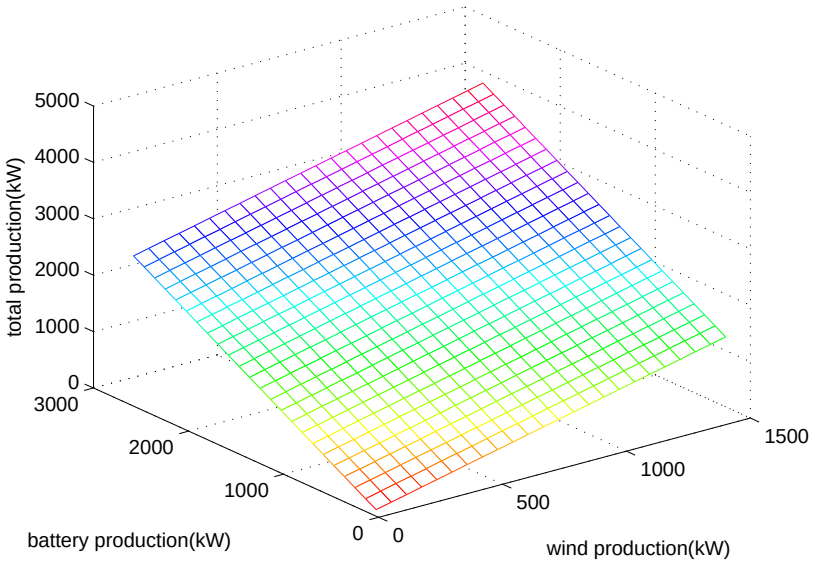

Figure 3.17: Daily power production at average wind speed 5 m/sec

These results are translated to levelized cost of energy as shown in Figure 3.18; it is clear that the total cost of energy for both the wind turbines and batteries in the case of wind speed time series of average value 5 m/s is much lower than the total cost of energy in the case of wind speed time series of average value 2 m/s. The levelized costs of energy for both wind turbines and batteries are summed, taking into consideration that the cycle life of the Vanadium Redox are high and equal to 12,000 and subsequently their life time are appreciated as 30 years, according to [114].

To this end, the higher mean wind speed does not provide a higher energy production and economic performance for the wind turbines only, but for the storage systems as well, if the both generation units are employed in a multi-objective function.

The objective of the Chapter is the economic evaluation for both the wind turbines and energy storage systems; the previous interesting results of the daily battery production, which show the possibility of reducing its cost of energy through the performance of wind turbines. Thus, the next Section will conduct the economic evaluation for microgrids supplied by various wind turbines and batteries. The batteries will be analysed under different capital costs, according to their efficiencies.

3.5 Economic Evaluation for Microgrids Supplied by Various Wind Turbines and Batteries

The microgrid energy management systems (EMS) are responsible for dispatching the energy among different generators in microgrids. EMS makes decision to which energy storage devices to dispatch for various types of contingencies.

Electric energy storage systems including different types as batteries, capacitors and flywheels are required to supplement the DER generators during low voltage transients on the distribution system, or when operating in isolated mode, or actual electric outages as a result of motor starts or other short term overloads. Some types of DERs as microturbines have little inertia for successful starting motors, unless some sort of storage is supplied. Hence, the energy storage systems as batteries can handle such problems by managing the

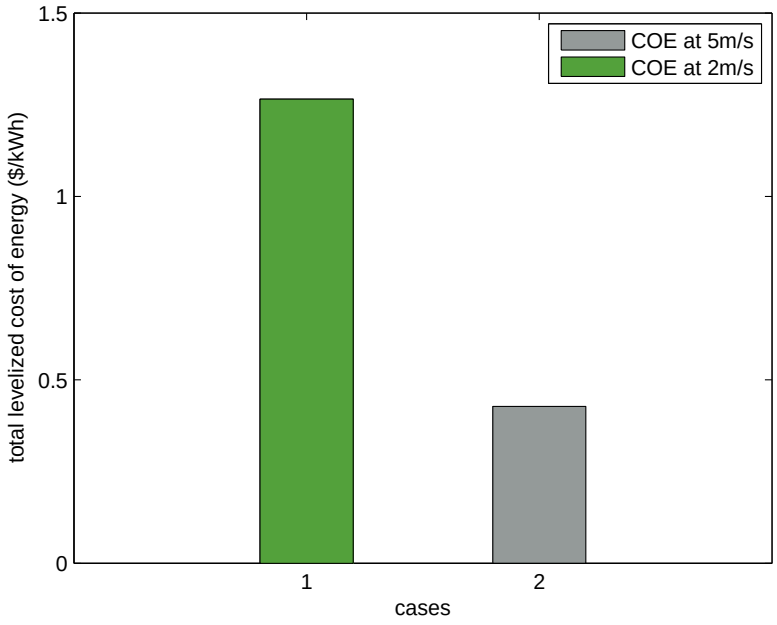

Figure 3.18: Total levelized cost of energy at different wind speed levels

power control during the transient moments. If a network is supplied by synchronous machines, which are characterized by high inertia, they cannot ride through the high power demand in a little time, leading to some power quality problems, such as frequency dips and different ranks of harmonics included in the voltage waveforms. In some cases, the harmonics are extreme that an equipment being powered from these generators may fail. Therefore, the energy storage devices can be employed to overcome such urgent problems, by providing power during sag moments, and to keep the voltage at buses always constant.

The continuous risk results from high penetration of intermittent wind energy sources in power systems, as shown in [115], has been a crucial principle of the energy storage systems supplying power grids during moments of low wind speed. Most analyses regarding wind integration in the power system have focused on more engineering aspects, such as grid stability, load-balance and system security. Some of these analyses have shown benefits from using energy storage as an alternative to other dispatchable generators, in order to manage wind uncertainty, but the economic evaluations for power systems supplied by wind energy in parallel with energy storage systems have not been cleared.

Through this Section, the energy storage devices are represented by various types of batteries. The economic evaluations of the proposed microgird supplied by wind turbines and various batteries are performed. The simulations considers batteries of the most widely used for small-medium scale storage applications, such as Lead-Acid, Nickel-Cadmium, Lithium-Ion and Vanadium Redox batteries.

The Lead-Acid battery is one of the most mature types of batteries and they are widely used for small-medium scale storage applications. However, one of the main disadvantages of the Lead-Acid battery is the poor performance at low and high ambient temperatures. In addition, the necessity for periodic water maintenance for flooded batteries and low specific energy and power. Furthermore, Lead-Acid batteries show difficulties in providing frequent power cycling [116].

The Nickel-Cadmium batteries compete with Lead-Acid batteries because they have a higher energy density; the technology of the Nickel-Cadmium battery has been under development since 1950. On the other hand, the main disadvantage of Nickel-Cadmium batteries is the memory effect. If Nickel-Cadmium batteries are not fully discharged before being recharged, the battery will start losing its capacity. Consequently, the Nickel-Cadmium batteries cannot operate economically, in parallel with non-dispatchable generators [117].

The Vanadium Redox batteries are suitable for small and medium scale applications. There are currently over 20 MWh of installed Vanadium Redox batteries in the world. The installed Vanadium Redox batteries are used for remote area power systems and renewable energy stabilization. Vanadium Redox plants can be upgraded at a low incremental cost, by increasing the volume of electrolytes for more stored energy or by adding new cell stacks for additional power. The drawback of Vanadium Redox battery is referred to its low specific energy and energy density [118].

The Lithium-Ion batteries are under growing demand, due to their high efficiencies of over 95%, long life cycle of and fast discharge capabilities. The main problem of Lithium-Ion batteries are their high costs [119].

This Section tries to answer a question regarding the possibility to reduce energy cost of a high capital cost-high efficient battery supplying a grid, in parallel with wind turbines. For this reason, the microgrid shown in Figure 3.8 is four times simulated at wind speed time series of average value 4 m/s; through

each simulation the microgrid is supplied by a different type of battery, such as Nickel Cadmium, Lithium, Vanadium-Redox or Lead-Acid.

Figure 3.19 shows the capital costs of the proposed batteries, as mentioned in [120]. The battery price differs from an article to another, depending on the manufacturer, the cycle efficiency, the life time and the discharge rate. Each battery is processed in separate simulation, in order to minimize the energy cost of the whole microgrid through the multi-objective function as shown by equation (3.19). The charge-discharge equations for all the simulated batteries, according to [106], are shown by equations (3.7)-(3.9).

The characteristics of the proposed batteries are detailed in Table 3.5, according to [121] and [122].

$$min \sum_{i=1}^{n} \left(\frac{F_{wt}(E_{wt})}{E_{wt}} + \frac{F_{bat}(E_{bat})}{E_{bat}} \right) \tag{3.19}$$

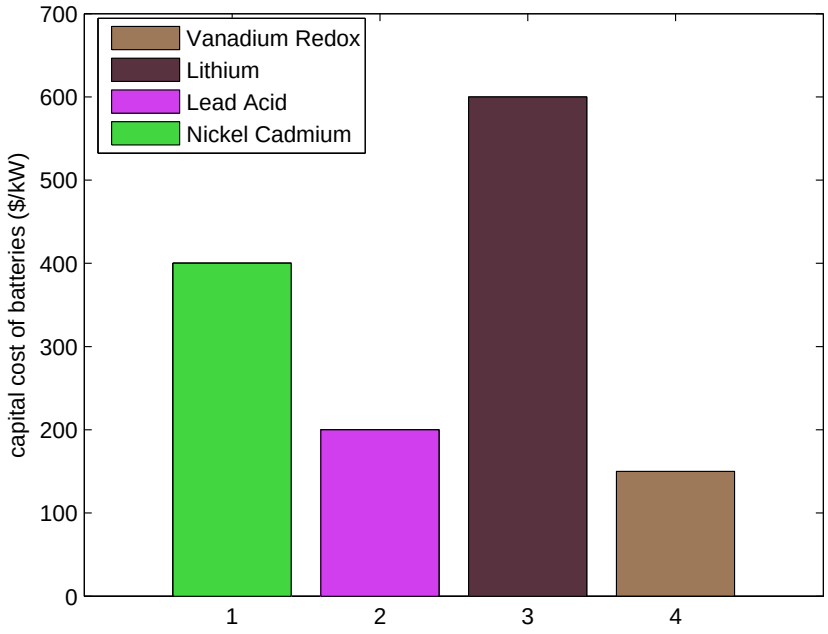

Figure 3.19: Capital cost of batteries

3.5.1 Optimization Results

Figure 3.20 express a comparison of generation percentage between Lithium and Vanadium batteries respectively, as the both figures explain the contri-

Table 3.5: Characteristics of the Simulated Batteries

Energy storage technology	Cycle efficiency %	Cycle life	Energy density (Wh/kg)
Lead-Acid battery	70-90	500-1000	30-50
Nickel-Cadmium battery	72	2000-2500	50-75
Lithium-Ion battery	almost 100	1000-10,000	75-200
Vanadium-Redox battery	85	12,000	10-30

bution between the wind turbines and batteries at supplying the microgrid, whereas the annual energy production of the two batteries is shown in Figure 3.22.

Both pie charts in Figure 3.20 brief the conclusion of the current simulation, as it is a comparison between the lowest capital cost battery (Vanadium) and the highest capital cost one (Lithium). The wind power production is the same, because the ratings of the wind turbines and the mean wind speed are the same in the both cases, but the battery power flow in the both cases are different. The optimization solver which is used in the simulations must balance between the wind turbines term $\left(\frac{F_{wt}(E_{wt})}{E_{wt}}\right)$ and battery term $\left(\frac{F_{bat}(E_{bat})}{E_{bat}}\right)$.

Clearly, the capital cost in the case of Lithium batteries is higher than Vanadium case, and so the optimization solver searches for another equilibrium point to reach the minimum cost of energy.

In the case of Lithium batteries, more power flows to the SRU. By end of the day, the SRU backs this energy again to the Lithium batteries to achieve the battery daily operation as shown in Figure 3.2. Therefore, the total power which flows to the load is the same in case of Lithium and Vanadium batteries to achieve P_{gen}=P_{demand}. The total power flow from Lithium batteries to the SRU is much higher than the case of Vanadium batteries.

This result indicates the ability of the high capital cost-high efficient battery to provide optimum economic performance and high energy production,

if the problem is performed by a multi-objective function.

The previous conclusion could be translated to cost of energy and annual energy production, as shown in Figures 3.21 and 3.22. The energy cost of the Lithium battery which has capital cost (600 $/kw) equals to the cost of energy of the Nickel-Cadmium battery which has capital cost (400 $/kw). This can be explained by Figure 3.22, as the annual energy production in the case of Lithium battery is higher than the Nickel-Cadmium case, due to higher power flow to the SRU in the case of Lithium battery.

Until now, some important results were concluded regarding supplying isolated microgrids by wind turbines and batteries. Next Section will show the aggregation effect of wind turbines capacities on the economic performance and energy production for microgrids.

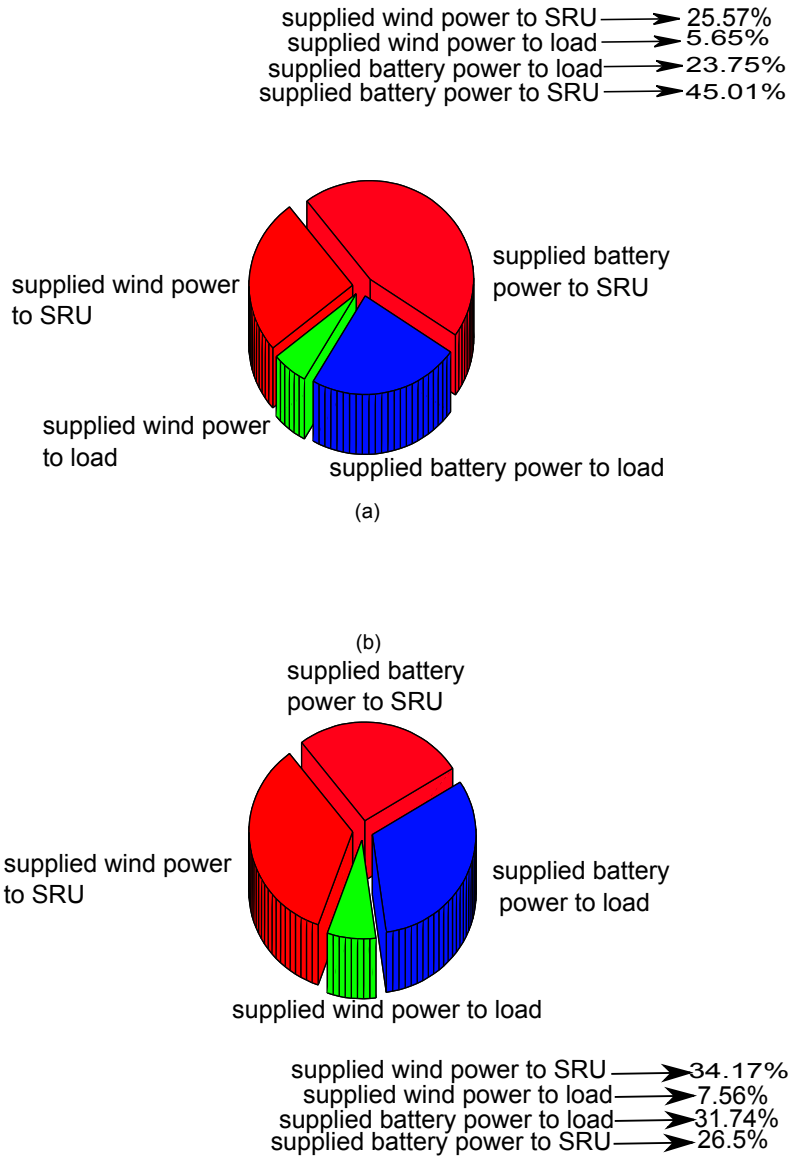

Figure 3.20: Daily power generation percentage: (a) Lithium battery case. (b) Vanadium battery case.

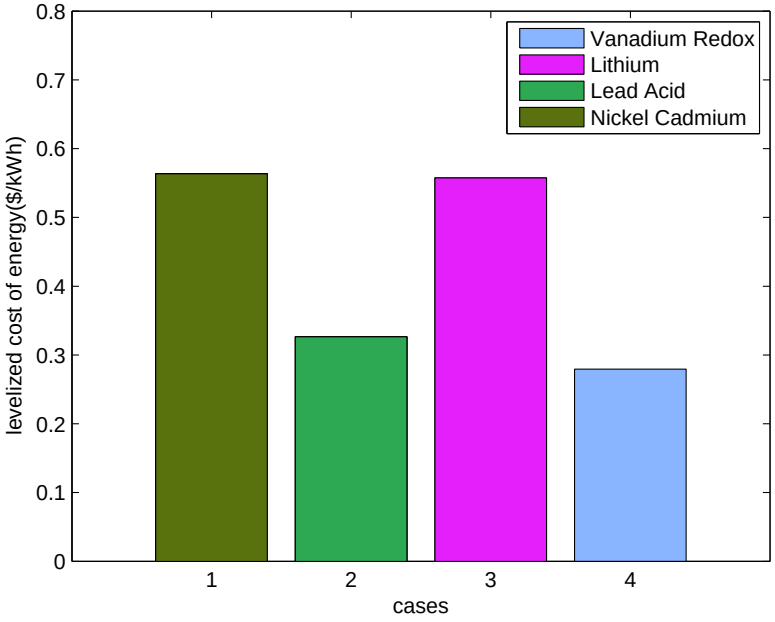

Figure 3.21: Batteries levelized cost of energy

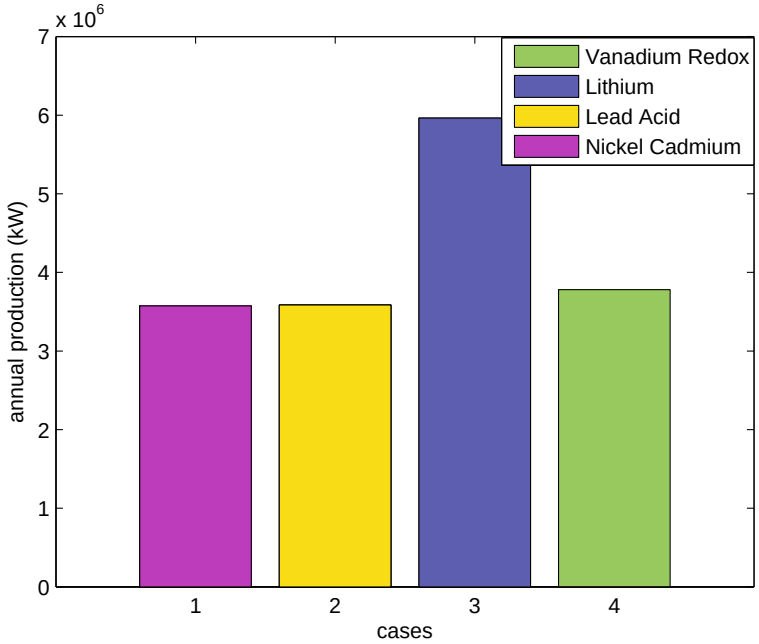

Figure 3.22: Batteries annual energy production

3.6 The Aggregation Effect of Wind Turbines on the Economic Performance

Most conducted analyses regarding the wind turbine aggregation have concentrated mainly on technical issues, as different simulation algorithms have been proposed to represent aggregated models of wind turbines without unnecessarily increasing the wind farm model. After occurrence of several aggregated wind farm models, the effect of such models on steady state and dynamic analyses have been shown in many papers. However, the economic evaluation of aggregated wind farm models on power systems have not been considered.

Through this Section, the economic evaluations of aggregated wind farms are performed. The economic evaluations of the aggregated wind farms are provided by the cost of energy, simple pay back and net present value.

The comparison is conducted among three cases:

- The first case employs three dispersed Enercon-600 kW wind turbines, to supply the microgrid with a set of batteries;
- The second case employs one Enercon-2000 kW wind turbine only to supply the microgrid with a set of batteries (Aggregation case);
- The third case employs one Vestas-1800 kW wind turbine only to supply the microgrid with a set of batteries (Aggregation case).

The microgrid layout for the first case is shown in Figure 3.1, while the layout of the second and third cases is shown by Figure 3.24. Moreover, the micorgrid is supplied in the first, second and third cases by Vanadium Redox batteries interfaced through MSUs, in order to share power supply with the proposed wind turbines of each case. The simulations are performed for each case at wind speed time series of average values 4 and 5 m/s respectively, by the same function shown in equation (3.19).

Figure 3.23a shows the curve fitting of Enercon-600 kW; Figure 3.23b shows the curve fitting of Vestas-1800 kW; Figure 3.23c shows the curve fitting of Enercon-2000 kW; diamonds indicate the manufacturer data.

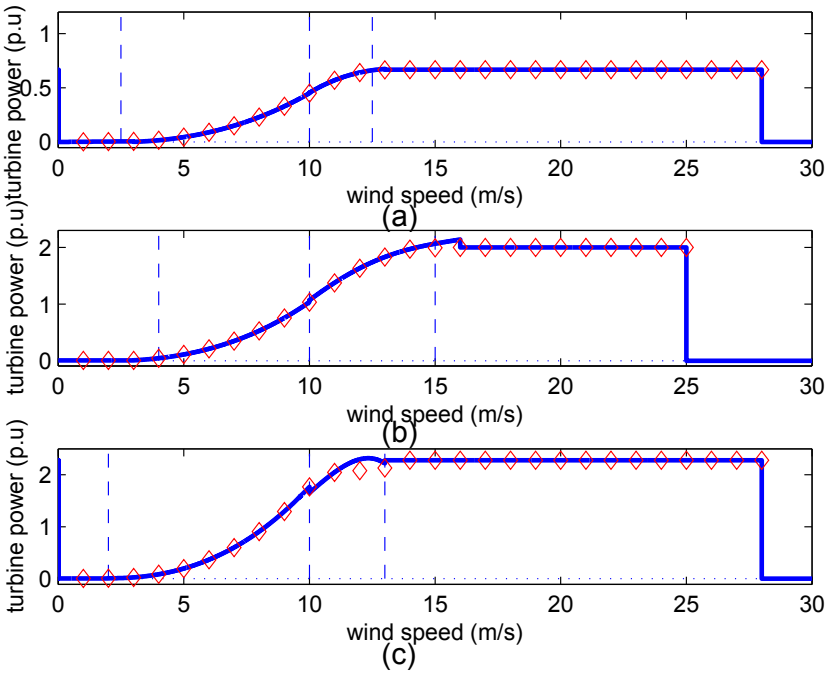

Figure 3.23: Curve fitting of contributing wind turbines: (a) Enercon-600 kW. (b) Vestas-1800 kW. (c) Enercon-2000 kW.

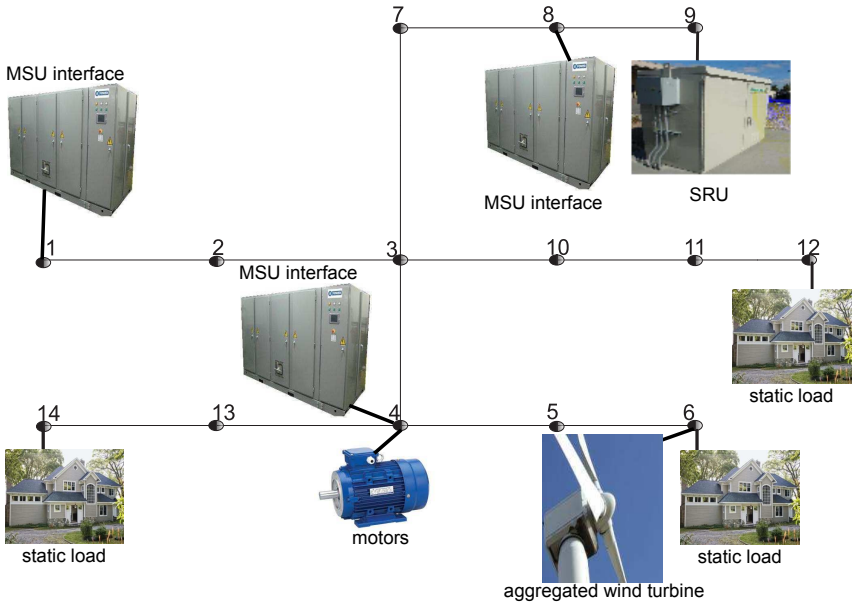

Figure 3.24: Microgrid layout

3.6.1 Optimization Results

Figures 3.25, 3.26 and 3.27 show that the turbines with higher w_i/w_r ratio still have the highest capacity factor, the highest annual energy production and the lowest cost of energy. Enercon-E40-600 kW turbines have the lowest w_i/w_r ratio, and so the case of supplying the microgrid by Enercon-E40-600 kW turbines shows the lowest capacity factor and the highest energy cost.

The annual wind turbine energy production is higher in both cases of Vestas-1800 kW and Enercon-E82-2000 kW than the Enercon-E40 600 kW turbines case, as shown from Figure 3.26.

The benefits of aggregation are not for wind turbines only, as the annual energy production for batteries in the both cases of Vestas-1800 kW and Enercon-E82-2000 kW, are higher than the Enercon-E40 600 kW case, as shown from Figure 3.28. Therefore, the batteries energy cost in both cases of Vestas-1800 kW and Enercon-E82-2000 kW are less than the Enercon-E40 600 kW case, as shown from Figure 3.29. Consequently, the total energy cost in both cases of Vestas-1800 kW and Enercon-E82-2000 kW are less than the Enercon-E40 600 kW case, as shown in Figure 3.30.

It could be concluded from the previous simulations, in order to provide a better economic performance and energy production, the aggregation of wind turbines capacities can be a better choice than dispersing the same capacities of wind turbines at different microgrid nodes. Moreover, the cases of wind turbines aggregation show more profitable gains than smaller capacity dispersed turbines (600 kW), as shown Figure 3.31, 3.32 and 3.33.

Figure 3.34 shows the percentage of power generation for Enercon-600 kW at mean wind speeds 4 and 5 m/s respectively. Figure 3.35 shows the percentage of power generation for Vestas-1800 kW at mean wind speeds 4 and 5 m/s respectively. Figure 3.36 shows the percentage of power generation for Enercon-2000 kW at mean wind speeds 4 and 5 m/s respectively. Finally, Tables 3.6 and 3.7 show the results of the economic evaluation models and energy production.

Up to this point, all the possible scenarios for economic evaluation of microgrids, supplied by wind energy and batteries were conducted; however, the objective of optimizing the energy production and economic feasibility for microgrids must be extended to include additional constraints related to the

operation of microgrids, as the objective is to enhance the minimum generation cost with stable power flow limits. For this sake, the small signal stability analyses will be conducted in Chapter 4.

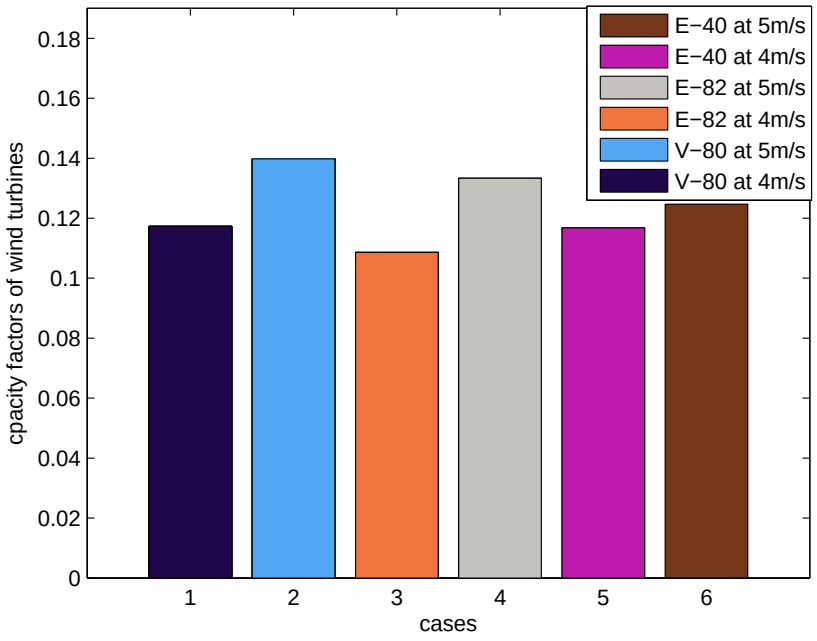

Figure 3.25: Wind turbines capacity factor

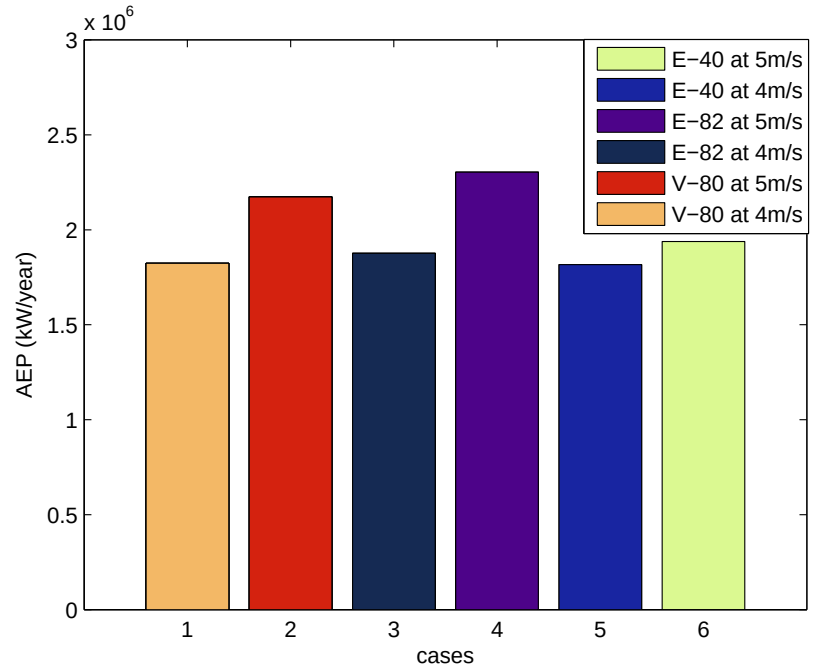

Figure 3.26: Wind turbines annual energy production

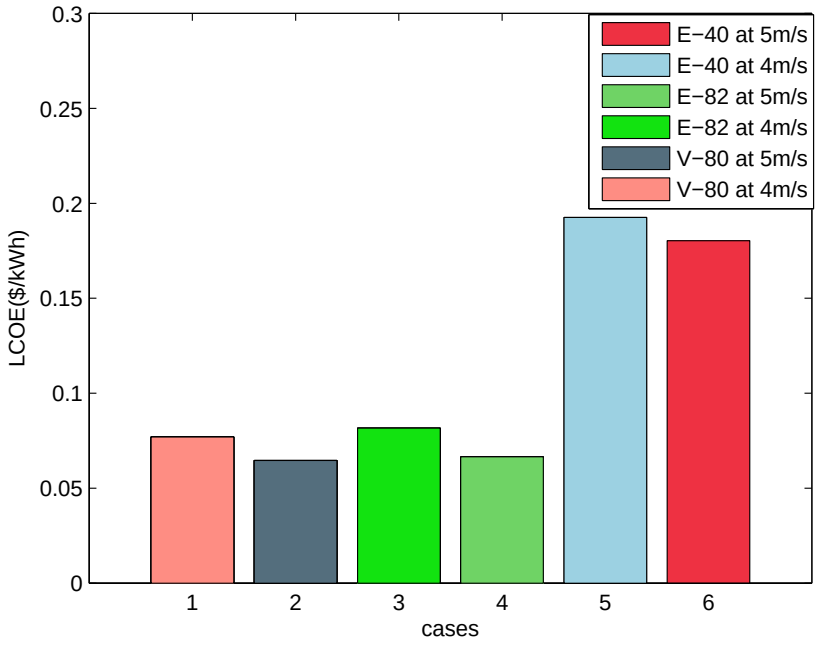

Figure 3.27: Wind turbines levelized cost of energy

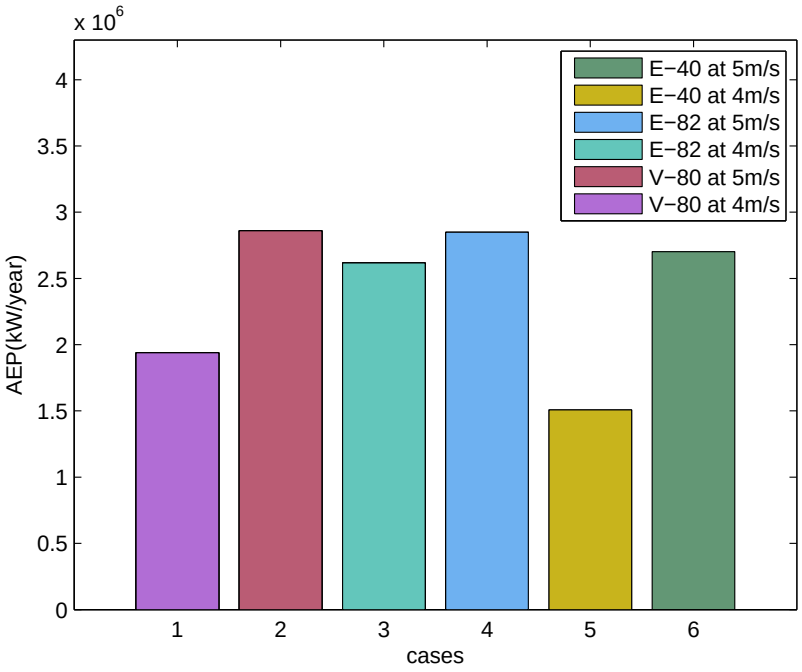

Figure 3.28: Batteries annual energy production

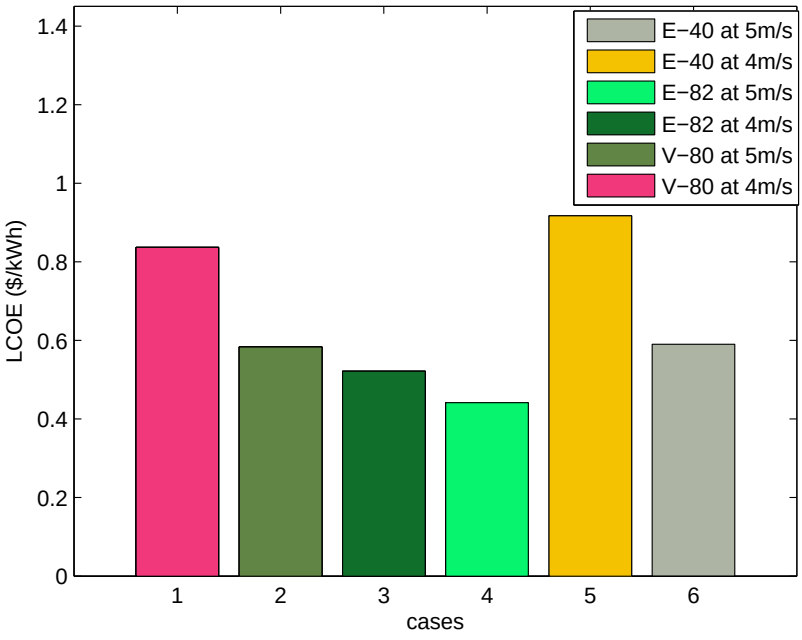

Figure 3.29: Batteries levelized cost of energy

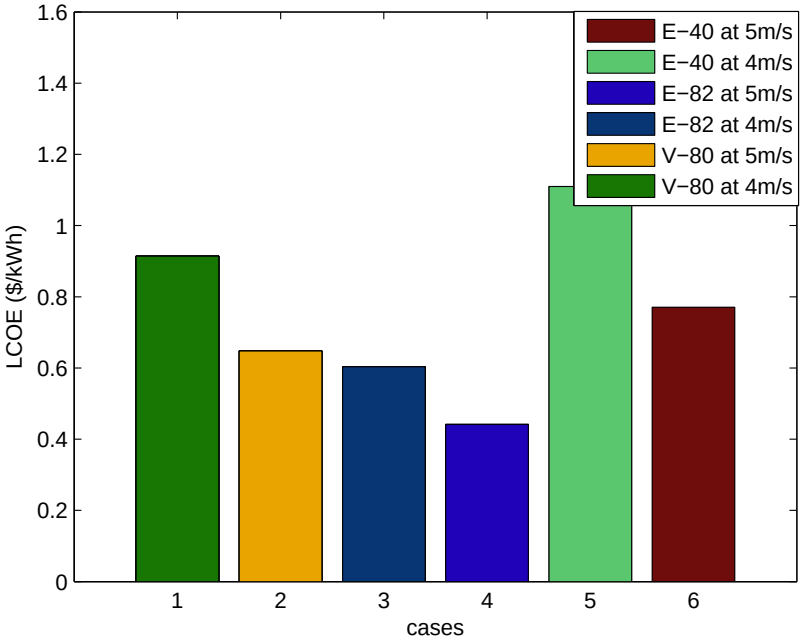

Figure 3.30: Total levelized cost of energy

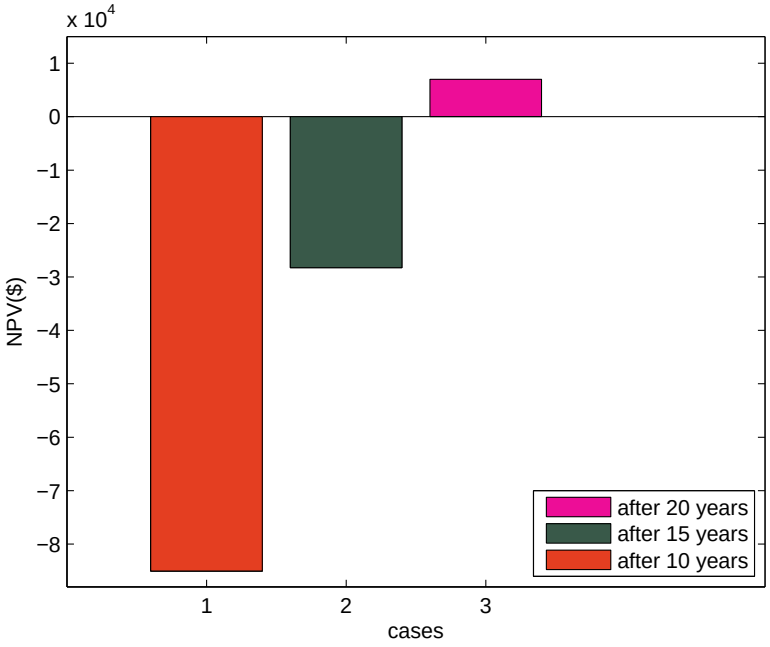

Figure 3.31: Net present value, Enercon-600 kW

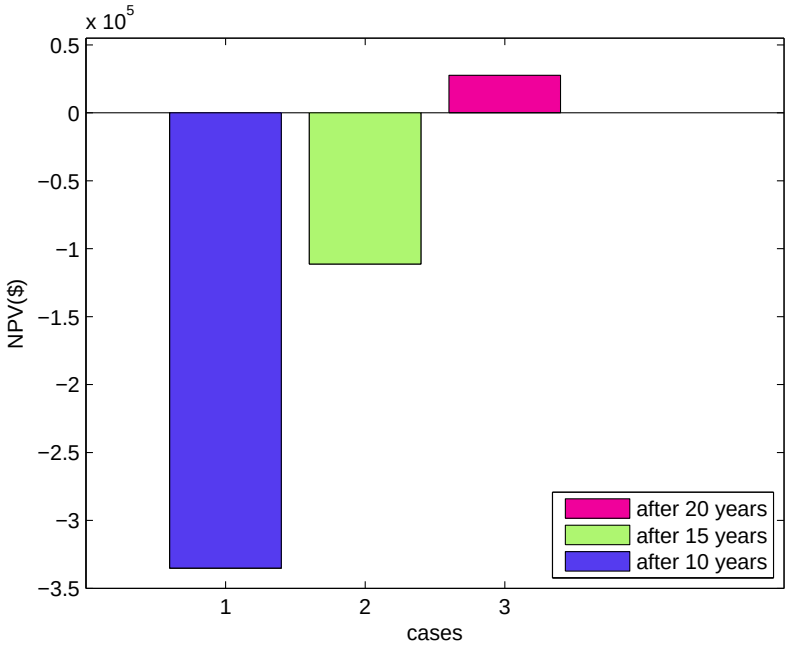

Figure 3.32: Net present value, Enercon-2000 kW

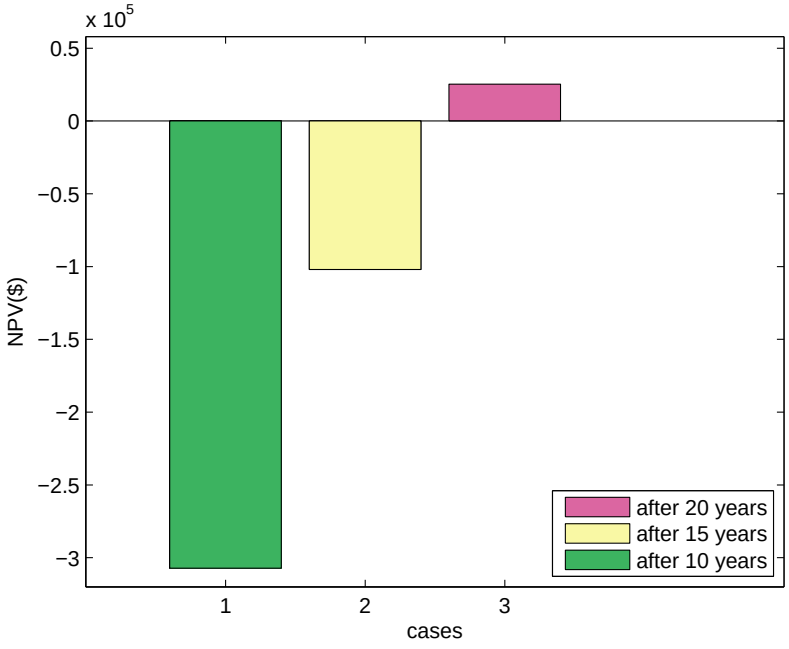

Figure 3.33: Net present value, Vestas-1800 kW

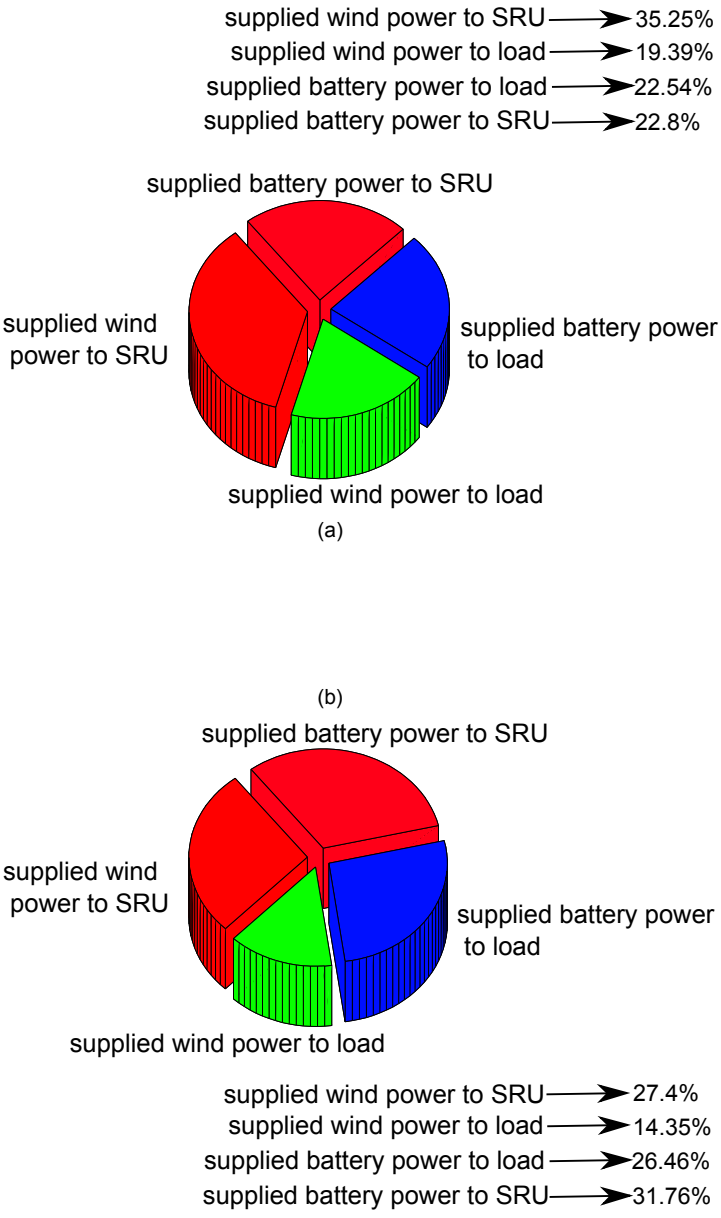

Figure 3.34: Daily power percentage, Enercon-600 kW: (a) mean wind speed (4 m/s). (b) mean wind speed (5 m/s).

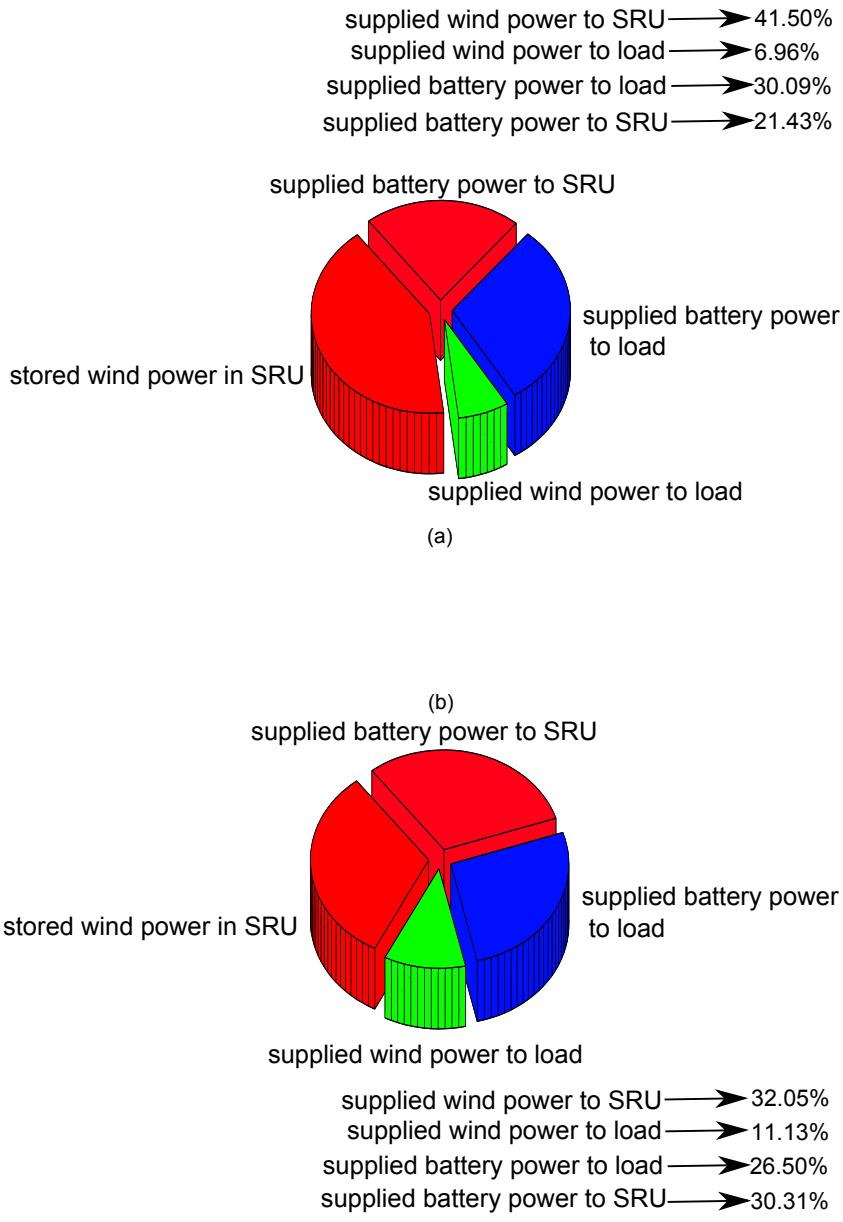

Figure 3.35: Daily power generation percentage, Vestas-1800 kW: (a) mean wind speed (4 m/s). (b) mean wind speed (5 m/s).

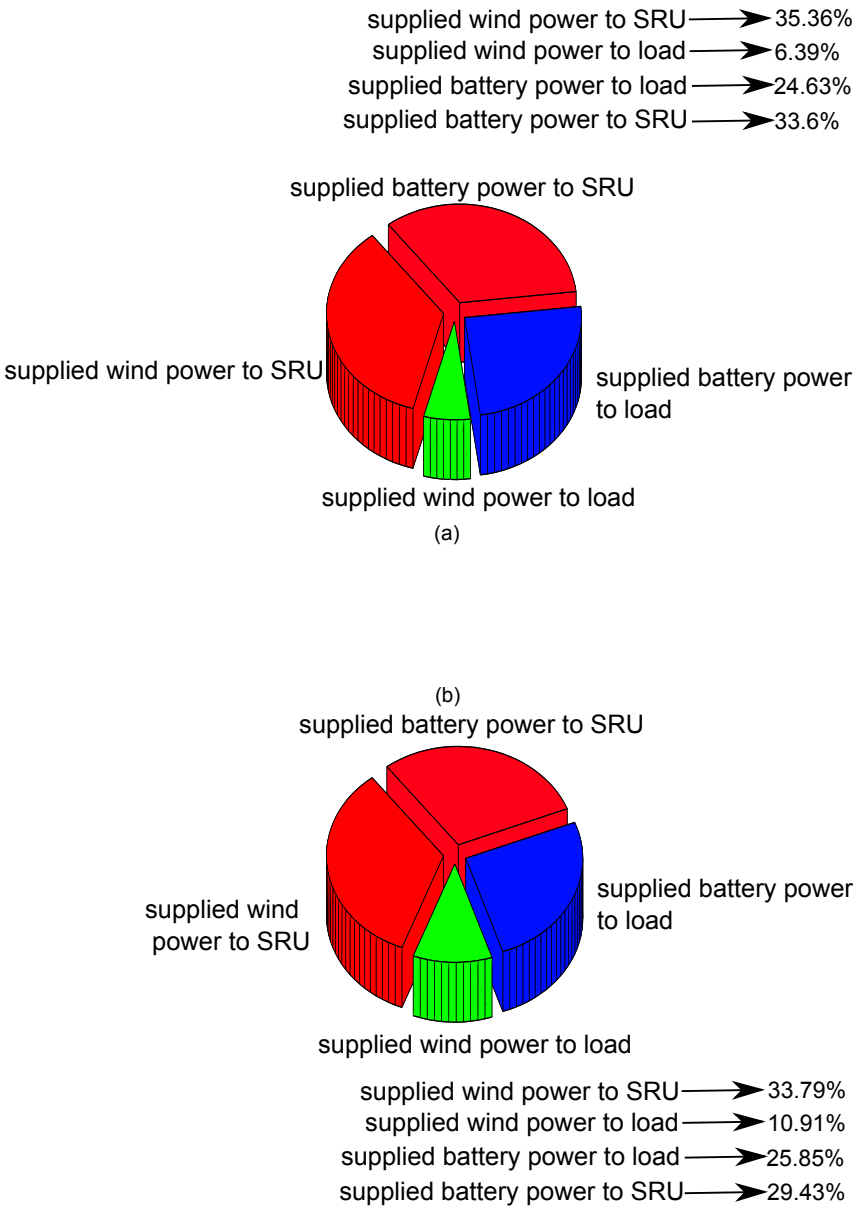

Figure 3.36: Daily power percentage, Enercon-2000 kW: (a) mean wind speed (4 m/s). (b) mean wind speed (5 m/s).

Table 3.6: Economic Evaluation at Mean Wind Speed: 4m/s-Aggregation Scenario

Item	Vestas-1800 kW	Three Enercon-600 kW	Enercon-2000 kW
Capital Cost	1.1694×10^6	9.7143×10^5	1.2759×10^6
Capacity factor	0.1173	0.1168 (for each turbine)	0.1086
Diameter	80	40 (for each turbine)	
Cost of energy	0.0769	0.1926	0.0816
Simple pay back	8.3333	8.3283(for each turbine)	8.3333
NPV(15 years)	-1.0205×10^5	-2.8259×10^4(for each turbine)	-1.1135×10^5
AEP (wind turbines)	1.8239×10^6	5.4507×10^6	1.8764×10^6

Table 3.7: Economic Evaluation at Mean Wind Speed: 5m/s-Aggregation Scenario

Item	Vestas-1800 kW	Three Enercon-600 kW	Enercon-2000 kW
Capital Cost	1.1694×10^6	9.7143×10^5	1.2759×10^6
Capacity factor	0.1398	0.3741	0.1333
Diameter	80	40 (for each turbine)	82
Cost of energy	0.0646	0.1803 (for each turbine)	0.0665
Simple pay back	8.3333	8.3371 (for each turbine)	8.3333
NPV(15 years)	-1.0205×10^5	-2.8259×10^4 (for each turbine)	-1.1135×10^5
AEP (wind turbines)	2.1735×10^6	5.8164×10^6	2.3033×10^6

Chapter 4

Microgrid Stability Analysis

4.1 Introduction

The previous Chapter discussed the economic evaluation and capacity factor analysis of microgrids based on maximizing the annual energy production. However, the objective of optimizing the energy production and economic feasibility for microgrids must be extended to satisfy the power balance and generation limit among different microgrid generators. The electric power system instability can be interpreted using various methods depending on the system configuration and operational status.

Traditionally, the question of stability has been connected to maintaining synchronous operations. The production of electricity in the conventional utility is secured primarily using synchronous generators, and for this reason it is important to secure their synchronism and parallel operation. Therefore, the question of stability in conventional power systems is mainly based on the stability of synchronous machinery and on the relationship between the active power and rotor angle of the generator.

Usually, the operation of conventional generation systems is based on centralized control of utility generators, delivering power through an extensive transmission and distribution system, to meet the given demands of widely dispersed users. Nowadays, the justification for the large centralized station is weakening due to depleting conventional resources, increased transmission and distribution costs, deregulation trends and environmental concerns. Distributed generation is commonly used for small scale generations and can offer solution to many of centralized generation challenges.

The proposed microgird in this Chapter is supplied by inverter-interfaced generators and doubly-fed induction generators (DFIGs). Typically, the increase of inverter-interfaced distributed generators penetration might not only lead to problems under faulty conditions, but also to instability under small disturbances, such as small changes in loads and power transfers that occur during normal power system operation. This type of stability is known as the small-signal stability. Moreover, the modelling and operation of the DFIGs are totally different from the synchronous generators; as they are intermittent sources and depend on stochastic wind parameters.

Many recent microgrid small signal stability studies belong to either isolated microgrids supplied by wind energy and connected to utility grids [33] and [34], or to isolated microgrids supplied by inverter-interfaced distributed generators without penetration of any intermittent energy sources have been conducted, but the stability analysis of isolated microgrids supplied by the both sources of generation have not been studied before. Thus, in this Chapter, the small signal stability analysis of isolated microgrids supplied by DFIGs and inverter-interfaced distributed generators are conducted.

The small signal stability is the ability of a power system to maintain stability when it is subjected to small disturbances. A disturbance is considered to be small, if the linearized system around the equilibrium point, still adequately represents dynamics of the original nonlinear system under this disturbance [2]. Small-signal stability problems are normally divided into two types, one type of problems is associated with the steady-state stability limits of the power system elements (voltage-frequency stability). The power system is usually controlled in such a way that an increase of the voltage angle leads to active power transfer increase and an increase of reactive power injection by a generator leads to load voltage magnitude increase. The other type of small-signal stability problems is related to the oscillatory instability, due to inefficient generators control strategies. The other possible reason for oscillatory problems is related to large power transfers through weak links, and so inter-area oscillations may appear. The different types of small signal instability are directly related to the system eigenvalues.

In this Chapter, eigenvalue analyses are used to reveal the information of different stability modes of microgrids small signal stability problems, such as wind speed variations, power demand increment and different power exchange

levels among DGs interfaced by electronic inverters.

In this Chapter, the small signal dynamic model of a microgrid is constructed, based on [123], for some important purposes, such as realizing the reliable operating points of DGs, identifying the most dominant DGs control parameters which can affect the microgrid stability. Therefore, in future work, the most dominant DGs control parameters can be set appropriately and an adequate control strategy can be developed to keep the microgrid stable. The following Section shows the main outlines of this Chapter.

4.2 Chapter Outlines

In order to conduct the small signal stability analysis of a microgrid, the microgrid state space modelling is conducted, where eigenvalue analyses are used to reveal the data of the microgrid stability modes. Thereafter, the stability analysis is conducted under different wind speed levels, droop constants increment of inverter-interfaced generators, power demand increment.

This Chapter is divided into the following Sections:

- Microgrid layout, (Section 4.3);
- Microgrid state space modelling, (Section 4.4);
- Conducting participation factor and time response (Section 4.5);
- Wind variation impact on the microgrid stability, (Section 4.6);
- Droop constants variation impact on the microgrid stability, (Section 4.7);
- Power demand increment impact on the microgrid stability, (Section 4.8).

4.3 Microgrid Layout

The base power of the microgrid is 2.97 MW, and the proposed microgrid for the isolated mode and grid-connected mode is configured and briefed as follows:

- Fourteen nodes distribution system;

- Static loads at nodes (2, 4, 6, 8, 9, 11, 12 and 14);
- Four doubly-fed induction generators rated at 1.27 MW at nodes (6, 9, 12 and 14).

In the case of isolated mode, the microgrid is supplied by additional four voltage-frequency inverters at nodes (8, 10, 11 and 13), as shown in Figure 4.1. The power and frequency are regulated from voltage-frequency inverters by droop control constants, which are valued to be 9.4×10^{-7} rad/W/s, whereas in the case of grid-connected mode, the microgrid is connected and supplied by the infinite bus at node 1, as shown in Figure 4.2.

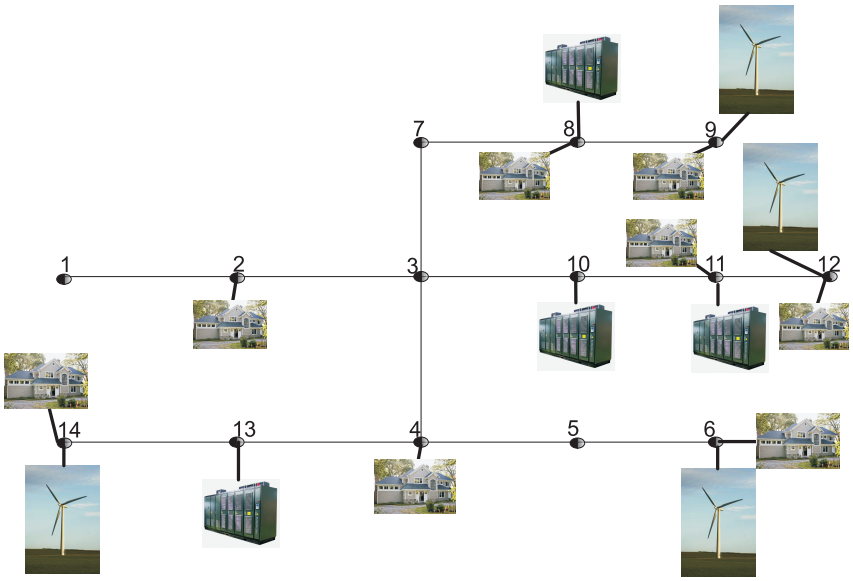

Figure 4.1: Isolated micorgrid layout

4.4 Microgrid State Space Modelling

4.4.1 Introduction

The small signal stability is defined as the capability of system to return to a stable operating point after the occurrence of a disturbance that leads to an incremental change in one or more of the state variables of the power system. The power system state variables are usually different from one state space model to another one. Some examples of power system state variables can be considered, such as generator load angles, magnetic flux linkages, generator

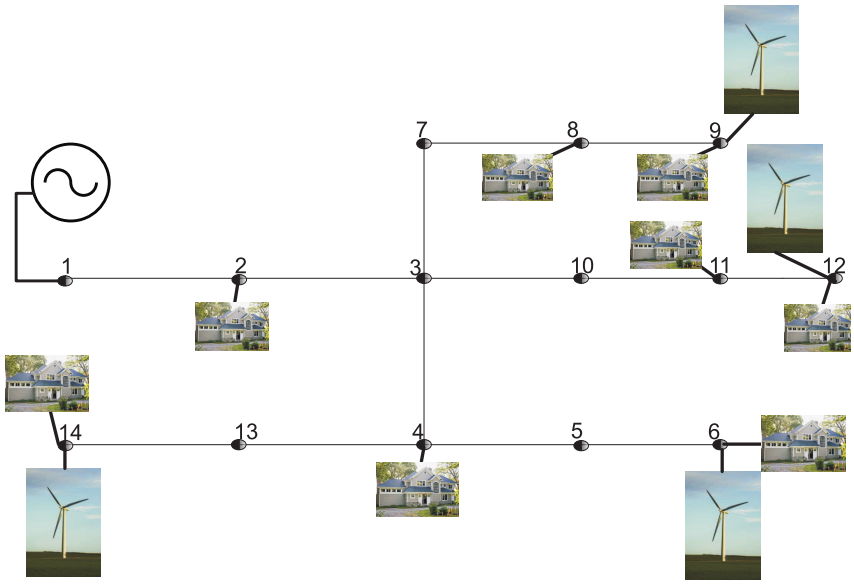

Figure 4.2: Layout of the microgrid connected to the infinite bus

currents and voltages.

The microgrid state variables in this Chapter are chosen based on microgrid elements which are capable of storing energy. These elements can be accounted, such as inductive, capacitive and integrator elements [124], which are included in the proposed microgrid plant model to be controlled.

If a disturbance causes a change in the value of one or more of these state variables, the system is driven from the equilibrium. If thereafter the system returns to its steady state, then it is stable; whereas, if the initial deviation from the steady state becomes larger, then it is unstable.

The main difference between transient stability and small signal stability is that, if a steady state is reached after a disturbance leading to a transient phenomenon, producing a change in the system topology, such as tripping of a generator or a line, the new steady state might be different from the initial state; this case is known as transient stability. In contrast, if a system returns to a steady state after an incremental change in a state variable, this steady state is identical to the initial state, because no change in the network topology has occurred; this case is known as small signal stability.

In this Chapter, eigenvalue analyses are used to reveal the informations of different stability modes. The aim is to illustrate the correspondence between the eigenvalues of the microgrid and their dynamic behaviour. The

linearization of the state equations of the microgrid is applied. Thereafter, the microgrid dominant eigenvalues can be detected, and also the relation between the behaviour of such dominant eigenvalues and the time domain can be obtained.

The behaviour of an electrical power system dynamics can be described based on [124] by equations (4.1) and (4.2).

$$\dot{x}(t) = f(x(t), u(t)) \tag{4.1}$$

$$y(t) = g(x(t), u(t)) \tag{4.2}$$

By assuming that:

f: Vector contains the microgrid first-order non-linear differential equations;

x: Vector contains the microgrid state variables;

u: Vector contains the microgrid control variables;

g: Vector contains the microgrid non-linear algebraic equations;

y: Vector contains the microgrid algebraic output variables;

t: The proposed time of a state variable change.

By assuming that the system indicated by equations (4.1) and (4.2) is time invariant, then the time part can be excluded from these equations.
Equations (4.1) and (4.2) can be linearized based on [2], and the resulting linearized description of the system can be used to investigate its response to small variations in the input or state variables, starting from an equilibrium point. To this end, equations (4.1) and (4.2) are expressed in terms of their Taylor's series expansion. The second and higher orders of the partial derivatives of f and g are excluded and only taking into account the first-order terms. Consequently, the final form can be described by equations (4.3) and (4.4).

$$\Delta\dot{x}(t) = A\Delta x(t) + B\Delta u(t) \tag{4.3}$$

$$\Delta y(t) = C\Delta x(t) + D\Delta u(t) \tag{4.4}$$

Where A, B, C and D are the matrices containing the coefficients of the state variables and system output equations. The proposed microgrid dynamic

model in this Chapter differentiates between the open-loop and closed-loop system. The open loop includes microgrid plant and controller models, whereas the closed loop system applies feed-back concept. As mentioned before that the microgrid state variables in this Chapter are chosen based on microgrid elements which are capable of storing energy. These elements can be accounted, such as inductive, capacitive and integrator elements, which are included in the proposed microgrid plant model to be controlled.

A model of RLC filter will be highlighted in the following part, to clear how the state variables are obtained, and how the linearization model is conducted. Thus, by the same manner, the state space model can be conducted for all the microgrid elements, such as voltage-frequency inverters, doubly-fed induction generators, distribution lines and static loads.

By considering the RLC filter as shown in Figure 4.3, the single phase current and voltage of the inductive part can be regarded as $i_i(t)$ and $v_L(t)$, while the same correspondent values of capacitive part can be regarded as as $i_c(t)$ and $v_c(t)$. Applying the voltage drop equation for the inductive part of the filter as function of time as shown in equation (4.5).

$$v_L(t) = R_f i_i(t) + L_f \frac{d\, i_i(t)}{dt} \tag{4.5}$$

The proposed state space modelling in this Chapter considers all the mi-

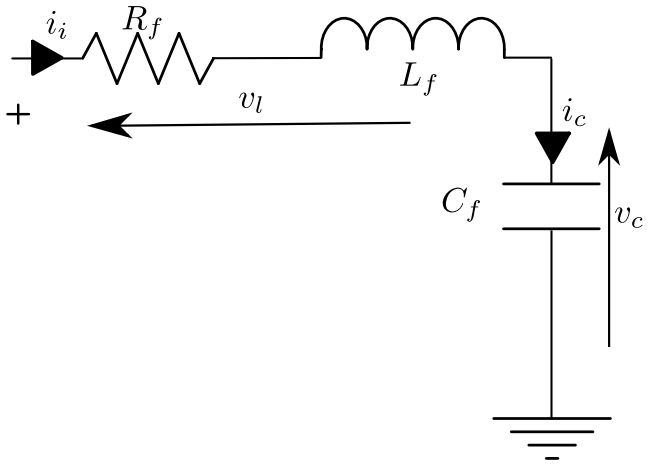

Figure 4.3: RLC filter

crogird state variables are constructed on a synchronous reference frame whose rotation frequency is ω. Therefore, the differentiation considers both the time and rotation frequency, as follows: $(\frac{d}{dt} + j\omega)$. Consequently, equation (4.5) can

be rewritten as follows:

$$v_L(t) = R_f i_i(t) + (\frac{d}{dt} + j\omega) L_f i_i(t) \tag{4.6}$$

The dynamic equations of the filter inductive part can be obtained as shown in equation (4.7).

$$\begin{cases} \dot{i}_{i_d} = \frac{-R_f}{L_f} i_{i_d} + \omega i_{i_q} + \frac{1}{Lf} v_{L_d} \\ \dot{i}_{i_q} = -\omega i_{i_d} + \frac{-R_f}{L_f} i_{i_q} + \frac{1}{Lf} v_{Lq} \end{cases} \tag{4.7}$$

Where:

i_i: Inductance filter current;

ω: Operating frequency;

v_L: Filter inductance voltage drop.

Typically, the microgrid frequency is variable with respect to time, during normal cases of power exchange among the microgrid generators and during transient cases. Thus, equation (4.7) is considered non-linear equation. The considered non-linear terms in equation (4.7) are (ωi_{i_q}) and $(-\omega i_{i_d})$. The linearized equation for the filter inductive part is shown by equation (4.8). The operator Δ indicates the linearized variables, while the subscript 0 indicates the linearization around the considered system operating point.

$$\begin{bmatrix} \Delta\dot{i}_{i_d} \\ \Delta\dot{i}_{i_q} \end{bmatrix} = \begin{bmatrix} \frac{-R_f}{L_f} & \omega_0 \\ -\omega_0 & \frac{-R_f}{L_f} \end{bmatrix} \begin{bmatrix} \Delta i_{i_d} \\ \Delta i_{i_q} \end{bmatrix} + \begin{bmatrix} \frac{1}{L_f} & 0 \\ 0 & \frac{1}{L_f} \end{bmatrix} \begin{bmatrix} \Delta v_{Ld} \\ \Delta v_{Lq} \end{bmatrix} + \begin{bmatrix} I_{i_q} \\ -I_{i_d} \end{bmatrix} \begin{bmatrix} \Delta\omega \end{bmatrix} \tag{4.8}$$

The linearized equation of the filter capacitive part can be derived by the same manner. The current in the filter capacitive part can be indicated by equation (4.9). By assuming that internal resistance $R_c = 0$, the final linearized equation of the capacitive part is shown by equation (4.10)

$$i_c(t) = R_c v_c(t) + (\frac{d}{dt} + j\omega) C_f v_c(t) \tag{4.9}$$

$$\begin{bmatrix} \Delta\dot{v}_{c_d} \\ \Delta\dot{v}_{c_q} \end{bmatrix} = \begin{bmatrix} 0 & \omega_0 \\ -\omega_0 & 0 \end{bmatrix} \begin{bmatrix} \Delta v_{c_d} \\ \Delta v_{c_q} \end{bmatrix} + \begin{bmatrix} \frac{1}{C_f} & 0 \\ 0 & \frac{1}{C_f} \end{bmatrix} \begin{bmatrix} \Delta i_{cd} \\ \Delta i_{cq} \end{bmatrix} + \begin{bmatrix} V_{c_q} \\ -V_{c_d} \end{bmatrix} \begin{bmatrix} \Delta\omega \end{bmatrix} \tag{4.10}$$

Where:

v_c: Tension of capacitor filter;

i_c: Filter capacitor current.

The state space modelling of the rest microgrid elements can be obtained by the same manner of the RLC filter. The following Section shows the state space modelling of the voltage-frequency inverter based on the droop control strategy as shown in equations (2.7) and (2.8).

4.4.2 Voltage-Frequency Inverter State Space Modelling

The proposed model of the voltage-frequency inverter is shown in Figure 4.4, as it consists of LCL output filter and controllers of power, voltage and current. The inverter dc bus dynamics are neglected with respect to high switching frequencies (4-10 kHz).

The reason for LCL filter choice is that the droop control is mainly based on the assumption that the output impedance of the generator is pure inductive, due to the large impedance of the filter and power lines. However, the impedance of power lines in low voltage application, as the case of microgrids is mainly resistive. This problem can be overcome by adding an output inductor, leading to LCL output filter.

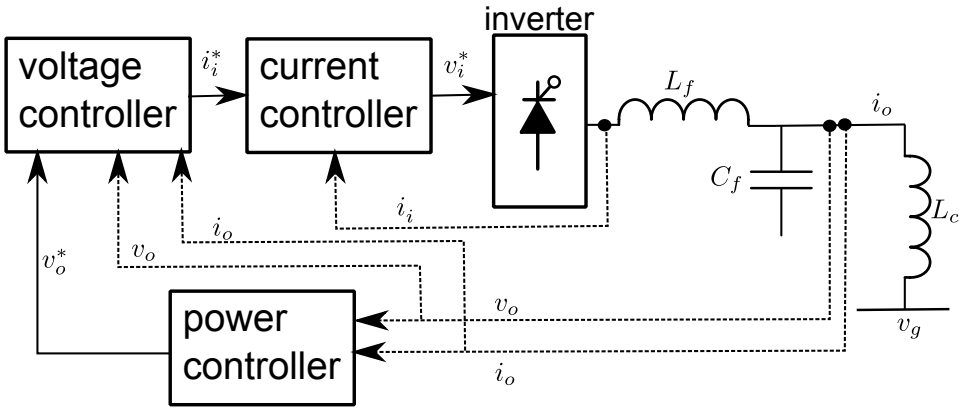

Figure 4.4: Voltage-frequency inverter

As mentioned in the previous Section, in order to derive the state space modelling, the separation between open-loop and closed-loop circuits must be cleared. Thus, in case of voltage-frequency inverter, the open-loop is considered as the LCL filter and the controllers of the inverter. The feed-back part

considers the introduced control variables to the inverter controllers, as shown in Figure 4.4.

LCL Filter

The detailed LCL filter is shown in Figure 4.5. By considering the same manner for modelling the RLC filter, the state variables of LCL filter are chosen as the inductance currents i_i, i_o and the voltage across the capacitor v_o. The linearized model of the LCL filter is shown by the following equation.

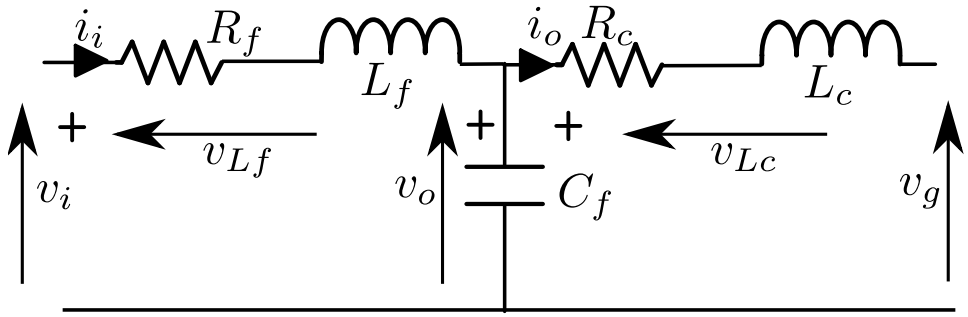

Figure 4.5: LCL filter

$$\begin{bmatrix} \Delta\dot{i}_{i_d} \\ \Delta\dot{i}_{i_q} \\ \Delta\dot{v}_{o_d} \\ \Delta\dot{v}_{o_q} \\ \Delta\dot{i}_{o_d} \\ \Delta\dot{i}_{o_q} \end{bmatrix} = \begin{bmatrix} \frac{-R_f}{L_f} & \omega_0 & \frac{-1}{L_f} & 0 & 0 & 0 \\ -\omega_0 & \frac{-R_f}{L_f} & 0 & \frac{-1}{L_f} & 0 & 0 \\ \frac{1}{C_f} & 0 & 0 & \omega_0 & \frac{-1}{C_f} & 0 \\ 0 & \frac{1}{C_f} & -\omega_0 & 0 & 0 & \frac{-1}{C_f} \\ 0 & 0 & \frac{1}{L_c} & 0 & 0 & \omega_0 \\ 0 & 0 & 0 & \frac{1}{L_c} & -\omega_0 & 0 \end{bmatrix} \begin{bmatrix} \Delta i_{i_d} \\ \Delta i_{i_q} \\ \Delta v_{o_d} \\ \Delta v_{o_q} \\ \Delta i_{o_d} \\ \Delta i_{o_q} \end{bmatrix} + \begin{bmatrix} \frac{1}{Lf} & 0 & 0 & 0 \\ 0 & \frac{1}{Lf} & 0 & 0 \\ 0 & 0 & 0 & 0 \\ 0 & 0 & 0 & 0 \\ 0 & 0 & \frac{-1}{Lc} & 0 \\ 0 & 0 & 0 & \frac{-1}{Lc} \end{bmatrix} \begin{bmatrix} \Delta v_{i_d} \\ \Delta v_{i_q} \\ \Delta v_{g_d} \\ \Delta v_{g_q} \end{bmatrix}$$
$$+ \begin{bmatrix} I_{i_q} \\ -I_{i_d} \\ Vo_q \\ -Vo_d \\ I_{o_q} \\ -I_{o_d} \end{bmatrix} \begin{bmatrix} \Delta\omega \end{bmatrix} \tag{4.11}$$

Where:

i_i: Inductance filter current;

i_o: Output filter current of the inverter;

v_o: Filter capacitor tension;

v_g: Microgrid node tension.

Power Controller

The external power control loop sets the magnitude of the frequency and inverter output voltage, according to the droop characteristics for the real and reactive power. The instantaneous active and reactive power components $\tilde{p}$ and $\tilde{q}$ respectively are calculated from the measured output voltage and current as shown by equation (4.12).

$$\begin{cases} \tilde{p} = 1.5(v_{od}i_{od} + v_{oq}i_{oq}) \\ \tilde{q} = 1.5(v_{oq}i_{od} - v_{od}i_{oq}) \end{cases} \tag{4.12}$$

Where:

$\tilde{q}$: Instantaneous reactive power;

$\tilde{p}$: Instantaneous active power.

The instantaneous power components are passed through low-pass filters of cut-off frequency ω_c, to limit the high transient variation, as shown in equation (4.13) and Figure 4.6.

$$\begin{cases} P = \frac{\omega_c}{s+\omega c}1.5(v_{od}i_{od} + v_{oq}i_{oq}) \\ Q = \frac{\omega_c}{s+\omega c}1.5(v_{oq}i_{od} - v_{od}i_{oq}) \end{cases} \tag{4.13}$$

The linearized equation of the power controller is indicated by equation(4.14), where the variables P and Q are considered as state variables. The operator

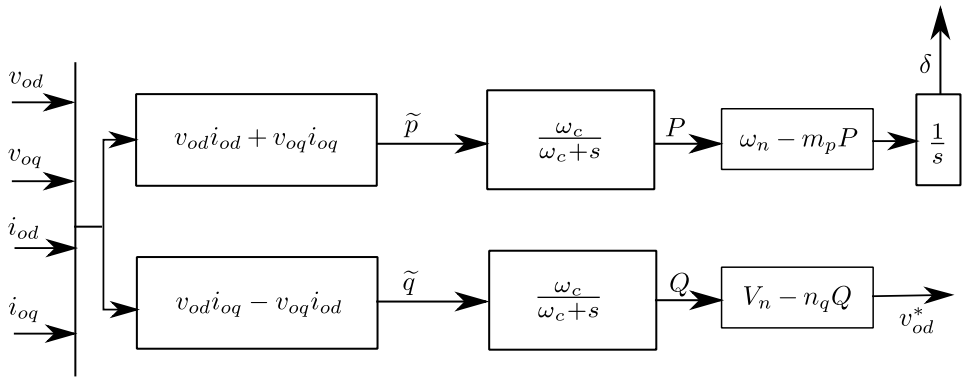

Figure 4.6: Inverter power controller

Δ indicates to the linearized variables, while variables $I_{od}, I_{oq}, V_{od}, V_{oq}$ are the variables of the considered operating point.

$$\begin{cases} \Delta\dot{P} = -\omega_c\Delta P + 1.5\omega_c(\Delta v_{od}I_{od} + \Delta v_{oq}I_{oq} + V_{od}\Delta i_{od} + V_{oq}\Delta i_{oq}) \\ \Delta\dot{Q} = -\omega_c\Delta Q + 1.5\omega_c(\Delta v_{oq}I_{od} - \Delta v_{od}I_{oq} + V_{oq}\Delta i_{od} - V_{od}\Delta i_{oq}) \end{cases} \tag{4.14}$$

Voltage and Current Controller

The output voltage and current are processed by the voltage-current controller. The output voltage control is achieved through PI controllers, taking into consideration that the inverter voltage is decomposed into dq coordinates, and the voltage across the q coordinate is assumed to be zero. The proposed current controller is employed to limit the high transient current, and improves the control dynamics of the system; therefore, the semiconductor protection can be ensured.

Figure 4.7 shows the inverter voltage-current controller; the dynamic equations of the voltage-current controller are shown by equation (4.15), where $s = \frac{d}{dt}$. The state variables in this case output from the controller integrators. Thereby, the terms $\Phi_{vd}, \Phi_{vq}, \zeta id, \zeta iq$ are considered as the state variables.

$$\begin{cases} i^*_{id} - i_{id} = e_{id} = s\zeta id \Longrightarrow \dot{\zeta} id = i^*_{id} - v_{id} \\ i^*_{iq} - i_{iq} = e_{iq} = s\zeta iq \Longrightarrow \dot{\zeta} iq = i^*_{iq} - v_{iq} \\ v^*_{od} - v_{od} = e_{vd} = s\Phi_{vd} \Longrightarrow \dot{\Phi}_{vd} \\ v^*_{oq} - v_{oq} = e_{vq} = s\Phi_{vq} \Longrightarrow \dot{\Phi}_{vq} \end{cases} \tag{4.15}$$

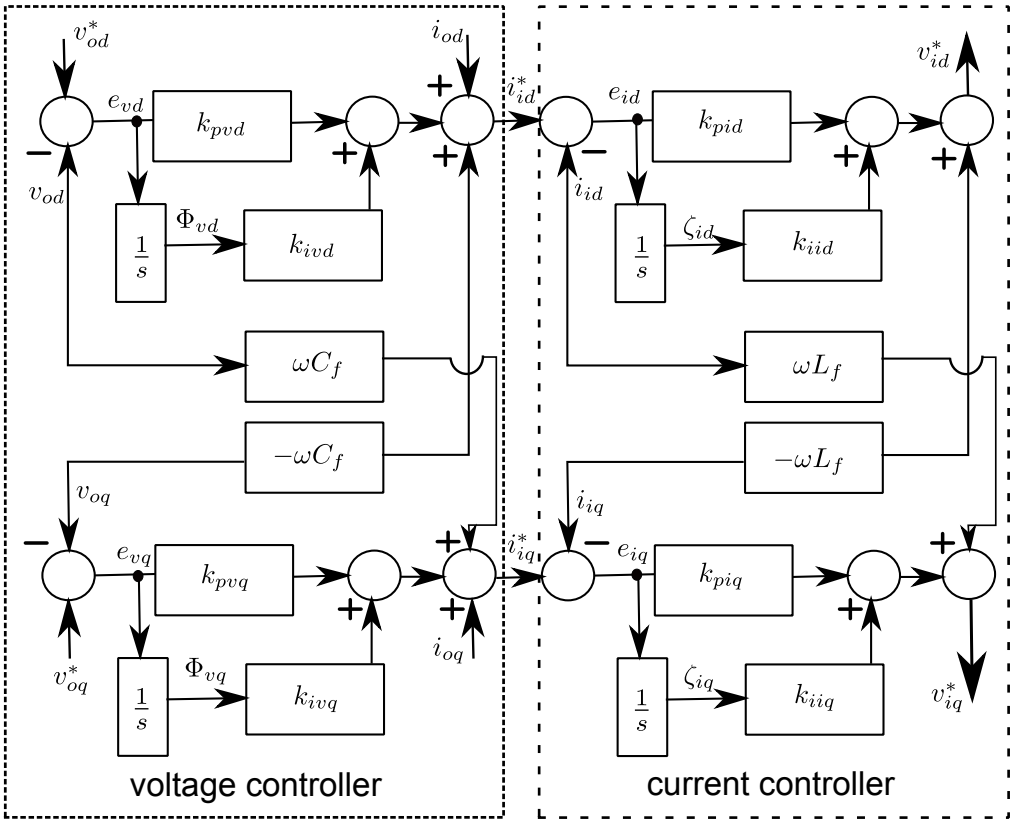

Figure 4.7: Inverter voltage-current controller

Microgrid Reference Frame

In the case of isolated microgrid, the network state space modelling is represented on the reference frame of one of the individual inverters (the master inverter), whereas in the case of grid-connected mode, the reference frame is considered as the infinite bus. This reference frame is regarded as the common reference frame, and all the other inverters are referred to it. The common reference frame must be chosen to rotate at the same frequency of the microgrid. The output voltage of each inverter is related directly to the microgrid. Therefore, it is a good choice to consider the output voltage of the master inverter as the common reference for the whole microgrid state variables.

Figure 4.8 shows the common reference frame of the master voltage-frequency inverter. This frame is denoted by DQ coordinates, and pulsating by the same frequency of the master inverter in dq1 coordinates by frequency $\omega = \omega_1$. If another inverter is decomposed into dq2 coordinates, and to be connected

to the microgrid, this inverter will be aligned to the master inverter frame by an angle δ_2, as shown in equation(4.16).

By considering the droop relation between the frequency and active power, which is indicated by $\Delta\omega = -m_p\Delta P$, and in order to relate each inverter rotating frame to the common reference frame, each inverter reference frame can be referred to the master one by equation (4.17). Consequently, each inverter output voltage can be referred to the common reference frame by transformation as shown in equation(4.18). Finally, the linearized equations of the new derived inverter voltage can be rewritten as indicated by equation (4.19).

$$\dot{\delta}_2 = \omega_2 - \omega_1 \tag{4.16}$$

$$\Delta\dot{\delta}_j = \omega_j - \omega_1 = -m_{pj}\Delta P_j + m_{p1}\Delta P_1 \tag{4.17}$$

$$\begin{cases} v_{oDj} = v_{odj}\, cos(\delta_j) - v_{oqj}\, sin(\delta_j) \\ v_{oQj} = v_{odj}\, sin(\delta_j) + v_{oqj}\, cos(\delta_j) \end{cases} \tag{4.18}$$

$$\begin{cases} \Delta v_{oDj} = cos(\delta_{j_o})\, \Delta v_{odj} - sin(\delta_{j_o})\, \Delta v_{oqj} - V_{odj}\, sin(\delta_{j_o})\Delta\delta_j - V_{oqj}\, cos(\delta_{j_o})\Delta\delta_j \\ \Delta v_{oQj} = sin(\delta_{j_o})\, \Delta v_{odj} + cos(\delta_{j_o})\, \Delta v_{oqj} + V_{odj}\, cos(\delta_{j_o})\Delta\delta_j - V_{oqj}\, sin(\delta_{j_o})\Delta\delta_j \end{cases} \tag{4.19}$$

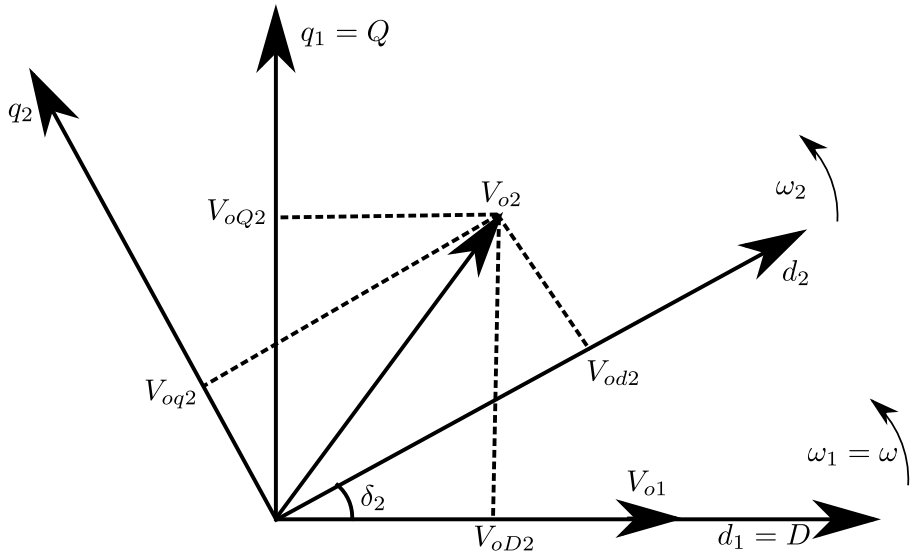

Figure 4.8: Reference frame transformation

As mentioned in the previous Section, the proposed model in this Chapter

differentiates between the open-loop and closed-loop system. The controller gains are defined by a separate matrix included by the feedback system. Therefore the effect of the controller gains change can be observed. The state space modelling can be defined by the following form:

$$\left[\begin{array}{c|c} \dot{x} \\ \hline 0 \end{array}\right] = \left[\begin{array}{c|c} J_{1A} & J_{2A} \\ \hline J_3 & J_4 \end{array}\right] \left[\begin{array}{c|c} x \\ \hline z \end{array}\right] + \left[\begin{array}{c|c} J_{5A} \\ \hline J_6 \end{array}\right] \left[\begin{array}{c} u \end{array}\right]$$

$$\left[\begin{array}{c|c} y \\ \hline 0 \end{array}\right] = \left[\begin{array}{c|c} J_{1C} & J_{2C} \\ \hline J_3 & J_4 \end{array}\right] \left[\begin{array}{c|c} x \\ \hline z \end{array}\right] + \left[\begin{array}{c|c} J_{5C} \\ \hline J_6 \end{array}\right] \left[\begin{array}{c} u \end{array}\right]$$

Where x is the state variables matrix, z is the algebraic variables matrix, u is the control variables matrix and y is the output variables matrix. The proposed model of the inverter in this Chapter considers the following matrices:

$$\Delta x = [\Delta i_{id} \quad \Delta i_{iq} \quad \Delta v_{od} \quad \Delta v_{oq} \quad \Delta i_{od} \quad \Delta i_{oq} \quad \Delta \zeta_{id} \quad \Delta \zeta_{iq} \quad \Delta \Phi_{vd} \quad \Delta \Phi_{vq} \quad \ldots$$

$$\Delta P \quad \Delta Q \quad \Delta \delta]^T$$

$$\Delta u = [\Delta v_{id} \quad \Delta v_{iq} \quad \Delta i_{id} \quad \Delta i_{iq}]^T$$

$$\Delta z = [\Delta V_{gD} \quad \Delta V_{gQ}]^T$$

4.4.3 Doubly-Fed Induction Generator State Space Modelling

The doubly-fed induction machine is basically a wound rotor induction machine with its stator windings directly connected to the grid and its rotor windings connected to the grid through a converter. The AC/DC/AC Converter is divided into the rotor side converter and grid side converter. These converters use force commutated power electronic devices to synthesize an AC Voltage from a DC source. A capacitor connected on the DC side acts as the DC voltage source.

Figure 4.9 shows the Power flow in the DFIG. The electro-magnetic torque T_e is positive for power generation and the electrical frequency ω_s is positive and constant for a constant grid frequency. P_r is positive, if the DFIG mechanical speed is greater than the synchronous speed, and it is negative, if the

mechanical speed is lower than the synchronous speed. The rotor side and the grid side converters have the capability of generating or absorbing reactive power and can be used to control the reactive power or the voltage at the grid terminals. The rotor side converter is used to control the wind turbine output real power, whereas the reactive power control is assumed deactivated in the proposed DFIG model in this Chapter, as the reactive power control is managed only by the voltage-frequency inverters. The grid side converter is used to regulate the voltage of the DC bus capacitor.

By the same manner of the inverter state space modelling, the DFIG model can be derived. The model separates between open-loop and closed-loop systems. The open-loop includes the induction generator part and the regulators regarding grid side converter (GSC) and the rotor side converter (RSC), while the feedback system includes the control variables which are introduced to GSC and RSC controllers.

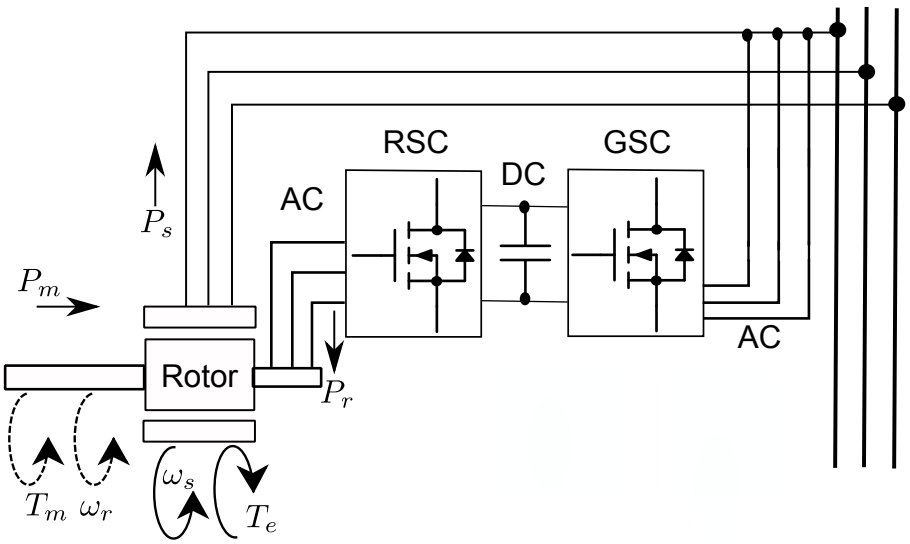

Figure 4.9: DFIG power flow

Induction Generator

The induction machine can be represented by the transformer per phase equivalent circuit model, where R_r and X_r are the rotor resistance and reactance before being referred to the stator side, as shown in Figure 4.10. The DFIG induction machine steady state model is decomposed into the dq coordinates, and can be briefed by equations (4.4.3)-(4.4.3).

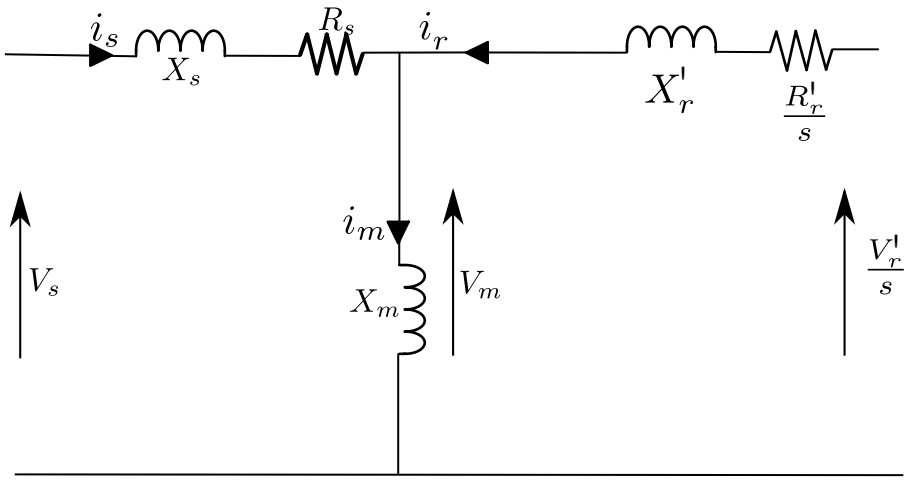

Figure 4.10: Induction machine equivalent circuit

$$\begin{cases} V_{md} = R_s i_{sd} + \omega_{pll} i_{sq} L_{sd} + V_{sd} \\ V_{mq} = V_{sq} - R_s i_{sq} - \omega_{pll} i_{sd} L_{sd} \\ \Psi_s = \frac{\sqrt{(V_{sd} - R_s i_{sd})^2 + (V_{sq} - R_s i_{sq})^2}}{\omega_{pll}} \end{cases} \tag{4.19}$$

$$\begin{cases} V_{md} = V_{rd} + \omega_{pll} L_{rd} i_{rq} - R_r i_{rd} - \omega_r L_m i_{mq} \\ V_{mq} = V_{rq} - \omega_{pll} L_{rd} i_{rd} - R_r i_{rq} + \omega_r L_m i_{md} \end{cases} \tag{4.19}$$

$$\begin{cases} V_{md} = -\omega_{pll} L_m i_{mq} \\ V_{mq} = \omega_{pll} L_m i_{md} \end{cases} \tag{4.19}$$

$$T_m = T_e + F \,.\, \frac{\omega_r}{p} \tag{4.19}$$

Where:

i_m: DFIG magnetization current;

i_r: DFIG rotor current;

i_s: DFIG stator current;

T_e: DFIG electromagnetic torque;

T_m: DFIG mechanical torque;

v_m: DFIG magnetization circuit tension;

v_r: DFIG rotor tension;

v_s: DFIG stator tension;

ω_r: Wind turbine mechanical speed;

ω_{pll}: DFIG pulsation frequency;

F: Wind turbine friction constant;

p: DFIG poles number.

The linearized model of the induction generator can be derived by the same manner of the RLC filter. The induction generator linearized equations are briefed by equations (4.4.3)-(4.4.3).

$$\begin{cases} \Delta\dot{i_{sd}} = -\frac{R_s}{L_{sd}}\Delta i_{sd} + \omega_{pll}\Delta i_{sq} + \frac{1}{L_{sd}}\Delta V_{sd} - \frac{1}{L_{sd}}\Delta V_{md} + I_{sq}\Delta\omega_{pll} \\ \Delta\dot{i_{sq}} = -\omega_{pll}\Delta i_{sd} - \frac{R_s}{L_{sd}}\Delta i_{sq} + \frac{1}{L_{sd}}\Delta V_{sq} - \frac{1}{L_{sd}}\Delta V_{mq} - I_{sd}\Delta\omega_{pll} \end{cases} \tag{4.19}$$

$$\begin{cases} \Delta\dot{i_{rd}} = -\frac{R_r}{L_{rd}}\Delta i_{rd} + (\omega_{pll} - \omega_r)\Delta i_{rq} + \frac{1}{L_{rd}}\Delta V^*_{rd} - \frac{1}{L_{rd}}\Delta V_{md} - \frac{L_m}{L_{rd}}\omega_r\Delta i_{mq} \\ +(-I_{rq} - \frac{L_m}{L_{rd}}I_{mq})\Delta\omega_r + I_{rq}\Delta\omega_{pll} \\ \Delta\dot{i_{rq}} = -\frac{R_r}{L_{rd}}\Delta i_{rq} - (\omega_{pll} - \omega_r)\Delta i_{rd} + \frac{1}{L_{rd}}\Delta V^*_{rq} - \frac{1}{L_{rd}}\Delta V_{mq} + \frac{L_m}{L_{rd}}\omega_r\Delta i_{md} \\ +(I_{rd} + \frac{L_m}{L_{rd}}I_{md})\Delta\omega_r - I_{rd}\Delta\omega_{pll} \end{cases}$$

$$\begin{cases} \Delta\dot{i_{md}} = \omega_{pll}\Delta i_{mq} + \frac{1}{L_m}\Delta V_{md} + I_{mq}\Delta\omega_{pll} \\ \Delta\dot{i_{mq}} = -\omega_{pll}\Delta i_{md} + \frac{1}{L_m}\Delta V_{mq} - I_{md}\Delta\omega_{pll} \end{cases} \tag{4.19}$$

$$\Delta\dot{\omega_{r_{elec}}} = \frac{p.T_m}{J} - \frac{F}{J}.\omega_r - \frac{p.T_e}{J} \tag{4.19}$$

Where:

J: Wind turbine inertia constant.

Rotor-Side Converter

The proposed control scheme of the rotor-side converter is illustrated in Figure 4.11. In order to decouple the electromagnetic torque and rotor excitation current, the induction generator is controlled in a synchronously rotating

stator-flux-oriented reference frame, with its d-axis oriented along the stator-flux vector position. The PI controllers are used for rotor current regulation.

The first part of the RSC controller aims at controlling the active power, so as to track the P_{ref}, which is shown by Figure 4.11b. The reference active power is determined by the wind turbine power speed characteristic $(C_p - \lambda)$ curve for maximum power extraction. The second part of the RSC controller is shown by Figure 4.11a, and aims at controlling the reactive power, but it is deactivated in the proposed model.

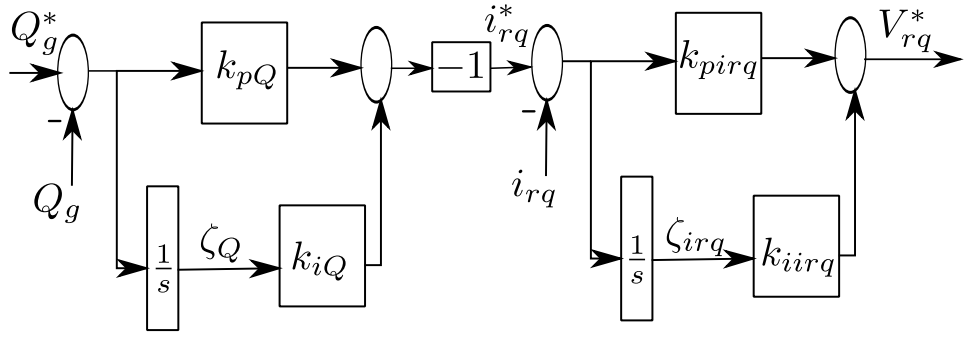

Figure 4.11: Control scheme of the rotor-side converter: (a) Reactive power controller. (b) Active power controller.

The linearized model of the RSC is shown by equation (4.20).

$$\begin{cases} \Delta\dot{\zeta_Q} = -\Delta Q_g = 1.5I_{gq}\Delta V_{sd} - 1.5I_{gd}\Delta V_{sq} + 1.5V_{sd}\Delta i_{igq} - 1.5V_{sq}\Delta i_{gd} \\ \Delta\dot{\zeta_{ird}} = \Delta i_{rd}^* - \Delta i_{rd} = -\frac{L_m+L_{sd}}{1.5pL_m\,.\,\Psi_s^2}T_e^*\,.\,\Delta\Psi_s + \frac{L_m+L_{sd}}{1.5pL_m\,.\,\Psi_s}\Delta T_e^* - \Delta i_{rd} \\ \Delta\dot{\zeta_{irq}} = \Delta i_{rq}^* - \Delta i_{rq} \end{cases} \tag{4.20}$$

Where:

Ψ_s: DFIG stator flux linkage;

ζ_Q: Integral term of DFIG rotor side converter state variable;

i_g: Output current from DFIG to the microgrid;

ζ_{i_r}: Integral term of DFIG rotor side converter;

Q: Reactive power.

DC-link capacitor

The equation which describes the energy balance of the DC-link capacitor is indicated in equation (4.21), while the DC-link circuit is shown by Figure 4.12.

$$\begin{cases} i_{C_{dc}}V_{dc} = 1.5(i_{rd}V_{rd} + i_{rq}V_{rq}) \\ i_{C_{dc}}V_{dc} = 1.5(i_{bd}V_{bd} + i_{bq}V_{bq}) \end{cases} \tag{4.21}$$

The linearized model of the DC-link circuit is shown by equation (4.22)

$$\Delta\dot{V_{dc}} = \frac{\Delta i_b}{C_{dc}} - \frac{\Delta i_r}{C_{dc}} \tag{4.22}$$

Where:

i_b: Input current to DC-link circuit;

i_{Cdc}: DC-link capacitor current;

v_b: DC-link tension.

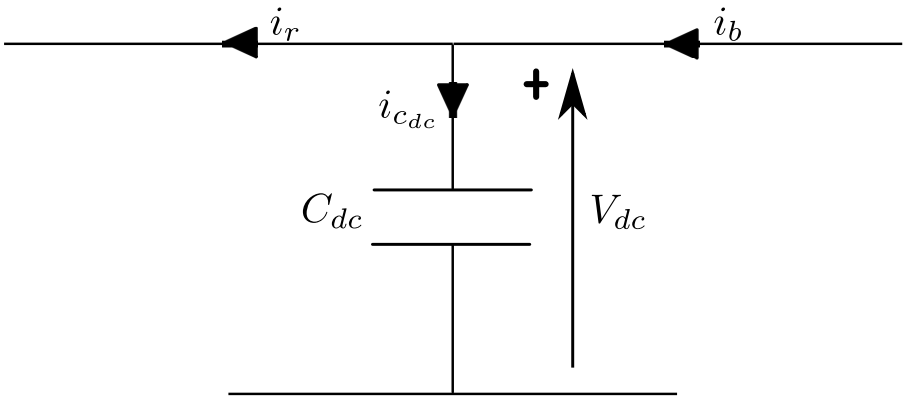

Figure 4.12: DC-link circuit

Grid-Side Converter

Figure 4.13a shows the DFIG reference frame transformation, as the DFIG stator voltage must be synthesized with the microgrid frequency. Thus, the stator voltage reference frame is transformed to the common reference frame, by the same manner as mentioned in the voltage-frequency inverter modelling. Figure 4.13b shows the DFIG phase-locked loop circuit, as the pulsation of the DFIG reference frame is obtained from the DFIG stator voltage.

Figures 4.14a and 4.14b show the control scheme of the grid-side converter. The converter control operates in the synchronously rotating grid voltage-oriented reference frame with its d-axis oriented along the grid voltage vector position. The PI controllers are used for DC-link voltage regulation. The reference signal for the DC voltage V_{dc}^* is set to a constant value independent of the wind speed.

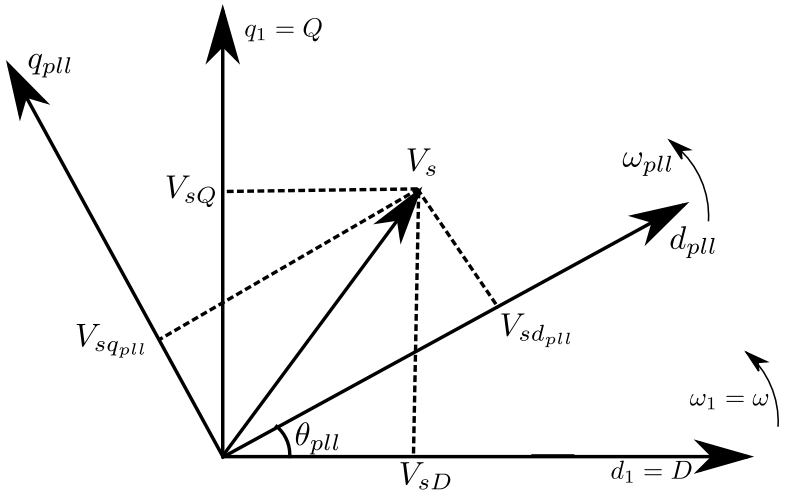

(a)

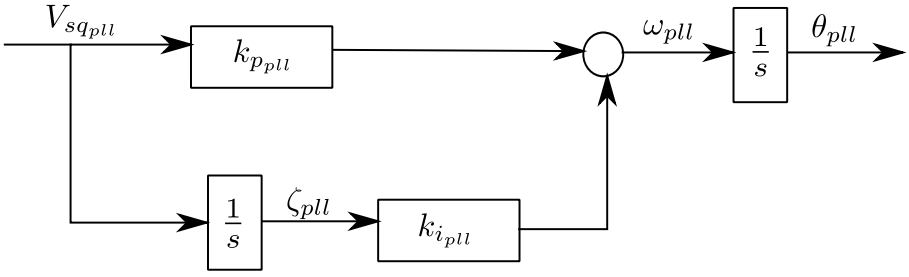

(b)

Figure 4.13: DFIG reference frame: (a) DFIG reference frame transformation. (b) DFIG phase-locked loop circuit.

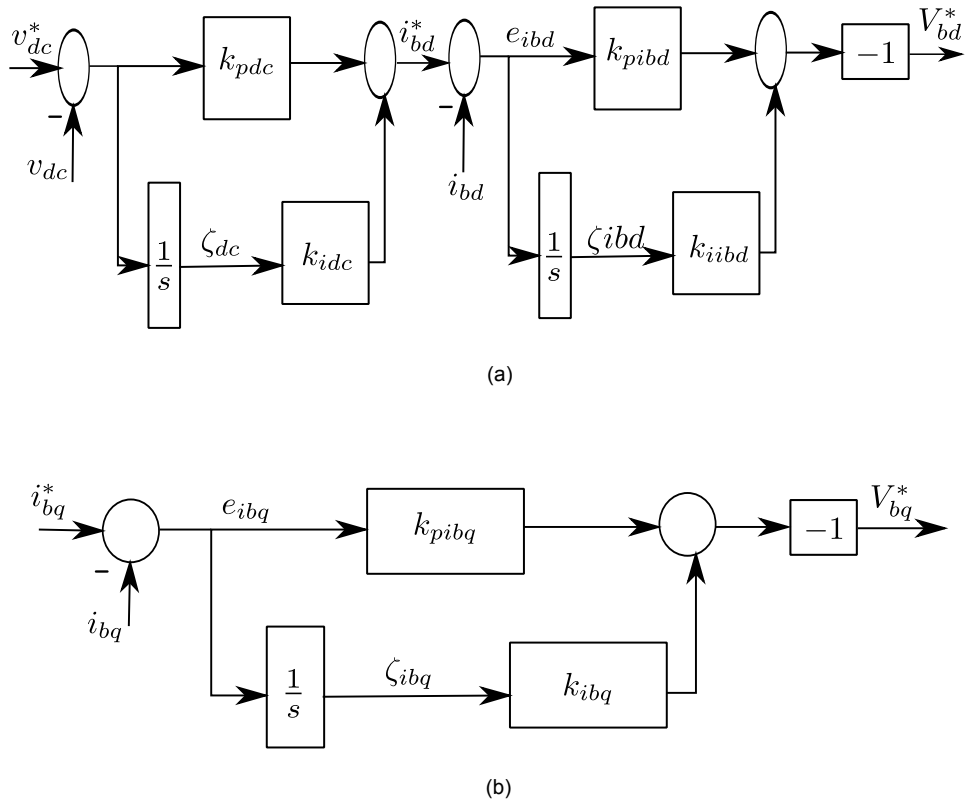

Figure 4.14: Control scheme of the grid-side converter: (a) Control scheme in the coordinate-d. (b) Control scheme in the coordinate-q

The linearized model of the GSC is shown by equation (4.23)

$$\begin{cases} \Delta\dot{(i_{bd})} = -\frac{R_b}{L_b}\Delta i_{bd} + \omega_{pll}\Delta i_{bq} + \frac{1}{L_b}\Delta V_{sd} - \frac{1}{L_b}\Delta V_{bd} + I_{bq}\Delta\omega_{pll} \\ \Delta\dot{(i_{bq})} = -\frac{R_b}{L_b}\Delta i_{bd} - \omega_{pll}\Delta i_{bd} + \frac{1}{L_b}\Delta V_{sq} - \frac{1}{L_b}\Delta V_{bq} - I_{bd}\Delta\omega_{pll} \\ \Delta\dot{\zeta_{dc}} = -\Delta V_{dc} \\ \Delta\dot{\zeta_{ibd}} = \Delta ibd^* - \Delta ibd \\ \Delta\dot{\zeta_{ibq}} = -\Delta ibq \\ \Delta\dot{\zeta_{pll}} = \Delta V_{sq_{pll}} \\ \Delta\dot{\theta} = \Delta\omega_{pll} - \Delta\omega_1 \end{cases} \tag{4.23}$$

The proposed model of the DFIG in this Chapter considers the following matrices:

$$\Delta x = [\Delta i_{sd} \quad \Delta i_{sq} \quad \Delta i_{rd} \quad \Delta i_{rq} \quad \Delta i_{md} \quad \Delta i_{mq} \quad \Delta\omega_r \quad \Delta\zeta_Q \quad \Delta\zeta_{i_{rd}} \quad \dots$$

$$\Delta\zeta_{i_{rq}} \quad \Delta i_{bd} \quad \Delta i_{bq} \quad \Delta v_{dc} \quad \Delta\zeta_{dc} \quad \Delta\zeta_{i_{bd}} \quad \Delta\zeta_{pll} \quad \Delta\theta_{pll}]^T$$

$$\Delta u = [\Delta v_{rd} \quad \Delta v_{rq} \quad \Delta i_{bd} \quad \Delta v_{bd} \quad \Delta v_{bq} \quad \Delta i_{rq} \quad \Delta\omega_{pll} \quad]^T$$

$$\Delta z = [\Delta v_{md} \quad \Delta v_{mq} \quad \Delta v_{sd} \quad \Delta v_{sq} \quad \Delta i_{gd} \quad \Delta i_{gq} \quad \Delta i_{C_{dc}} \quad \Delta T_e \quad \dots$$

$$\Delta T_m \quad \Delta T_e^* \quad \Delta\psi_s \quad \Delta\lambda_i \quad \Delta C_p]^T$$

4.4.4 Distribution Line State Space Modelling

In conventional power systems, the network dynamics are neglected, due to the high time constant of rotating machines and their controls. In contrast, DGs in microgrids are interfaced by inverters and their response times are small. Therefore network dynamics influence the system stability.
Figure 4.15 shows the modelling of the proposed short distribution line in this Chapter, based on [125]. The model considers both the inductive and resistive terms of the distribution line.

By the same manner, the linearized form of the microgrid distribution lines

can be derived as shown in equation(4.4.4). Where Δ operator corresponds to the linearized variables, whereas I_{line_d} and I_{line_q} are the distribution line variables corresponding to the considered operating point.

$$\begin{bmatrix} \Delta \dot{i}_{line_d} \\ \Delta \dot{i}_{line_q} \end{bmatrix} = \begin{bmatrix} \frac{-R_{line}}{L_{line}} & \omega_0 \\ -\omega_0 & \frac{-R_{line}}{L_{line}} \end{bmatrix} \begin{bmatrix} \Delta i_{line_d} \\ \Delta i_{line_q} \end{bmatrix} + \begin{bmatrix} \frac{1}{L_{line}} & 0 \\ 0 & \frac{1}{L_{line}} \end{bmatrix} \begin{bmatrix} \Delta v_{gi} \\ \Delta v_{gi} \end{bmatrix} + \begin{bmatrix} \frac{-1}{L_{line}} & 0 \\ 0 & \frac{-1}{L_{line}} \end{bmatrix} \begin{bmatrix} \Delta v_{gj} \\ \Delta v_{gj} \end{bmatrix} \begin{bmatrix} I_{line_q} \\ -I_{line_d} \end{bmatrix} \begin{bmatrix} \Delta\omega \end{bmatrix}$$

Where:

i_{line}: Distribution line current.

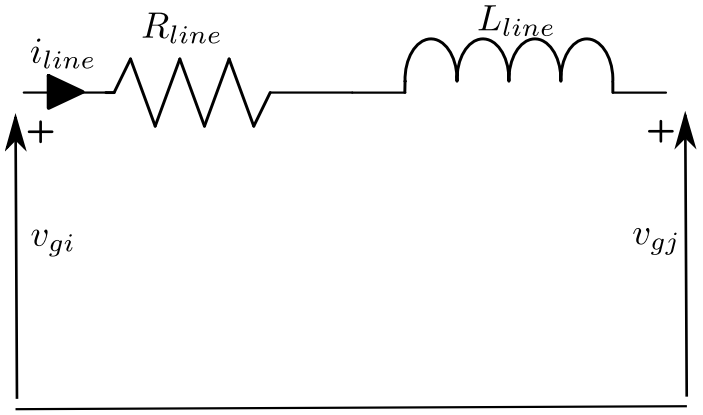

Figure 4.15: Microgrid distribution line

The proposed model of the distribution line in this Chapter considers the following matrices:

$\Delta x = [\Delta i_{lineD} \quad \Delta i_{lineQ}]^T$

$\Delta z = [\Delta V_{gD} \quad \Delta V_{gQ}]^T$

4.4.5 Static Load State Space Modelling

The proposed static load model is shown in Figure 4.16; each static load is connected between its correspondent microgrid node and a neutral point. The

state space modelling is shown by equation (4.4.5).

$$\begin{bmatrix} \dot{\Delta i_{load_d}} \\ \dot{\Delta i_{load_q}} \end{bmatrix} = \begin{bmatrix} \frac{-R_{load}}{L_{load}} & \omega_0 \\ -\omega_0 & \frac{-R_{load}}{L_{load}} \end{bmatrix} \begin{bmatrix} \Delta i_{load_d} \\ \Delta i_{load_q} \end{bmatrix} + \begin{bmatrix} \frac{1}{L_{load}} & 0 \\ 0 & \frac{1}{L_{load}} \end{bmatrix} \begin{bmatrix} \Delta v_{gj} \\ \Delta v_{gj} \end{bmatrix} + \begin{bmatrix} I_{load_q} \\ -I_{load_d} \end{bmatrix} \begin{bmatrix} \Delta\omega \end{bmatrix}$$

Where:

i_{load}: Static load current.

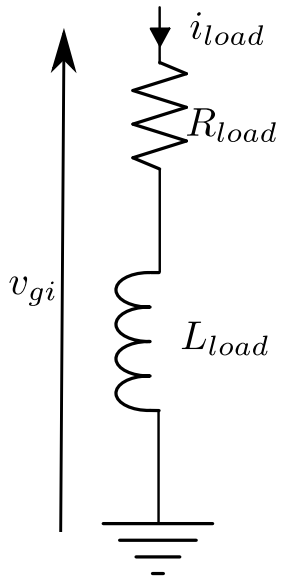

Figure 4.16: Microgrid static Load

The proposed model of the static load in this Chapter considers the following matrices:
$\Delta x = [\Delta i_{loadD} \quad \Delta i_{loadQ}]^T$

$\Delta z = [\Delta V_{gD} \quad \Delta V_{gQ}]^T$

The state space modelling of all proposed microgrid elements were detailed until now. The aim of the next Section is to conduct the eigenvalues of the state matrix. Thereafter, the influence of each dynamic state in the microgrid can be measured through the participation factor index. Also, the correspondence between the eigenvalues of the state matrix and the time domain will be defined.

4.5 Conducting Participation Factor and Time Response

Equations (4.3) and (4.4) can be Laplace transformed; thus, the state equations in the frequency domains are obtained as follows:

$$\begin{cases} s\Delta x(s) - \Delta x(0) = A\Delta x(s) + B\Delta u(s) \\ \Delta y(s) = C\Delta x(s) + D\Delta u(s) \end{cases} \tag{4.23}$$

Rearranging equation (4.5), a solution to the state equations can be obtained as:

$$(sI - A)\Delta x(s) = \Delta x(0) + B\Delta u(s) \tag{4.23}$$

Where I is an identity matrix.

Eigenvalues

The eigenvalues of the matrix A, which was mentioned by equation (4.3) are indicated by λ. The eigenvalues are obtained from the characteristic equation of the matrix A as follows:

$$det(A - \lambda I) = 0 \tag{4.23}$$

The eigenvalues of the matrix A provide information about the system response to a small disturbance, such as any oscillatory mode that exists in the system. The eigenvalues consist of real and imaginary components, and can be indicated as shown by equation (4.5).

$$\lambda = \sigma \pm j\omega \tag{4.23}$$

Typically, the real eigenvalues correspond to a non-oscillatory mode. A negative real eigenvalue represents a decaying mode, while a positive eigenvalue represents aperiodic instability. Complex conjugate eigenvalues correspond to an oscillatory mode.

Participation Factor

The participation matrix provides a measure of the influence of each dynamic state on a given mode. The normalized participation factor P_{ni} of the nth state variable into mode i is shown as follows:

$$P_{ni} = \frac{|\phi_{ni}||\psi_{in}|}{\sum_{i=1}^{n} |\phi_{ni}||\psi_{in}|} \tag{4.23}$$

Where n is the number of state variables, ϕ_{in} is the ith element of the nth right-eigenvector and ψ_{in} is the nth element of the ith left-eigenvector.

Time Response

According to [2], the time response of ith state variable can be shown as follows:

$$\Delta x_i(t) = \phi_{i1}c_1e^{\lambda_1 t} + \phi_{i2}c_2e^{\lambda_2 t} + \cdots + \phi_{in}c_ne^{\lambda_n t} \tag{4.23}$$

Where $c_n = \psi_n \Delta x(0)$. The derived form of this time response complies with the open loop systems only, but in current state space model, the closed loop system is applied. Therefore, another form of time response based on [123] is adopted to define the time response in this Chapter, and can be shown by equation (4.5).

$$\Delta \dot{x}(t) = (A - BKC)\Delta x(t) \tag{4.23}$$

Where K is the system gains matrix, and the term $(A-BKC)$ is the closed loop state variables matrix and can be indicated by A_c.

Thus far, the state space modelling of all proposed microgrid elements were detailed and the eigenvalues, participation factor and time response were defined. The next Sections will show the small signal stability analyses of microgrid under different scenarios.

4.6 Wind Variation Impact on the Microgrid Stability

4.6.1 Introduction

The wind energy is characterized by its fluctuating nature, and so the generated power of wind turbines is completely determined by the wind speed and not controlled any further. Typically, there are two impacts of connecting wind energy to the grid, local and wide impacts of wind power. The local impacts of wind power are the impacts that occur in the electrical vicinity of a wind turbine or wind park that can be attributed to a specific turbine or park.

These effects occur at each turbine or park, independently of the overall wind power penetration level in the system as a whole. Local impacts can be realized in some main points, such as power flow, voltage of power system nodes, harmonics and flickers. The system wide impacts, on the other hand are the impacts which cannot be localized, they cannot be attributed to individual turbines or parks. Nevertheless, they are strongly related to the penetration level in the system as a whole. The wide impacts can be realized in some other points, such as dynamic stability and voltage-frequency control.

Although wind power exploitation appear particularly attractive under ongoing energy policies, the integration of a substantial amount of wind power in isolated electrical systems needs careful consideration, in order to maintain a high degree of reliability and security of the system operation. The main problems concern operational scheduling, due to high production forecasting uncertainties, as well as steady state and dynamic operation disorder [126].

These problems may considerably limit the amount of wind generation that can be connected to the power systems, increasing the complexity of their operation. Thus, beyond voltage stability concerns, frequency stability must be ensured [127]. This depends on the ability of the system to restore balance between generation and load.

The doubly-fed induction generator (DFIG) is one of the most popular wind conversion systems due to its high energy efficiency, reduced mechanical stress on the wind turbine and low power rating of the connected power electronics converter [128]. As the penetration level of DFIG wind power generation into the grid increases, the stability issue of the DFIG wind turbine system is of

particular increasing concern.

The dynamic behaviour of DFIGs based on time-domain simulations have been studied to investigate the performance of the DFIG system and its impact on power system dynamics in [129] and [130]. In [131] and [132], detailed dynamic models of DFIGs have been presented and small signal stability analyses have been conducted. The small signal stability analyses can identify the effects of the system parameters and operating points on the system modes.

The purposes of the behaviour and stability analyses of the DFIG systems can offer better understanding of the system intrinsic dynamics, which can be useful for robust control design of such systems.

The main purpose of this Section, is to study the stability of microgrids supplied by DFIGs and other DGs interfaced through inverters, with respect to wind speed increment. The simulations are processed for the isolated microgrid, and also for grid-connected mode.

4.6.2 Processing Simulations

Through this Section, the wind speed increment is simulated, in order to determine the critical eigenvalues. The proposed microgrid is shown in Figure 4.1, where the microgrid is isolated. The wind speed is sampled from 1.5 m/s to 8 m/s for the first DFIG only at the 6th node of the microgrid, while the wind speeds at other DFIGs are assumed constant at 7 m/s; two hundred samples are taken, also the proportional and integral dc-link gains of all DFIGs supplying the microgrid k_{pdc}, k_{idc} are set as 1.1.

Figure 4.17 shows the loci of dominant eigenvalues of the isolated microgrid during wind speed increment. Figure 4.17a is related to the first DFIG magnetization current i_{mdq_1}; Figure 4.17b is related to the mode dominated by the dc-link state variables of the first DFIG v_{dc_1}, ζ_{dc_1}; Figure 4.17c is related to the mode of the voltage-frequency inverters affected by angle of rotation state variables $\delta_{2,3}$; Figure 4.17d belongs to the dc-link mode of the second, third and fourth DFIGs $v_{dc_{2,3}}, \zeta_{dc_{2,3,4}}$.

Table 4.1 shows the dominant modes of current simulation, participation factors and their damping ratios. In Table 4.1, the first three columns belong to the status of the dominant state variables at the first simulation sample, while the last column of remarks belong to the status of the dominant state

variables at the last simulation sample.

Table 4.1 and Figure 4.17 show that the system is stable through all the range of wind speed increment, because there are not any mode cross the imaginary axis creating a saddle node or Hopf bifurcations, but at the same time, its observed that oscillatory modes affected mainly by magnetization currents either of the first DFIG where the wind speed variations occur, or other DFIGs of constant wind speed overall simulation, move towards the imaginary axis.

The modes dominated by magnetization currents are divided into coupled modes, which are dominated by all DFIGs magnetization currents and other decoupled modes affected by magnetization current of first DFIG only, and the latter has lower damping ratio.

The modes dominated by dc-link state variables are decoupled, as ζ_{dc_1} of the first DFIG is a dominant mode, but its response clearly improves through moving to the left part at the real axis as shown in Figure 4.17b, while other DFIGs dc-link modes are out of interest, because of being far from the imaginary axis; thus, their analyses are ignored.

The mechanical speed variables of the DFIGs affect some modes, all of them lay at the real axis without any oscillation, and these modes are decoupled, as the modes dominated by the first DFIG of the changeable speed is separated from the rest DFIGs, and all the mechanical modes of the DFIGs are nearly fixed, they do not show better or worse behaviour during the wind speed increase.

The modes affected by inverters angle of rotation are oscillatory at low frequency (11.1 rad/sec) and far from the imaginary axis, and so they are not included in the analysis. These modes as shown in Figure 4.17c, and move by little values to higher frequencies far from the imaginary axis, such a movement is logic, due to different levels of power exchange during the wind speed variation, and so the inverters try to resynchronize and recover from power swings.

Clearly, the dominant modes through current simulation are dedicated to the mechanical speed, dc-link and magnetization currents of the DFIGs.

Table 4.1: Dominant Modes of the Isolated MG During Wind Speed Increment-Case 1

$\lambda = \sigma \pm j\omega$	f, HZ	Damping (ξ)	Dominant states	Participation factor	Remarks
-0.28+j311.05	49.49	0.0009	electrical, i_{mdq_1}	0.37	stable
-1.16	0	1	electrical, v_{dc_1}, ζ_{dc_1}	1	stable
-2.24	0	1	electrical, ζ_{dc_2}	0.96	stable
-0.96+j311.1	49.5	0.0031	electrical, $i_{mdq_{1,2,3,4}}$	0.13	stable
-0.28+j311	49.4	0.00099	electrical, $i_{mdq_{2,3}}$	0.29	stable
-0.0019	0	1	mechanical, w_{r_1}	1	stable
-0.009	0	1	mechanical, $w_{r_{2,3,4}}$	0.47	stable

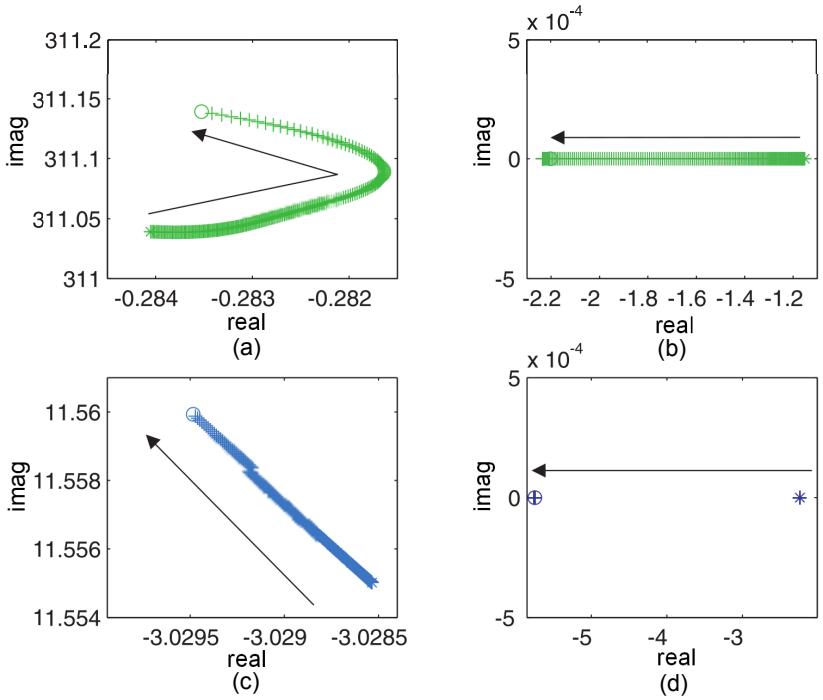

Figure 4.17: Loci of eigenvalues of the isolated microgrid during wind variation-case 1: (a) Magnetization current mode of the 1st DFIG i_{mdq_1}. (b) DC-link mode of the 1st DFIG $v_{dc_1} and \zeta_{dc_1}$. (c) Inverters angle of rotation mode θ_{pll}. (d) DC-link mode of the 2nd, 3rd and 4th DFIGs $v_{dc_{2,3}} and \zeta_{dc2,3,4}$.

The Effect of Reducing the DC-Link Control Gains on Isolated Microgrids

The previous simulation is processed for the isolated microgrid through different dc-link proportional and integral gains of DFIGs k_{pdc}, k_{idc}, as both of them are set as 0.1, in order to clear the effect of the dominant dc-link modes on the microgrid stability. The wind speed of the first DFIG at the 6th node is sampled from 1.5 m/s to 8 m/s by 200 samples, while the other DFIGs have constant wind speed 7 m/s.

Table 4.2 shows the dominant modes, as they are dedicated to DFIGs state variables, such as magnetization currents, dc-link and mechanical speed. In Table 4.2, the first three columns belong to the status of the dominant state variables at the first simulation sample, while the last column of remarks belong to the status of the dominant state variables at the last simulation sample.

Figure 4.18a shows the magnetization current mode of the first DFIG i_{mdq_1}; Figure 4.18b shows the mechanical modes affected by the contributing DFIGs $w_{r_{2,3,4}}$; Figure 4.18c shows the dc-link mode $v_{dc_{2,4}}$ of the second and fourth DFIGs; Figure 4.18d shows the dc-link mode v_{dc_1}, ζ_{dc_1} dominated by the first DFIG.

The obvious difference that occurs with decreasing the proportional and integral control gains of dc-link control circuit that the system turned to instability. The modes dictated by magnetization currents, are totally decoupled, as the magnetization current of the first DFIG affects an oscillatory mode, while the magnetization currents of the rest DFIGs influence other oscillatory modes, and the frequencies of all magnetization current modes increase during wind speed increment.

The trajectories of the mechanical modes involved by the DFIGs are nearly constant and do not move either to the right or to left side.

An interesting conclusion occurs, as the modes dominated by dc-link variables are the only responsible for instability in the microgrid, as shown in Figure 4.18c and 4.18d. The dc-link state variables of the second, third and fourth DFIGs dominate the unstable mode, shifting it to the right part, while the first DFIG dc-link state variables motivate a Hopf bifurcation by crossing the imaginary axis to the right side. Finally, the modes related to the inverters angle of rotation δ, are still out of interest, because they lay far from the imaginary axis.

Figure 4.19 shows the deteriorated behaviour at low dc-link control gain values versus the wind speed, as the dc-link tension reaches terrible values, which could damage the dc-link circuit.

Table 4.2: Dominant Modes of the Isolated MG During Wind Speed Increment-Case 2

$\lambda = \sigma \pm j\omega$	f, HZ	Damping (ξ)	Dominant states	Participation factor	Remarks
-0.28+j311.04	49.5	0.0009	electrical, i_{mdq_1}	0.39	stable
-0.28+j311.04	49.5	0.0009	electrical, $i_{mdq_{2,3,4}}$	0.36	stable
3.3	0	1	mechanical, $w_{r_{2,3,4}}$	0.56	stable
-0.3+j1.05	0.1671	0.27	electrical, ζ_{dc_1}, v_{dc_1}	0.52	unstable (Hopf)
3.38	0	1	electrical, $v_{dc_{2,4}}$	0.56	unstable
-0.002	0	1	mechanical, w_{r_1}	1	stable
-0.0091	0	1	mechanical, $w_{r_{2,3,4}}$	0.47	stable

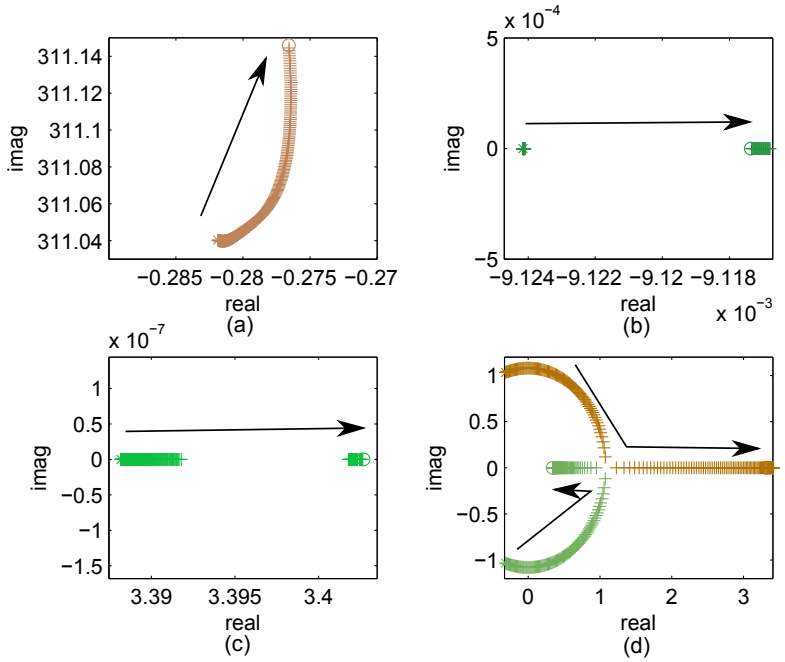

Figure 4.18: Loci of eigenvalues of the isolated microgrid during wind variation-case 2: (a) Magnetization current mode of the 1st DFIG i_{mdq_1}. (b) Mechanical speed mode of the 2nd, 3rd and 4th DFIGs $w_{r_{2,3,4}}$. (c) DC-link mode of the 2nd and 4th DFIGs $v_{dc_{2,4}}$. (d) DC-link mode of the 1st DFIG $\zeta_{dc_1}, v_{dc_1} and \zeta_{dc_1}$.

Wind Speed Increment, Grid-Connected Mode

Another simulation is conducted by connecting the microgrid to the infinite bus; the proposed microgrid is shown in Figure 4.2. The wind speed is sampled from 3 m/s to 8 m/s by 150 samples, and these samples are applied to the first DFIG only at the 6th node, while the wind speed of the other DFIGs are constant at 7 m/s, also the dc-link proportional and integral gains k_{pdc}, k_{idc} are set as 1.1.

Table 4.3 shows the dominant modes of the current simulation, participation factors and their damping ratios. In Table 4.3, the first three columns belong to the status of the dominant state variables at the first simulation sample, while the last column of remarks belong to the status of the dominant state variables at the last simulation sample.

Figure 4.20a shows the dc-link mode of the first DFIG v_{dc_1}, ζ_{dc_1}; Fig-

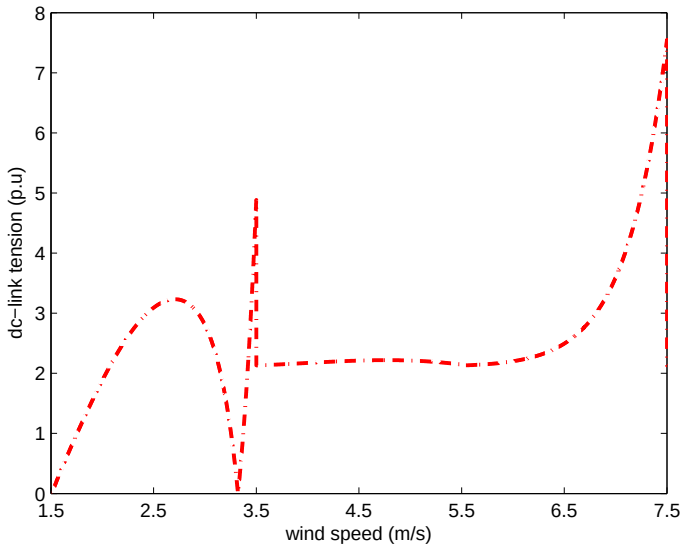

Figure 4.19: DC-link tension at low dc-link control gains versus the wind speed

ure 4.20b shows the dc-link mode related to the rest DFIGs $v_{dc_{2,3,4}}$; Figure 4.20c shows the mechanical speed mode of the first DFIG w_{r_1}; Figure 4.20d shows the mechanical speed mode related to the rest DFIGs $\omega_{r_{2,3,4}}$.

Unlike the isolated microgrid case, the modes affected by DFIGs magnetization currents disappear, and lay far from the imaginary axis, while the oscillatory modes dictated by dc-link state variables are more damped with wind speed increase in the current case than the isolated microgrid case, and they step to the left, acquiring more stability.

In addition, the stability of the mechanical speed mode related to the first DFIG improves during wind speed increase, while in the isolated microgrid simulations, this mode lays at the real axis near to the saddle node bifurcation limit and without any improvement.

Table 4.3: Dominant Modes of the Grid-Connected Mode During Wind Speed Increment-Case 1

$\lambda = \sigma \pm j\omega$	f, HZ	Damping (ξ)	Dominant states	Participation factor	Remarks
-1.25+j0.89	0.1416	0.8146	electrical, v_{dc_1}, ζ_{dc_1}	0.8	stable
-1.68+j0.76	0.1210	0.9111	electrical, $v_{dc_{2,3,4}}$	0.9	stable
-0.0019	0	1	mechanical, w_{r_1}	1	stable
-0.0045	0	1	mechanical, $w_{r_{2,3,4}}$	0.46	stable

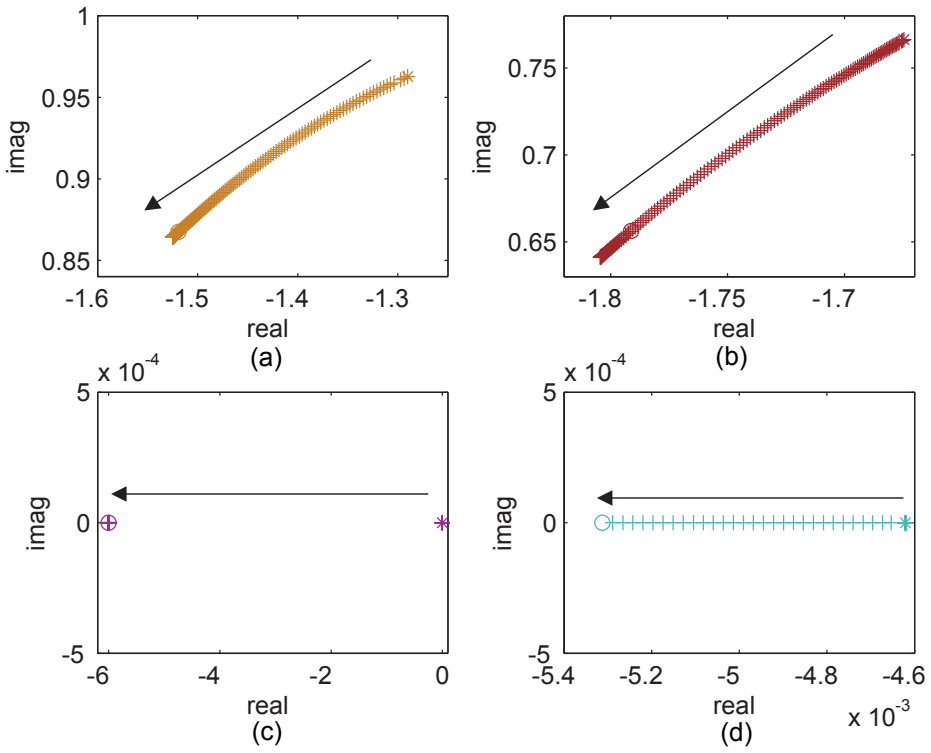

Figure 4.20: Loci of eigenvalues of the grid-connected mode during wind variation-case 1: (a) DC-link mode of 1st DFIG $v_{dc_1} and \zeta_{dc_1}$. (b) DC-link mode of 2nd, 3rd and 4th DFIGs $v_{dc_{2,3,4}}$. (c) Mechanical speed mode of 1st DFIG w_{r_1}. (d) Mechanical speed mode of 2nd, 3rd and 4th DFIGs $\omega_{r_{2,3,4}}$.

The Effect of Reducing the DC-Link Control Gains, Grid-Connected Mode

The previous simulation is conducted regarding the grid-connected mode, by setting the DFIGs proportional and integral gains of the dc-link circuits as 0.1, in order to clear the effect of these gains on the stability of the whole system.

Table 4.4 explains the dominant modes, their participation factors and damping ratios. In Table 4.4, the first three columns belong to the status of the dominant state variables at the first simulation sample, while the last column of remarks belong to the status of the dominant state variables at the last simulation sample.

Figure 4.21a shows the first DFIG dc-link mode $v_{dc_1,\zeta_{dc_1}}$; Figure 4.21b shows the magnetization current dominant mode of the second and third DFIGs $i_{mdq_{2,3}}$; Figure 4.21c shows the dc-link modes of the second and the fourth DFIGs $v_{dc_{2,4}}$.

The grid turns totally unstable; also the magnetization current modes acquire their dominant oscillatory nature again in the current case, and step towards the imaginary axis with increasing wind speed, raising a Hopf bifurcation possibility as shown in Figure 4.21b. Moreover, the modes influenced by dc-link state variables cross the imaginary axis with wind speed increase, creating a Hopf bifurcation, and lay at the unstable part.

The dominant modes shown in the simulations of this Section coincide with other studies as in [132] and [133], where the dominant modes are related to the dc-link and mechanical speed of DFIGs.

Table 4.4: Dominant Modes of the Grid-Connected Mode During Wind Speed Increment-Case 2

$\lambda = \sigma \pm j\omega$	f, HZ	Damping (ξ)	Dominant states	Participation factor	Remarks
-0.2815+j314.12	49.5	0.0008	electrical, $i_{mdq_{2,3}}$	0.43	stable
-0.004	0	1	mechanical, w_{r_1}	0.99	stable
3.58	0	1	electrical, $v_{dc_{2,4}}$	0.68	unstable
0.4+j1.1	0.17	-0.34	electrical, ζ_{dc_1}, v_{dc_1}	0.52	unstable

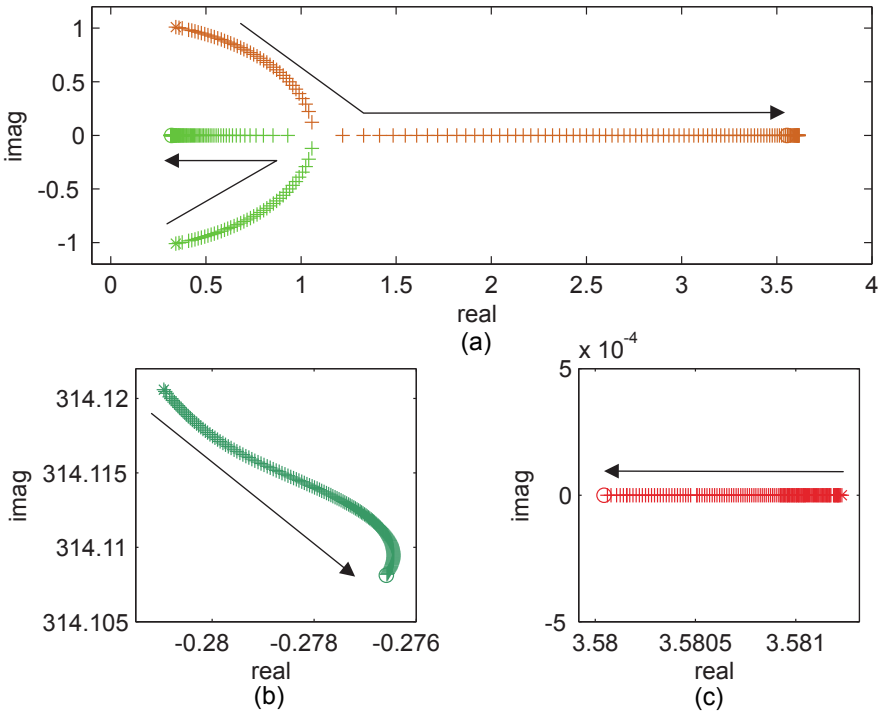

Figure 4.21: Loci of eigenvalues of the grid-connected mode during wind variation-case 2: (a) DC-link mode of 1st DFIG $\zeta_{dc_1} and v_{dc_1}$. (b) Magnetization current mode of 2nd and 3rd DFIGs $i_{mdq_{2,3}}$. (c) DC-link mode of 2nd, 3rd and 4th DFIGs $v_{dc_{2,4}}$.

The conclusions of this Section are briefed hereunder:

- The stability of the microgrid vanishes with decreasing the DFIGs dc-link proportional and integral gains, either in the isolated mode or grid-connected mode;
- By increasing the wind speed, the oscillatory dominant modes move towards the imaginary axis, raising the possibility of a Hopf bifurcation, this result coincide with other papers as in [132] and [33];
- For both the stable isolated microgrid and grid-connected mode, the stability of the mechanical speed modes of the DFIGs improve with increasing the wind speed;
- The oscillatory modes in the case of isolated microgrid are related to the magnetization currents of the DFIGs, and move towards the imaginary axis with wind speed increase, whereas in the case of grid-connected mode, the oscillatory modes are related to the dc-link state variables and move far from the imaginary axis with higher damping ratio with increasing the wind speed;
- In the case of stable isolated microgrid, the dc-link mode of the DFIG, where wind speed increments, is decoupled from dc-link modes of the other DFIGs, where their wind speeds are constant. Moreover, the mechanical mode of the DFIG, where wind speed increments, is decoupled from the other mechanical modes of DFIGs, where their wind speeds are constant.

The stability analysis of microgrids either in the isolated mode or connected to the infinite bus were conducted in this Section during wind speed increment. The simulated microgrid through this Chapter is supplied by both DGs interfaced by inverters and DFIGs. Therefore, the stability study during inverters droop regulation is necessary, because they play the main role for stable power exchange and safe resynchronization. Simulations regarding microgrid stability during inverters droop regulations will be conducted in the following Section.

4.7 Droop Constants variation Impact on the Microgrid Stability

4.7.1 Introduction

The microgrids are usually built using low-inertia generators that can easily adapt to a rapidly changing environment. Although the benefits of low-inertia generation, the drawback is that large demand steps can cause a system to become unstable and losing synchronism. A control system is necessary to bring stability while providing efficient electricity to the microgrid.
The droop control uses only local power to detect changes in the system and adjust the operating points of the generators accordingly.

The droop control uses the real power out of a generator to calculate the ideal operating frequency.

In [134] it was concluded that DGs may have significant impact on the power system stability, if the power system is not properly compensated by reactive power. In [135] it was shown that DGs could have significant impacts on transmission system stability at heavy penetration levels. Typically, a DG unit affects the system stability by generating or consuming active and reactive power. Thus, the power control performance of a DG unit determines its impact on the microgrid, whether in the isolated or grid-connected mode. When the power control strategy can handle successfully the load demand, the DG unit can be used as a mean to enhance the system stability and improve the power quality; otherwise it could undermine the system stability.

Due to the large demand uncertainties, the DGs interfaced by inverters suffer more challenges which call for the needs of stability analyses. First of all, the DGs interfaced by inverters have much less over current capability compared to rotation machine units [136]. Secondly, the intermittent nature of non-dispatchable generators supplying power systems, as in the case of the propsoed microgrid in this Chapter. Thirdly, the microgrid normally has a wide-band dynamics due to the presence of fast response of DGs interfaced by inverters and multiple small DGs with different power capability [137].

Due to all previous challenges, there is a strong need for stability analyses to guarantee proper and stable system operations in the microgrid. Through the first trials to study the stability of DGs interfaced by inverters, the stability

analyses have been conducted by Bode plots using the phase margin and gain margin. In single LCL grid-tie inverter systems, bode plots have been used to study the effects of changing some important parameters, such as feedback, plant parameters and controller gains as shown in [138] and [139].

The stability of large scale DG systems with droop control is usually analysed by the state-space models. The purpose of this Section is small signal stability analysis of the isolated microgrid, supplied by wind energy and DGs interfaced through inverters operating by the droop control, under droop constants increment. Therefore, the stability of the isolated microgrid can be evaluated.

4.7.2 Processing Simulations

Through this Section, the droop constants of the inverter-interfaced generators supplying the isolated microgrid are increased gradually through eighty samples, in order to determine the critical eigenvalues.

Figure 4.22 explains the dominant modes trajectories of the isolated microgrid during inverters droop constants increment, when the simulation is processed at high wind speed equals to 10 m/s. Figure 4.22a shows the trajectory of DFIGs magnetization current mode $i_{mdq_{1,2,3,4}}$; Figures 4.22b show the trajectories of the modes related to the inverters angle of rotation $\delta_{2,3}$; Figure 4.22c shows the trajectories of the modes dominated by the integral terms of inverters voltage controllers $\Phi_{vd_{1,2,3,4}}$; Figure 4.22d shows the dc-link mode related to the DFIGs $\zeta_{dc_{1,2}}$.

Table 4.5 shows the dominant modes of the current simulation, participation factors and their damping ratios. In Table 4.5, the first three columns belong to the status of the dominant state variables at the first simulation sample, while the last column of remarks belong to the status of the dominant state variables at the last simulation sample.

It is clear that the system is stable, as no critical eigenvalues cross the imaginary axis. The modes affected by DFIGs magnetization current shift towards the imaginary axis. In Figure 4.22b, the angle of rotation of the inverters influence modes near to the imaginary axis and turn them to oscillatory modes, moving clock wise towards the imaginary axis again to cross it creating a Hopf bifurcation with incrementing the droops. In Figure 4.22c, other modes related

to voltage controller variables of the inverters move at the real axis towards the imaginary axis, by incrementing the droops, these modes turn unstable.

The Modes dominated by DFIGs dc-link variables step towards the imaginary axis as in Figure 4.22d; other modes dominated by dc-link variables move far from the imaginary axis with incrementing the droops. Mechanical speed modes of the DFIGs shift far from the imaginary axis by little values.

Table 4.5: Dominant Modes of the Isolated MG During Inverters Droop Constants Increment-Case 1

$\lambda = \sigma \pm j\omega$	f, HZ	Damping (ξ)	Dominant states	Participation factor	Remarks
-0.58+j313	49.8	0.0019	electrical, $i_{mq_{1,2,3,4}}$	0.127	stable
-3+j11.5	1.83	0.2524	electrical, $\delta_{2,3}$	0.414	unstable (Hopf-bifurcation
-0.26	0	1	electrical, $\zeta_{dc_{1,2}}$	0.35	stable
-0.029	0	1	mechanical, w_{r_4}	0.53	stable

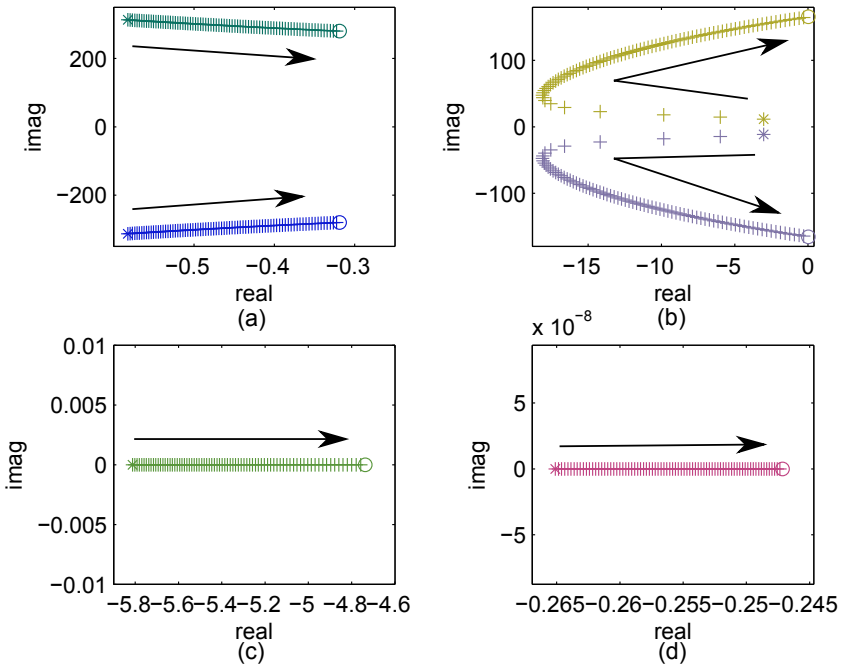

Figure 4.22: Loci of eigenvalues of the isolated microgrid during inverters droop increment-case 1: (a) Magnetization current mode of DFIGs $i_{mdq_{1,2,3,4}}$. (b) Inverters angle of rotation modes $\delta_{2,3}$. (c) Integral term of inverters voltage controller modes $\Phi_{vd_{1,2,3,4}}$. (d) DC-link mode of DFIGs $\zeta_{dc_{1,2}}$.

The Effect of the Droop constants Increment at Low Wind Speeds

The previous simulation is conducted at mean wind speed equals to 3 m/s, by incrementing the droops of the inverter-interfaced generators. The system turn to be unstable as shown in Figure 4.23. Figure 4.23a shows the trajectory of the DFIGs magnetization current mode $i_{mdq_{1,2,3,4}}$; Figures 4.23b and Figure 4.23c show the trajectories of the inverters angle of rotation modes $\delta_{2,3}$; Figure 4.23d shows the dc-link mode related to the third DFIG v_{dc_3}, ζ_{dc_3}.
Table 4.6 shows the dominant modes of the current simulation, participation factors and their damping ratios. In Table 4.6, the first three columns belong to the status of the dominant state variables at the first simulation sample, while the last column of remarks belong to the status of the dominant state variables at the last simulation sample.

Clearly, the modes dominated by the inverters angle of rotation turn unstable and cross the imaginary axis by incrementing the droops, producing a Hopf bifurcation; other modes affected by angles of rotation as shown in Figure 4.23c step towards the imaginary axis through different trajectories, but they are still stable. The modes dominated by dc-link variables of the third DFIG move towards the imaginary axis by incrementing the droops as shown in Figure 4.23d. DFIG magnetization current modes shift towards the imaginary axis as in Figure 4.23a.

It can be observed that DFIG magnetization current modes have the same response, by incrementing the droops of inverters, during the low and high wind speed cases (3 and 10 m/s) respectively, as they move towards the imaginary axis. Moroever, The inverters angle of rotation modes have the same trajectory for all wind speed cases, as they influence oscillatory modes and move clock wise towards the imaginary axis again to cross it causing a Hopf bifurcation, with incrementing the droops. In addition, during the low wind speed case (3 m/s), the inverters angle of rotation modes turn unstable more rapidly. Furthermore, for the dc-link and mechanical speed modes of the DFIGs, it is clear that during the high wind speed case (10 m/s), the stability of such modes improve by incrementing the droops, and during the low wind speed case (3 m/s), these modes shift towards the imaginary axis and their stability worsen. The dominant modes of the current simulations coincide with the dominant modes shown in [140], [23] and [48].

Figure 4.24 shows the behaviour of the microgrid during the inverters droops increment through the low wind speed case (3 m/s). Figure 4.24a explains that the inverters keep stable, till certain droop limit, and the increment over this droop limit motivates synchronization problems and the inverter-interfaced generators start to experience power swing moments as shown in Figure 4.24b. Figure 4.24c clears the frequency collapse in the microgrid, which is created from inverters droops increment. Figure 4.24 shows clearly that the instability case experienced from the droop increment is (oscillatory) instability.

Table 4.6: Dominant Modes of the Isolated MG During Inverters Droop Constants Increment-Case 2

$\lambda = \sigma \pm j\omega$	f, HZ	Damping (ξ)	Dominant states	Participation factor	Remarks
-0.99+j311	49.49	0.0032	electrical, $i_{mdq_{1,2,3,4}}$	0.127	stable
-3+j11.6	1.83	0.2524	electrical, $\delta_{2,3}$	0.39	unstable (Hopf-bifurcation
-1.3	0	1	electrical, v_{dc_3}, ζ_{dc_3}	1	stable
-0.0038	0	1	mechanical, w_{r_3}	0.5	stable

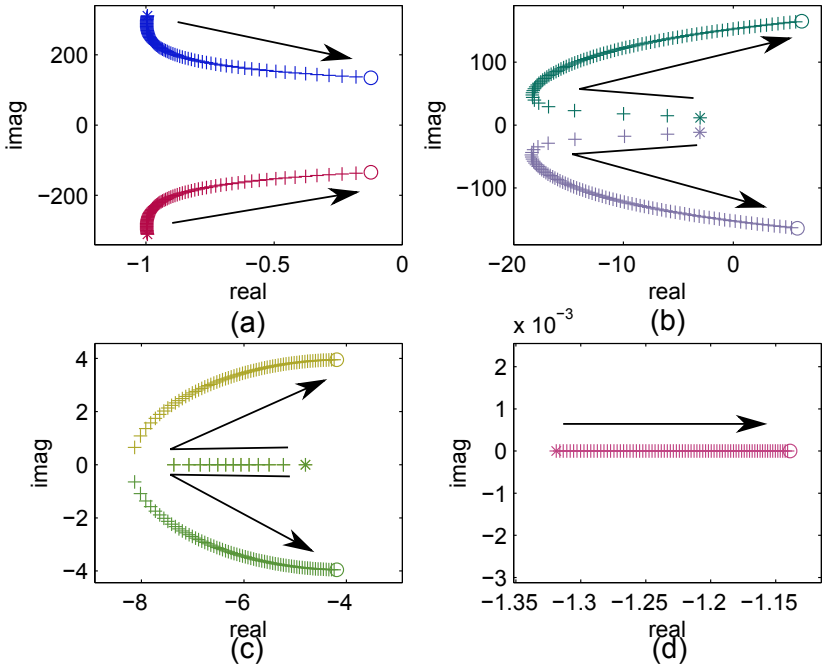

Figure 4.23: Loci of eigenvalues of the isolated microgrid during inverters droop increment-case 2: (a) Magnetization current mode of DFIGs $i_{mdq_{1,2,3,4}}$. (b) Inverters angle of rotation modes $\delta_{2,3}$. (c) Inverters angle of rotation modes δ_2. (d) DC-link mode of the 3rd DFIG v_{dc_3}, ζ_{dc_3}.

The conclusions of this Section are briefed hereunder:

- The magnetization current modes of the DFIGs have the same response during the low and high wind speed cases, as by incrementing the inverters droops, these modes have oscillatory motion towards the imaginary axis;
- The inverters angle of rotation modes have the same trajectory during the low and high wind speed cases, as they influence oscillatory modes near to the imaginary axis and move clock wise, to cross it, causing a Hopf bifurcation by incrementing the droops;
- The stability of dc-link and mechanical speed modes related to the DFIGs worsens by incrementing the droops during the low wind speed case;
- The stability of the microgrid through inverters droop increment worsens earlier during the low wind speed case than the high wind speed case.

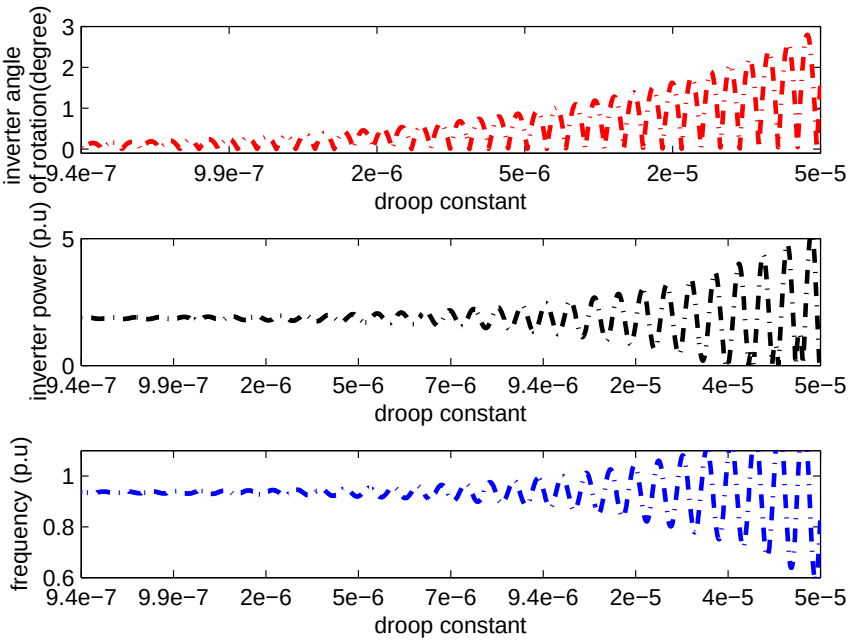

Figure 4.24: Effect of inverters droop increment: (a) Inverter angle of rotation. (b) Inverter power. (c) Frequency.

Till now, the stability analyses of microgrids were conducted, as a result of inverters droop increment and wind energy increase, but the analysis of the power demand increment is necessary, in order to clear the behaviour of microgrid generators in response to such variations. In the following Section, the demand increment impact on the microgrid stability will be conducted.

4.8 Power Demand Increment Impact on the Microgrid Stability

4.8.1 Introduction

As the loading of a power system increases, the system reaches a critical point, where it can no longer deliver the expected demand power. This point is known by the Saddle-Node Bifurcation limit (SNB), where the system is characterized by a singular Jacobian, and so the system loses stability in terms of voltage. The bifurcation usually occurs in single parameter families of ordinary differential equations (ODEs), which are mainly related to Saddle Node and Hopf Bifurcations.

The bifurcation effect becomes clearer by the limitation of the reactive power that can be generated by the system due to voltage collapse, as it is a well-established fact that voltage collapse in power systems is associated with system demand increase beyond certain limits. Typically, if the reactive power demand is greater than the supply reactive power, the voltage will decrease. As the voltage decreases, the difference between reactive power supply and demand increases and the voltage falls even more until it eventually falls to a very small value. The bifurcation limit is critical for the operation and planning of a power system, to be able to prevent instability.

Typically, Voltage stability is defined as the ability of the system to maintain steady voltages after being subjected to a disturbance. Therefore, possible outcome of voltage instability is loss of load in an area, or tripping of transmission lines and other elements by their protective systems leading to cascading outages. Consequently, generators loss of synchronism may result from these outages.

Power system maximum loadability has been discussed in many papers as in [141], where maximum loading point was estimated in normal steady state condition and also in different line outage conditions. In [142], the sensitivities of the load parameter with respect to the load bus power injections are evaluated for each optimal power flow solution, also the participation of the load buses in both active power generation and critical loadability has been conducted.

The proposed small signal stability analyses in this Section are conducted

for microgrids supplied by DGs interfaced through inverters and doubly-fed induction generators, under continuous power demand increment for the microgird, whether in the isolated mode or grid-connected mode. Doubly-fed induction generators are typically nonlinear systems; bifurcation phenomena in such nonlinear systems may occur under certain conditions, leading to oscillatory instability. Therefore, a special attention must be paid to bifurcation phenomena through DFIG stability analysis, because the stability analysis of DFIG from a bifurcation perspective has not been cleared well in most papers, which have focussed on DFIGs stability.

Based on the proposed DFIG model in this Chapter, the dominant eigenvalues are analyzed, revealing that a Hopf bifurcation is likely to happen in the system under load demand increase.

4.8.2 Processing Simulations

Through this Section, the load demand is increased gradually through four hundred samples, from 7.5 p.u to 12 p.u, and simulations are processed for the isolated microgrid mode and grid-connected mode, in order to determine the critical eigenvalues.

Table 4.7 shows the dominant modes, participation factors and their damping ratios in the isolated microgrid. The simulation is processed at mean wind speed equals to 7 m/s. In Table 4.7, the first three columns belong to the status of the dominant state variables at the first simulation sample, while the last column of remarks belong to the status of the dominant state variables at the last simulation sample.

Figures 4.25a and 4.25b show the different DFIGs magnetization current mode trajectories; Figures 4.25c and 4.25d show different trajectories of the inverters angle of rotation modes; Figure 4.26a shows the DFIGs dc-link modes; Figure 4.26b shows the trajectory of DFIGs mechanical speed mode.

From the previous figures, it is clear that the instability originates from a mode influenced by DFIGs dc-link state variables, as it moves to the right at the real axis and turn oscillatory to cross the imaginary axis and causing a Hopf bifurcation, as shown in Figure 4.26a. The rest modes have different response to the load demand increase, but all of them are stable.
Some modes related to DFIGs magnetization currents move counter clock wise

towards the imaginary axis, while other modes influenced by DFIGs magnetization currents step far from the imaginary axis. Inverters angle of rotation modes have two different trajectories, but both of them step towards the imaginary axis. Finally, DFIGs mechanical speed mode shows a slight response to the load demand increment and moves far from the imaginary axis by little values.

Table 4.7: Dominant Modes of the Isolated MG During Demand Increment at Mean Wind Speed: 7 m/s

$\lambda = \sigma \pm j\omega$	f, HZ	Damping (ξ)	Dominant states	Participation factor	Remarks
-0.95+j311	49.49	0.0031	electrical, $i_{mdq_{1,2,3,4}}$	0.12	stable
-0.31+j311	49.49	0.0009	electrical, $i_{mdq_{1,2,4}}$	0.16	stable
-3+j11.5	1.83	0.0096	electrical, $\delta_{2,3}$	0.39	stable
-5.7	0	1	electrical, $v_{dc_{2,4}}$	0.73	unstable (Hopf-bifurcation)
-0.009	0	1	mechanical, w_{r_3}	0.46	stable

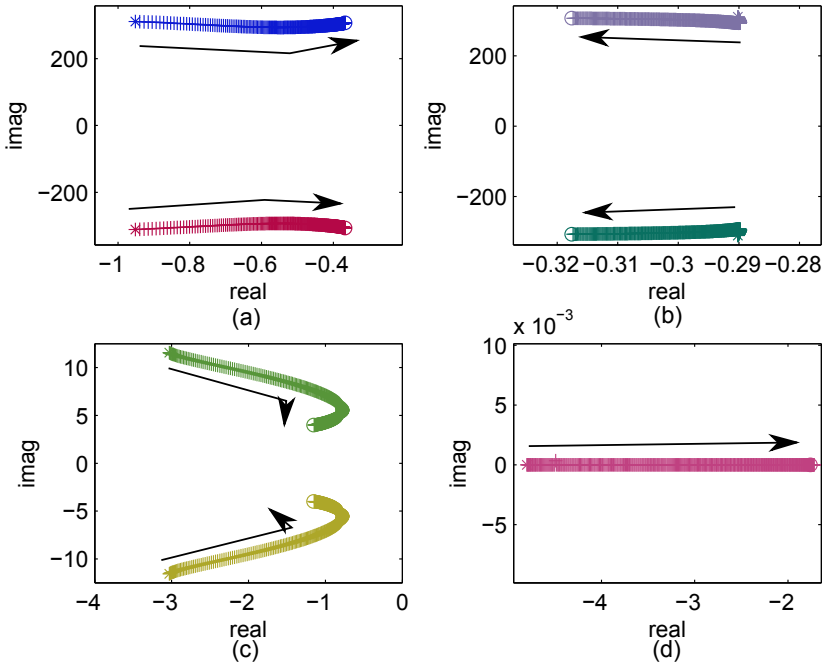

Figure 4.25: Loci of eigenvalues of the isolated microgrid during demand increment at mean wind speed 7 m/s: (a) Magnetization current mode of DFIGs $i_{mdq_{1,2,3,4}}$. (b) Magnetization current mode of DFIGs $i_{mdq_{1,2,4}}$. (c) Inverters angle of rotation modes $\delta_{2,3}$. (d) Inverters angle of rotation modes δ_2.

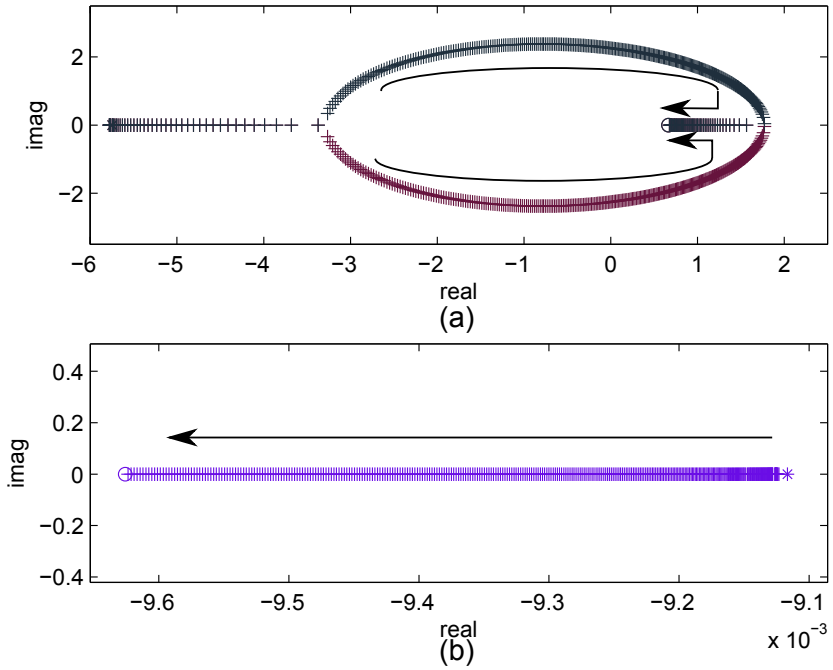

Figure 4.26: The rest of critical eigenvalues trajectories of the isolated microgrid during demand increment at mean wind speed 7 m/s: (a) DC-link mode $v_{dc_{2,4}} and \zeta_{dc_{2,4}}$. (b) DFIG mechanical speed mode $\omega_{r_{2,3,4}}$.

Load Demand Increment at Mean Wind Speed 7 m/s, Grid-Connected Mode

Table 4.8 shows the dominant modes, participation factors and their damping ratios in the case of load demand increment from 7.5 p.u to 12 p.u for the grid-connected mode. The simulation is processed at mean wind speed equals to 7 m/s. In Table 4.8, the first three columns belong to the status of the dominant state variables at the first simulation sample, while the last column of remarks belong to the status of the dominant state variables at the last simulation sample.

Figures 4.27a and 4.27b show different DFIGs magnetization current modes trajectories; Figure 4.27c shows the trajectory of modes dictated by DFIGs integral terms of phased-locked loop circuits; Figures 4.27d and 4.28a show the DFIGs dc-link modes; Figure 4.27b shows the trajectory of DFIGs mechanical speed mode.

The modes dictated by DFIGs dc-link variables are still the source of instability in the system, by crossing the imaginary axis to the unstable part. Some modes related to DIFGs magnetization currents move towards the imaginary axis and their frequencies increase with incrementing the load demand as in Figure 4.27a, while other modes affected by DIFGs magnetization currents step far from the imaginary axis as in Figure 4.27b. In Figure 4.28b, DFIGs mechanical speed mode shows a slight response to the load demand increment and moves far from the imaginary axis by little values. DFIGs integral terms of phased-locked loop circuit modes are far from the imaginary axis and out of the analysis scope, as shown in Figure 4.27c.

Table 4.8: Dominant Modes of the Grid-Connected Mode During Demand Increment at Mean Wind Speed: 7 m/s

$\lambda = \sigma \pm j\omega$	f, HZ	Damping (ξ)	Dominant states	Participation factor	Remarks
-3.6+j313	49.8	0.0115	electrical, $i_{mdq_{1,2,3,4}}$	0.12	stable
-0.28+j314	49.97	0.00089	electrical, $i_{mdq_{1,4}}$	0.27	stable
-26.2	0	1	electrical, $\zeta_{pll_{1,2,3,4}}$	0.3	stable
-3.45+0.3j	0.047	0.99	electrical, $v_{dc_{1,2,3,4}}$	1	unstable
-2.48	0	1	electrical, $\zeta_{dc_{1,2}}$	1	unstable
-0.009	0	1	electrical, $w_{r_{1,4}}$	0.54	stable

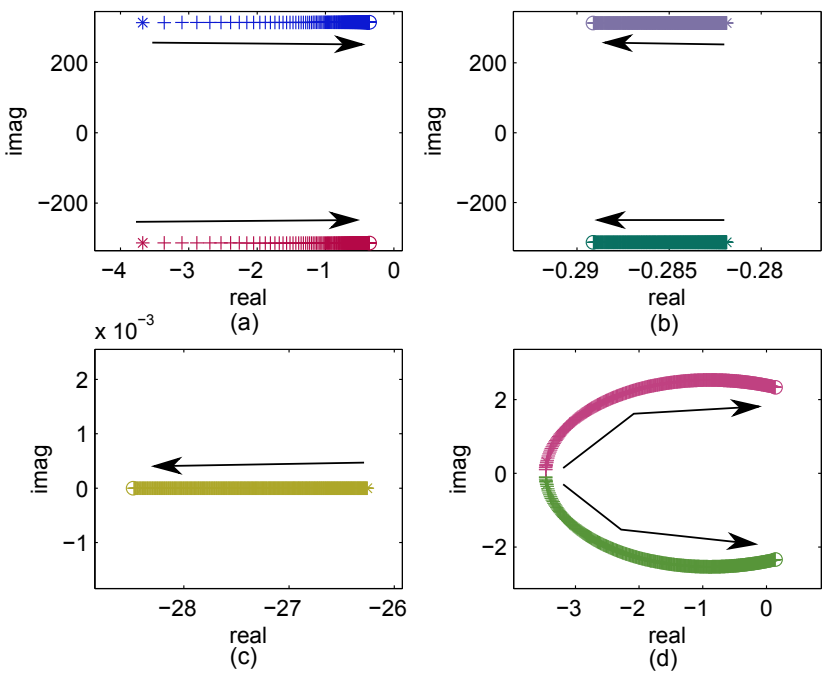

Figure 4.27: Loci of eigenvalues of the grid-connected mode during demand increment at mean wind speed 7 m/s: (a)Magnetization current mode of DFIGs $i_{mdq_{1,2,3,4}}$. (b) Magnetization current mode of DFIGs $i_{mdq_{1,4}}$. (c) DFIGs integral terms of phased-locked loop $\zeta_{pll_{1,2,3,4}}$. (d) DC-link mode $v_{dc_{1,2,3,4}}$.

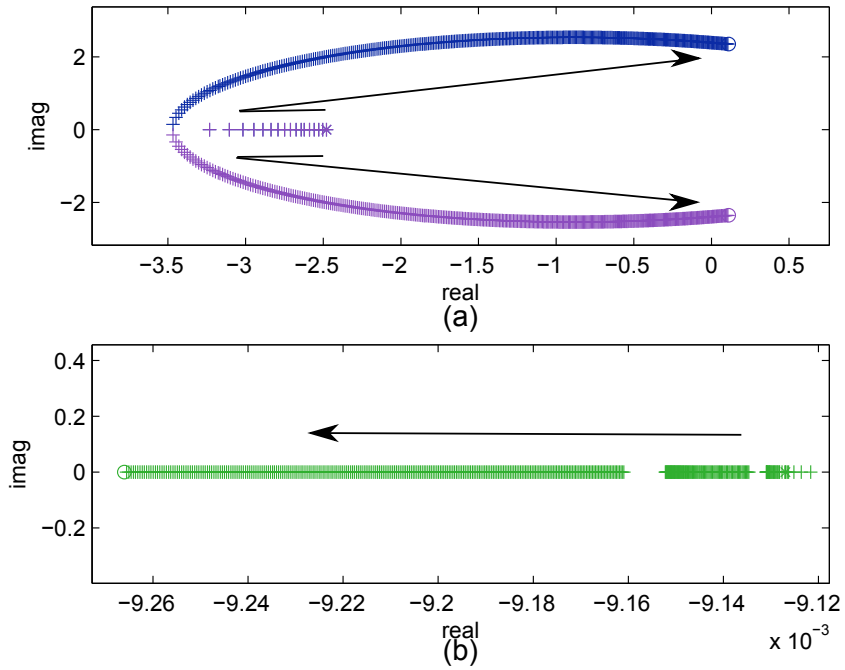

Figure 4.28: The rest of critical eigenvalues trajectories of the grid-connected mode during demand increment at mean wind speed 7 m/s: (a) DC-link mode $v_{dc_{1,2}}$. (b) DFIG mechanical speed mode $\omega_{r_{1,4}}$.

Load Demand Increment at Mean Wind Speed 12 m/s, Isolated Microgrid

Table 4.9 shows the dominant modes, participation factors and their damping ratios, in the case of load demand increment from 7.5 p.u to 12 p.u in the isolated microgrid, the simulation is processed at mean wind speed equals to 12 m/s. In Table 4.9, the first three columns belong to the status of the dominant state variables at the first simulation sample, while the last column of remarks belong to the status of the dominant state variables at the last simulation sample.

Figure 4.29a shows the DFIGs magnetization current mode trajectories; Figures 4.29b and 4.29c show the modes related to the inverters angle of rotation modes; Figures 4.29d and 4.30a show the trajectories of the DFIGs integral terms of dc-link modes; Figure 4.30b shows the trajectory of the DFIGs mechanical speed.

Through the simulation of low wind speed case (7 m/s), where the source of instability in this case was related to the modes dominated by dc-link variables only, but in the current case of wind speed equals to 12 m/s, the instability source of the system originates from two dominant modes, those influenced by the inverters angle of rotation and the DFIGs dc-link state variables. DFIGs magnetization currents mode steps towards the imaginary axis, while DFIGs mechanical speed mode shifts slightly far from the imaginary axis through load demand increment.

Table 4.9: Dominant Modes of the Isolated MG During Demand Increment at Mean Wind Speed: 12 m/s

$\lambda = \sigma \pm j\omega$	f, HZ	Damping (ξ)	Dominant states	Participation factor	Remarks
-0.79+j312	49.65	0.0025	electrical, $i_{mdq_{1,2,3,4}}$	0.12	stable
-3+j11.6	1.84	0.2504	electrical, $\delta_{2,3}$	0.39	stable
-0.68	0	1	electrical, ζ_{dc_2}	0.68	unstable (Hopf-bifurcation)
-0.68	0	1	electrical, $\zeta_{dc_{1,4}}$	0.63	unstable (Hopf-bifurcation)
-0.0157	0	1	electrical, $w_{r_{1,4}}$	0.5	stable

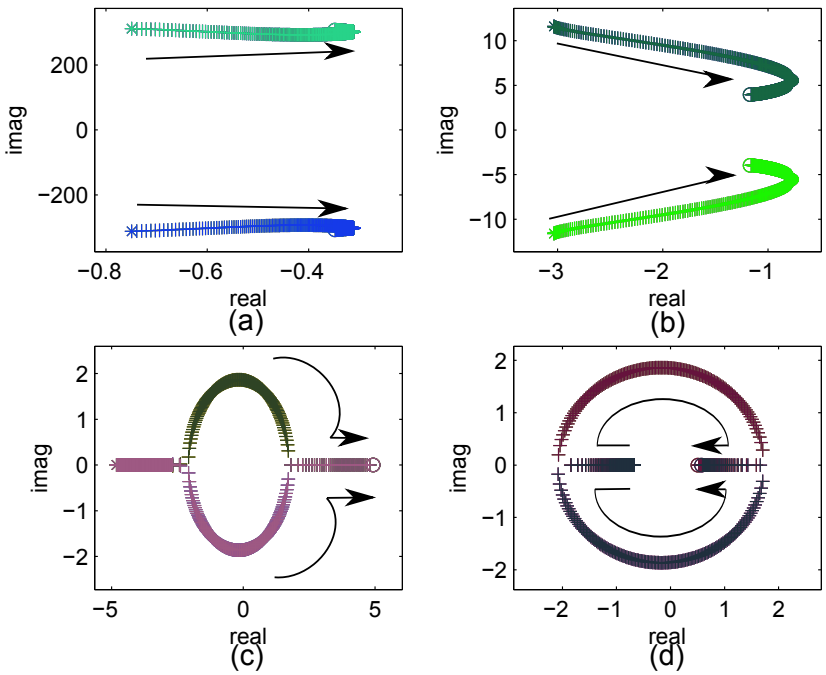

Figure 4.29: Loci of eigenvalues of the isolated microgrid during demand increment at mean wind speed 12 m/s: (a) Magnetization current mode of DFIGs $i_{mdq_{1,2,3,4}}$. (b) Inverters angle of rotation modes $\delta_{2,3}$. (c) Inverters angle of rotation mode δ_2. (d) DC-link mode $\zeta_{dc_{3,4}}$.

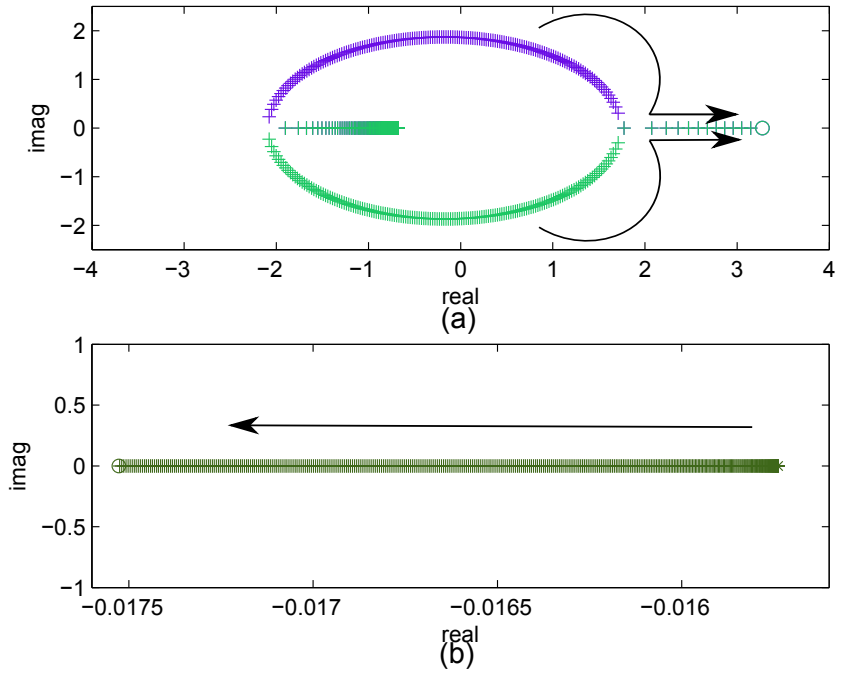

Figure 4.30: The rest of critical eigenvalues trajectories of the isolated microgrid during demand increment at mean wind speed 12 m/s: (a) DC-link mode $\zeta_{dc_{1,4}}$. (b) DFIG mechanical speed mode $\omega_{r_{1,4}}$.

Load Demand Increment at Mean Wind Speed 12 m/s, Grid-Connected Mode

Table 4.10 shows the dominant modes, participation factors and their damping ratios, in the case of load demand increment from 7.5 p.u to 12 p.u for the grid-connected mode. The simulation is processed at mean wind speed equals to 12 m/s. In Table 4.10, the first three columns belong to the status of the dominant state variables at the first simulation sample, while the last column of remarks belong to the status of the dominant state variables at the last simulation sample.

Figures 4.31a and 4.31b show the trajectory of the DFIGs magnetization current modes; Figure 4.31c shows the modes related to the DFIGs integral terms of phased-locked loop circuit; Figures 4.31d and 4.32a show the trajectory of the DFIGs integral terms of dc-link circuit; Figure 4.32b shows the mode influenced by the DFIGs mechanical speed.

The current case is totally stable and no mode is observed crossing the imaginary axis to the unstable part creating Hopf or saddle node bifurcations. The modes dominated by all DFIGs magnetization currents still move towards the imaginary axis with lower frequencies. The DFIGs mechanical speed mode still show the same response as previous cases, and it moves slightly far from the imaginary axis. The modes dictated by dc-link variables v_{dc} step towards the imaginary axis as shown in Figure 4.31d, while the modes dominated by ζ_{dc} move far from the imaginary axis as shown in Figure 4.32a, but still the both modes are stable.

Figure 4.33 shows a comparison between the isolated microgrid mode and grid-connected mode. It is observed that in the isolated microgrid case, the load demand increment leads to a frequency collapse, while in the grid-connected mode, the frequency is stable because a sufficient reserve coming from the infinite bus.

Table 4.10: Dominant Modes of the Grid-connected Mode During Demand Increment at Mean Wind Speed: 12 m/s

$\lambda = \sigma \pm j\omega$	f, HZ	Damping (ξ)	Dominant states	Participation factor	Remarks
-2.1+j312	49.7	0.0067	electrical, $i_{mdq_{1,2,3,4}}$	0.12	stable
-0.29+j314	49.9	0.00092	electrical, $i_{mdq_{1,4}}$	0.27	stable
-26.2	0	1	electrical, $\zeta_{pll_{1,2,3,4}}$	0.28	stable
-14.7	0	1	electrical, $v_{dc_{1,2,3,4}}$	0.256	stable
-0.87	0	1	electrical, $\zeta_{dc_{1,2,3,4}}$	0.26	stable
-0.015	0	1	electrical, $w_{r_{1,2,3,4}}$	0.25	stable

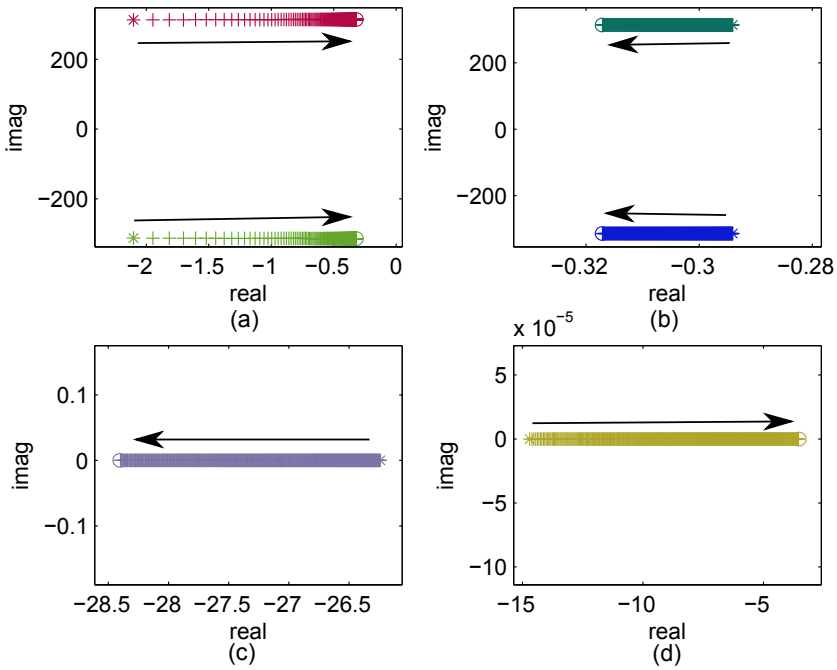

Figure 4.31: Loci of eigenvalues of the grid-connected mode during demand increment at mean wind speed 12 m/s: (a) Magnetization current mode of DFIGs $i_{mdq_{1,2,3,4}}$. (b) DFIGs magnetization current mode of $i_{mdq_{1,4}}$. (c) DFIGs integral terms of phased-locked loop mode $\zeta_{pll_{1,2,3,4}}$. (d) DC-link mode $v_{dc_{1,2,3,4}}$.

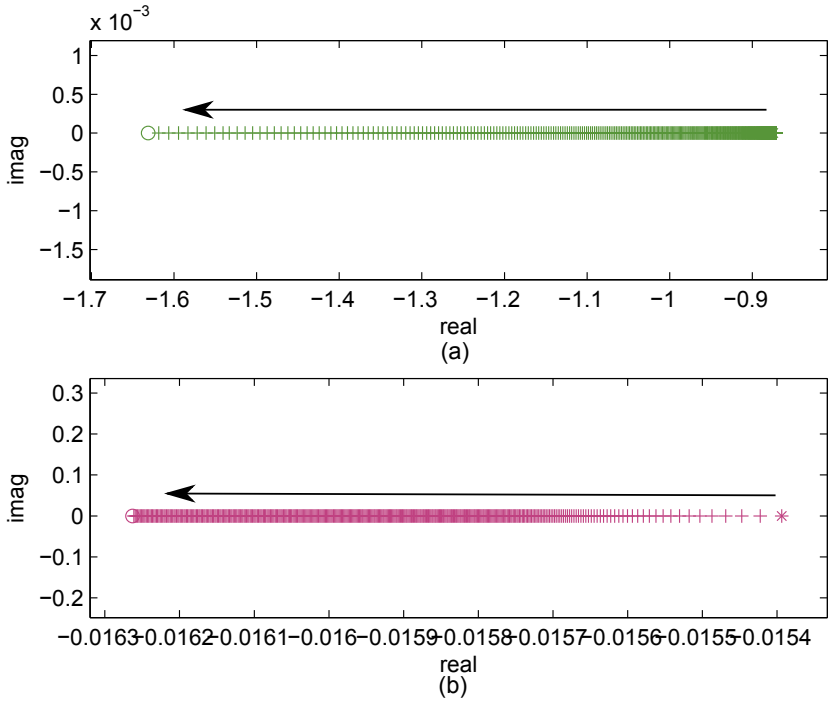

Figure 4.32: The rest of critical eigenvalues trajectories of the grid-connected mode during demand increment at mean wind speed 12 m/s: (a) DC-link mode $\zeta_{dc_{1,2,3,4}}$. (b) DFIG mechanical speed mode $\omega_{r_{1,2,3,4}}$.

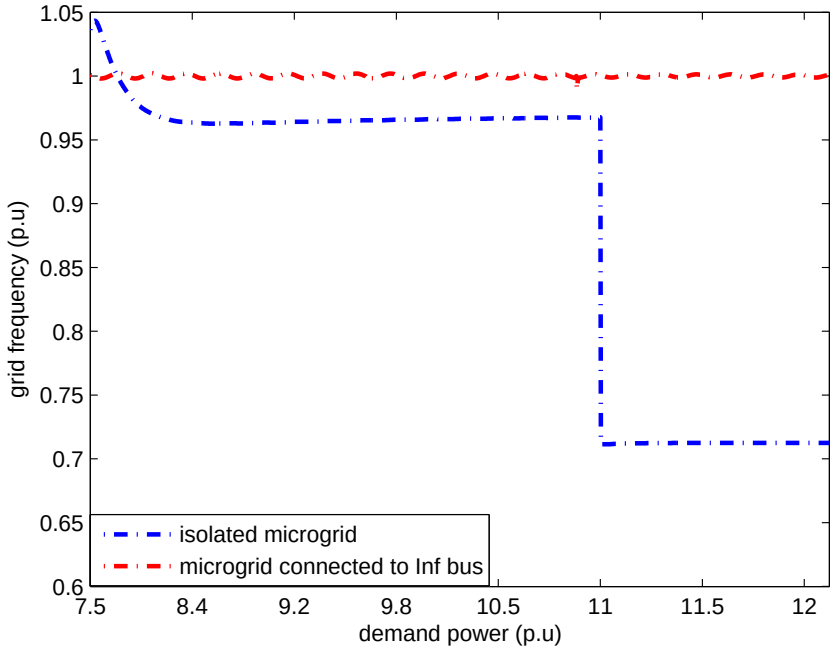

Figure 4.33: Frequency vs demand increment

The conclusions of all the load demand increment scenarios are briefed hereunder:

- For the both cases of isolated microgrid and grid-connected mode, and during the low wind speed case (7 m/s), the source of instability is the mode influenced by the DFIGs dc-link state variables, which strikes the imaginary axis and produces a Hopf bifurcation;
- For the isolated microgrid and during the high wind speed case (12 m/s), two sources of instability can be considered which are the DFIGs dc-link and the inverters angle of rotation modes, as both of them cross the imaginary axis motivating a Hopf bifurcations;
- The best response is shown in the grid-connected mode, and during the high wind speed case (12 m/s), as the system is totally stable, and the frequency is stiff and not affected by load demand increment.

Chapter 5

Conclusions, Published Articles and Future Work

5.1 Conclusions

In this thesis, several technical and economic analyses were conducted, regarding microgrids, such as providing an insight about site matching suitability for droop-regulated microgrids supplied by wind generators, optimizing both energy production and economic performance for isolated microgrids supplied by wind energy and batteries and finally predicting some stability constraints for generation sources by small signal stability analysis. The conclusions of this thesis are briefed hereunder:

- The applied LHS sampling technique serves to sample the wind speed, by ensuring a better spread of sample points through the overall wind speed probability domain in comparison with conventional MCS techniques. Therefore, more precise estimation of wind turbines states and capacity factor can be ensured. Moreover, the conducted correlation strategy based on Cholesky decomposition technique ensures an efficient correlation among different wind turbines, without intensive computations;

- Thesis provided that the wind turbines aggregation modelling in microgrids is not accurate; the estimation of injected power into a microgrid cannot be measured by multiplying directly the injected power of one

generator by number of generators of the grid. Regardless losses in each branch among the microgrid nodes, the correlations among wind turbine generators play an important role in such discrepancies. Moreover, if the dynamic response is to be considered, the small signal stability analysis of this thesis show that varying the wind speed input for only one wind generator has a stability effect on other microgrid wind generators;

- Thesis provided that the maximum loadability of a droop-regulated microgrid is restricted, and so the total maximum power of the microgrid can be less than the sum of power injections by each generation unit, due to existence of DGs interfaced by electronic inverters, which operate by the droop control. The more restriction on the maximum power constraint of each inverter, the earlier bifurcation will be, because the voltage is continuously degraded down to a point in which a saddle-node bifurcation occurs;

- The wind turbine cut-in to rated speed (w_i/w_r) ratio is a vital element to enhance the annual energy production of the wind turbine. The higher (w_i/w_r) ratio, the higher annual energy production and minimum cost of energy can be ensured. Moreover, high wind turbines (w_i/w_r) ratios do not provide a better economic performance and higher energy production for wind turbines only, but for storage systems which operate in parallel with wind turbines as well, if both generation units are employed in a multi-objective function, in order to minimize the cost of energy;

- For a microgrid supplied by wind energy and batteries, there is a possibility of employing high capital cost-high efficient batteries to provide optimum economic performance, if the problem is employed in a multi-objective function, including both wind generation and battery units;

- It could be concluded that in order to provide optimum economic performance and high energy production, the aggregation of wind turbines capacities can be a better choice than dispersing the same turbines capacities at different microgrid nodes;

- Several small signal stability analyses were conducted in this thesis, in order to study the dominant variables which can violate the stability of microgrids. These dominant modes are related mainly to DFIGs state

variables, such as mechanical speed, dc-link and magnetization currents state variables. Moreover, other modes related to DGs interfaced by inverters, which are angle of rotation state variables;

- The experienced bifurcations through the different scenarios of the small signal stability analysis are related to Hopf bifurcations. Thus, to eliminate or damp those variables, which violate the stability of microgrids, an appropriate control strategy must be developed to keep microgrids stable.

5.2 Published Articles

Author: Guzmán Díaz; Ahmed M. Abd-el-Motaleb; Verónica Mier.

Title: "On the Capacity Factor of Distributed Wind Generation in Droop-Regulated Microgrids"

Journal: IEEE Transactions on Power Systems, vol.PP, pp.1 September 2012

DOI: 10.1109/TPWRS.2012.2222941

Abstract: This paper presents the methodological basis for the computation of the capacity factor (CF) of the power delivered by an off-grid droop-regulated microgrid when the power is injected by distributed stochastic generation. More particularly, the paper is focused on wind generation and its modeling particularities. It shows how the availability of power can be efficiently sampled by a low variation Latin Hypercube Sampling (LHS) method, supplemented with a restricted pairing technique to account for correlation among generating units. The paper also presents a minimization problem that, combined with a Fischer-Burmeister-based formulation, permits obtaining the maximum deliverable power at each sample. This paper additionally shows a first numerical analysis of a 14-node microgrid supplied by five Enercon E40. The analysis includes an investigation into the best model that represents the CF of the microgrid, and highlights the effects of correlation and maximum loadability.

5.3 Future Work

In Chapter 4, several small signal stability analyses were conducted, in order to determine the dominant variables which can violate the stability of microgrids. The critical state variables were determined, and the proposed future work will be dedicated to develop power flow models with stable constraints for isolated microgrids. The proposed future work will extend to the following items:

- Possible solutions may include reconstruction of demand and generation models, to ensure the dispatching and loading within the small signal stability constraints. Probabilistic stability analyses must be taken into consideration, which can ensure the robustness of the solution for various system operation modes. In order to cover this point, more uncertainties and refine of probabilistic models of the demand and generation with electricity market considerations must be conducted;

- Participation factor analyses of the dominant modes, which were performed in Chapter 4 can be used to select the most effective input signal to enhance the damping of relevant oscillation modes. Thereafter, adding damping controllers for the dominant state variables is necessary. The dominant state variables of Chapter 4 are related to the DFIGs dc-link and inverters angle of rotation state variables.

  Regarding the DFIGs, the impact of damping controllers on such dominant modes must be studied. Thus, an efficient tuning method must be adopted to enhance the damping of the DFIGs dominant state variables. In [32] Mishra showed a coordinated tuning of a damping controller for a DFIG, using bacterial foraging technique. In [34] Yang proposed a multi-objective controller design for a DFIG, including the damping ratios and real parts of the dominant eigenvalues. Thus, restricting the damping ratios of the dominant modes within pre-defined values and sufficient stability margins could be ensured.

  Regarding the generators interfaced by inverters, an efficient method

must be applied to tune the inverter droops according to stability constraints. In [23] Barklund proposed a tuning algorithm for droop-regulated generators by inverters, which takes into consideration the power demand level and economic dispatch of the interfaced generators. In [143] Guerrero introduced a method to locally tune droop-regulated batteries by inverters, taking into consideration the batteries charge levels and an equal harmonic sharing among the inverters;

- It is also possible to add additional controllers into the microgrid, such as FACTS devices for security enhancement. Chapter 4 proved that the disturbances caused mainly by a power demand increment provide catastrophic results on DFIGs especially, as the dc-link tension could reach terrible values that could damage the dc-link circuit. In addition, the power quality could be affected due to voltage-frequency sags, and so grid code requirements cannot be ensured. Therefore, in order to protect DFIGs from isolation, the implementation of FACTS devices as grid code requirements restorer can be adopted.
  In [144] and [145] Kenneth and Qiao showed that proper coordinated reactive power control strategies between the wind farm and the FACTS can be adopted to reduce the level of sags and comply with grid code requirements.

Chapter 5

Conclusiones, Artículos Publicados y Trabajos Futuros

5.1 Conclusiones

En esta tesis se han realizado diversos estudios técnicos y económicos sobre microredes y sobre la elección del emplazamiento de las mismas, alimentadas por generadores eólicos y reguladas mediante droop. Buscando la optimización tanto de la producción de energía como del rendimiento económico y por último, la predicción de algunas restricciones de estabilidad para las fuentes de generación, mediante el análisis de estabilidad de pequeña señal. Las conclusiones de la tesis se resumen a continuación:

- La técnica de muestreo aplicada, LHS, sirve para muestrear la velocidad del viento, al garantizar una mejor difusión de los puntos de la muestra a través del dominio global de probabilidad de la velocidad del viento, en comparación con las técnicas convencionales MCS. Asimismo, la estrategia de correlación llevaba a cabo, basada en la técnica de descomposición de Cholesky, garantiza una correlación eficaz entre las diversas turbinas eólicas, evitando cálculos laboriosos.

- La tesis determinó que los modelos de agregación de turbinas eólicas en microredes no son correctos. La estimación de la potencia inyectada en una microred no puede calcularse multiplicando directamente la potencia inyectada de un generador por el número de generadores de la red.

- La tesis concluyó que la capacidad de carga máxima de una microred

regulada mediante droop es limitada y por lo tanto, la potencia máxima total de la microred puede ser inferior a la suma de inyecciones de potencia de cada unidad de generación, debido a la existencia de DG conectadas mediante convertidores electrónicos que operan a través del control droop.

- El índice de conexión-desconexión (w_i/w_r) de la turbina eólica es un elemento de suma importancia para mejorar la producción anual de energía de la turbina eólica. Cuanto mayor sea el índice (w_i/w_r), mayor será la producción anual de energía y menor el coste de energía. Además, los altos índices (w_i/w_r) de turbinas eólicas no sólo proporcionan un mejor rendimiento económico y una mayor producción energética para las turbinas eólicas, sino también para los sistemas de almacenamiento que operan en paralelo con turbinas eólicas, si ambas unidades de generación se emplean en una función multiobjetivo para minimizar el coste de energía.

- Podría concluirse que para proporcionar un rendimiento económico óptimo y una alta producción energética, la agregación de capacidades de turbinas eólicas puede resultar mejor que la dispersión de las mismas capacidades de las turbinas en diferentes nodos de la microred.

- En la tesis se han llevado a cabo diversos análisis de estabilidad de pequeña señal para estudiar las variables dominantes que pueden amenazar la estabilidad de las microredes. Estos modos dominantes se relacionan fundamentalmente con variables de estado de los DFIG, como las variables de estado de velocidad mecánica, de enlace de continua y de corrientes de magnetización. Asimismo, otros modos relacionados con las DG se conectaron mediante convertidores, que constituyen ángulos de rotación de las variables de estado.

- Las bifurcaciones experimentadas a través de diferentes escenarios de análisis de estabilidad de pequeña señal están relacionadas con las bifurcaciones de Hopf. Por consiguiente, para eliminar o amortiguar esas variables que amenazan la estabilidad de las microredes, debe desarrollarse una estrategia adecuada de control para mantener la estabilidad de las microredes.

5.2 Artículos Publicados

Author: Guzmán Díaz; Ahmed M. Abd-el-Motaleb; Verónica Mier.

Title: "On the Capacity Factor of Distributed Wind Generation in Droop-Regulated Microgrids"

Journal: IEEE Transactions on Power Systems, vol.PP, pp.1 September 2012

DOI: 10.1109/TPWRS.2012.2222941

Abstract: This paper presents the methodological basis for the computation of the capacity factor (CF) of the power delivered by an off-grid droop-regulated microgrid when the power is injected by distributed stochastic generation. More particularly, the paper is focused on wind generation and its modeling particularities. It shows how the availability of power can be efficiently sampled by a low variation Latin Hypercube Sampling (LHS) method, supplemented with a restricted pairing technique to account for correlation among generating units. The paper also presents a minimization problem that, combined with a Fischer-Burmeister-based formulation, permits obtaining the maximum deliverable power at each sample. This paper additionally shows a first numerical analysis of a 14-node microgrid supplied by five Enercon E40. The analysis includes an investigation into the best model that represents the CF of the microgrid, and highlights the effects of correlation and maximum loadability.

5.3 Trabajos Futuros

En el Capítulo 4, se han llevado a cabo varios análisis de estabilidad de señal pequeña para determinar las variables principales que pueden amenazar la estabilidad de las microredes. Se determinaron las variables de estado críticas y el trabajo futuro propuesto se centrará en desarrollar modelos de flujo de potencia con restricciones estables para las microredes aisladas. Los trabajos futuros propuestos abarcarán los siguientes aspectos:

- Soluciones posibles, entre las que se pueden incluir la reconstrucción de modelos de demanda y generación para garantizar los límites estables del flujo de potencia. Los análisis de estabilidad probabilísticos deben tenerse en cuenta ya que pueden garantizar la robustez de la solución para varios modos de operación de los sistemas.

- Los análisis sobre el factor de participación de los modos dominantes que se presentaron en el Capítulo 4, pueden utilizarse para seleccionar la señal de entrada más eficaz con el fin de mejorar el amortiguamiento de los modos de oscilación pertinentes. Por lo tanto, es necesario añadir controladores de amortiguamiento para las variables de estado dominantes. Las variables de estado dominantes del Capítulo 4 se relacionan con el enlace de corriente continua de los DFIG. Además, los ángulos de rotación de los generadores operan a través de convertidores.

- Por último, también es posible añadir controladores adicionales en la microred, como los dispositivos FACTS, para la mejora de la seguridad. El Capítulo 4 demostró que las perturbaciones causadas principalmente por un incremento en la demanda de potencia, ocasionaron resultados devastadores especialmente en los DFIG, ya que la tensión de enlace de corriente continua podría alcanzar valores nefastos que podrían dañar el circuito de enlace de continua. Asimismo, la calidad de la potencia podría verse afectada por los huecos de tensión-frecuencia y por lo tanto, no pueden garantizarse los requisitos de código de la red. Para proteger a los DFIG del aislamiento, puede adoptarse la implementación de dispositivos FACTS, como el restaurador de requisitos de código de red.

Bibliography

[1] G. Diaz, A. M. Abd-el Motaleb, and V. Mier. On the capacity factor of distributed wind generation in droop-regulated microgrids. *Power Systems, IEEE Transactions on*, PP(99):1, 2012.

[2] P. Kundur. *Power system stability and control.* Epri Power System Engineering Series. McGraw-Hill, 1994.

[3] Paul M. Anderson and A.A. Fouad. *Power system control and stability.* IEEE Press power engineering series. IEEE Press, 2003.

[4] C. Marnay, H. Asano, S. Papathanassiou, and G. Strbac. Policy making for microgrids. *Power and Energy Magazine, IEEE*, 6(3):66 –77, may-june 2008.

[5] R.H Lasseter. Smart distribution: coupled microgrids. *Proceedings of the IEEE*, 99(6):1074–1082, june 2011.

[6] B. Kroposki, R. Lasseter, T. Ise, S. Morozumi, S. Papatlianassiou, and N. Hatziargyriou. Making microgrids work. *Power and Energy Magazine, IEEE*, 6(3):40 –53, may-june 2008.

[7] Ronald L. Iman and W. J. Conover. A distribution-free approach to inducing rank correlation among input variables. *Communications in Statistics - Simulation and Computation*, 11(3):311–334, 1982.

[8] A. Chuang and M. McGranaghan. Master controller requirements specification for perfect power systems. Technical report, EPRI for The Galvin Electricity Initiative, 2007.

[9] P. Piagi and R.H. Lasseter. Autonomous control of microgrids. In *Power Engineering Society General Meeting, 2006. IEEE*, page 8 pp., 0-0 2006.

[10] H. Nikkhajoei and R.H. Lasseter. Distributed generation interface to the certs microgrid. *Power Delivery, IEEE Transactions on*, 24(3):1598 –1608, july 2009.

[11] R.H. Lasseter. Extended certs microgrid. In *Power and Energy Society General Meeting - Conversion and Delivery of Electrical Energy in the 21st Century, 2008 IEEE*, pages 1 –5, july 2008.

[12] R.H. Lasseter, J.H. Eto, B. Schenkman, J. Stevens, H. Vollkommer, D. Klapp, E. Linton, H. Hurtado, and J. Roy. Certs microgrid laboratory test bed. *Power Delivery, IEEE Transactions on*, 26(1):325 –332, jan. 2011.

[13] A. Losi and M. Russo. Dispersed generation modeling for object-oriented distribution load flow. *Power Delivery, IEEE Transactions on*, 20(2):1532 – 1540, april 2005.

[14] Hassan Nikkhajoei and Reza Iravani. Steady-state model and power flow analysis of electronically-coupled distributed resource units. *Power Delivery, IEEE Transactions on*, 22(1):721 –728, jan. 2007.

[15] M.Z. Kamh and R. Iravani. Unbalanced model and power-flow analysis of microgrids and active distribution systems. *Power Delivery, IEEE Transactions on*, 25(4):2851 –2858, oct. 2010.

[16] K.L. Lo and C. Zhang. Decomposed three-phase power flow solution using the sequence component frame. *Generation, Transmission and Distribution, IEE Proceedings C*, 140(3):181 –188, may 1993.

[17] J. Morren, S.W.H. de Haan, W.L. Kling, and J.A. Ferreira. Wind turbines emulating inertia and supporting primary frequency control. *Power Systems, IEEE Transactions on*, 21(1):433 – 434, feb. 2006.

[18] R.G. de Almeida and J.A.P. Lopes. Participation of doubly fed induction wind generators in system frequency regulation. *Power Systems, IEEE Transactions on*, 22(3):944 –950, aug. 2007.

[19] O. Anaya-Lara, F.M. Hughes, N. Jenkins, and G. Strbac. Contribution of dfig-based wind farms to power system short-term frequency regu-

lation. *Generation, Transmission and Distribution, IEE Proceedings-*, 153(2):164 – 170, march 2006.

[20] J.A.P. Lopes, C.L. Moreira, and A.G. Madureira. Defining control strategies for microgrids islanded operation. *Power Systems, IEEE Transactions on*, 21(2):916 – 924, may 2006.

[21] M. Prodanovic and T.C. Green. High-quality power generation through distributed control of a power park microgrid. *Industrial Electronics, IEEE Transactions on*, 53(5):1471 –1482, oct. 2006.

[22] C. L. Moreira, F. O. Resende, and J. A. P. Lopes. Using low voltage microgrids for service restoration. *Power Systems, IEEE Transactions on*, 22(1):395 –403, feb. 2007.

[23] E. Barklund, N. Pogaku, M. Prodanovic, C. Hernandez-Aramburo, and T.C. Green. Energy management in autonomous microgrid using stability-constrained droop control of inverters. *Power Electronics, IEEE Transactions on*, 23(5):2346 –2352, sept. 2008.

[24] Seon-Ju Ahn, Jin-Woo Park, Il-Yop Chung, Seung-Il Moon, Sang-Hee Kang, and Soon-Ryul Nam. Power-sharing method of multiple distributed generators considering control modes and configurations of a microgrid. *Power Delivery, IEEE Transactions on*, 25(3):2007 –2016, july 2010.

[25] E. Serban and H. Serban. A control strategy for a distributed power generation microgrid application with voltage- and current-controlled source converter. *Power Electronics, IEEE Transactions on*, 25(12):2981 –2992, dec. 2010.

[26] A. Molderink, V. Bakker, M.G.C. Bosman, J.L. Hurink, and G.J.M. Smit. Management and control of domestic smart grid technology. *Smart Grid, IEEE Transactions on*, 1(2):109 –119, sept. 2010.

[27] M.G. Molina and P.E. Mercado. Power flow stabilization and control of microgrid with wind generation by superconducting magnetic energy storage. *Power Electronics, IEEE Transactions on*, 26(3):910 –922, march 2011.

[28] Changhee Cho, Jin-Hong Jeon, Jong-Yul Kim, Soonman Kwon, Kyongyop Park, and Sungshin Kim. Active synchronizing control of a microgrid. *Power Electronics, IEEE Transactions on*, 26(12):3707 –3719, dec. 2011.

[29] A. Colet-Subirachs, A. Ruiz-Alvarez, O. Gomis-Bellmunt, F. Alvarez-Cuevas-Figuerola, and A. Sudria-Andreu. Centralized and distributed active and reactive power control of a utility connected microgrid using iec61850. *Systems Journal, IEEE*, 6(1):58 –67, march 2012.

[30] Zhixin Miao, A. Domijan, and Lingling Fan. Investigation of microgrids with both inverter interfaced and direct ac-connected distributed energy resources. *Power Delivery, IEEE Transactions on*, 26(3):1634 –1642, july 2011.

[31] A. Ostadi, A. Yazdani, and R.K. Varma. Modeling and stability analysis of a dfig-based wind-power generator interfaced with a series-compensated line. *Power Delivery, IEEE Transactions on*, 24(3):1504 –1514, july 2009.

[32] Y. Mishra, S. Mishra, Fangxing Li, Zhao Yang Dong, and R.C. Bansal. Small-signal stability analysis of a dfig-based wind power system under different modes of operation. *Energy Conversion, IEEE Transactions on*, 24(4):972 –982, dec. 2009.

[33] Lihui Yang, Zhao Xu, J. Ø andstergaard, Zhao Yang Dong, Kit Po Wong, and Xikui Ma. Oscillatory stability and eigenvalue sensitivity analysis of a dfig wind turbine system. *Energy Conversion, IEEE Transactions on*, 26(1):328 –339, march 2011.

[34] Yang G.Y. Yang, L and Z. Xu. Optimal controller design of a doubly-fed induction generator wind turbine system for small signal stability enhancement. *Generation, Transmission Distribution, IET*, 4(5):579 – 597, may 2010.

[35] H. Holttinen. Hourly wind power variations in the nordic countries. *Wind Energy*, 8(2):173–195, 2004.

[36] D.A. Bechrakis and P.D. Sparis. Correlation of wind speed between neighboring measuring stations. *Energy Conversion, IEEE Transactions on*, 19(2):400 – 406, june 2004.

[37] Wijarn Wangdee. Considering load-carrying capability and wind speed correlation of wecs in generation adequacy assessment. *IEEE Transactions on Energy Conversion*, 21(3):734– 741, 2006.

[38] Y. Gao. Adequacy assessment of generating systems containing wind power considering wind speed correlation. *IET Renewable Power Generation*, 3(2):217–226, 2009.

[39] Hui Li and Zhe Chen. Design optimization and evaluation of different wind generator systems. In *Electrical Machines and Systems, 2008. ICEMS 2008. International Conference on*, pages 2396 –2401, oct. 2008.

[40] S.H. Jangamshetti and V.G. Ran. Optimum siting of wind turbine generators. *Energy Conversion, IEEE Transactions on*, 16(1):8–13, 2001.

[41] Tai-Her Yeh and Li Wang. A study on generator capacity for wind turbines under various tower heights and rated wind speeds using weibull distribution. *Energy Conversion, IEEE Transactions on*, 23(2):592 –602, june 2008.

[42] We-Jen Lee Zhe Chen Li Wang, Tai-Her Yeh. Benefit evaluation of wind turbine generators in wind farms using capacity-factor analysis and economic-cost methods. *IEEE Transactions on Power Systems*, 24(2), may 2009.

[43] U. Sureshkumar, P.S. Manoharan, and A.P.S. Ramalakshmi. Economic cost analysis of hybrid renewable energy system using homer. In *Advances in Engineering, Science and Management (ICAESM), 2012 International Conference on*, pages 94 –99, march 2012.

[44] N.A.b.A. Razak, M.M. bin Othman, and I. Musirin. Optimal sizing and operational strategy of hybrid renewable energy system using homer. In *Power Engineering and Optimization Conference (PEOCO), 2010 4th International*, pages 495 –501, june 2010.

[45] A.K. Srivastava, A.A. Kumar, and N.N. Schulz. Impact of distributed generations with energy storage devices on the electric grid. *Systems Journal, IEEE*, 6(1):110 –117, march 2012.

[46] K.W. Wang, C.Y. Chung, C.T. Tse, and K.M. Tsang. Multimachine eigenvalue sensitivities of power system parameters. In *Power Engineering Society Winter Meeting, 2000. IEEE*, volume 2, page 1434 vol.2, 2000.

[47] E.E. Souza Lima and L.F. De Jesus Fernandes. Assessing eigenvalue sensitivities [power system control simulation]. *Power Systems, IEEE Transactions on*, 15(1):299 –306, feb 2000.

[48] N. Pogaku, M. Prodanovic, and T.C. Green. Modeling, analysis and testing of autonomous operation of an inverter-based microgrid. *Power Electronics, IEEE Transactions on*, 22(2):613 –625, march 2007.

[49] A.P. Leite, C.L.T. Borges, and D.M. Falcao. Probabilistic wind farms generation model for reliability studies applied to brazilian sites. *Power Systems, IEEE Transactions on*, 21(4):1493 –1501, nov. 2006.

[50] R. Billinton, Yi Gao, and R. Karki. Composite system adequacy assessment incorporating large-scale wind energy conversion systems considering wind speed correlation. *Power Systems, IEEE Transactions on*, 24(3):1375 –1382, aug. 2009.

[51] F. Vallee, G. Brunieau, M. Pirlot, O. Deblecker, and J. Lobry. Optimal wind clustering methodology for adequacy evaluation in system generation studies using nonsequential monte carlo simulation. *Power Systems, IEEE Transactions on*, 26(4):2173 –2184, nov. 2011.

[52] F. Katiraei and M.R. Iravani. Power management strategies for a microgrid with multiple distributed generation units. *Power Systems, IEEE Transactions on*, 21(4):1821 –1831, nov. 2006.

[53] R. Majumder, A. Ghosh, G. Ledwich, and F. Zare. Power management and power flow control with back-to-back converters in a utility connected microgrid. *Power Systems, IEEE Transactions on*, 25(2):821 –834, may 2010.

[54] R. Billinton. *Power System Reliability Evaluation.* Gordon and Breach, Science Publ., 1970.

[55] R.Y. Redlinger and P.D Andersen. *Wind energy in the 21st century: economics, policy, technology and the changing electricity industry.* Palgrave Macmillan, 2002.

[56] C. Abbey, F. Katiraei, C. Brothers, L. Dignard-Bailey, and G. Joos. Integration of distributed generation and wind energy in canada. In *Power Engineering Society General Meeting, 2006. IEEE*, page 7 pp., 0-0 2006.

[57] B. Fox. *Wind power integration: connection and system operational aspects.* IET power and energy series. The Institution of Engineering and Technology, 2007.

[58] M. P. Connor. *The UK Renewable Obligation*, chapter 7 of book: Switching of Renewable Power. 2005.

[59] J. Moccia and A. Arapogianni. Pure power. Technical report, European Wind Energy Association, 2011.

[60] I Abouzahr and R Ramakumar. An approach to assess the performance of utility-interactive wind electric conversion systems. *Energy Conversion, IEEE Transactions on*, 6(4):627– 638, Dec 1991.

[61] P. Giorsetto and K.F. Utsurogi. Development of a new procedure for reliability modeling of wind turbine generators. *Power Apparatus and Systems, IEEE Transactions on*, PAS-102(1):134–143, 1983.

[62] P. Hu R. Karki and R. Billinton. Reliability evaluation of a wind power delivery system using an approximate wind model. In *41st International Universities Power Engineering Conference, Newcastle, UK*, 2006.

[63] R. Karki and Po Hu. Wind power simulation model for reliability evaluation. In *Electrical and Computer Engineering, 2005. Canadian Conference on*, pages 541–544, 2005.

[64] Iman R. L. Steck, G. P. and Dahlgren. *Probablistic analysis of lOCA , annual report.* SAND76-0535, Sandia National Laboratories, Albuquerque, NM, 1976.

[65] Ali Naci Celik. A statistical analysis of wind power density based on the weibull and rayleigh models at the southern region of turkey. *Renewable Energy*, 29(4):593–604, July 2003.

[66] P. Ramírezb J.A. Cartaa and S. Velázquezc. A review of wind speed probability distributions used in wind energy analysis: Case studies in the canary islands. *Renewable and Sustainable Energy Reviews*, 13(5):933–955, June 2009.

[67] B. Stephen S. Gill and S. Galloway. Wind turbine condition assessment through power curve copula modeling. *Sustainable Energy, IEEE Transactions on*, 3(1):94 –101, jan. 2012.

[68] O.A. Jaramillo and M.A. Borja. Wind speed analysis in la ventosa, mexico: a bimodal probability distribution case. *Renewable Energy*, 29(10):1613–1630, August 2004.

[69] M. Cabello andJ.A.G. Orza. Wind speed analysis in the province of alicante, spain. potential for small-scale wind turbines. *Renew Sust Energ*, 14(9):3185–3191, 2010.

[70] R. J. Beckman M. D. Mckay and W. J. Conover. A comparison of three methods for selecting values of input variables in the analysis of output from a computer code. *Technometrics*, 42(1):55–61, 2000.

[71] R.L. Iman and M.J. Shortencarier. *A FORTRAN 77 program and user's guide for the generation of latin hypercube and random samples for use with computer models*. NUREG/CR. The Division, 1984.

[72] A. E. Feijo. Wind speed simulation in wind farms for steady-state security assessment of electrical power systems. *IEEE Transactions on Energy Conversion*, 14(4):1582– 1588, 1999.

[73] Roy Billinton. Composite system adequacy assessment incorporating large-scale wind energy conversion systems considering wind speed correlation. *IEEE Transactions on Power Systems*, 24(3):1375– 1382, 2009.

[74] James R. Salmon and John L. Walmsley. A two-site correlation model for wind speed, direction and energy estimates. *Journal of Wind Engineering and Industrial Aerodynamics*, 79(3):233–268, 1999.

[75] M.C. Alexiadis, P.S. Dokopoulos, and H.S. Sahsamanoglou. Wind speed and power forecasting based on spatial correlation models. *Energy Conversion, IEEE Transactions on*, 14(3):836 –842, sep 1999.

[76] Michael Stein. Large sample properties of simulations using latin hypercube sampling. *Technometrics*, 29(2):143–151, 1987.

[77] M.H Albadi and E. F. El-Saadany. Wind turbines capacity factor modeling—a novel approach. *Power Systems, IEEE Transactions*, 24(3):1637–1638, Aug 2009.

[78] Cristina L. Archer and Mark Z. Jacobson. Supplying base load power and reducing transmission requirements by interconnecting wind farms. *Applied Meteorology and Climatology*, 46, november 2007.

[79] S. Bazaraa, H.D. Sherali, and C.M. Shetty. *Nonlinear programming: theory and algorithms*. Wiley-Interscience, 2006.

[80] G. Claeskens and N.L. Hjort. *Model selection and model averaging*. Cambridge Series on Statistical and Probabilistic Mathematics. Cambridge University Press, 2008.

[81] Hamparsum Bozdogan. Akaike's information criterion and recent developments in information complexity. *Mathematical Psychology*, 44:62–91, 2000.

[82] H Akaike. A new look at the statistical model identification. *Automatic Control, IEEE Transactions*, 19(6)(6):716–723, Dec 1974.

[83] Gideon E Schwarz. Estimating the dimension of a model. *Annals of Statistics*, 6(2):461–464, 1978.

[84] R. Tibsharani Hastie, T and J. Friedman. *The elements of statistical learning*. Springer, New York, 2001.

[85] Markon KE and Krueger RF. An empirical comparison of information-theoretic selection criteria for multivariate behavior genetic models. *Behaviour Genetics*, 34(6):593–610, 2004.

[86] R. Billinton and A.A. Chowdhury. Incorporation of wind energy conversion systems in conventional generating capacity adequacy assessment. *Generation, Transmission and Distribution, IEE Proceedings C*, 139(1):47–56, 1992.

[87] A.J.M. van Wijk and N. Halberg. Capacity credit of wind power in the netherlands. *Electric Power Systems Research*, 23(3):189–200, May 1992.

[88] R.M.G. Castro and L.A.F.M. Ferreira. A comparison between chronological and probabilistic methods to estimate wind power capacity credit. *Power Systems, IEEE Transactions on*, 16(4):904–909, 2001.

[89] M Milligan and K. Porter. Determining the capacity value of wind: an updated survey of methods and implementation. Technical report, National Renewable Energy Laboratory, 2008.

[90] Aynur Ucar and Figen Balo. Evaluation of wind energy potential and electricity generation at six locations in turkey. *Applied energy*, 86(10):1864–1872, October 2009.

[91] Z.M. Salameh and I. Safari. The effect of the windmill's parameters on the capacity factor. *Energy Conversion, IEEE Transactions on*, 10(4):747–751, 1995.

[92] K.R. Padiyar. *Power System Dynamics: Stability and Control*. Anshan Pub, 2004.

[93] Jan Machowski, J.W. Bialek, and J.R. Bumby. *Power system dynamics and stability*. John Wiley, 1997.

[94] G. Diaz, C. Gonzalez-Moran, J. Gomez-Aleixandre, and A. Diez. Composite loads in stand-alone inverter based microgrids-modeling procedure and effects on load margin. *Power Systems, IEEE Transactions on*, 25(2):894–905, 2010.

[95] A.P. Agalgaonkar, C.V. Dobariya, M.G. Kanabar, S.A. Khaparde, and S.V. Kulkarni. Optimal sizing of distributed generators in microgrid. In *Power India Conference, 2006 IEEE*, page 8 pp., 0-0 2006.

[96] R.W. Wies, R.A. Johnson, A.N. Agrawal, and T.J. Chubb. Simulink model for economic analysis and environmental impacts of a pv with diesel-battery system for remote villages. *Power Systems, IEEE Transactions on*, 20(2):692 – 700, may 2005.

[97] William Isherwooda and J.Ray Smith. Remote power systems with advanced storage technologies for alaskan villages. *Energy*, 25(10):1005–1020, 2000.

[98] DF Ancona and P.R. Goldman. Wind program technological developments in the united states. *Renew Energy*, 10:253–8, 1997.

[99] Mark Bolinger Lori Bird and Troy Gagliano. Policies and market factors driving wind power development in the united states. *Energy Pol*, 33(1):397–407, 2005.

[100] Jager-Waldau and Heinz Ossenbrink. Progress of electricity from biomass, wind and photovoltaics in the european union. *Renew Sustain Energy*, 8(1):57–82, 2004.

[101] Smith JC and DeMeo EA. Wind power impacts on electric power system operating costs: summary and perspective on work to date. *Presented at the American wind energy association global wind power conference*, 2004.

[102] L.L. Lai. *Power system restructuring and deregulation: trading, performance and information technology*. Wiley, 2001.

[103] Sally Hunt and Graham Shuttleworth. *Competition and choice in electricity*. John Wiley, may 1996.

[104] A. Kusiak and Z. Song. Design of wind farm layout for maximum wind energy capture. *Renewable Energy*, 35:658–694, 2010.

[105] G. Diaz and C. Gonzalez-Moran. Fischer-burmeister-based method for calculating equilibrium points of droop-regulated microgrids. *Power Systems, IEEE Transactions on*, 27(2):959–967, 2012.

[106] S.X. Chen, H.B. Gooi, and M.Q. Wang. Sizing of energy storage for microgrids. *Smart Grid, IEEE Transactions on*, 3(1):142–151, 2012.

[107] L. M. Hand Fingersh and A. Laxson. Wind turbine design cost and scaling model. Technical report, National Renewable Energy Laboratory, june 2006.

[108] F.A. Chacra, P. Bastard, G. Fleury, and R. Clavreul. Impact of energy storage costs on economical performance in a distribution substation. *Power Systems, IEEE Transactions on*, 20(2):684 – 691, may 2005.

[109] M. Kintner-Meyer and Chunlian Jin. Energy storage for variable renewable energy resource integration-a regional assessment for the northwest power pool. In *Power Systems Conference and Exposition (PSCE), IEEE/PES*, pages 1 –7, march 2011.

[110] Susan Schoeenung and Jim Eyer. Benefit and cost comparisons of energy storage technologies for three engineering value propositions. In *presented at EESAT, San Francisco, California*, 2005.

[111] D.G. Newnan, J.P. Lavelle, and T.G. Eschenbach. *Essentials of engineering economic analysis*. Oxford University Press, 2002.

[112] M. Preindl and S. Bolognani. Optimization of the generator to rotor ratio of mw wind turbines based on the cost of energy with focus on low wind speeds. In *IECON 2011 - 37th Annual Conference on IEEE Industrial Electronics Society*, pages 906 –911, nov. 2011.

[113] Samir Succar and David C. Denkenbergerc. Optimization of specific rating for wind turbine arrays coupled to compressed air energy storage. *Applied energy*, 96:222–234, December 2011.

[114] Patrick Mazza Christopher Schaber and Roel Hammerschlag. Utility-scale storage of renewable energy. *Electricity Journal*, 17(6):21–29, 2004.

[115] G. Desrochers, M. Blanchard, and S. Sud. A monte-carlo simulation method for the economic assessment of the contribution of wind energy to power systems. *Energy Conversion, IEEE Transactions on*, EC-1(4):50–56, 1986.

[116] Parker CD. Lead-acid battery energy-storage systems for electricity supply networks. *Power Sources*, 100:18–28, 2001.

[117] Y. Moriokaa Y and S. Narukawab. State-of-the-art of alkaline rechargeable batteries. *Power Sources*, 100(1):107–1161, 2001.

[118] C. Ponce de Leon and A. Frias-Ferrer. Redox flow cells for energy conversion. *Power Sources*, 160:716–732, 2006.

[119] M. Wakihara. Recent developments in lithium ion batteries. *Materials Science and Engineering*, 33:109–134, 2001.

[120] Anthony Schellenberglabe Marc Beaudin, Hamidreza Zareipour and William Rosehart. Energy storage for mitigating the variability of renewable electricity sources: an updated review. *Energy for sustainable development*, 14(4):302–314, September 2010.

[121] Haisheng Chen and Thang Ngoc Cong. Progress in electrical energy storage system: A critical review. *Progress in Natural Science*, 19(3):291–312, March 2009.

[122] SusanmM Schoenung. Characteristics and technologies for long- vs. short-term energy storage: A study by the doe energy storage systems program. Technical report, Sandia National Labs, 2001.

[123] Cristina González Morán. *Optimizacion en el espacio de estaods del funcionamiento en modo autonomo de una microred.* PhD thesis, Universidad de oviedo, 2010.

[124] E. S. Kuh and R. A. Rohrer. The state-variable approach to network analysis. *Proceedings of the IEEE*, 53(7):672–686, 1965.

[125] IEEE Std 399-1997. *IEEE recommended practice for industrial and commercial power systems analysis.* 1998.

[126] E.N. Dialynas and N.D. Hatziargyriou. Effect of high wind power penetration on the reliability and security of isolated power systems. In *presented at 37th session, CIGRE, Paris*, august 1998.

[127] N.D. Hatziargyrious and E.S. karapidakis. Frequency stability of power systems in large islands with high wind power penetration. In *Bulk Power Systems dynamics and Control Symposium*, august 1998.

[128] A.D. Hansen. *Generators and power electronics for wind turbines*, chapter 5 of book: Wind power in power systems, pages 53–78. Wiley, 2004.

[129] Slootweg J.G. *Wind power modelling and impact on power systems dynamics*. PhD thesis, Delft University of Technology, Delft, The Netherlands, 2003.

[130] M.V. Nunes and A.J Lopesa. Influence of the variable-speed wind generators in transient stability margin of the conventional generators integrated in electrical grids. *IEEE Trans. Energy Convers*, 19(4):692–701, 2004.

[131] F. Mei and B.C. Pal. Modelling and small-signal analysis of a grid connected doubly-fed induction generator. In *Power Engineering Society General Meeting, 2005. IEEE*, pages 2101 – 2108 Vol. 3, june 2005.

[132] F. Mei and B Pal. Modal analysis of grid-connected doubly fed induction generators. *Energy Conversion, IEEE Transactions on*, 22(3):728 –736, sept. 2007.

[133] B.C. Pal and F. Mei. Modelling adequacy of the doubly fed induction generator for small-signal stability studies in power systems. *Renewable Power Generation, IET*, 2(3):181 –190, september 2008.

[134] R. J. Thomas and A. G. Phadke. Operational characteristics of a large wind-farm utility system with a controllable ac–dc–ac interface. *IEEE Trans. Power Syst*, PS-3(1):220–225, Feb 1988.

[135] M. K. Donnelly and J.E. Dagle. Impacts of the distributed utility on transmission system stability. *IEEE Trans. Power Syst*, 11(2):741–746, May 1996.

[136] R C. Dugan and T. S. Key. Distributed resources standards. *IEEE Industry Applications Magazine*, 12:27–34, Feb 2006.

[137] F. Katiraei and M. R. Iravani. Power management strategies for a microgrid with multiple distributed generation units. *IEEE Trans. Power Syst*, 21:1821–1831, Nov 2006.

[138] Guoqiao Shen and Xuancai Zhu. A new feedback method for pr current control of lcl-filter-based grid-connected inverter. *IEEE Trans. Ind. Electron*, 57(6):2033–2041, June 2010.

[139] Fei Liu and Yan Zhou. Parameter design of a two current-loop controller used in a grid-connected inverter system with lcl filter. *IEEE Trans. Ind. Electron*, 56(11):4483–4491, Nov 2009.

[140] Y. Mohamed and E.F. El-Saadany. Adaptive decentralized droop controller to preserve power sharing stability of paralleled inverters in distributed generation microgrids. *Power Electronics, IEEE Transactions on*, 23(6):2806 –2816, nov. 2008.

[141] A. Anbarasan. Identification of maximum loading point in power system under critical line outage condition. *European Journal of Scientific Research*, 68(2):274–282, 2012.

[142] C.F. Moyano, R. Salgado, and L.V. Barboza. Calculating participation factors in the maximum loadability. In *Power Tech Conference Proceedings, 2003 IEEE Bologna*, volume 2, page 6 pp. Vol.2, june 2003.

[143] J.M. Guerrero, J.C. Vasquez, J. Matas, M. Castilla, and L.G. de Vicuna. Control strategy for flexible microgrid based on parallel line-interactive ups systems. *Industrial Electronics, IEEE Transactions on*, 56(3):726 –736, march 2009.

[144] Wei Qiao, R.G. Harley, and G.K. Venayagamoorthy. Coordinated reactive power control of a large wind farm and a statcom using heuristic dynamic programming. *Energy Conversion, IEEE Transactions on*, 24(2):493 –503, june 2009.

[145] Kenneth E. Okedu. Stability enhancement of dfig-based variable speed wind turbine with a crowbar by facts device as per grid requirement. *International Journal of Renewable Energy Ressearch*, 2(3), 2012.

88.0pt